PROCESS DEVELOPMENT FOR THE PRODUCTION OF DICYCLOPENTADIENE FROM PYROLYSIS GASOLINE (PYGAS)

A THESIS SUBMITTED TO
THE GRADUATE SCHOOL OF NATURAL AND APPLIED SCIENCES
OF
MIDDLE EAST TECHNICAL UNIVERSITY

BY

DENİZ SESLİ UYSAL

IN PARTIAL FULFILLMENT OF THE REQUIREMENTS
FOR
THE DEGREE OF MASTER OF SCIENCE
IN
CHEMICAL ENGINEERING

SEPTEMBER 2023

Approval of the thesis:

PROCESS DEVELOPMENT FOR THE PRODUCTION OF DICYCLOPENTADIENE FROM PYROLYSIS GASOLINE (PYGAS)

submitted by **DENİZ SESLİ UYSAL** in partial fulfillment of the requirements for the degree of **Master of Science** i**n Chemical Engineering, Middle East Technical University** by,

Prof. Dr. Halil Kalıpçılar
Dean, Graduate School of **Natural and Applied Sciences** _____

Prof. Dr. Pınar Çalık
Head of Department, **Chemical Engineering** _____

Prof. Dr. Gürkan Karakaş
Supervisor, **Chemical Engineering, METU** _____

Prof. Dr. Halil Kalıpçılar
Co-Supervisor, **Chemical Engineering, METU** _____

Examining Committee Members:

Prof. Dr. Yusuf Uludağ
Chemical Engineering, METU _____

Prof. Dr. Gürkan Karakaş
Chemical Engineering, METU _____

Prof. Dr. Halil Kalıpçılar
Chemical Engineering, METU _____

Prof. Dr. Nuray Oktar
Chemical Engineering, Gazi Uni. _____

Assoc. Prof. Dr. Çerağ Dilek Hacıhabiboğlu
Chemical Engineering, METU _____

Date: 11.09.2023

I hereby declare that all information in this document has been obtained and presented in accordance with academic rules and ethical conduct. I also declare that, as required by these rules and conduct, I have fully cited and referenced all material and results that are not original to this work.

Name, Last Name: Deniz Sesli Uysal

Signature :

ABSTRACT

PROCESS DEVELOPMENT FOR THE PRODUCTION OF DICYCLOPENTADIENE FROM PYROLYSIS GASOLINE (PYGAS)

Sesli Uysal, Deniz
Master of Science, Chemical Engineering
Supervisor: Prof. Dr. Gürkan Karakaş
Co-Supervisor: Prof. Dr. Halil Kalıpçılar

September 2023, 237 pages

Dicyclopentadiene (DCPD) is an essential intermediate utilized in various products. It is the dimer of cyclopentadiene (CPD) and potentially precious component of pyrolysis gasoline (PYGAS).

This study aims to develop a process for the recovery of CPD through monomerization of DCPD and subsequent separation from other hydrocarbons in the PYGAS mixture. For this purpose, reactive distillation can be employed. DCPD can finally be produced by dimerization of highly pure CPD.

The PYGAS samples from SOCAR Turkey were analyzed in GC-MS. Vapor-liquid equilibrium of DCPD in PYGAS was investigated in rotary evaporator to obtain equilibrium compositions within the temperature and pressure range of 40°C-135°C and 70-650 mbar. DCPD monomerization was examined in a single-stage reactive distillation system within the temperature range of 150°C-160°C under atmospheric pressure. The decomposition kinetics of DCPD were investigated in detail by conducting *in-situ* GC-MS reaction experiments at the temperature range of 80°C-350°C. The compositions obtained in experiments were compared with Aspen Plus

simulations. Results show that PYGAS separation and DCPD monomerization can be modeled by using Peng Robinson Equation of State with confidence under the experimental conditions applied. The PYGAS feed composition and obtained reaction rate expression were further used to ascertain the multicomponent distillation separation sequence in Aspen Plus. In this study, a novel method for the production of DCPD with high purity (≥ 90%wt) by reactive distillation is proposed. DCPD can be retrieved from PYGAS in a single equipment, with a yield of 94%, decreasing the equipment and the operational costs compared to conventional methods.

Keywords: Dicyclopentadiene, Cyclopentadiene, Pyrolysis Gasoline, Reactive Distillation

ÖZ

PİROLİZ BENZİNİNDEN (PYGAS) DİSİKLOPENTADİEN ÜRETİMİ İÇİN PROSES GELİŞTİRİLMESİ

Sesli Uysal, Deniz
Yüksek Lisans, Kimya Mühendisliği
Tez Yöneticisi: Prof. Dr. Gürkan Karakaş
Ortak Tez Yöneticisi: Prof. Dr. Halil Kalıpçılar

Eylül 2023, 237 sayfa

Disiklopentadien (DCPD), çeşitli ürünlerde kullanılan önemli bir ara maddedir. Disiklopentadien, siklopentadienin (CPD) dimeridir piroliz benzininden (PYGAS) elde edilebilen potansiyel olarak değerli bir bileşendir.

Bu çalışma, DCPD'nin monomerizasyonu ve ardından PYGAS karışımındaki diğer hidrokarbonlardan ayrılması yoluyla CPD'nin geri kazanılmasına yönelik bir süreç geliştirmeyi amaçlamaktadır. Bu amaçla, reaktif distilasyon kullanılması önerilmiştir. Bu işlemden sonra, yüksek derecede saf CPD'nin dimerizasyonu ile DCPD üretilebilmektedir.

PYGAS numuneleri SOCAR Türkiye'den temin edilmiş ve GC-MS kullanılarak analizleri yapılmıştır. DCPD'nin PYGAS içerisindeki buhar-sıvı dengesi davranışı döner buharlaştırıcı kullanılarak incelenmiş ve 40°C-135°C ile 70-650 mbar aralığında çeşitli sıcaklık ve basınçlarda denge kompozisyonları elde edilmiştir. DCPD monomerizasyon reaksiyonunu, atmosferik basınçta 150°C-160°C aralığında çeşitli sıcaklıklarda, tek kademeli reaktif distilasyon sisteminde deneysel olarak incelenmiştir. DCPD'nin ayrışma kinetiği, 80°C-350°C sıcaklık aralığında yerinde GC-MS reaksiyon deneyleri yapılarak da ayrıntılı olarak incelenmiştir. Deneylerde

elde edilen kompozisyonlar Aspen Plus simülasyon çalışmalarından elde edilen sonuçlarla da kıyaslanmıştır. Elde edilen sonuçlar, PYGAS ayrımının ve DCPD monomerizasyonunun, uygulanan deneysel koşullar altında Peng Robinson Hal Denklemi kullanılarak güvenle modellenebileceğini göstermektedir. Besleme komposizyonu ve elde edilen reaksiyon kinetiği, Aspen Plus'ta çok bileşenli distilasyon sürecinin belirlenmesi için kullanılmıştır. Bu çalışmada, reaktif distilasyon sisteminde yüksek saflıkta (≥ %90 wt) DCPD üretimi için yeni bir yöntem önerilmiştir. DCPD, PYGAS'tan tek bir ekipmanda, geleneksel yöntemlere kıyasla ekipman ve işletme maliyetlerini düşürerek, %94 verimle geri kazanılabilmektedir.

Anahtar Kelimeler: Disiklopentadien, Siklopentadien, Piroliz Benzin, Reaktif Distilasyon

To my beloved family

ACKNOWLEDGMENTS

I wish to express my sincerest and deepest gratitude to my supervisors Prof. Dr. Gürkan Karakaş and Prof. Dr. Halil Kalıpçılar for their guidance, vision, patience, and advice throughout the master study. It is a great honor to find a chance to conduct research with them, feed from their assistance, and knowledge. I feel privileged and deeply indebted to my supervisors.

I am grateful to Roketsan Inc. for giving me the opportunity to conduct master's studies during my profession and supported my work by providing me with time, knowledge, experience, and resources. I am deeply thankful to my colleagues in Chemical Material Processes Design Unit, Material Characterization Unit, and Material Technologies Unit for their support and guidance.

I would like to thank my supervisor Bora Bilgiç and my coworkers Murat Öztürk, Nihat Özer Uçar, Necati Güzel, Murat Yiğit, Sezgin Akdeniz, Coşkun Kaya, Enes Polat, and Yiğit Sarışen. I would like to extend my sincere thanks to Kıvanç Aydıncak for his advice, guidance, and patience. I could not have undertaken this journey without Zeynep Öztan. And at last, words can not express my gratitude for Ümüt Şen whose tenacity and stance, I admire.

Most of all, my greatest gratitude is for my family; my mother Birsen Sesli whom I never thank enough for making me who I am, being there for me, providing me with support, and continuous encouragement, and my father Cihangir Sesli for “fuelling” me with love, support, tolerance, and good wishes when I needed the most. Last but not least, this endeavor would not have been possible without my husband, Evren Uysal. I am deeply thankful for his suggestions, efforts, and reviews.

TABLE OF CONTENTS

ABSTRACT v

ÖZ vii

ACKNOWLEDGMENTS x

TABLE OF CONTENTS xi

LIST OF TABLES xiv

LIST OF FIGURES xvi

LIST OF ABBREVIATIONS xxx

1 INTRODUCTION 1

1.1 Dicyclopentadiene and Cyclopentadiene 1

1.2 Dicyclopentadiene and Cyclopentadiene Production 2

1.3 Major Problems of the Dicyclopentadiene and Cyclopentadiene Production 3

1.4 Objectives 4

2 LITERATURE REVIEW 5

2.1 Usage Areas of Dicylopentadiene and Cyclopentadiene 5

2.2 Pyrolysis Gasoline 11

2.3 Production of DCPD from PYGAS 14

2.3.1 Production of DCPD from C5 fraction of PYGAS 16

2.3.2 Production of DCPD from Crude DCPD 22

2.4 Kinetic Studies for Monomerization and Dimerization Reaction of DCPD 29

3 EXPERIMENTAL AND SIMULATION METHODS 37
3.1 Characterization of PYGAS and DCPD 37
3.2 Phase Equilibrium Experimental Studies and Model Prediction 38
3.2.1 Phase Equilibrium Experimental Studies 38
3.2.2 Phase Equilibrium Model Prediction 41
3.3 Monomerization Reaction Kinetics and Model Prediction 42
3.3.1 GC-MS Reaction Experiments 43
3.3.2 Reactive Distillation Experimental Studies 43
3.3.3 Reactive Distillation Model Prediction 46
3.4 Aspen Simulation of Seperation Sequence for the Production of CPD from PYGAS 46
4 RESULTS AND DISCUSSION 49
4.1 Characterization Results of PYGAS and DCPD 49
4.2 Phase Equilibrium Experiments and Modelling Results 54
4.3 Monomerization Reaction Kinetics and Modelling Results 75
4.3.1 GC-MS Reaction Experiment Results 75
4.3.2 Reactive Distillation Experiments and Modelling Results 84
4.4 Aspen Simulation of Seperation Sequence for the Production of CPD from PYGAS in an Industrial Scale 93
4.4.1 Batch Distillation Column Simulation 95
4.4.2 Continuous Operating Column Simulation 111
4.4.3 Comparison of Batch and Continuous Operating Column Simulation Results 118
5 CONCLUSION 121
REFERENCES 123

APPENDICES

A. Sample Chromatogram for PYGAS 131

B. Sample Chromatogram for DCPD 149

C. Experimental Procedure for Phase Equilibrium Experiment 14 153

D. Experimental Procedure for Reactive Distillation Experiment 39 155

E. Sample Chromatogram for Phase Equilibrium Experiment 14 Steps 156

F. Sample Chromatogram for GC-MS Reaction Experiment of DCPD in Heptane 177

G. Sample Chromatogram for GC-MS Reaction Experiments of DCPD in Toluene 191

H. Sample Chromatograms for GC-MS Reaction Experiments of PYGAS in Heptane 207

I. Sample Chromatogram for Reactive Distillation Experiment 27 Liquid Compositions 219

J. Sample Chromatogram for Reactive Distillation Experiment 39 Vapor and Liquid Compositions 229

LIST OF TABLES

TABLES

Table 1.1: Physical and chemical properties of CPD and DCPD (Claus, Claus, Claus, Hönicke, Födisch, & Olson, 2016), (Cheung, 2000). 1
Table 2.1: Areas of usage for CPD/DCPD with different purity ranges (Herink et al., 2022), (Cheung, 2000) 6
Table 2.2: Physical and chemical properties of pyrolysis gasoline from SOCAR 13
Table 2.3: C5 fraction composition of used PYGAS (Nurullina et al., 2001) 16
Table 2.4: Typical composition of used crude DCPD (Li et al., 2013) 22
Table 2.5: System parameters for the reactive distillation system (Cai et al., 2009) 24
Table 2.6: Summary table for production routes of CPD/DCPD 25
Table 2.7: Kinetic parameters for the reversible monomerization reaction of DCPD 30
Table 2.8: Kinetic parameters for the reversible dimerization reaction of CPD 33
Table 3.1: Phase equilibrium experiment sets 41
Table 3.2: Reactive distillation experiment sets 45
Table 4.1: Composition analysis of major PYGAS (SOCAR) constituents 50
Table 4.2: Composition analysis of DCPD (ZET) 51
Table 4.3: Physical properties of stored PYGAS (SOCAR) sample 54
Table 4.4: Experimental parameters and results of phase equilibrium experiments performed by using PYGAS sample (stored) 57
Table 4.5: PYGAS sample constituents grouping 68
Table 4.6: Aspen Plus inputs for the simulation of phase equilibrium experiments 75
Table 4.7: GC-MS reaction experiment sets and results for 10 mL/min He 77
Table 4.8: Regression analysis results of POLYMATH for reaction rate expression 82

Table 4.9: Comparison of regression analysis results and experimental results.... 82
Table 4.10: Comparison of the pre-exponential factors and activation energies of DCPD monomerization reaction 83
Table 4.11: Reactive distillation experiments and results..... 85
Table 4.12: Aspen Plus inputs for the simulation of reactive distillation experiment 89
Table 4.13: Aspen Plus inputs for the batch operating simulation of industrial scale removal of benzene and lighter hydrocarbons 96
Table 4.14: Aspen Plus inputs for the batch operating simulation of industrial scale production of CPD 104
Table 4.15: Aspen Plus inputs for the continuous operating simulation of industrial scale removal of benzene and lighter hydrocarbons 111
Table 4.16: Aspen Plus inputs for the continuous operating simulation of industrial scale production of CPD 112
Table 4.17: Comparison of the Aspen Plus results for the batch and continuous operating simulation of benzene and lighter hydrocarbon removal stage 118
Table 4.18: Comparison of the Aspen Plus results for the batch and continuous operating simulation of industrial scale production of CPD..... 119
Table A 1: Method information for characterization of PYGAS..... 131
Table B 1: Method information for characterization of DCPD 149
Table E 1: Method information for phase equilibrium experiment samples 156
Table F 1: Method information for DCPD reaction in GC-MS in heptane 177
Table G 1: Method information for DCPD reaction in GC-MS in toluene 191
Table H 1: Method information for PYGAS reaction in GC-MS in heptane 207
Table I 1: Method information for Reactive Distillation Experiment 27 samples219
Table J 1: Method information for Reactive Distillation Experiment 39 samples 229

LIST OF FIGURES

FIGURES

Figure 2.1: Structures of endo-DCPD and exo-DCPD 9
Figure 2.2: Reversible monomerization reaction of DCPD 14
Figure 2.3: DCDP production route from C5 fraction of PYGAS (Nurullina et al., 2001) 17
Figure 2.4: Alternative DCDP production route from C5 fraction of PYGAS (Kim, et al., 2019) 19
Figure 2.5: Production route for DCPD from Light PYGAS (Herink et al., 2022) 21
Figure 3.1: Phase equilibrium experimental set-up 39
Figure 3.2: Multi step separation of the PYGAS in phase equilibrium experiments 40
Figure 3.3:Experimental set-up for the reactive distillation system 44
Figure 4.1: Thermogram of PYGAS 52
Figure 4.2: Thermogram of DCPD 52
Figure 4.3: Comparison of PYGAS and DCPD thermograms 53
Figure 4.4: Composition analysis of Step 1 (Experiment 14x), started with inital flask containing PYGAS sample 69
Figure 4.5: Composition analysis of Step 2 (Experiment 14y), started with flask of Step 1 69
Figure 4.6: Composition analysis of Step 3 (Experiment 14z), started with condensate of Step 2 70
Figure 4.7: Comparison of experimental and simulation results for Step 1 (Experiment 14x) condensate 72
Figure 4.8: Comparison of experimental and simulation results for Step 1 (Experiment 14x) flask 72
Figure 4.9: Comparison of experimental and simulation results for Step 2 (Experiment 14y) condensate 73

Figure 4.10: Comparison of experimental and simulation results for Step 2 (Experiment 14y) flask 73
Figure 4.11: Comparison of experimental and simulation results for Step 3 (Experiment 14z) condensate 74
Figure 4.12: Comparison of experimental and simulation results for Step 3 (Experiment 14z) flask 74
Figure 4.13: Effect of temperature on weight fraction of CPD and DCPD for 10 mL/min He and 20 mL/min He 78
Figure 4.14: Effect of temperature on weight fraction of Met-CPD, Met-DCPD and toluene for 20 mL/min He 79
Figure 4.15: Effect of temperature on weight fraction of CPD, DCPD and benzene for 20 mL/min He 79
Figure 4.16: Temperature effect on conversion (XDCPD) for pure DCPD and DCPD in PYGAS 80
Figure 4.17: Weight percentage of DCPD over time at 160°C 87
Figure 4.18: Weight percentages of CPD and TCPD over at 160°C 88
Figure 4.19: Condensate volume over time for experiments and model simulation 90
Figure 4.20: Model simulation for literature kinetics and the experimental kinetics for vapor phase (condensate) CPD's weight percentage 90
Figure 4.21: Model simulation for literature kinetics and the experimental kinetics for vapor phase (condensate) DCPD's weight percentage 91
Figure 4.22: Model simulation for literature kinetics and the experimental kinetics for liquid phase (reaction flask) CPD's weight percentage 92
Figure 4.23: Model simulation for literature kinetics and the experimental kinetics for liquid phase (reaction flask) DCPD's weight percentage 92
Figure 4.24: Pot temperature over time for lighter hydrocarbon separation simulation 98
Figure 4.25: Pot composition of CPD, benzene and DCPD over time for lighter hydrocarbon separation simulation 98

Figure 4.26: Effect of column pressure on mass fraction of DCPD in pot for lighter hydrocarbon separation simulations 99
Figure 4.27: Effect of column pressure on DCPD mass in pot for lighter hydrocarbon separation simulations 99
Figure 4.28: Effect of column pressure on benzene mass in pot for lighter hydrocarbon separation simulations 100
Figure 4.29: Effect of column pressure on pot temperature for lighter hydrocarbon separation simulations 100
Figure 4.30: Effect of reflux ratio on mass fraction of DCPD in pot for lighter hydrocarbon separation simulations 101
Figure 4.31: Effect of reflux ratio on DCPD mass in pot for lighter hydrocarbon separation simulations 101
Figure 4.32: Effect of reflux ratio on benzene mass in pot for lighter hydrocarbon separation simulations 102
Figure 4.33: Effect of reflux ratio on pot temperature for lighter hydrocarbon separation simulations 102
Figure 4.34: Pot temperature over time for reactive distillation simulation..... 105
Figure 4.35: Distillate composition of CPD and DCPD over time for reactive distillation simulation 105
Figure 4.36: Reaction rates over time for CPD, DCPD, Met-CPD and Met-DCPD 106
Figure 4.37: Compositions of CPD, DCPD, Met-CPD and Met-DCPD over time in pot 107
Figure 4.38: Effect of pressure on mass fraction of CPD in distillate for reactive distillation simulations..... 108
Figure 4.39: Effect of pressure on CPD mass in distillate for reactive distillation simulations..... 108
Figure 4.40: Effect of pressure on pot temperature for reactive distillation simulations..... 109

Figure 4.41: Effect of reflux ratio on mass fraction of CPD in distillate for reactive distillation simulations 109
Figure 4.42: Effect of reflux ratio on CPD mass in distillate for reactive distillation simulations 110
Figure 4.43: Effect of reflux ratio on pot temperature for reactive distillation simulations 110
Figure 4.44: Temperature profile of continuous operating column for lighter hydrocarbon separation simulation 114
Figure 4.45: Temperature profile of continuous operating column for reactive distillation simulation..... 115
Figure 4.46: Composition profile of continuous operating column for lighter hydrocarbon separation simulation 116
Figure 4.47: Composition profile of continuous operating column for reactive distillation simulation..... 117
Figure A 1: Sample chromatogram for PYGAS in heptane 132
Figure A 2: Sample chromatogram for PYGAS constituents between 2.3 RTmin and 3.4 RTmin 132
Figure A 3: Sample chromatogram for PYGAS constituents between 3.4 RTmin and 5.6 RTmin 133
Figure A 4: Sample chromatogram for PYGAS constituents between 10.6 RTmin and 12.1 RTmin 133
Figure A 5: Sample chromatogram for PYGAS constituents between 24.6 RTmin and 30.8 RTmin 134
Figure A 6: Sample chromatogram for PYGAS constituents between 48 RTmin and 54.5 RTmin 134
Figure A 7: Mass spectra and library match for peak at 2.33 RTmin..... 135
Figure A 8: Mass spectra and library match for peak at 2.36 RTmin..... 135
Figure A 9: Mass spectra and library match for peak at 2.43 RTmin..... 136
Figure A 10: Mass spectra and library match for peak at 2.46 RTmin..... 136
Figure A 11: Mass spectra and library match for peak at 2.49 RTmin..... 137

Figure A 12: Mass spectra and library match for peak at 2.52 RTmin 137
Figure A 13: Mass spectra and library match for peak at 2.58 RTmin 138
Figure A 14: Mass spectra and library match for peak at 2.65 RTmin 138
Figure A 15: Mass spectra and library match for peak at 2.69 RTmin 139
Figure A 16: Mass spectra and library match for peak at 2.77 RTmin 139
Figure A 17: Mass spectra and library match for peak at 2.87 RTmin 140
Figure A 18: Mass spectra and library match for peak at 3.12 RTmin 140
Figure A 19: Mass spectra and library match for peak at 3.23 RTmin 141
Figure A 20: Mass spectra and library match for peak at 3.29 RTmin 141
Figure A 21: Mass spectra and library match for peak at 3.36 RTmin 142
Figure A 22: Mass spectra and library match for peak at 3.48 RTmin 142
Figure A 23: Mass spectra and library match for peak at 3.57 RTmin 143
Figure A 24: Mass spectra and library match for peak at 3.78 RTmin 143
Figure A 25: Mass spectra and library match for peak at 4.05 RTmin 144
Figure A 26: Mass spectra and library match for peak at 5.43 RTmin 144
Figure A 27: Mass spectra and library match for peak at 10.95 RTmin 145
Figure A 28: Mass spectra and library match for peak at 24.69 RTmin 145
Figure A 29: Mass spectra and library match for peak at 28.09 RTmin 146
Figure A 30: Mass spectra and library match for peak at 30.43 RTmin 146
Figure A 31: Mass spectra and library match for peak at 48.39 RTmin 147
Figure A 32: Mass spectra and library match for peak at 51.72 RTmin 147
Figure A 33: Mass spectra and library match for peak at 54.18 RTmin 148
Figure B 1: Sample chromatogram for DCPD constituents in toluene 150
Figure B 2: Sample chromatogram for DCPD constituents between 7.5 RTmin and 9.9 RTmin 150
Figure B 3: Mass spectra and library match for peak at 3.32 RTmin 151
Figure B 4: Mass spectra and library match for peak at 8.08 RTmin 151
Figure B 5: Mass spectra and library match for peak at 9.01 RTmin 152
Figure B 6: Mass spectra and library match for peak at 9.66 RTmin 152

Figure E 1: Sample chromatogram for Step 1 condensate constituents between 2 RTmin and 15.5 RTmin 157
Figure E 2: Sample chromatogram for Step 1 condensate constituents between 2 RTmin and 5.3 RTmin 157
Figure E 3: Sample chromatogram for Step 1 condensate constituents between 9.35 RTmin and 10.2 RTmin 158
Figure E 4: Sample chromatogram for Step 1 condensate constituents between 13.25 RTmin and 15.65 RTmin 158
Figure E 5: Sample chromatogram for Step 1 flask constituents between 0.5 RTmin and 15 RTmin 159
Figure E 6: Sample Chromatogram for Step 1 flask Constituents between 2.2 RTmin and 5.2 RTmin 159
Figure E 7: Sample chromatogram for Step 1 flask constituents between 8 RTmin and 8.27 RTmin 160
Figure E 8: Sample chromatogram for Step 1 flask constituents between 8.95 RTmin and 9.85 RTmin 160
Figure E 9: Sample chromatogram for Step 1 flask constituents between 10.5 RTmin and 11 RTmin 161
Figure E 10: Sample chromatogram for Step 1 flask constituents between 13 RTmin and 15 RTmin 161
Figure E 11: Sample chromatogram for Step 2 condensate constituents between 2 RTmin and 15 RTmin 162
Figure E 12: Sample chromatogram for Step 2 condensate constituents between 2.35 RTmin and 3.45 RTmin 162
Figure E 13: Sample chromatogram for Step 2 condensate constituents between 4.75 RTmin and 4.90 RTmin 163
Figure E 14: Sample chromatogram for Step 2 condensate constituents between 7.2 RTmin and 11.60 RTmin 163
Figure E 15: Sample chromatogram for Step 2 condensate constituents between 12.70 RTmin and 15 RTmin 164

Figure E 16: Sample chromatogram for Step 2 flask constituents between 2 RTmin and 39.3 RTmin 164
Figure E 17: Sample chromatogram for Step 2 flask constituents between 7.4 RTmin and 13 RTmin 165
Figure E 18: Sample chromatogram for Step 2 flask constituents between 12.6 RTmin and 16.6 RTmin 165
Figure E 19: Sample chromatogram for Step 2 flask constituents between 17 RTmin and 18.9 RTmin 166
Figure E 20: Sample chromatogram for Step 2 flask constituents between 19.20 RTmin and 23.00 RTmin 166
Figure E 21: Sample chromatogram for Step 2 flask constituents between 23 RTmin and 32.5 RTmin 167
Figure E 22: Sample chromatogram for Step 3 condensate constituents between 1.5 RTmin and 15.5 RTmin 167
Figure E 23: Sample chromatogram for Step 3 condensate constituents between 2.6 RTmin and 4.8 RTmin 168
Figure E 24 : Sample chromatogram for Step 3 condensate constituents between 13.20 RTmin and 14.7 RTmin 168
Figure E 25: Sample chromatogram for Step 3 flask constituents between 1 RTmin and 15.5 RTmin 169
Figure E 26 : Sample chromatogram for Step 3 condensate constituents between 7.5 RTmin and 14.5 RTmin 169
Figure E 27: Mass spectra and library match for peak at 2.40 RTmin 170
Figure E 28:Mass spectra and library match for peak at 2.62 RTmin 170
Figure E 29: Mass spectra and library match for peak at 3.25 RTmin 171
Figure E 30: Mass spectra and library match for peak at 4.81 RTmin 171
Figure E 31: Mass spectra and library match for peak at 8.13 RTmin 172
Figure E 32: Mass spectra and library match for peak at 9.58 RTmin 172
Figure E 33: Mass spectra and library match for peak at 13.35 RTmin 173
Figure E 34:Mass spectra and library match for peak at 13.97 RTmin 173

Figure E 35:Mass spectra and library match for peak at 14.62 RTmin 174
Figure E 36:Mass spectra and library match for peak at 18.10 RTmin 174
Figure E 37. Mass spectra and library match for peak at 24.16 RTmin 175
Figure E 38: Mass spectra and library match for peak at 30.83 RTmin 175
Figure E 39: Mass spectra and library match for peak at 21.47 RTmin 176
Figure E 40: Mass spectra and library match for peak at 16.34 RTmin 176
Figure F 1: Sample chromatogram for GC-MS reaction experiment constituents between 2 RTmin and 38 RTmin at 250°C and 10 mL/min Helium flow..... 178
Figure F 2: Sample chromatogram for GC-MS reaction experiment constituents between 24 RTmin and 31.5 RTmin at 250°C and 10 mL/min Helium flow..... 178
Figure F 3: Sample Chromatogram for GC-MS reaction experiment constituents between 2 RTmin and 38 RTmin at 250°C and 20 mL/min Helium flow..... 179
Figure F 4: Sample chromatogram for GC-MS reaction experiment constituents between 24 RTmin and 31 RTmin at 250°C and 20 mL/min Helium flow..... 179
Figure F 5: Sample chromatogram for GC-MS reaction experiment constituents between 2 RTmin and 38 RTmin at 270°C and 10 mL/min Helium flow..... 180
Figure F 6: Sample chromatogram for GC-MS reaction experiment constituents between 24 RTmin and 32 RTmin at 270°C and 10 mL/min Helium flow..... 180
Figure F 7: Sample chromatogram for GC-MS reaction experiment constituents between 2 RTmin and 38 RTmin at 270°C and 20 mL/min Helium flow..... 181
Figure F 8: Sample chromatogram for GC-MS reaction experiment constituents between 24 RTmin and 31.5 RTmin at 270°C and 20 mL/min Helium flow..... 181
Figure F 9: Sample chromatogram for GC-MS reaction experiment constituents between 2 RTmin and 38 RTmin at 290°C and 10 mL/min Helium flow..... 182
Figure F 10: Sample chromatogram for GC-MS reaction experiment constituents between 24 RTmin and 31 RTmin at 290°C and 10 mL/min Helium flow..... 182
Figure F 11: Sample chromatogram for GC-MS reaction experiment constituents between 2 RTmin and 38 RTmin at 290°C and 20 mL/min Helium flow..... 183
Figure F 12: Sample chromatogram for GC-MS reaction experiment constituents between 24 RTmin and 31 RTmin at 290°C and 20 mL/min Helium flow..... 183

Figure F 13: Sample chromatogram for GC-MS reaction experiment constituents between 2 RTmin and 38 RTmin at 330°C and 10 mL/min Helium flow 184
Figure F 14: Sample chromatogram for GC-MS reaction experiment constituents between 24 RTmin and 31 RTmin at 330°C and 10 mL/min Helium flow 184
Figure F 15: Sample chromatogram for GC-MS reaction experiment constituents between 2 RTmin and 38 RTmin at 330°C and 20 mL/min Helium flow 185
Figure F 16:Sample chromatogram for GC-MS reaction experiment constituents between 24 RTmin and 31 RTmin at 330°C and 20 mL/min Helium flow 185
Figure F 17: Sample chromatogram for GC-MS reaction experiment constituents between 2 RTmin and 38 RTmin at 350°C and 10 mL/min Helium flow 186
Figure F 18: Sample chromatogram for GC-MS reaction experiment constituents between 24 RTmin and 31.5 RTmin at 350°C and 10 mL/min Helium flow 186
Figure F 19: Sample chromatogram for GC-MS reaction experiment constituents between 2 RTmin and 38 RTmin at 350°C and 20 mL/min Helium flow 187
Figure F 20: Sample chromatogram for GC-MS reaction experiment constituents between 24 RTmin and 31.5 RTmin at 350°C and 20 mL/min Helium flow 187
Figure F 21: Mass spectra and library match for peak at 2.59 RTmin 188
Figure F 22: Mass spectra and library match for peak at 4.25 RTmin 188
Figure F 23: Mass spectra and library match for peak at 4.49 RTmin 189
Figure F 24: Mass spectra and library match for peak at 28.03 RTmin 189
Figure F 25: Mass spectra and library match for peak at 31.17 RTmin 190
Figure G 1: Sample chromatogram for GC-MS reaction experiment constituents between 1 RTmin and 24 RTmin at 80°C in toluene 192
Figure G 2: Sample chromatogram for GC-MS reaction experiment constituents between 7.5 RTmin and 10 RTmin at 80°C in toluene 192
Figure G 3: Sample Chromatogram for GC-MS Reaction Experiment Constituents between 1 RTmin and 24 RTmin at 250°C in toluene 193
Figure G 4: Sample chromatogram for GC-MS reaction experiment constituents between 7.6 RTmin and 9.9 RTmin at 250°C in toluene 193

Figure G 5: Sample chromatogram for GC-MS reaction experiment constituents between 0.5 RTmin and 10.5 RTmin at 260°C in toluene 194
Figure G 6: Sample chromatogram for GC-MS reaction experiment constituents between 7.7 RTmin and 9.8 RTmin at 260°C in toluene 194
Figure G 7: Sample chromatogram for GC-MS reaction experiment constituents between 1 RTmin and 24 RTmin at 270°C in toluene 195
Figure G 8: Sample chromatogram for GC-MS reaction experiment constituents between 7.4 RTmin and 9.8 RTmin at 270°C in toluene 195
Figure G 9: Sample chromatogram for GC-MS reaction experiment constituents between 1 RTmin and 24 RTmin at 280°C in toluene 196
Figure G 10: Sample chromatogram for GC-MS reaction experiment constituents between 7.7 RTmin and 9.8 RTmin at 280°C in toluene 196
Figure G 11: Sample chromatogram for GC-MS reaction experiment constituents between 1 RTmin and 24 RTmin at 290°C in toluene 197
Figure G 12: Sample chromatogram for GC-MS reaction experiment constituents between 7.8 RTmin and 9.8 RTmin at 290°C in toluene 197
Figure G 13: Sample chromatogram for GC-MS reaction experiment constituents between 1 RTmin and 24 RTmin at 300°C in toluene 198
Figure G 14: Sample chromatogram for GC-MS reaction experiment constituents between 7.7 RTmin and 9.8 RTmin at 300°C in toluene 198
Figure G 15: Sample chromatogram for GC-MS reaction experiment constituents between 1 RTmin and 24 RTmin at 310°C in toluene 199
Figure G 16: Sample chromatogram for GC-MS reaction experiment constituents between 8.7 RTmin and 9.8 RTmin at 310°C in toluene 199
Figure G 17: Sample chromatogram for GC-MS reaction experiment constituents between 1 RTmin and 24 RTmin at 320°C in toluene 200
Figure G 18: Sample chromatogram for GC-MS reaction experiment constituents between 7.7 RTmin and 9.8 RTmin at 320°C in toluene 200
Figure G 19: Sample chromatogram for GC-MS reaction experiment constituents between 1 RTmin and 24 RTmin at 330°C in toluene 201

Figure G 20: Sample chromatogram for GC-MS reaction experiment constituents between 8.9 RTmin and 9.8 RTmin at 330°C in toluene 201
Figure G 21: Sample chromatogram for GC-MS reaction experiment constituents between 1 RTmin and 24 RTmin at 340°C in toluene 202
Figure G 22: Sample chromatogram for GC-MS reaction experiment constituents between 8.8 RTmin and 9.8 RTmin at 340°C in Toluene 202
Figure G 23: Sample chromatogram for GC-MS reaction experiment constituents between 1 RTmin and 24 RTmin at 350°C in toluene 203
Figure G 24: Sample chromatogram for GC-MS reaction experiment constituents between 8.8 RTmin and 10.05 RTmin at 350°C in toluene 203
Figure G 25: Mass spectra and library match for peak at 2.29 RTmin 204
Figure G 26: Mass spectra and library match for peak at 3.32 RTmin 204
Figure G 27: Mass spectra and library match for peak at 8.10 RTmin 205
Figure G 28: Mass spectra and library match for peak at 9.01 RTmin 205
Figure G 29: Mass spectra and library match for peak at 9.66 RTmin 206
Figure H 1: Sample chromatogram for PYGAS GC-MS reaction experiment constituents between 2 RTmin and 58 RTmin at 260°C in heptane..... 208
Figure H 2: Sample chromatogram for PYGAS GC-MS reaction experiment constituents between 2.2 RTmin and 3.35 RTmin at 260°C in heptane..... 208
Figure H 3: Sample chromatogram for PYGAS GC-MS reaction experiment constituents between 3.25 RTmin and 4.45 RTmin at 260°C in heptane..... 209
Figure H 4: Sample chromatogram for PYGAS GC-MS reaction experiment constituents between 24.668 RTmin and 30.5 RTmin at 260°C in heptane..... 209
Figure H 5: Sample chromatogram for PYGAS GC-MS reaction experiment constituents between 48 RTmin and 54.50 RTmin at 260°C in heptane..... 210
Figure H 6: Sample chromatogram for PYGAS GC-MS reaction experiment constituents between 2 RTmin and 58 RTmin at 270°C in heptane..... 210
Figure H 7: Sample chromatogram for PYGAS GC-MS reaction experiment constituents between 2.35 RTmin and 3.25 RTmin at 270°C in heptane..... 211

Figure H 8: Sample chromatogram for PYGAS GC-MS reaction experiment constituents between 3.15 RTmin and 4.85 RTmin at 270°C in heptane 211
Figure H 9: Sample chromatogram for PYGAS GC-MS reaction experiment constituents between 24.5 RTmin and 30.5 RTmin at 270°C in heptane 212
Figure H 10: Sample chromatogram for PYGAS GC-MS reaction experiment constituents between 48 RTmin and 54.5 RTmin at 270°C in heptane 212
Figure H 11: Sample chromatogram for PYGAS GC-MS reaction experiment constituents between 2 RTmin and 58 RTmin at 300°C in heptane 213
Figure H 12: Sample chromatogram for PYGAS GC-MS reaction experiment constituents between 2.35 RTmin and 3.35 RTmin at 300°C in heptane 213
Figure H 13: Sample chromatogram for PYGAS GC-MS reaction experiment constituents between 3.2 RTmin and 4.55 RTmin at 300°C in heptane 214
Figure H 14: Sample chromatogram for PYGAS GC-MS reaction experiment constituents between 24.5 RTmin and 30.5 RTmin at 300°C in heptane 214
Figure H 15: Sample chromatogram for PYGAS GC-MS reaction experiment constituents between 48.2 RTmin and 54.4 RTmin at 300°C in heptane 215
Figure H 16: Sample chromatogram for PYGAS GC-MS reaction experiment constituents between 2 RTmin and 58 RTmin at 320°C in heptane 215
Figure H 17: Sample chromatogram for PYGAS GC-MS reaction experiment constituents between 2.3 RTmin and 3.4 RTmin at 320°C in heptane 216
Figure H 18: Sample chromatogram for PYGAS GC-MS reaction experiment constituents between 3.05 RTmin and 4.55 RTmin at 320°C in heptane 216
Figure H 19: Sample chromatogram for PYGAS GC-MS reaction experiment constituents between 28.9 RTmin and 31.6RTmin at 320°C in heptane 217
Figure H 20: Sample chromatogram for PYGAS GC-MS reaction experiment constituents between 2 RTmin and 58 RTmin at 350°C in heptane 217
Figure H 21: Sample chromatogram for PYGAS GC-MS reaction experiment constituents between 2.3 RTmin and 3.3 RTmin at 350°C in heptane 218
Figure H 22: Sample chromatogram for PYGAS GC-MS reaction experiment constituents between 3 RTmin and 5 RTmin at 350°C in heptane 218

Figure I 1: Sample chromatogram of liquid phase at 15 minute for Reactive Distillation Experiment 27 220
Figure I 2: Sample chromatogram of liquid phase at 30 minute for Reactive Distillation Experiment 27 220
Figure I 3: Sample chromatogram of liquid phase at 45 minute for Reactive Distillation Experiment 27 221
Figure I 4: Sample chromatogram of liquid phase at 60 minute for Reactive Distillation Experiment 27 221
Figure I 5: sample chromatogram of liquid phase at 75 minute for Reactive Distillation Experiment 27 222
Figure I 6: Sample chromatogram of liquid phase at 90 minute for Reactive Distillation Experiment 27 222
Figure I 7: Sample chromatogram of liquid phase at 105 minute for Reactive Distillation Experiment 27 223
Figure I 8: Sample chromatogram of liquid phase at 120 minute for Reactive Distillation Experiment 27 223
Figure I 9: Sample chromatogram of liquid phase at 135 minute for Reactive Distillation Experiment 27 224
Figure I 10: Sample chromatogram of liquid phase at 150 minute for Reactive Distillation Experiment 27 224
Figure I 11: Sample chromatogram of liquid phase at 165 minute for Reactive Distillation Experiment 27 225
Figure I 12: Sample Chromatogram of Liquid Phase at 180 Minute for Reactive Distillation Experiment 27 225
Figure I 13: Mass Spectra and Library Match for Peak at 2.27 RTmin 226
Figure I 14: Mass Spectra and Library Match for Peak at 2.36 RTmin 226
Figure I 15: Mass Spectra and Library Match for Peak at 8.92 RTmin 227
Figure I 16: Mass Spectra and Library Match for Peak at 9.55RTmin 227
Figure I 17: Mass Spectra and Library Match for Peak at 36.66 RTmin 228

Figure J 1: Sample chromatogram of vapor phase at 10 minute for Reactive Distillation Experiment 39 230
Figure J 2: Sample chromatogram of liquid phase at 10 minute for Reactive Distillation Experiment 39 230
Figure J 3: Sample chromatogram of vapor phase at 20 minute for Reactive Distillation Experiment 39 231
Figure J 4: Sample chromatogram of liquid phase at 20 minute for Reactive Distillation Experiment 39 231
Figure J 5: Sample chromatogram of vapor phase at 30 minute for Reactive Distillation Experiment 39 232
Figure J 6: Sample chromatogram of liquid phase at 30 minute for Reactive Distillation Experiment 39 232
Figure J 7: Sample chromatogram of vapor phase at 40 minute for Reactive Distillation Experiment 39 233
Figure J 8: Sample chromatogram of liquid phase at 40 minute for Reactive Distillation Experiment 39 233
Figure J 9: Sample chromatogram of vapor phase at 50 minute for Reactive Distillation Experiment 39 234
Figure J 10: Sample chromatogram of liquid phase at 50 minute for Reactive Distillation Experiment 39 234
Figure J 11: Sample chromatogram of vapor phase at 60 minute for Reactive Distillation Experiment 39 235
Figure J 12: Sample chromatogram of liquid phase at 60 minute for Reactive Distillation Experiment 39 235
Figure J 13: Mass spectra and library match for peak at 2.665 RTmin 236
Figure J 14: Mass spectra and library match for peak at 2.771 RTmin 236
Figure J 15: Mass spectra and library match for peak at 10.441 RTmin 237
Figure J 16: Mass spectra and library match for peak at 11.156 RTmin 237

LIST OF ABBREVIATIONS

ABBREVIATIONS	
3D	3 Dimensional
C4	4 Carbon Cut
C5	5 Carbon Cut
C9	9 Carbon Cut
COC	Cyclic Olefin Copolymer
CPD	Cyclopentadiene
DCDP	Dicyclopentadiene
ECD	Electron Capture Detection
ENB	Ethylidene Norbornene
EOS	Equation of State
Endo-THDCPD	Endotetrahydrodicyclopentadiene
EPDM	Ethylene Propylene Diene Monomer
Exo-THDCPD	Exotetrahydrodicyclopentadiene
FID	Flame Ionization Detection
FRC	Fiber Reinforced Composites
GC-MS	Gas Chromatography–Mass Spectrometry
Met-CPD	Methyl Cyclopentadiene
Met-DCPD	Methyl Dicyclopentadiene
Poly-DCPD	Polydicyclopentadiene

PYGAS	Pyrolysis Gasoline
RIM	Reaction Injection Molding
ROMP	Ring Opening Metathesis Polymerization
RTmin	Retention Time in Minute
STA	Simultaneous Thermal Analysis
TCPD	Tricyclopentadiene
UPR	Unsaturated Polyester Resin
USD	United States Dollar
VLE	Vapor Liquid Equilibrium
VOC	Volatile Organic Compounds

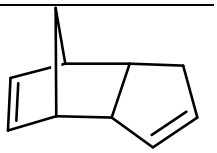
CHAPTER 1

INTRODUCTION

1.1 Dicyclopentadiene and Cyclopentadiene

Dicyclopentadiene (DCPD) is a speciality chemical that is used widely in the chemical industry in automative parts, optical lenses, resins, co-polymers and electronics (Cheung, 2000).

Table 1.1: Physical and chemical properties of CPD and DCPD (Claus, Claus, Claus, Hönicke, Födisch, & Olson, 2016), (Cheung, 2000).

Property	*CPD*	*DCPD*
Structure		
Molecular Weight (g/mol)	66.1	132.2
Boiling Point (°C at 1 bar)	40.0	170.0
Freezing Point (°C)	-97.2	32.0
Heat of Combustion (kJ/mol)	2929.0	5767.0
Heat of Vaporization (kJ/mol)	28.9	38.5
Liquid Specific Heat Capacity (kJ $kg^{-1}K^{-1}$)	1.8	1.3
Vapor Pressure (bar at 20°C)	0.45	0.0004
Standart State Enthalpy of Formation (kJ/mol)	130.8	196.1
Standart State Gibbs Energy of Formation (kJ/mol)	172.6	375.0
Autoignition Temperature (°C)	640.0	510.0
Flash Point (°C)	≤ -46.2	32.2

DCPD is the dimer of cyclopentadiene (CPD) and at or above room temperature CPD spontaneously dimerizes to its more stable dimer, DCPD. The physical and chemical properties of DCPD and CPD are given in Table 1.1.As a highly reactive molecule due to its cyclic olefinic structure, CPD acts as both diene and dienophile and can go under Dies-Alder, alkylation, polymerization, condensation, hydrogenation, oxidation, and halogenation reactions (Cheung, 2000), (Monson,1971).

1.2 Dicyclopentadiene and Cyclopentadiene Production

Global DCPD demand was reported as 811,000 tonnes in 2017 (Herink, Fulín, Krupka & Pašek, 2022). The United States of America, Europe, China, Japan, Singapore, and South Korea are the largest consumers of DCPD in 2018 globally (Perrot, Hyršl, Bandžuch, Waňousová, Hájek, Jenčík & Herink, 2023). Projections show that the DCPD demand can increase by 20% in Europe, 40% in the United States of America, and 60% in Asia by 2030 where the current DCPD producers are Dow Chemicals, Shell and ExxonMobil (Herink et al.,2022). The current market size of DCPD is stated at around 915.9 million US dollars in 2021 and expected to increase up to 1,501.5 million USD by 2030 (Global Market Insights, 2022).

CPD/DCPD can be produced by synthesis from cyclopentane, recovery from oils, and pyrolysis of hydrocarbons. CPD can be synthesized by dehydrogenation of cyclopentane around 500-600°C at elevated pressures by using dehydrogenating catalysts. Formerly, CPD/DCPD was discovered in coking plants. CPD presence in the forerun fraction of the distillation of coke-oven light oil was reported. DCPD was encountered during the recovery of oils containing dienes when heated around 100°C under pressure. It was also observed that the phenols can be pyrolyzed to CPD around 750°C (Szekeres, Siklos, Nagy & Jelinek, 1977), (Wilson & Wells, 1944).

DCPD was recovered from the coal tar with a yield of %0.00001 to %0.00002 by weight per tonne of coal. However, with the advancements in the petrochemical industry and the pyrolysis of petroleum products, production with higher yields was

enlarged. Today, DCPD and CPD are vastly produced in steam cracking reactors of hydrocarbons such as naphtha or ethylene, from side products. (Claus et al., 2016), (Xu, Al Shoaibi, Wang, Carstensen & Dean, 2011).

The side product of the steam cracking units, or pyrolysis gasoline (PYGAS), is a primary source for the production of CPD/DCPD. DCPD can be retrieved from naphtha with a yield of %1.4 by weight per tonne of feed in steam cracking units (Claus et al., 2016). Pyrolysis gasoline contains approximately 25% by weight CPD, however, the yield, production capacity, purity of CPD/DCPD, or the remaining 75%'s residual composition is directly related to the parameters of the pyrolysis reactor and feed stream, therefore, depending on the source, can change (Szekeres et al., 1977), (Claus et al., 2016), (Bondaletov, Bondaletova, Van Thanh & Baikova, 2015).

1.3 Major Problems of the Dicyclopentadiene and Cyclopentadiene Production

In general, CPD/DCPD can be produced from pyrolysis gasoline with sequential equipment sets. These equipment involve a reactor to dimerize CPD to DCPD, distillation columns to separate DCPD from lower carbon compounds, and reactors in order to monomerize DCPD, separation units to recover CPD and reactors to re-dimerize CPD in controlled conditions to increase purity (Claus et al., 2016). The need for the monomerization-dimerization of DCPD results from the CPD loss due to side products of co-dimers in the first dimerization reactor (Claus et al., 2016), (Cao, Liu, Zhang, Shi, Song & Yao, 2015), (Xu, Jocz, Wiest, Sarngadharan, Milina, Coleman, Iaccino, Pollet, Sievers & Liotta, 2019). Also, CPD forms an azeotrope with other five-carbon PYGAS constituents therefore, separation by distillation with desired purity can be challenging. Extractive distillation methods followed by monomerization and re-dimerization of DCPD are common to produce CPD/DCPD (Cheung, 2000), (Miki, 2019). The high energy consumption, high capital cost, and

handling issues of sequential distillation and reactor systems to obtain high purity DCPD are also adressed in literature (Hsu, Wang, Ou & Wong, 2015).

Therefore the main bottleneck problems for the production of DCPD can be listed as the side product formations with co-monomers in the PYGAS mixture, the high capital and operational costs due to sequential processes to retrieve DCPD from PYGAS.

1.4 Objectives

This study aims to develop an integrated and lean process for high purity DCPD production from PYGAS. PYGAS samples were obtained from SOCAR, Turkey and the composition analysis of PYGAS and DCPD were conducted by using GC-MS. Phase equilibrium behavior of DCPD in PYGAS was investigated by using a rotary evaporator and GC-MS, and kinetics of monomerization reaction of DCPD to CPD were investigated by *in-situ* GC-MS analysis. DCPD-CPD conversion and purification was conducted by single stage reactive distillation to observe simultaneous effects of phase equilibrium and monomerization. A reactive distillation system was then proposed for the removal of CPD from the PYGAS mixture. The prominent experiments were simulated by using Aspen Plus to find a fitted equation of state for industrial scale simulations. A novel process is proposed where benzene and lighter hydrocarbons are separated from the PYGAS mixture by distillation, therefore, eliminating the side product formation with CPD, and the recovery of CPD from the remaining PYGAS mixture by reactive distillation system in a single equipment. In the proposed novel method, industrial scale Aspen Plus simulations show that DCPD can be obtained from PYGAS with a purity of higher than 90%wt in the reactive distillation by monomerization and redimerization of CPD.

CHAPTER 2

LITERATURE REVIEW

The literature review of the process development for the production of dicyclopentadiene (DCPD) from pyrolysis gasoline (PYGAS) is presented by addressing through following aspects;

- Usage areas of CPD and DCPD
- Pyrolysis Gasoline (PYGAS)
- DCPD production from different sources of PYGAS
- Reaction kinetics of reversible DCPD monomerization

2.1 Usage Areas of Dicylopentadiene and Cyclopentadiene

Depending on the purity and application, there are several categories of intermediate or end industrial uses of CPD and DCPD. The purity range for industrial applications are categorized as 65-80% low purity, 80-90% intermediate purity, 90-95% high purity, to 95-100% ultra high purity. Table 2.1 depicts the industrial intermediate or end uses of CPD/DCPD depending on the purity range (Herink et al., 2022), (Cheung, 2000).

DCPD is widely used in hydrocarbon resins as adhesives, tires, coatings, and printing inks. Hydrocarbon resins can be produced by the oligomerization reaction of DCPD and other co-dimers of DCPD such as CPD-isoprene, CPD-methyl cyclopentadiene, or CPD-piperylene (Herink et al.,2022).

CPD can also form organic metallic complexes that can be used as polymerization catalysts (Cheung, 2000), (Monson,1971).

Polyester resins that are based on DCPD are reported to show an improved character to those that are based on phthalic anhydride as far as the low cost and the less styrene emission are concerned since DCPD-based polyester resins need less styrene during production. Furthermore, due to its lower viscosity, DCPD-based resins tend to cooperate well with even low-cost fillers, making the resin easier to shape and preferable for marine and automotive applications where the aesthetics are concerned (Herink et al., 2022), (Cheung, 2000). Currently, unsaturated polyester resin (UPR) production dominates the DCPD market globally (Perrot et al., 2023).

Table 2.1: Areas of usage for CPD/DCPD with different purity ranges (Herink et al., 2022), (Cheung, 2000)

DCPD Purity	Low Purity (65-80%)	Intermediate Purity (80-90%)	High Purity (90-95%)	Ultra High Purity (95-100%)
Industrial Application	Hydrocarbon Resins	Unsaturated Polyester Resins	Co-Polymers	Speciality Chemicals
	• Adhesives • Tires • Diapers and sanitary pads • Coatings	• Boat constituents • Jet skis • Automotive Industry • Safety Helmets • Tubs	• EPDM • ENB • COC • Optics • Automotive Industry	• Poly-DCPD • High Energy Fuels • RIM Applications • Electronics • Automotive Industry

DCPD and other CPD derivatives such as ethylidene norbornene (ENB) are used in Ethylene-propylene-diene monomer (EPDM) rubber production for the automotive

industry where diene character brings flexibility to the polymer by crosslinking. DCPD and CPD derivatives are also preferred chemicals for cyclic olefin copolymer (COC) applications. Having excellent properties in optics such as transparency, low density, chemical resistance, and low double refraction, DCPD and CPD derivative based COC's are utilized in optical disks, optical lenses, or high performance films. Speciality goods that require molding techniques such as bumpers and body panels of vehicles or golf carts use the DCPD polymerization end product, poly dicyclopentadiene (poly-DCPD). Due to its rapid polymerization reaction in the presence of a catalyst, DCPD and poly-DCPD are reported to be used in reaction injection molding applications as well (Cheung, 2000). Due to crosslinking within the structure, Poly-DCPD shows higher strength at both high and low temperatures. (Cuthbert, Li & Wulff, 2019). In fact, poly-DCPD shows excellent cryogenic properties where it can be used as a matrix component for fiber reinforced composites (FRC) in cryogenic applications (Toplosky & Walsh, 2006). Although the required DCPD purity to produce poly-DCPD is ultra high, the production route from low purity DCPD is also investigated (Gumerov, Yurasov, Shafigullin, Romanov, Romanova, Shafigullina & Sokolova, 2018).

Chlorinated cyclopentadiene derivatives are used as raw material for the production of pesticides such as aldrin and chlorodane. Chlorinated cyclopentadiene derivatives are also used in constructional flame retardants such as showers, panels, and lavatories for unsaturated polyester resins (Cheung, 2000). Due to polarity, hydrophobicity, low moisture absorption, and relatively low cost of DCPD, it is widely preferred in low dielectric polymers without comprising the thermal properties. Therefore DCPD derivatives show good flame retardancy to be used in electronics (Hwang, Lin, & Wang, 2008).

Another application of CPD and DCPD is in value-added chemicals such as pharmaceuticals and perfumery (Herink et al.,2022).

DCPD can be utilized as an additive to diesel fuels to enhance properties. The addition of the DCPD to diesel fuels can reduce pollution by decreasing particulate

emissions of CO, NO_x, SO_x, and other volatile organic compounds (VOC) that may cause cancer, cardiovascular problems, or global warming. Therefore, DCPD is a cheaper alternative to diesel particulate filters and also contributes to the cetane number of diesel fuels (Alrefaai, Guerrero Peña, Raj, Stephen, Anjana, & Dindi, 2018).

Due to their high density and strain energy, polycyclic hydrocarbons are good candidates for high energy fuels. Tricyclopentadiene (TCPD), a trimer of CPD, can be used as a liquid high energy density fuel precursor for this purpose (Zhang, Jiang, Xiong, Zou, Wang, & Mi, 2008), (Park, Kim, Yim, Han, Kwon, Park & Jeon, 2016), (Li, Zou, Zhang, Wang & Mi, 2010). TCPD can be selectively synthesized by stopping Dies Alder oligomerization at a certain time when the end products are higher oligomers (Shan & Mei, 2013). High energy density fuels such as RJ-4, RJ-5, RJ-,6 and RJ-7 are obtained from hydrogenated end products of CPD, DCPD, or TCPD and utilized in racing cars, jets, or missiles by having more propulsive energy when compared with conventional kerosene (Cheung, 2000), (Zhang et al., 2008), (Chung, Chen, Kremer, Boulton & Burdette, 1999). The most targeted among these is currently exo-tetrahydrodicyclopentadiene (exo-THDCPD) which is the primary constituent of JP-10 jet propellant with high propulsion abilities (Khan, Ali, Chodimella, Farooqui, Anand & Sinha, 2021). DCPD itself can also be used as aircraft fuel, however, due to its high viscosity injection problems may occur in the spray nozzle. Therefore, adding viscosity-lowering agents are suggested to DCPD to overcome injection problems by decreasing the viscosity (Touazi, Didaoui, Khimeche & Benziane, 2020).

CPD can be further hydrogenated to cyclopentane to be utilized in the production of polypentenamer in the rubber industry and COC's (Krupka, Pasek, Fila, Patera & Severa, 2005).

DCPD is also used for the applications of self healing polymers and composites where DCPD is added to the micro capsulated systems as a repair agent with suspended catalysts. In case of a crack in a self healing material, DCPD is released

from the microcapsules, and healing of the cracked surface is ensured by the ring opening metathesis polymerization (ROMP) over the surface (Sottos, White, & Bond, 2007) (Sharma, Pandey, Shukla & Pandey, 2018). Encapsulation of the DCPD can be achieved by using polyurea-formaldehyde (Mauldin, Rule, Sottos, White & Moore, 2007).

Along with DCPD, other CPD derivates can also be used in microcapsule systems as healing agents. Self healing polymers and composites based on DCPD and CPD derivatives are attracting growing interest in the military, aerospace, and marine applications regarding low material and maintenance costs (Vintila, Iovu, Alcea, Cucuruz, Mandoc & Vasile, 2020).

DCPD is also used in additive manufacturing as a poly-DCPD, a thermoset. Three-dimensional (3D) printing ink can contain DCPD, a polymerization catalyst such as Grubbs's ruthenium catalyst where 3D printed ink polymerized to form crosslinked poly-DCPD in a fast manner. 3D printing applications are desirable in the medical, aerospace, and robotics industry as far as the simplification of the manufacturing process, low cost, and flexibility are concerned (Wang, Zhang, Pei, Qiu & Wang, 2020).

DCPD occurs in endo and exo isomers. Depending on the application DCPD can be selectively produced. The 3D orientation of endo and exo isomers of DCPD are depicted in Figure 2.1.

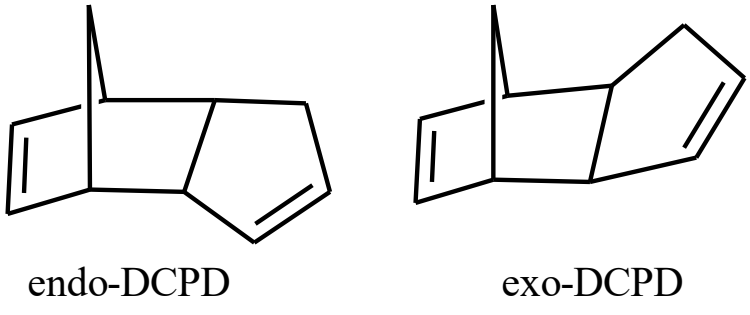


Figure 2.1: Structures of endo-DCPD and exo-DCPD

Endo-DCPD is majorly formed when the temperature of the dimerization reaction of CPD is below 150°C, however, at higher temperatures the major isomer is exo-DCPD (Szekeres et al., 1977). Although the exo-DCPD is considered to be a more thermally stable isomer, the endo isomer is kinetically favored. In fact, endo-DCPD monomerization to CPD starts around 140°C, while exo isomer is stated to remain unreacted even at 170°C. Therefore, the C5 fraction of pyrolysis gasoline (PYGAS) or commercially available DCPD contains majorly endo isomer. Thermal dimerization of CPD favors the formation of endo-DCPD with the amounts of 99.5% endo and 0.5% exo isomer respectively. Photochemical dimerization, on the other hand, allows the formation of an equimolar mixture of endo and exo isomers (Jamróz, Gałka & Dobrowolski, 2003), (Han, Zou, Zhang, Wang & Wang, 2009), (Zou, Xu, Zhang & Wang, 2012), (Herndon, Grayson & Manion,1967). Exo isomer is claimed to have better characteristics when compared to endo isomer for polymers and jet fuels in terms of rigidity, polymerization speed, and having better low temperature performance respectively (Zhang, Jiang, Jiang, Zou, Wang, & Mi, 2007), (Sottos et al., 2007). Self healing polymers that use exo-DPCD able to reach 20 times faster healing rate when compared to endo isomers where fast healing rates are preferred (Mauldin et al., 2007). Therefore the production of exo-DCPD is also an important target for the industry (Zhang et al., 2007), (Sottos et al., 2007). Exo-DCPD can not directly isomerize to endo-DCPD without monomerizing to CPD (Narayan, Wang, Nava Medina, Mannan, Cheng & Wang, 2016). Studies show that, for the isomerization of endo isomer to exo, a monomerization reaction at elevated temperatures and pressures is required where the endo/exo isomer ratio is greatly affected by reaction parameters. During the monomerization reaction, duration is crucial as far as the oligomerization of the CPD is concerned. Therefore, shorter reaction times, high pressures, and milder temperatures are preferred for the exo isomerization with a higher yield (Zhang et al., 2007). However novel studies are present in the literature to isomerize endo isomer to exo isomer. Isomerization of endo-DCPD in the liquid phase over acidic zeolites is proposed for practical applications where the oligomer formation can be eliminated (Han et al., 2009). Due

to either intermediate or end-use areas, high purity dicyclopentadiene production is an important target for the chemical industry.

At or above room temperatures, CPD goes under a spontaneous exothermic dimerization reaction to produce DCPD with heat release of 75 kJ/mol, therefore a production route for CPD also offers a production route for DCPD. In fact, if the heat dissipation due to spontaneous dimerization reaction is not handled properly, runaway reactions may occur within the storing unit such that the build-up pressure may cause explosion hazards. Therefore, CPD is preferred to be handled, transferred, or stored in DCPD form. However, to produce CPD, DCPD should go under a thermal monomerization reaction and should be kept at a temperature below -20°C in order to prevent re-dimerization. DCPD monomerization reaction can undergo in both liquid phase and vapor phase depending on the application (Cheung, 2000), (Claus et al., 2016), (Jamróz et al., 2003).

2.2 Pyrolysis Gasoline

DCPD is primarily produced from pyrolysis gasoline (PYGAS) in industry. PYGAS is a hydrocarbon-rich mixture and mainly produced from steam cracking reactors for the production of ethylene as a side product (Cheung et al., 2000). Depending on the feed and the pyrolysis conditions, the constituents and the composition of the PYGAS may vary. PYGAS can contain unsaturated, saturated, cyclic, olefinic, or aromatic petroleum compounds containing two to eleven or higher carbon containing hydrocarbons (Bondaletov et al., 2015), (Herrera, Murgia, de Hazos & Lubkowitz, 1981). Mixtures that contain numerous types of petroleum derivatives are usually not preferred to separate all the components into their pure forms. Therefore, these hydrocarbon rich petroleum mixtures are distilled or fractionated into their fractions. Fractions or cuts, refer to mixtures that have similar properties such as boiling point (Towler & Sinnot, 2013).

C3 and C4 fractions of the PYGAS are widely processed in the petrochemical industry due to their activity. Butadiene, butene, isobutylene, and mixed butanes can be directly isolated and utilized from the PYGAS mixture. C5 and higher carbon fractions can be directly used as fuels or completely hydrogenated to alkanes. (Kim, Lee, Lim & Seo, 2019). C5 and C9 fractions of PYGAS are generally used in petroleum resins and depending on the composition of these fractions, resin quality can change (Bondaletov et al., 2015), (Rahmatpour & Meymandi, 2021). Dearomatization of the PYGAS is also an important target for the petrochemical industry (Ayuso, Navarro, Moya, Moreno, Palomar, García & Rodríguez, 2022). Benzene, toluene, and xylene fractions are used as raw materials for petrochemical applications and can be obtained by extractive distillation of PYGAS (Abushwireb, Elakrami & Emtir, 2007), (Larriba, Navarro, González, García & Rodríguez, 2015), (Larriba, Navarro, Delgado-Mellado, Stanisci, García & Rodríguez, 2017).

In fact, PYGAS is used as a primary source for the production of benzene and toluene in Western Europe and Asia Pacific due to its low cost. The amount of the PYGAS produced from the steam cracking reactor is proportional to the feed constituents' molecular weight. For instance, naphtha cracking yields more PYGAS when compared to butane cracking per kilogram of ethylene produced. For this reason, PYGAS is not a primary source for the production of C5 olefins or aromatics in the United States of America since lighter feeds such as ethane and propane are generally used for cracking, unlike in Europe or Asia (Wittcoff, Reuben & Plotkin, 2013).

PYGAS can be directly hydrogenated for stabilization to prevent gum formation during storage or downstream processing (Enache, Landon, Lok, Pollington & Stitt, 2005), (Medeiros, Araújo, Gaspar, Silva, & Britto, 2007).

Constituents of the PYGAS mixture have close boiling points and some of which form an azeotrope with each other, therefore separation of the components by common distillation methods can be challenging (Abushwireb et al., 2007).

Table 2.2: Physical and chemical properties of pyrolysis gasoline from SOCAR

Property	*Value*	*Unit*
Density (15°C, under vacuum)	0.8293-0.8692	g/cm^3
API Gravity (15°C/15°C, under vacuum)	31-39	-
Boiling Point		
• First Boiling Point, min.	35	°C
• %10 Fraction, min.	57	°C
• %50 Fraction, min.	88	°C
• %90 Fraction, min.	152	°C
• Last Boiling Point, min	180	°C
Boiling Point Range	45-340	°C
Flash Point Range	-20.5-35	°C
Vapor Pressure (at 20 °C)	21.33-249.69	hPa
Dynamic Viscosity (at 20 °C)	0.59-0.95	mPa.s
Dynamic Viscosity (at 40 °C)	0.47-0.73	mPa.s
Solubility in Water	0.035-0.16	g/L
Surface Tension	70.2-72	mN/m
Autoignition Temperature	401-502	°C
Gum Content, max.	60	mg/100mL

PYGAS can be obtained as a side product in the ethylene production unit from SOCAR in Turkey. Non-aromatic compounds, dienes, benzene, toluene, ethyl-benzene, xylene, styrene C9, and heavier compounds are stated to be present in the PYGAS mixture. PYGAS mixture from SOCAR is liquid at room temperature and has a straw yellow color. The physical and chemical properties of the PYGAS mixture obtained from SOCAR are given in Table 2.2. (SOCAR, 2019), (SOCAR, 2020).

2.3 Production of DCPD from PYGAS

Generally, DCPD is produced from PYGAS with CPD/DCPD content of 15% to 25% by weight in the chemical industry. Depending on the storage CPD and DCPD content of PYGAS may vary. As CPD spontaneously dimerizes to DCPD by the reaction shown in Figure 2.2, major portion of the CPD in the PYGAS is in the form of DCPD if the PYGAS is stored.

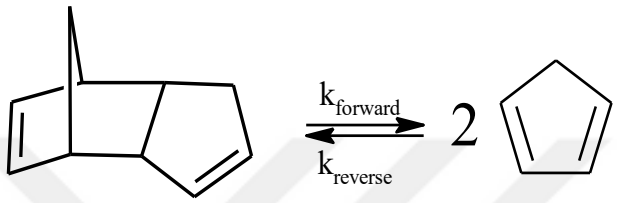


Figure 2.2: Reversible monomerization reaction of DCPD

Stored PYGAS mixture is processed in dimerization reactor where the remaining fraction of the CPD converts to DCPD. Depending on the storage of the used PYGAS, the first dimerization reactor can be bypassed if all CPD content was dimerized to DCPD. Then DCPD enrichened PYGAS is sent to sequential distillation columns where C5 to C11 fractions are separated to form crude DCPD (Claus et al., 2016), (Cheung, 2000). Crude DCPD can also be obtained by the dimerization of CPD in the C5 fraction and the distillation of DCPD from the C5 mixture (Li, Shen & Ling, 2013). Typical DCPD content in the crude DCPD varies from 87%wt to 90%wt (Li et al., 2013), (Cai, Shen, Liu, Xin & Ling, 2009). Crude DCPD mixture can be subjected to subsequent monomerization and dimerization reactions in controlled conditions to increase purity (Claus et al., 2016). The need for the additional monomerization-dimerization of DCPD results from the CPD loss due to side products of co-dimers in the first dimerization reactor. These side products can be CPD+1,3 butadiene, CPD+1,3 pentadiene, CPD+ isoprene, CPD+1-pentene, CPD+methyl butene (Cao, Liu, Zhang, Shi, Song & Yao, 2015), (Xu, Jocz, Wiest, Sarngadharan, Milina, Coleman, Iaccino, Pollet, Sievers & Liotta, 2019), (Krupka & Kolena, 2012). Yet another side product of co-dimer is methyl

dicyclopentadiene. Methyl dicyclopentadiene (Met-DCPD) is also a potentially valuable compound of PYGAS. Met-DCPD can be used as additive in unsaturated polyester resins to increase the quality of polyester grade DCPD (Perrot, Hyršl, Bandžuch, Waňousová, Hájek, Jenčík & Herink, 2021). Due to its low cost, Met-DCPD and derivatives can also be used in epoxy resins, rubbers, adhesives, or varnishes. Met-DCPD can be utilized from low purity DCPD or separately in technical grade. Met-DCPD has many isomers where the methyl group is attached to 2, 3, 4, 5, or 7 positions and isomerization kinetics are present in the literature (Krupka, 2011). Met-DCPD also goes under Dies Alder reactions to produce cyclopentadiene (CPD), methyl cyclopentadiene (Met-CPD), or dimethyl cyclopentadiene (DMet-CPD) therefore Met-DCPD is also a potential source for CPD from monomerization reaction. Met-DCPD kinetic study is also an important target to develop a model for reaction mediums involving Met-DCPD as well. Kinetic parameters for the reversible co-dimerization reaction of Met-CPD is given as $3.7x10^6$ $(L/mol)s^{-1}$ for k_0 and 71.6 kJ/mol for E_a. Activation energy for the reversible co-dimerization reaction of Met-CPD with CPD is close to CPD dimerization reaction activation energy value (Krupka, 2010).

Separation of CPD from PYGAS directly by distillation can be challenging as CPD forms an azeotrope with other five-carbon PYGAS constituents such as n-Pentane, 2-Methyl-2-butene, and cis-2-Pentene. Therefore extractive distillation methods followed by monomerization and re-dimerization of DCPD can be applied to produce high purity DCPD (Cheung, 2000), (Miki, 2019). To separate CPD from other close boiling point or azeotropic compounds in C5 fraction, usually acetonitrile, dimethyl formamide, and N-methyl-2-pyrrolidone are selected as solvent for extractive distillation (Hsu, Wang, Ou, & Wong, 2015). DCPD can also be produced by the separated C5 fraction of PYGAS. Subsequent monomerization and dimerization reactions can be employed to further increase the DCPD purity (Nurullina, Solov'eva, Liakumovich & Samuilov, 2001)

2.3.1 Production of DCPD from C5 fraction of PYGAS

The typical C5 fraction composition of used PYGAS is given in Table 2.3 (Nurullina et al., 2001). High purity target for DCPD from C5 fraction of PYGAS can not be achieved by conventional separation methods directly, because of the azeotrope formations with CPD and other C5 constituents of PYGAS as mentioned in earlier sections (Cheung, 2000), (Miki, 2019).

Table 2.3: C5 fraction composition of used PYGAS (Nurullina et al., 2001)

Compound Name	*wt %*
1,4 Pentadiene	1.3
Isopentane	12.9
n-Pentane	24.8
1-Pentene	4.1
2-Methyl-1-butene	8.7
2-Pentene (cis and trans)	6.1
2-Methyl-2-butene	1.9
Piperylene (cis and trans)	11.9
Isoprene	12.6
Cyclopentadiene	13.1
Cyclopentene	2.5

Therefore, dimerization of CPD in C5 fraction to DCPD, and separation of DCPD from C5 fraction by boiling point difference are proposed as DCPD has higher boiling point when compared to other C5 fraction constituents. However, co-dimers of isoprene and piperylene from reversible reactions are also formed during the dimerization reaction. The resulting mixture from the dimerization reaction and separation is called crude DCPD, where co-dimers of isoprene and piperylene along with DCPD are present as impurities. The crude DCPD mixture is then subjected to monomerization where CPD is majorly produced as the co-dimers are more stable than DCPD. Then the monomerization and re-dimerization stages followed by

distillation can continue until the desired purity of DCPD is achieved (Nurullina et al., 2001). Monomerization and re-dimerization steps are depicted in Figure 2.3.

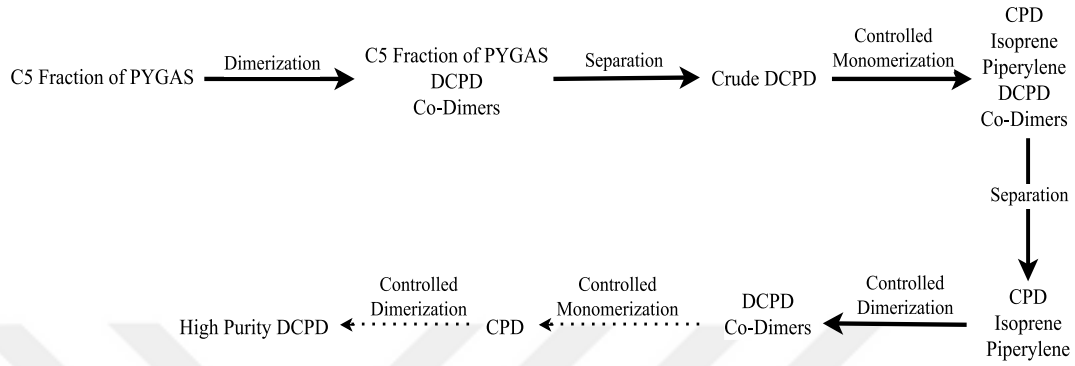


Figure 2.3: DCDP production route from C5 fraction of PYGAS (Nurullina et al., 2001)

The rate of reaction of DCPD is higher than co-dimers and the rate of reaction of co-dimerization with isoprene is higher than that of piperylene making the isoprene-CPD dimer a major impurity. Co-dimer impurities increase with reaction temperature, reaction time, and CPD conversion for dimerization. Therefore the reactions should not go to completion. The dimerization reaction of CPD becomes limited as the reaction proceeds. The decrease in the CPD concentration in the medium leads to the reaction rate of piperylene and isoprene being higher as the CPD dimerization reaction is second order with respect to CPD. According to the experiments conducted, co-dimer impurities, are affected by dimerization temperature, dimerization time, and the conversion of CPD to DCPD during controlled dimerization. For optimum DCPD yield in dimerization, temperature should be selected as 50°C and the reaction time should be selected as 110 hours. For the monomerization step, decrease in the the side products with monomerization temperature is observed due to reaction kinetics of the co-dimers. Therefore for optimum DCPD monomerization, reaction temperature should be 160°C to 200°C. Then, the re-dimerization step can be performed around 50°C for 14 to 18 hours. To remove the C5 fraction, distillation is performed and the product DCPD purity of

99.5% to 99.9% can be achieved. As a last step, high-boiling point inert solvent (heptadecane) and a radical scavenger (hydroquinone) are added to inhibit polymerization (Nurullina et al., 2001).

Kim, et al. (2019) suggest an alternative route for the production of DCPD from the C5 fraction of PYGAS. This process is proposed as an alternative to the conventional route which involves a series of distillation steps requiring high energy consumption along with expensive equipment. Furthermore, oligomers such as CPD trimer (TCPD) may be formed around the reboiler due high temperatures. In order to overcome the oligomer formation issues, the reboiler temperature should be decreased as the pressure, making the column size increase. Therefore, an alternative operation strategy to produce DCPD is suggested. As an alternative to conventional serial distillation operations, membrane separation is proposed. It is aimed to reduce the energy consumption and the impurities in the mixture by using 1,1,3,3-tetraethoxy1,3-dimethyl disiloxane (TEDMDS)/silica composite membrane. By starting the C5 fraction of PYGAS, all CPD content in C5 is dimerized and separated from lower boiling compounds by distillation. The crude DCPD mixture is then monomerized and dimerized for further purification steps. The effluent of the second dimerization reactor can be separated by a membrane. CPD and other C5 molecules being permeated under pervaporation conditions and the DCPD being a retentate over the TEDMDS membrane, ultra-high purity (98 %) of DCPD can be achieved. A comparison of the conventional method and the membrane separation is given in Figure 2.4.

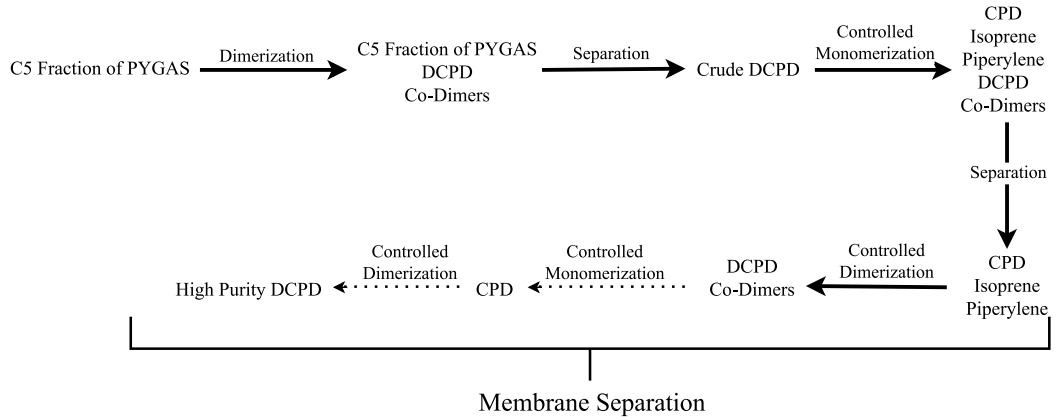


Figure 2.4: Alternative DCDP production route from C5 fraction of PYGAS (Kim, et al., 2019)

Hsu, Wang, Ou, and Wong (2015) also pointed out the problems regarding the high energy consumption, capital cost, and handling issues of sequential distillation and reactor systems to obtain high purity DCPD and other valuable hydrocarbons such as isoprene or pentadiene. In fact, energy consumption for distillation processes covers %3 of global energy consumption. Therefore, there is a need for process intensification and simplification for DCPD production. Although there are various strategies to produce high purity DCPD in industry, the common DCPD production route includes dimerization, monomerization, and separation steps as mentioned in earlier sections. The number of dimerization and monomerization units depends on the target DCPD purity. Other than thermal monomerization, acid-catalyzed monomerization can also be used for monomerization of DCPD. Simulations are performed for the separation of the C5 fraction of PYGAS in Aspen Plus. For vapor-liquid equilibrium relations, NRTL model is used and the model is stated to be in compliance with experimental data for relative volatilities. Reaction information is also provided for the simulations which are in agreement with reaction experiments. Although the optimum selectivity for DCPD formation could be achieved at 40°C, the reaction is slow due to the low temperature. If the reaction temperature exceeds 110 °C then the side product formation with isoprene and pentadiene increases. Therefore, the optimum temperature for the dimerization reaction of CPD is suggested as 75-110°C (Hsu et al., 2015). In the suggested simplified process by

Hsu, Wang, Ou, and Wong (2017), the number of reactors and columns is decreased by separating the CPD from the C5 fraction before the dimerization reaction by extractive distillation. The simplified process consists of a reactor and six distillation columns. In this way, 98.84% pure DCPD can be obtained by reducing the capital cost by decreasing the equipment cost. Moreover, external heat integration and thermal coupling can also be applied to the process to further reduce energy consumption (Hsu et al., 2017).

In addition to extractive distillation, reactive distillation can also be adapted to C5 fraction separation (Guo, Wang, Li & Wang, 2017). Reactive distillation systems allow reaction and separation to occur simultaneously in the same equipment. Reactive distillation systems are preferred in industry to overcome the equilibrium restriction by removing the product from the reaction medium. Moreover, equipment costs are reduced as the same equipment is used for reaction and distillation (Towler & Sinnot, 2013).

Without using a dimerization reactor, the C5 fraction of PYGAS can be used as a direct feedstock for reactive distillation system where 5 carbon molecules such as pentadiene or isoprene can be drawn out as distillate and DCPD is obtained as bottom stream where the CPD dimerizes to DCPD within the column. In fact, due to its high dimerization affinity, CPD is readily converted to DCPD within the column and it is reported that the dimerization is largely completed in the feed plate (Guo et al., 2017). As CPD content decreases within the column due to dimerization, co-dimer formation gets limited. Temperature, number of stages, and operation time should be determined carefully in order to have sufficient DCPD yield with minimal co-dimer formation. For instance, at temperatures above 100°C, isoprene loss due to co-dimer impurities increases to 10% and CPD conversion to DCPD increases with the number of stages (Wang, 2014), (Guo, Wang, Li & Wang, 2016), (Guo et al., 2017). In order to sustain the separation of the C5 fraction, the addition of the liquid hold-up areas within the packed column is suggested to increase the residence time of liquid phase, therefore, increase the CPD conversion. It is observed that the conversion of CPD to DCPD increases as the number of the liquid holdup regions, operating pressure,

and residence time increase with a trade off in the increase in conversion of the co-dimer. However, higher reflux ratios allow higher conversions of CPD with higher selectivities. The reactive distillation column for the C5 separation could be operated in a temperature and pressure range of 50°C-90°C and 2.3-2.6 bar, under the reflux ratio of 8-12 at the cost of high utility consumption and the risk of flooding to achieve desired conversion and selectivity for DCPD (Guo et al., 2017).

Large scale production of DCPD in the purity range of 80% or 93 to 95% with methyl dicyclopentadiene (Met-DCPD) as a major impurity, is investigated by Herink et al. (2022). Light pyrolysis gasoline (LPYGAS) mainly contains C5 and C6 and used as feedstock for the DCPD production. The separation process consists of a reactor (R1) and four serial distillation columns (DC1, DC2, DC3, DC4) and the process flow is given in Figure 2.5.

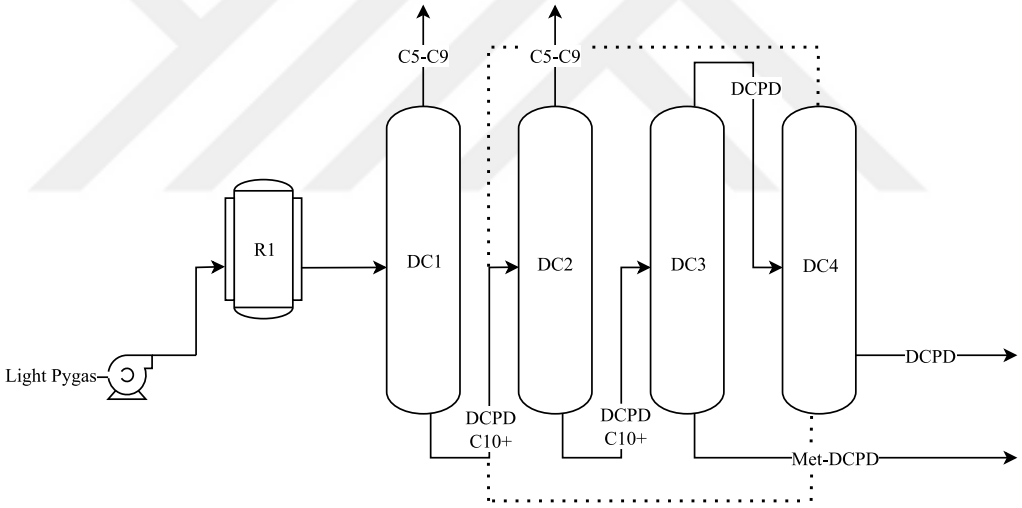


Figure 2.5: Production route for DCPD from Light PYGAS (Herink et al., 2022)

In this process, CPD in the LPYGAS is dimerized to DCPD in the reactor (R1). Then the reactor outlet stream is fractionated in the distillation column sequence in order to separate the C5-C9 fractions as distillate in columns DC1 and DC2 while the bottoms product of DC2 contains heavier compounds and DCPD having the purity of 50-70%. Then the DCPD is further purified in DC3 and DC4 till the desired purity

of the DCPD is achieved. One advantage of the process is that the distillation sequience allows the isolation of co-dimer Met-DCPD (Herink et al., 2022).

2.3.2 Production of DCPD from Crude DCPD

Li, Shen and Ling (2013), studied the production of CPD from crude DCPD mixture. Typical crude DCPD composition used in the study is given in Table 2.4.

Table 2.4: Typical composition of used crude DCPD (Li et al., 2013)

Compound Name	*wt %*
Cyclopentadiene	0.1
Norbornene (Co-Dimer with Isoprene)	6.4
Dicyclopentadiene	89.9
Other Impurities	3.6

High purity CPD production is achieved by the monomerization reaction of DCPD. The monomerization reaction of the DCPD is an endothermic and reversible reaction therefore, CPD should be removed from the reaction system in order to shift the reaction towards the product's side and higher temperatures and lower pressures should be preferred for higher equilibrium conversions. Monomerization of DPCD can be conducted in both liquid and gas phases. Liquid phase monomerizations are limited in flow rates to reduce the concentration of DCPD that may lead to coke deposition. Coke deposition taking place under the high temperatures, long reaction times and high concentrations of reactants in reactor causes serious heat transfer problems and increases the maintenance cost (Li et al., 2013). On the other hand high monomerization rates could be achieved in gas phase monomerization of DCPD which enables high conversion rates. Therefore, gas phase monomerization is more adventageous for large scale production and coke formation problem can be eliminated by using inert diluents (Cai, Shen, Xin, Liu, & Ling 2011). Li, Shen and Ling (2013) also states that adding inert diluents not only decreases the coke

formation but also increases the cracking efficiency. If the water or steam are used as the diluents, the DCPD and other heavy compounds can easily be separated from the mixture as bottoms products since the water forms an azeotrope with DCPD. However, H_2 can be used as a diluent to overcome coking issues for its reusable and separable character. Gas phase monomerization experiments are conducted at 0.12 MPa with different flow rates, H_2 to DCPD ratios, and temperatures. It is stated that the increase in the reaction temperature increases both conversion and yield of DCPD. The maximum DCPD conversion is reported at 320°C as 97%. However, when that temperature exceeds 340°C, a decrease in both conversion and yield is observed due to coke formation. It is also observed that the flow rates should not be too high, and reaction rate requires longer residence times than four seconds to obtain appreciable conversion. Similarly, H_2 to DCPD ratios should be adjusted between 30 and 50 in order to achieve sufficient space time in the reactor. It is reported that, under 320 °C reaction temperature and H_2 to DCPD ratio of 50, reaction could be carried out without observing coke formation. The monomerized CPD is purified by batch distillation under atmospheric pressure by purging nitrogen into the system for the removal of air and prevent oxidation reactions. Batch distillation was performed initially at total reflux until the steady state is reached and constant reflux ratios are applied (Li et al., 2013).

The reactive distillation method was also studied for the production of CPD with liquid phase monomerization of Crude DCPD mixture by Cai, Shen, Liu, Xin and Ling (2009). Liquid phase monomerization is closely investigated where hydrocarbons with high boiling point as solvents are used for dilution. Although the reaction temperatures applied are relatively lower than gas phase monomerization (200°C to 300 °C), lower CPD yield is reported because of the formation of undesired oligomers which may also cause problems such as clogging in the reactor. Therefore, a reactive distillation system is offered rather than the series of reaction-distillation steps which is helpful for shifting equilibrium to product side, reduction in plant cost, and improved selectivity. DCPD monomerization with an autoclave reactor and reactive distillation with continuous column experimental studies are

conducted. CPD and DCPD concentration also directly affects the oligomerization of CPD and DCPD therefore high boiling point diluent such as dodecane is added to the system. In addition to the diluents, oligomerization inhibitors such as o-nitrophenol, and para-tert-butylcatechol can also be added to the system. Also, the oligomerization rate is reported to be more sensitive to CPD concentration than that of DCPD concentration. Therefore removing the CPD from the mixture supresses the oligomer formation within the system. By reactive distillation, DCPD is forced to monomerize rather than oligomerize with CPD as CPD is continuously removed from the reaction medium. Reactive distillation system parameters applied in the study of Cai, Shen, Liu, Xin and Ling (2009) are summarized in Table 2.5 which yields 90% CPD with 98 wt % purity.

Table 2.5: System parameters for the reactive distillation system (Cai et al., 2009)

Parameter	*Value*
Tray Number	15
Feed Location	11
Tray Diameter	*30 mm*
Tray Spacing	*40 mm*
Liquid Holdup for Each Tray	*1.4 mL*
Distillate Heat Transfer	Ice Bath
Reboiler Heat Transfer	*Electric Heater (175^{o}C)*
Reflux Ratio	*4*
Pressure	*Atmospheric*
Operation Time	*1 h*

The feedstok, operating conditions and the performances of the DCPD production routes presented above are summarized in Table 2.6.

Table 2.6: Summary table for production routes of CPD/DCPD

Source Used	*Initial CPD/DCPD Content*	*Method*	*CPD/DCPD Purity*
C5 fraction of PYGAS (Nurulinna et al.,2001)	13.1 % CPD	Dimerization-Monomerization Followed by Separation Cycle Dimerization Temperature: 50°C Monomerization Temperature: 160-200°C	≥ 99.0 % DCPD
C5 fraction of PYGAS (Kim et al., 2019)	9.0 % DCPD	Membrane Separation Feed Temperature: 50-70°C	≥ 98.0 % DCPD

Table 2.6 (continued)

Source Used	*Initial CPD/DCPD Content*	*Method*	*CPD/DCPD Purity*
C5 fraction of PYGAS (Hsu et al., 2015)	NA	Simplified Reaction- Extractive Distillation Complex Dimerization Temperature: 75-110°C	≥ 98.0 % DCPD
C5 fraction of PYGAS (Guo et al., 2017)	16.97 % CPD and 2.17 % DCPD	Reactive Distillation to Dimerize CPD Column Temperature: 50-90°C Column Pressure: 2.3-2.6 bar	NA

Table 2.6 (continued)

Source Used	*Initial CPD/DCPD Content*	*Method*	*CPD/DCPD Purity*
Light PYGAS (Herink et al., 2022)	NA	Reactor and Distillation Complex	80.0 % or 93.0–95.0% DCPD
Crude DCPD (Li et al., 2013)	89.9% DCPD	Gas Phase Monomerization to CPD Monomerization Temperature: 320°C H_2 to DCPD ratio: 50	99.3% CPD

Table 2.6 (continued)

Source Used	*Initial CPD/DCPD Content*	*Method*	*CPD/DCPD Purity*
Crude DCPD (Cai et al., 2011)	89.2% DCPD	Gas Phase Monomerization to CPD Monomerization Temperature: 320°C H_2 to DCPD ratio: 50	NA
Crude DCPD (Cai et al., 2009)	87.0% DCPD	Liquid Phase Reactive Distillation to Monomerize DCPD Reboiler Temperature: 175°C Column Pressure: Atmospheric	98.0 % CPD

2.4 Kinetic Studies for Monomerization and Dimerization Reaction of DCPD

Kinetic parameters for thermal dimerization of CPD, monomerization of DCPD, and side reactions with co-dimers and oligomers are thoroughly investigated over the years in literature. Kinetic studies for the reversible monomerization and dimerization reactions of DCPD (Figure 2.2) are summarized in Table 2.7 and Table 2.8, respectively. Kinetic parameters of the reactions are categorized according to the temperature range, reaction medium, and the DCPD isomer that is used. Although the type of DCPD isomer is not specified in some studies, it is extracted from the context by considering the fact that endo-DCPD formation reaction has lower activation energy than that of exo-DCPD. The type of solvent in the reaction medium is stated not to have a significant effect on the kinetic parameters. (Krupka, 2010). Monomerization of both endo and exo-DCPD take place by first order reaction, and dimerization follows second order kinetics.

Table 2.7: Kinetic parameters for the reversible monomerization reaction of DCPD

Source	*DCPD Isomer*	*k_0 forward s^{-1}*	*E_a forward (kJ/mol)*	*Temperature Range (^oC)*	*Reaction Medium*
Herndon, Grayson & Manion, 1967	endo-DCPD	$1.1x10^{13}$	142.1	150-210	DCPD in Gas Phase, Flow Reactor Under Nitrogen
Herndon, Grayson & Manion, 1967	exo-DCPD	$5.3x10^{13}$	161.0	200-350	DCPD in Gas Phase, Flow Reactor Under Nitrogen
Griffith, Chu & Langer, 1987	endo-DCPD	$4.0x10^{14}$	157.7	190-210	DCPD in Gas Phase, Multi Column GC Reactor
Langer and Patton, 1972	endo-DCPD	$5.0x10^{14}$	156.1	180-200	DCPD in Gas Phase, in Versamid 900 Solvent, GC Column as Reactor
Nurulinna et al., 2001	NA	$2.6x10^{13}$	142.3	NA	C5 Fraction of PYGAS
Guo et al., 2017	NA	$5.7x10^{12}$	142.0	50-100	C5 Fraction of PYGAS, Vapor-Liquid Medium, Autoclave Reactor

Table 2.7 (continued)

Source	*DCPD Isomer*	*k_0 forward s^{-1}*	*E_a forward (kJ/mol)*	*Temperature Range (^oC)*	*Reaction Medium*
Yao, Xu, Dong, Liu, Yuan, Wang, Cao& Luo, 2020	endo-DCPD	$3.0x10^{13}$	131.0	180-240	DCPD with Toluene in Microreactor
Yao, Xu, Dong, Liu, Yuan, Wang, Cao& Luo, 2020	exo-DCPD	$1.4x10^{14}$	157.0	180-240	DCPD with Toluene in Microreactor
Xu et al., 2019	endo-DCPD	$1.2x10^{15}$	157.2	80-160	C5 fraction with Toluene, Liquid Phase
Cai et al., 2011	NA	$2.8x10^{7}$	77.6	280-330	Crude DCPD, Gas Phase Reaction, Flow Reactor

Table 2.7 (continued)

Source	*DCPD Isomer*	*k_0 forward s^{-1}*	*E_a forward (kJ/mol)*	*Temperature Range (^oC)*	*Reaction Medium*
Palmová, Kosek, Schöngut, Marek& Štěpánek, 2001	NA	$5.3x10^{10}$	161.0	*150-220*	DCPD, Reactor with Overhead Condenser, Vapor-Liquid Medium, Gas Phase Reaction

Table 2.8: Kinetic parameters for the reversible dimerization reaction of CPD

Source	*DCPD Isomer*	*k_0 reverse* *$(L/mol)s^{-1}$*	*E_a reverse* *(kJ/mol)*	*Temperature Range* *(^oC)*	*Reaction Medium*
Szekeres et al., 1977	NA	$1.9x10^6$	68.6	60-120	C5 Fraction of PYGAS, Steel Vessel
Guo et al., 2017	NA	$4.4x10^5$	65.8	50-100	C5 Fraction of PYGAS, Vapor-Liquid Medium, Autoclave Reactor
Nurulinna et al., 2001	NA	$1.2x10^6$	68.6	NA	C5 Fraction of PYGAS
Yao et al., 2020	endo-DCPD	$5.3x10^6$	62.0	180-240	DCPD with Toluene in Microreactor
Yao et al., 2020	exo-DCPD	$4.1x10^6$	69.0	180-240	DCPD with Toluene in Microreactor
Palmová et al., 2001	NA	$1.9x10^7$	75.0	150-220	DCPD, Reactor with Overhead Condenser, Vapor-Liquid Medium, Liquid Phase Reaction
Palmová et al., 2001	NA	$1.2x10^6$	70.0	150-220	DCPD, Reactor with Overhead Condenser, Vapor-Liquid Medium, Gas Phase Reaction
Bělohlav et al., 2000	NA	$3.4\ x10^6$	71.3	30-190	DCPD in Decaline, Vapor-Liquid Medium, Reaction Flask

Table 2.8 (continued)

Source	*DCPD Isomer*	*k_0 reverse (L/mol)s^{-1}*	*E_a reverse (kJ/mol)*	*Temperature Range (^oC)*	*Reaction Medium*
Krupka, 2010 Krupka, Pašek, Lederer & Bílková, 2014	endo-DCPD	$2.7x10^6$	70.6	40-120	CPD, Liquid Phase, with Cyclohexane, Batch Reactor
Krupka, 2010 Krupka, Pašek, Lederer & Bílková, 2014	exo-DCPD	$4.5x10^5$	80.2	40-120	CPD, Liquid Phase, with Cyclohexane, Batch Reactor
Krupka, 2010	endo-DCPD	$3.6x10^6$	71.1	40-120	CPD and Met-DCPD, Liquid Phase, with Cyclohexane, Batch Reactor
Cai et al., 2011	NA	$6.3x10^3$	51.45	280-330	Crude DCPD, Gas Phase Reaction, Flow Reactor

Table 2.8 (continued)

Source	*DCPD Isomer*	*k_0 reverse (L/mol)s^{-1}*	*E_a reverse (kJ/mol)*	*Temperature Range (^oC)*	*Reaction Medium*
Xu et al., 2019	endo-DCPD	$1.4x10^6$	68.8	80-160	C5 fraction with Toluene, Liquid Phase
Xu et al., 2019	exo-DCPD	$8.5x10^5$	82	80-160	C5 fraction with Toluene, Liquid Phase
Kumar and Pawar, 2004*	NA	$3.2x10^{-4}$	7-11	30-40	CPD Dimerization, with %45 $AlCl_3$ in EMIC Ionic Liquid

* Pre-exponential factor and the activation energy are calculated from reaction rate constants at different temperatures: $k_{45\%AlCl3}(30^oC,10^{-6}\ Ms^{-1}) = 2.99$, $k_{45\%AlCl3}(35^oC,10^{-6}\ Ms^{-1}) = 3.27$, $k_{45\%AlCl3}(40^oC,10^{-6}\ Ms^{-1}) = 3.47$

As it is shown in tables 2.7 and 2.8, reaction kinetics data reported in literature were determined in the presence of different reaction mediums. The influence of the solvents on Dies Alder reactions is also well documented in the literature. Different solvent types can have an impact on the reaction rate depending on the dienophile type (Bini, Chiappe, Mestre, Pomelli & Welton, 2008), (Sheehan and Sharratt, 1999), (Zhang et al., 2008). However, the effect of the solvent type on the reaction rate is stated as negligible for reversible CPD dimerization reaction (Krupka, 2010), (Griffith et al., 1987), (Langer and Patton, 1972). Langer and Patton (1972), Griffith et al. (1987) and Herndon et al. (1967) assumes no reverse reaction for the dimerization of DCPD at the given temperature ranges.

CHAPTER 3

EXPERIMENTAL AND SIMULATION METHODS

This chapter presents details regarding the characterization methods, experimental procedures, experimental set-up, and simulation methods in order to produce high purity DCPD (≥ 90%wt) from PYGAS mixture. Characterization methods include composition analysis, thermal behavior analysis, and property estimation of PYGAS. Experimental methods comprise two parts; phase equilibrium and reaction experiments. Simulation studies performed for the digital twin of the prominent experimental studies in Aspen Plus software version V12.1 are also detailed in this chapter.

3.1 Characterization of PYGAS and DCPD

A series of composition analyses were conducted for DCPD (≥ 99%wt, ZET) and PYGAS samples (SOCAR) to correctly identify the constituents and composition along with defining feed streams for the digital twin of the system to be developed. Agilent Technologies GC 7890B and MS 5977E were used for characterization purposes for DCPD and PYGAS. Agilent Technologies HP-5ms capillary GC column was selected due to its low bleed characteristics and inertness. A split liner was used for dilution with a split ratio of 50. The injection volume was kept at 0.2 µL for Automatic Liquid Sampler (ALS). Inlet temperature was kept at 80°C-320°C for PYGAS and 80°C-160°C for DCPD characterization. Column pressure was adjusted as 1.1 bar. The oven temperature was kept at 50°C. Helium gas was used as the carrier gas, while heptane (for gas chromatography ECD and FID SupraSolv®, ≥99.5%, Merck), hexane (for gas chromatography, ≥98%wt, Merck), and toluene (for gas chromatography MS SupraSolv®, ≥99.8%, Merck) were used as dilution

solvents for DCPD and PYGAS samples. Detailed information about GC-MS analyses are provided in Appendix A and Appendix B.

In order to understand the thermal behavior of the DCPD and PYGAS, simultaneous thermal analyses with TGA/DSC-STA were conducted. Netzsch STA 449 F3 JUPITER was used for thermal analysis by using hermetically sealed sample cup (Ti Hermetic Pan). Tests were conducted under a nitrogen atmosphere where the heating rate was selected as 10°C/min, and the gas flow rate as 45 mL/min. Density and viscosity measurements of the PYGAS were carried out in order to check the property change of PYGAS that is stored for a prolonged period. Density measurements were conducted in a liquid pycnometer and the viscosity measurements were carried out by using the Brookfield Viscometer DV2TRV.

3.2 Phase Equilibrium Experimental Studies and Model Prediction

Phase equilibrium experiments were conducted in order to understand the phase equilibrium behavior of the PYGAS mixture, to determine the applicable equation of state, and provide consistent data to be used in process simulations for the production of DCPD from PYGAS in industrial scale.

3.2.1 Phase Equilibrium Experimental Studies

Phase equilibrium experiments were conducted by using Heidolph Rotary Evaporator, Laborota 4003 as a single stage distillation apparatus. PYGAS (SOCAR) and commercial DCPD samples (≥ 99%wt, ZET) were used as feedstock in these experiments. The rotary evaporator operated at temperatures between 20°C-180°C with an accuracy of +/-1 K and had a built-in temperature and vacuum controller which was connected to a vacuum pump and a vacuum trap. The condenser was connected to Huber Minichiller where the temperature of the cooling fluid can be controlled. The experimental setup for phase equilibrium experiments is depicted in Figure 3.1.

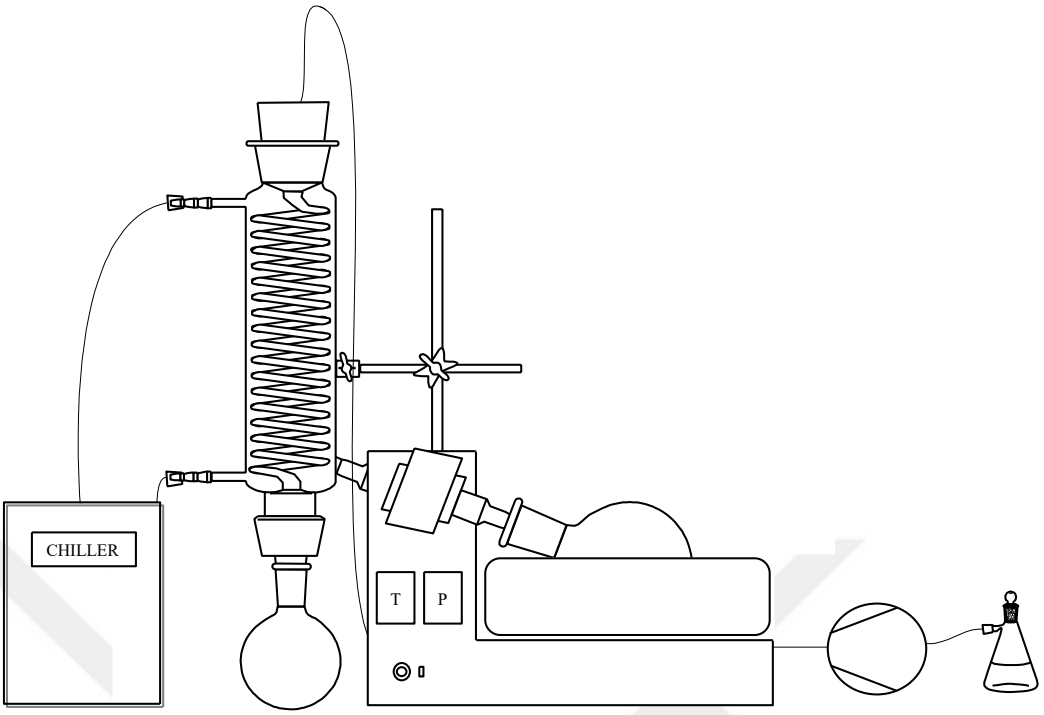


Figure 3.1: Phase equilibrium experimental set-up

A set of vapor-liquid equilibrium experiments for fractionation of the PYGAS in single equilibrium stage were carried out at different temperatures and pressures to explore fractions that can be separated.

Two groups of experiments were conducted. In the first group of experiments original PYGAS sample was separated to various fractions by applying appropriate temperature and pressure. The fraction collected in receiving flask in equilibrium with residual in evaporating (rotary) flask were analyzed by using GC-MS. It was determined that the benzene and lighter hydrocarbons can be removed from the PYGAS mixture at 80°C and 100 mbar at single step to a large extent. The second group of experiments were carried out by successive fractionations to determine the operating conditions and to envise possible fractions that can be obtained in multistage distillation. These experiments were conducted to separate benzene and lighter hydrocarbons, DCPD rich condensate and isolated DCPD as first, second and third step fractionation respectively.

Schematic explanation of the three step phase equilibrium experiments is given in Figure 3.2. Step 1 represents the stage where benzene and lighter hydrocarbons are separated from the PYGAS mixture. In Step 2, the flask of step 1 was filled into the evaporating flask and further distilled to retrieve DCPD in receiving flask (condensate) from the heavy residue. Then at Step 3, it was aimed to further purify the receiving flask (condensate) of Step 2. Set temperature and pressure values for single step experiments such as experiments 1, 2, 3 and multi step experiments such as 8, 9, 10, 14 are given in Table 3.1. During the experiments, an upper limit temperature was determined as 135°C to prevent DCPD monomerization in evaporative flask. The step-by-step procedure for experiment 14 is given in Appendix C.

All samples collected in receiving and evaporating (rotary) flasks were analyzed and composition of fractions were determined. GC-MS method information for characterization are provided in Appendix E.

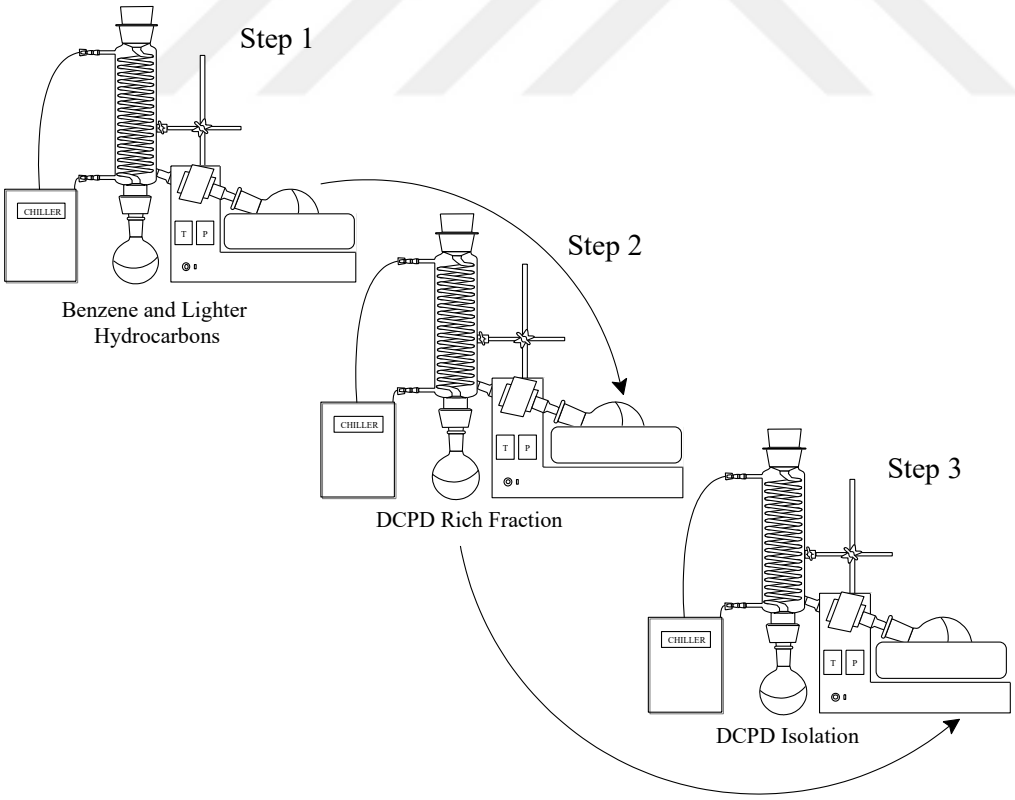


Figure 3.2: Multi step separation of the PYGAS in phase equilibrium experiments

Table 3.1: Phase equilibrium experiment sets

Experiment Number	*Set Temperature(°C)*	*Set Pressure(mbar)*
Experiment 1	*40*	*175*
Experiment 2	*80*	*650*
Experiment 3	*80*	*100*
Experiment 8x*	*80*	*100*
Experiment 8y*	*125*	*100*
Experiment 8z*	*135*	*100*
Experiment 9x*	*80*	*100*
Experiment 9y*	*125*	*100*
Experiment 9z*	*125*	*70*
Experiment 10x*	*80*	*100*
Experiment 10y*	*130*	*150*
Experiment 10z*	*130*	*90*
Experiment 14x*	*80*	*100*
Experiment 14y*	*125*	*100*
Experiment 14z*	*110*	*100*

*x represents the "Benzene and Lighter Hydrocarbons Removal Step (Step 1)", y represents the "DCPD Removal Step from the Heavy Residue (Step 2)" and z represents the "DCPD Isolation Step (Step 3)".

3.2.2 Phase Equilibrium Model Prediction

The quantitative analysis results of fractions obtained in phase equilibrium experiments were simulated in Aspen Plus software version V12.1 to test the compliance of various equation of states. For simplicity, constituents of the PYGAS mixture were grouped as representative mixture containing Light Hydrocarbons,

Benzene, Toluene, DCPD, and Methyl-DCPD. For property estimation methods, Braun K-10 (BK-10) by being suitable for vacuum applications for petroleum compounds, and Peng Robinson by being a better fit for the determination of thermodynamic properties for petrochemical compounds, were selected.

For digital twin of the experiments, BatchSep equipment in the Batch Models module was used. The physical dimensions of the rotary evaporator system used in experiments were compiled into Aspen Plus software version V12.1. The number of stages was selected as 2 comprising only the pot and condenser for the accurate modeling of the single-stage distillation with a reflux ratio of 0. The medium temperature was specified as the set temperature of the heating bath and the pressure was specified as the set pressure of the vacuum controller system. Condenser temperature was determined according to the temperature of the chiller that was connected to the rotary evaporator's condenser. The initial condition was selected as "Initial Charge" where the starting amount of PYGAS in the evaporating flask was specified. Condenser pressure was specified as 100 mbar as an operating step for batch operating simulation.

3.3 Monomerization Reaction Kinetics and Model Prediction

Monomerization kinetics of DCPD to CPD was studied to determine the reaction rate expression and reaction equilibrium. The reaction experiments were conducted in order to evaluate the viability of the production of DCPD from PYGAS by reactive distillation. By following this approach, monomerization of DCPD could be performed during distillation *in-situ* and formed CPD can be separated from PYGAS mixture by boiling point difference. In this study, kinetic analysis for monomerization and dimerization reactions were carried out and the kinetic data was provided for the simulation of the reactive distillation system.

3.3.1 GC-MS Reaction Experiments

The reaction kinetics of DCPD monomerization experiments were carried out by injecting DCPD samples into the heated injection port of GC-MS system where the reaction takes place and the reaction mixture was analyzed *in-situ*. For this purpose, GC-MS inlet liner of Agilent Technologies GC 7890B-MS 5977E system was used as a differential reactor for kinetic analysis by injecting the diluted solutions of DCPD (≥ 99%wt, ZET) in toluene (for gas chromatography MS SupraSolv®, ≥99.8%, Merck), in heptane (for gas chromatography ECD and FID SupraSolv®, ≥99.5%, Merck) and PYGAS (SOCAR) in heptane (for gas chromatography ECD and FID SupraSolv®, ≥99.5%, Merck) with a ratio of 1:20 by volume. HP-5ms capillary GC column was used for the anayses. A split liner with a volume of 990 µL was used in injection port for further dilution of injected samples. The injection volume was kept at 0.2 µL for Automatic Liquid Sampler (ALS). During the experiments, the injection port temperature was changed and the oven temperature was kept constant in order to make sure that the reactions only proceed in the GC-MS injection port liner and the formed reaction products were only eluted in the column without any change in reaction extent. Experiments were performed at 80°C, 240°C, 250°C. 270°C, 290°C, 310°C, 330°C and 350°C injection port temperatures at the constant oven temperature of 50°C. Helium gas was used as the carrier gas. The helium flow rate was altered to change the residence time in injection port. The resulting composition analyses at different reaction temperatures were collected. The same procedure was applied for PYGAS in order to check the compatibility of the results from pure DCPD reaction. Information about the applied methods are provided in Appendix F, Appendix G, and Appendix H.

3.3.2 Reactive Distillation Experimental Studies

The reactive distillation experiments were carried out by using single-stage reactive distillation system in order to monomerize the DCPD in the flask and separate CPD

from DCPD. In the experiments, DCPD (≥ 99%wt, ZET) was used. The experimental setup is shown in Figure 3.3.

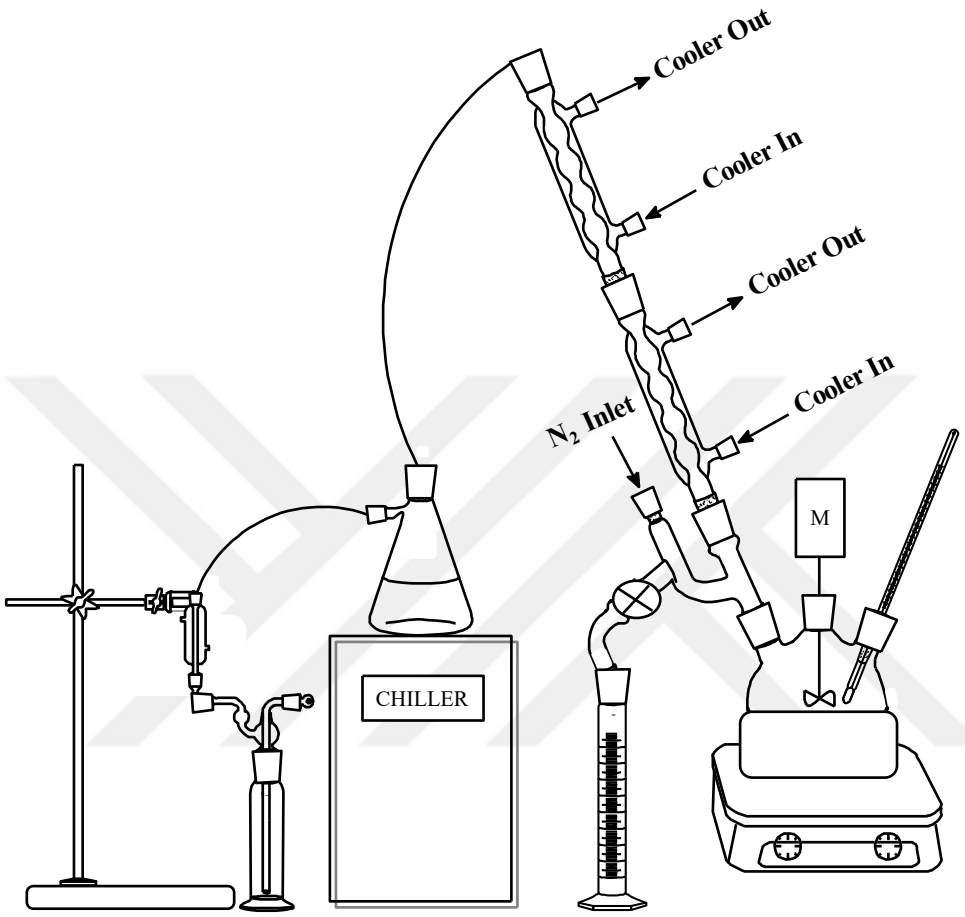


Figure 3.3:Experimental set-up for the reactive distillation system

The reactive distillation system was comprised of a reaction flask, condenser system, electric heater, nitrogen inlet, condensate collection valve connected to graduated cylinder, thermometer, thermocouple, stirrer, cold trap connected to the outlet of the sequential condenser system, relief valve connected to the cold trap and the final trap connected to the relief valve. A cold trap was cooled by liquid nitrogen and connected to the outlet of the sequential condenser system in order to capture the material losses. The relief valve was set to atmospheric pressure and the outlet was dipped into a cold water trap. The open position of the condensate collection valve allowed the collection of the condensate into a graduated cylinder while the closed

position operates the system under total reflux. The condensate collection valve was held in an open position when the sampling is needed without disturbing vapor liquid composition in the system. The experimental procedure for a single reactive distillation experiment is given in Appendix D while the modified parameters of the other experiments are given in Table 3.2.

Table 3.2: Reactive distillation experiment sets

Experiment Number	*Set Temperature (°C)*	*Duration (h)*	*Sampling Interval*	*Experiment Type*
Experiment 27	160	3	15 minutes	Total Reflux
Experiment 29	160	1	10 minutes	Total Reflux
Experiment 31	160	1	10 minutes	Condensate Collection Valve opened at 160°C
Experiment 34	155	1	10 minutes	Condensate Collection Valve opened at 155°C
Experiment 36	150	2.5	10 minutes	Condensate Collection Valve opened at 150°C
Experiment 39	155	1	10 minutes	Condensate Collection Valve opened at 20°C
Experiment 40	150	1	10 minutes	Condensate Collection Valve opened at 20°C

3.3.3 Reactive Distillation Model Prediction

Reactive distillation experiments were also simulated by using Aspen Software version V12.1 to check the validity and viability of the process in industrial scale and the results are compared. DCPD and CPD were selected as components. For the property method, Peng Robinson was selected as a better fit for the determination of thermodynamic properties for petrochemical compounds in reactive systems. For digital twin of the experiments, BatchSep equipment in the Batch Models module was used. Reactor and condenser dimensions were specified according to the reaction flask and condenser dimensions respectively in Aspen Plus. The number of stages was selected as 2 comprising only the pot and condenser for the accurate modeling of the reactive distillation system with a reflux ratio of 0. The medium temperature was specified as the set temperature of the electric heater and the pressure was specified as atmospheric pressure as the set pressure of the relief valve. Condenser temperature was determined according to the temperature of the cooling fluid of the chiller that was connected to the sequential condenser system. For reaction information, kinetic data that was obtained from both literature and data gathered in this work were tested. The system was purged with nitrogen before the reaction therefore the initial condition was specified as “Pad Gas Nitrogen”. The distillate mass flow rate was specified as 0.4 kg/min in compliance with the experimental results as an operating step for batch operating simulation.

3.4 Aspen Simulation of Seperation Sequence for the Production of CPD from PYGAS

In this study, production of DCPD from PYGAS with minimum 90%wt purity is aimed. Industrial scale production of the CPD from PYGAS was simulated by using the collected experimental data in Aspen Plus version V12.1. Constituents of the PYGAS mixture were added as components. The components that are not present in the material databases of Aspen Plus were added manually by defining the structure

of compounds and using the built in estimation module. For the property method, Peng Robinson equation of state was selected which gives results consistent with both phase equilibrium and reactive distillation experiments.

For the simulation of industrial scale production, both BatchSep equipment in the Batch Models module and RadFrac in the Columns module were used and compared.

CHAPTER 4

RESULTS AND DISCUSSION

In this chapter, detailed results of PYGAS and DCPD characterization, phase equilibrium experiments, monomerization reaction kinetic studies and modelling studies are presented and discussed. PYGAS and DCPD characterization studies include the determination of raw materials and products compositions, thermal behavior analysis, and property estimation of PYGAS and DCPD. Results of the phase equilibrium experiments performed to obtain VLE data of DCPD in PYGAS. Reactive distillation experiments and *in-situ* GC-MS reaction experiments were also performed to obtain DCPD monomerization kinetics. Simulation results of the digital twin of the prominent experimental studies and the industrial scale DCPD production in Aspen Plus software version V12.1 are also explained in detail in this chapter.

4.1 Characterization Results of PYGAS and DCPD

PYGAS sample obtained from SOCAR is a diene-rich mixture which contains more than 200 petroleum compounds. In Table 4.1 GC-MS composition analysis result of major constituents in stored PYGAS mixture for a prolonged time is given. For simplicity, more than 200 petroleum compound percentages of PYGAS constituents are distributed to 20 representatvie components according to their boiling points. GC-MS chromatograms and mass spectra are given in Appendix A. PYGAS samples were stored under cool and dry conditions in sealed containers for minimum 2 weeks before use and kept away from heat and direct sunlight. High ratio of DCPD to CPD can be explained by the storage of PYGAS sample for a long time. It was observed that the high temperature GC-MS analysis (≥180°C) allowed diene and norbornene structures to go under Dies-Alder reactions in the GC-MS inlet liner causing the increase in concentration of monomerization products. On the other hand, low

temperature GC-MS analysis (≤180°C) does not represent the actual PYGAS composition as failing to vaporize high boiling point compounds within the mixture in sampling port. PYGAS sample analyses allowed us to identify components in the mixture and the composition to plan phase equilibrium, distillation and reactive distilattion experiments.

Table 4.1: Composition analysis of major PYGAS (SOCAR) constituents

Compound Name	*%wt*
2-Methyl 1-Butene	0.2
Methyl Butane	2.0
n-Pentane	9.0
2-Methyl-1,3 Butadiene (Isoprene)	3.1
Pentene	0.8
1,3-Pentadiene (Piperylene)	2.0
1,3 Cyclopentadiene	3.6
Cyclopentene	1.5
Methyl Pentane	2.6
Methyl Cyclopentadiene	1.3
n-Hexane	2.7
Methyl Cyclopentane	1.8
Methyl Cyclopentene	0.7
Benzene	30.2
Toluene	1.5
5-Vinyl-2-Norbornene	3.0
Isopropenyl Norbornene	4.0
Exo-Dicyclopentadiene	0.3
Endo-Dicyclopentadiene	23.7
Methyl-Dicyclopentadiene	6.0

In addition to DCPD and CPD, other C5 dimers to co-dimers were observed in PYGAS sample. These co-dimers are methyl dicyclopentadiene (CPD+Met-CPD), 5-vinyl-2-norbornene (CPD+1,3 butadiene), isopropenyl norbornene (CPD+isoprene). However, the end-product of piperylene with cyclopentadiene was not observed due to the lower reaction activity of piperylene with CPD, which is in agreement with the literature (Nurulinna et al., 2001).

Commercial DCPD sample (≥99%wt, ZET) was also analyzed in GC-MS and the analysis results are given in Table 4.2. GC-MS chromatogram and mass spectra of the DCPD sample are given in Appendix B. DCPD sample contains %99.8 DCPD (endo DCPD+exo DCPD) therefore it is accepted as pure DCPD in our studies.

Table 4.2: Composition analysis of DCPD (ZET)

Compound Name	*%wt*
Isopropenyl Norbornene	0.2
Exo-Dicyclopentadiene	0.4
Endo-Dicyclopentadiene	99.4

Thermal behaviour of the PYGAS and DCPD were also investigated by using TGA/DSC-STA and the thermograms are shown in Figure 4.1 and 4.2 respectively. Figure 4.3 represents the overlaying thermograms.

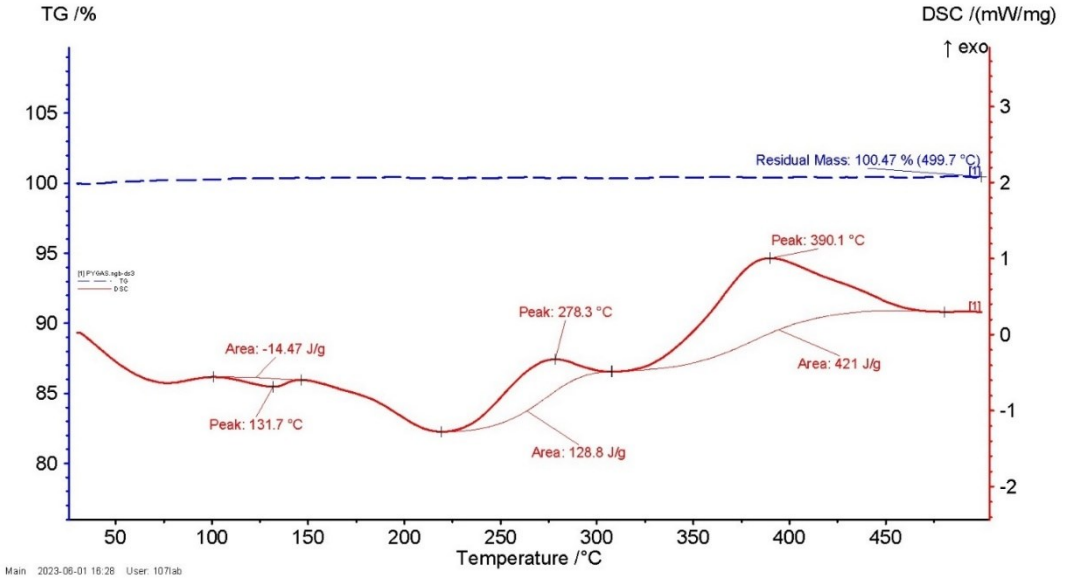


Figure 4.1: Thermogram of PYGAS

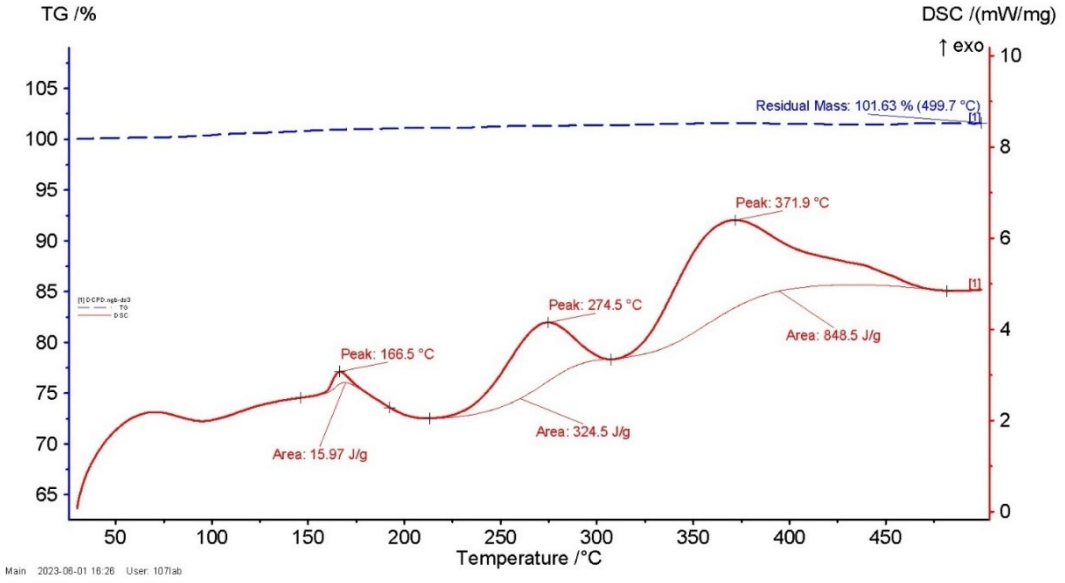


Figure 4.2: Thermogram of DCPD

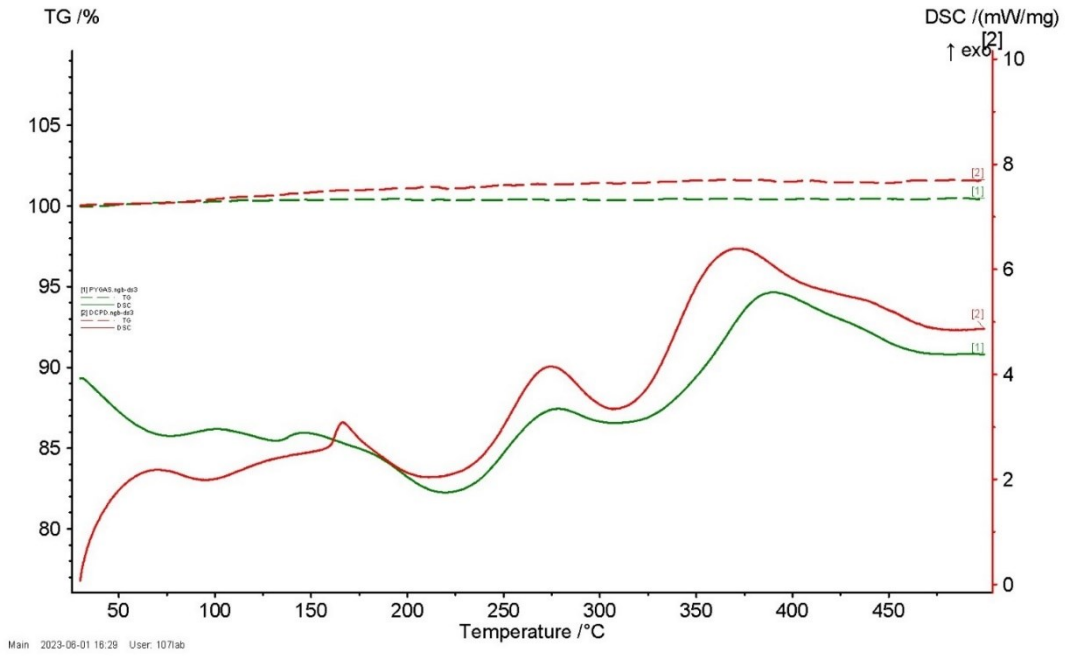


Figure 4.3: Comparison of PYGAS and DCPD thermograms

STA thermogram of DCPD (Figure 4.2) exhibit three exothermic peaks at 166.5°C, 274.5°C and 371.9°C while the heat released from these exotherms are determined as 15.97 J/g, 324.5 J/g, 848.5 J/g respectively. The first exotherm at 166.5°C was assigned as the monomerization reaction of DCPD while the peaks at 274.5°C and 371.9°C represent the higher-order oligomerization reactions of CPD. Am Ende, Whritenour and Coe (2007) investigated the thermal behavior of DCPD from 25°C to 400°C in DSC with 4°C/min heating rate, and an exothermic peak at 123.5°C along with secondary exothermic events starting from 200°C to 379.6°C were reported. For the PYGAS sample (Figure 4.1), the endotherm is observed at 131.7°C with 14.47 J/g heat release while the exotherms at 278.3°C and 390.1°C have heat releases of 128.8 J/g and 421 J/g, respectively. The first endotherm at 131.7°C indicates the vaporization of benzene and light hydrocarbons in a closed sample pan. It can be concluded that the thermal behavior of the DCPD and PYGAS shows similar trends above 200°C indicating the higher-order oligomerization reactions of CPD which is in compliance with literature (am Ende et al., 2007). Heat release

values are different for PYGAS and DCPD thermograms due to different concentrations of DCPD in both samples.

Density and viscosity measurements were conducted by using pycnometry and Brookfield Viscometer DV2TRV respectively. A comparison of the density and the viscosity of fresh and stored PYGAS sample are given in Table 4.3. An increase is observed in the viscosity of the stored PYGAS sample. This increase can be resulted from the dimerization and co-dimerization reactions occured in the mixture.

Table 4.3: Physical properties of stored PYGAS (SOCAR) sample

Property	*Value as Received from SOCAR*	*Experimental Value for Stored PYGAS*
Density	0.83-0.87 g/mL	0.78 g/mL
Viscosity (at 20°C)	0.59-0.95 mPa.s	4.50 mPa.s

4.2 Phase Equilibrium Experiments and Modelling Results

As stated in Section 3.2.1, single and multi step experiments were conducted to fractionate PYGAS. The fractions collected in receiving flask (condensate) are in equilibrium with residual in evaporating (rotary) flask at the applied temperature and pressure. With the primary aim of gathering phase equilibrium data, the upper limit of temperature was set to 135°C to prevent DCPD monomerization in evaporative flask.

Single step experiments (Experiments 1, 2 and 3 in Table 4.4) were conducted to determine the temperature and pressure values for separation of benzene and lighter hydrocarbons from the PYGAS mixture. Altough lighter hydrocarbons were separated from the PYGAS mixture and collected in condensate, Experiment 1 and Experiment 2 failed to remove benzene. Benzene was separated substantially in Experiment 3. It was observed that benzene and lighter hydrocarbons can be removed from the PYGAS mixture at 80°C and 100 mbar to a large extent, but DCPD can not be retrieved in a single step.

Therefore it was aimed to separate DCPD by multi step experiments at various temperatures and pressures (Experiments 8, 9, 10 and 14 in Table 4.4). Multi-step separation scheme was conducted to separate benzene and lighter hydrocarbons from PYGAS and to obtain DCPD rich condensate and isolate DCPD as first, second and third step fractionation respectively. The compositions (wt%) of the benzene, DCPD and Met-DCPD (as components without grouping) in fractionates of the phase equilibrium experiments at different temperatures and pressures are given in Table 4.4. The liquid fractions collected in receiving flask are labelled as condensate and the remainings in evaporating flask are labelled as flask for simplicity. GC-MS chromatogram and mass spectra of the PYGAS fraction samples are given in Appendix E.

Table 4.4: Experimental parameters and results of phase equilibrium experiments performed by using PYGAS sample (stored)

Experiment Number	*Set Temperature (°C)*	*Set Pressure (mbar)*	*%wt Benzene (as component)*	*%wt DCPD (as component)*	*%wt Met-DCPD (as component)*
PYGAS sample	NA	NA	30.00	24.00	6.00
Experiment 1 Flask, 34.0 g (Started with 79.6 g PYGAS as feed)	*40*	*175*	31.38	45.61	9.30
Experiment 1 Condensate, 13.3 g (Started with 79.6 g PYGAS as feed)	*40*	*175*	25.0	1.27	0
Experiment 2 Flask, 37.2 g (Started with 86.1 g PYGAS as feed)	*80*	*650*	35.77	42.70	8.75
Experiment 2 Condensate, 32.0 g (Started with 86.1 g PYGAS as feed)	*80*	*650*	21.20	1.67	0

Table 4.4 (Continued)

Experiment Number	*Set Temperature (°C)*	*Set Pressure (mbar)*	*%wt Benzene (as component)*	*%wt DCPD (as component)*	*%wt Met-DCPD (as component)*
Experiment 3 Flask, 22.9 g (Started with 78.1 g PYGAS as feed)	*80*	*100*	2.60	67.77	22.88
Experiment 3 Condensate, 31.6 g (Started with 78.1 g PYGAS as feed)	*80*	*100*	73.20	13.26	0
Experiment 8x* Flask, 37.1 g (Started with 169.9 g PYGAS as feed)	*80*	*100*	1.55	65.67	24.69
Experiment 8x* Condensate, 62.1 g (Started with 169.9 g PYGAS as feed)	*80*	*100*	70.18	8.90	2.17

Table 4.4 (Continued)

Experiment Number	*Set Temperature (°C)*	*Set Pressure (mbar)*	*%wt Benzene (as component)*	*%wt DCPD (as component)*	*%wt Met-DCPD (as component)*
Experiment 8y* Flask, 8.7 g (Started with Experiment 8x's flask as feed)	*125*	*100*	0.05	51.01	38.61
Experiment 8y* Condensate, 26.3 g (Started with Experiment 8x's flask as feed)	*125*	*100*	3.40	68.14	20.43
Experiment 8z* Flask, 3.5 g (Started with Experiment 8y's condensate as feed)	*135*	*100*	0	36.75	45.15

Table 4.4 (Continued)

Experiment Number	*Set Temperature (°C)*	*Set Pressure (mbar)*	*%wt Benzene (as component)*	*%wt DCPD (as component)*	*%wt Met-DCPD (as component)*
Experiment 8z* Condensate, 4.1 g (Started with Experiment 8y's condensate as feed)	*135*	*100*	0	63.32	30.03
Experiment 9x* Flask, 66.0 g (Started with 156.5 g PYGAS as feed)	*80*	*100*	3.01	65.260	24.35
Experiment 9x* Condensate, 86.8 g (Started with 156.5 g PYGAS as feed)	*80*	*100*	65.93	15.26	5.91
Experiment 9y* Flask, 5.5 g (Started with Experiment 9x's flask as feed)	*125*	*100*	0.02	41.9	43.30

Table 4.4 (Continued)

Experiment Number	*Set Temperature (°C)*	*Set Pressure (mbar)*	*%wt Benzene (as component)*	*%wt DCPD (as component)*	*%wt Met-DCPD (as component)*
Experiment 9y* Condensate, 28.2 g (Started with Experiment 9x's flask as feed)	*125*	*100*	3.16	68.49	21.19
Experiment 9z* Flask, Droplets (Started with Experiment 9y's condensate as feed)	*125*	*70*	0	27.97	48.71
Experiment 9z* Condensate, 5.0 g (Started with Experiment 9y's condensate)	*125*	*70*	0	68.59	21.19

Table 4.4 (Continued)

Experiment Number	*Set Temperature (°C)*	*Set Pressure (mbar)*	*%wt Benzene (as component)*	*%wt DCPD (as component)*	*%wt Met-DCPD (as component)*
Experiment 10x* Flask, 37.5 g (Started with 163.0 g PYGAS as feed)	*80*	*100*	2.65	64.66	24.42
Experiment 10x* Condensate, 100.5 g (Started with 163.0 g PYGAS as feed)	*80*	*100*	60.81	15.83	3.58
Experiment 10y* Flask, 4.3 g (Started with Experiment 10x's flask as feed)	*130*	*150*	0	35.15	46.09

Table 4.4 (Continued)

Experiment Number	*Set Temperature (°C)*	*Set Pressure (mbar)*	*%wt Benzene (as component)*	*%wt DCPD (as component)*	*%wt Met-DCPD (as component)*
Experiment 10y* Condensate, 30.8 g (Started with Experiment 10x's flask as feed)	*130*	*150*	2.89	67.57	21.10
Experiment 10z* Flask, Droplets (Started with Experiment 10y's condensate as feed)	*130*	*90*	0	26.97	49.48
Experiment 10z* Condensate, 3.0 g (Started with Experiment 10y's condensate as feed)	*130*	*90*	0	57.92	34.64

Table 4.4 (Continued)

Experiment Number	*Set Temperature (°C)*	*Set Pressure (mbar)*	*%wt Benzene (as component)*	*%wt DCPD (as component)*	*%wt Met-DCPD (as component)*
Experiment 14x* Flask, 100.0 g (Started with 450.0 g PYGAS as feed)	*80*	*100*	2.94	64.46	25.59
Experiment 14x* Condensate, 329.0 g (Started with 450.0 g PYGAS as feed)	*80*	*100*	58.90	6.35	0.73
Experiment 14y* Flask, 8.0 g (Started with Experiment 14x's flask as feed)	*125*	*100*	0	21.72	52.39

Table 4.4 (Continued)

Experiment Number	*Set Temperature (°C)*	*Set Pressure (mbar)*	*%wt Benzene (as component)*	*%wt DCPD (as component)*	*%wt Met-DCPD (as component)*
Experiment 14y* Condensate, 92.0 g (Started with Experiment 14x's flask as feed)	*125*	*100*	0.69	71.56	23.94
Experiment 14z* Flask, 41.0 g (Started with Experiment 14y's condensate as feed)	*110*	*100*	0	60.29	32.88

Table 4.4 (Continued)

Experiment Number	*Set Temperature (°C)*	*Set Pressure (mbar)*	*%wt Benzene (as component)*	*%wt DCPD (as component)*	*%wt Met-DCPD (as component)*
Experiment 14z* Condensate, 49.0 g (Started with Experiment 14y's condensate as feed)	*110*	*100*	0.86	75.75	19.36

*x represents the "Benzene and Lighter Hydrocarbons Removal Step (Step 1)", y represents the "DCPD Removal Step from the Heavy Residue (Step 2)" and z represents the "DCPD Isolation Step (Step 3)".

Results presented in Table 4.4 indicates that the DCPD can not be separated to a high purity in a single step for Experiment 1, 2 and 3. Therefore after separating the benzene and lighter hydrocarbons at 80°C and 100 mbar in the first, second and third steps were conducted at various temperatures and pressures between 125-135°C and 70-150 mbar. However, it was noticed that the DCPD could not be separated from the Met-DCPD to a high purity in second or even third steps under the experimental conditions applied due to temperature restrictions to prevent monomerization reaction of DCPD. DCPD purity varies between 64.46% and 65.67% wt in the flask for Step 1, 67.57% to 71.56% wt in the condensate for Step 2, and 63.32% and 75.75% wt in the condensate for Step 3 in the multi step experiments. The highest purity of DCPD was achieved in Experiment 14 Step 3 with %75.75 wt. It was also observed that the rotary evaporator system has considerable amount of vapor loss resulting from highly volatile compounds in PYGAS mixture. Vapor loss was substantially observed in Step 1 where lighter hydrocarbons were separated from the PYGAS mixture.

Experiment 14 is the most prominent experimental study in terms of DCPD purification. The weight percentage of the benzene, DCPD and Met-DCPD in the PYGAS mixture is presented in Table 4.4 and the weight percentage of other constituents of PYGAS for each step of Experiment 14 are given in Figure 4.4, 4.5, 4.6. For simplicity, compositions are given in terms of the representative compounds. Simulation of the compound rich petroleum mixtures such as PYGAS is challenging in terms of defining the compounds for simulation. For this purpose, pseudo or representative components are created to simulate cuts or fractions where the properties are similar. Pseudo or representative component is a single component that represents a mixture characteristics with close boiling points (Towler & Sinnot, 2013). Therefore, PYGAS sample constituents are classified into five groups by considering the boiling points of the components; Lighter Hydrocarbons, Benzene Group, Toluene Group, Dicyclopentadiene, and Methyl-Dicyclopentadiene Group as presented in Table 4.5. Pentadiene for lighter hydrocarbons, benzene for the benzene group, toluene for the toluene group, and methyl dicyclopentadiene for the

methyl dicyclopentadiene group were selected as representative components for the simulations.

Material characterization for condensate and flask samples for Step 1 (Experiment 14x), Step 2 (Experiment 14y), and Step 3 (Experiment 14z) along with the heavy compounds formed in the evaporative flask are presented in Appendix E. Experiment 14 was reproduced and the standard deviations are pointed in figures.

Table 4.5: PYGAS sample constituents grouping

Compound Name	*Classification*	*%wt*
2-Methyl 1-Butene Methyl Butane n-Pentane 2-Methyl-1,3 Butadiene (Isoprene) Pentene 1,3-Pentadiene (Piperylene) 1,3 Cyclopentadiene Cyclopentene	Lighter Hydrocarbons	22.2
Methyl Pentane Methyl Cyclopentadiene n-Hexane Methyl Cyclopentane Methyl Cyclopentene Benzene	Benzene Group	39.3
Toluene 5-Vinyl-2-Norbornene(CPD+1,3 butadiene)	Toluene Group	4.5
Exo-Dicyclopentadiene Endo-Dicyclopentadiene	Dicyclopentadiene	24.0
Isopropenyl Norbornene Methyl-Dicyclopentadiene	Methyl-Dicyclopentadiene Group	10.0

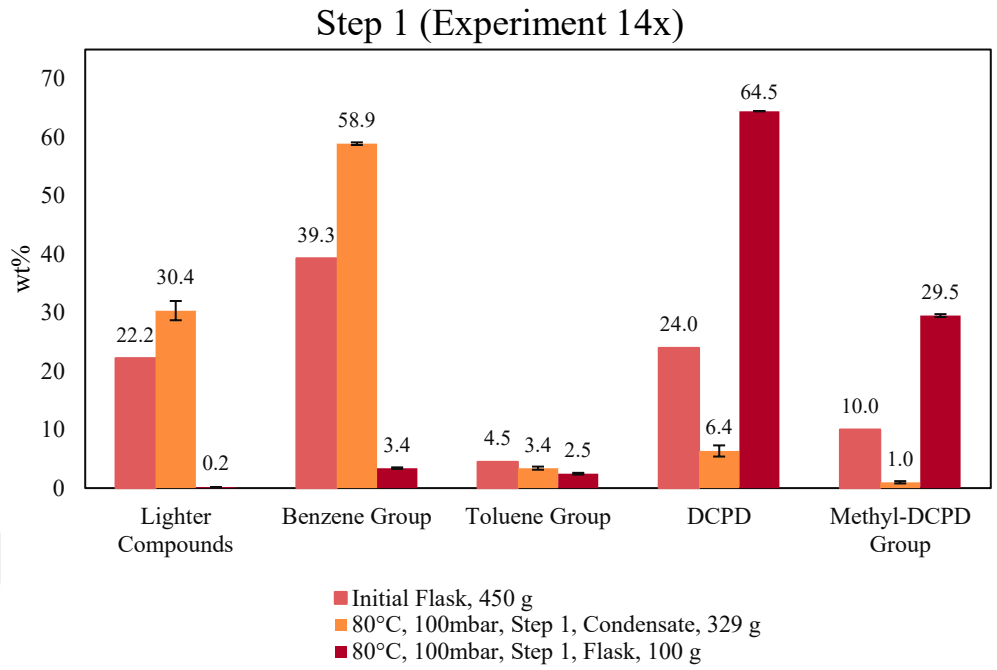


Figure 4.4: Composition analysis of Step 1 (Experiment 14x), started with inital flask containing PYGAS sample

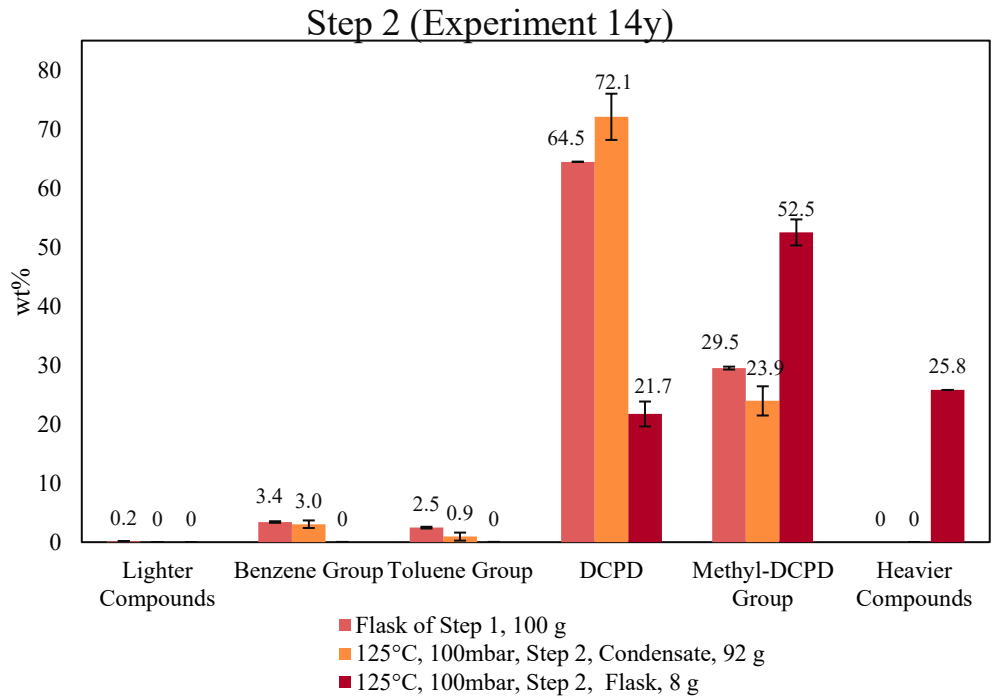


Figure 4.5: Composition analysis of Step 2 (Experiment 14y), started with flask of Step 1

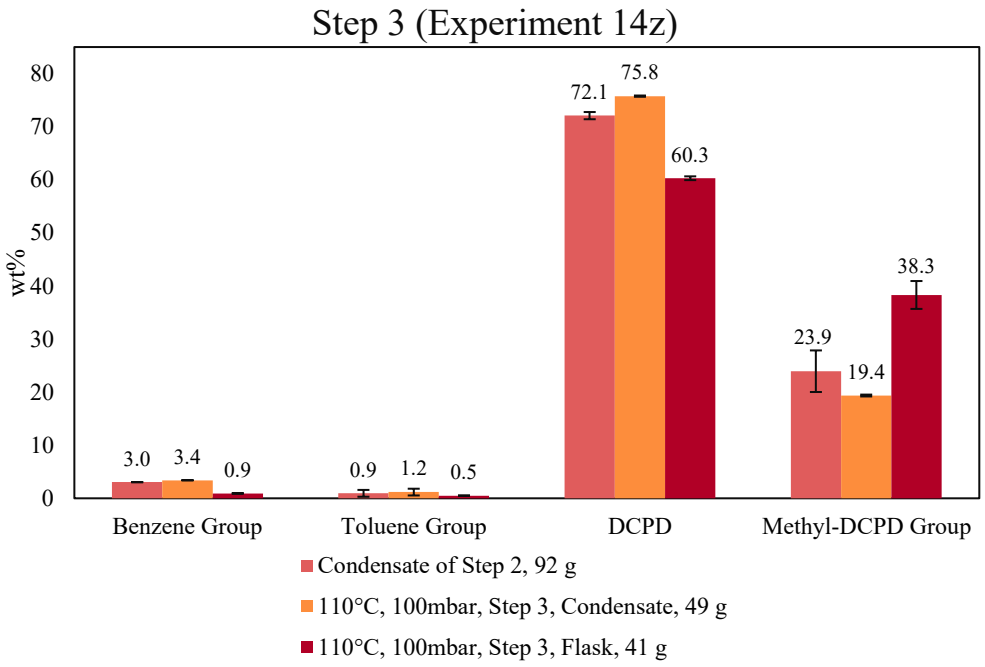


Figure 4.6: Composition analysis of Step 3 (Experiment 14z), started with condensate of Step 2

Phase Equilibrium Experiment 14 was conducted for fifteen minutes for Step 1 (Experiment 14x), two and a half hours for Step 2 (Experiment 14y), and one and half hours for Step 3 (Experiment 14z). Therefore it was concluded that the benzene and lighter hydrocarbons can easily be separated from the PYGAS mixture while DCPD can not be easily retrieved from the remainings under the experimental conditions applied. The formation of heavy compounds such as dicyclopentadiene oligomers, benzene derivatives, and naphthalene derivates which had not been observed in original PYGAS sample, were observed in Step 2 residual. The formation of residuals might be favored by prolong heating of flask.

Experiment 14 was also simulated in Aspen Plus by using 2 stage batch distillation column comprising only pot and condenser, similar to experimental set-up. The inputs for the simulation are shown in Table 4.6. The composition (mass fractions) of the original PYGAS mixture presented in Table 4.5 was used as the feed compositions in simulation of Step 1 as representative components.

The experiment 14 was simulated in ASPEN by using the final mass fractions of the pot of Step 1 as a feed composition for Step 2. Finally using the final composition of the receiver (distillate) of Step 2 as the feed composition for Step 3 as depicted in Figure 3.2. Comparison of the experimental results with the Aspen Plus simulation results are presented in Figure 4.7 and Figure 4.8 for Step 1, Figure 4.9 and Figure 4.10 for Step 2, Figure 4.11 and Figure 4.12 for Step 3.

Experimental studies for Step 1, Step 3 and the simulation results are in good agreement. The differences in the compositions between the experimental analyses and Aspen simulation results are within acceptible limits. Errors can be resulted from representative composition assumption, experimental composition analysis and vapor losses from rotary evaporator. The differences in the composition of DCPD and Met-DCPD in Step 2 between the experiment and Aspen simulation observed may arise from the formation of heavy products such as dicyclopentadiene oligomers, benzene derivatives and napthalene derivatives due to prolonged heating in Step 2. The formation of heavy components was not considered in Aspen simulation and no reaction information was provided into Aspen. Formation of heavier compounds was observed only when the experiment was extended over two hours. Therefore, prolonged heating of PYGAS fractions should be avoided to prevent unwanted oligomerizations.

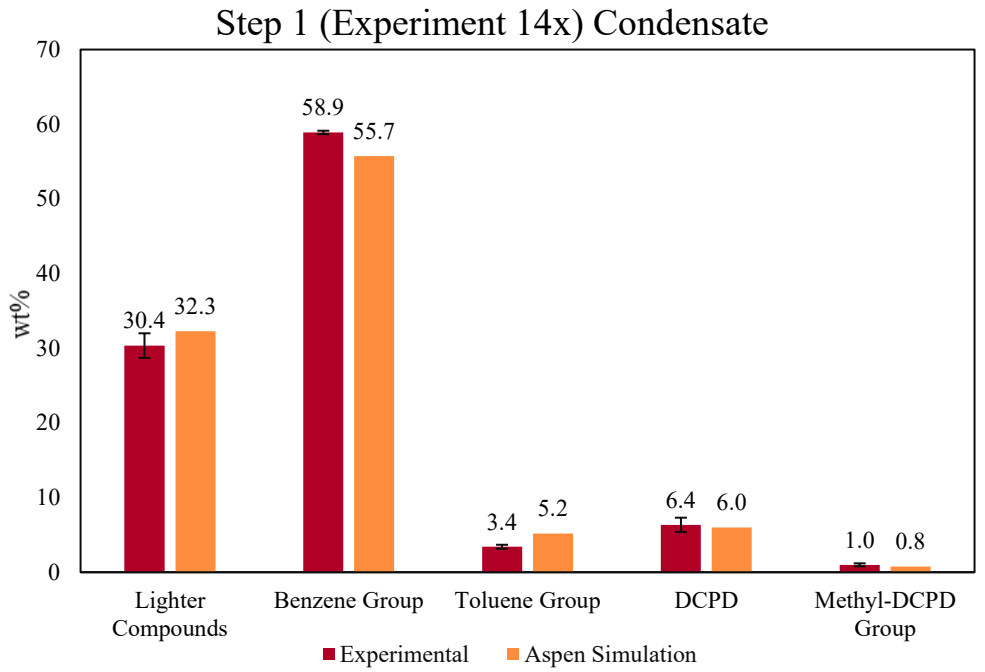


Figure 4.7: Comparison of experimental and simulation results for Step 1 (Experiment 14x) condensate

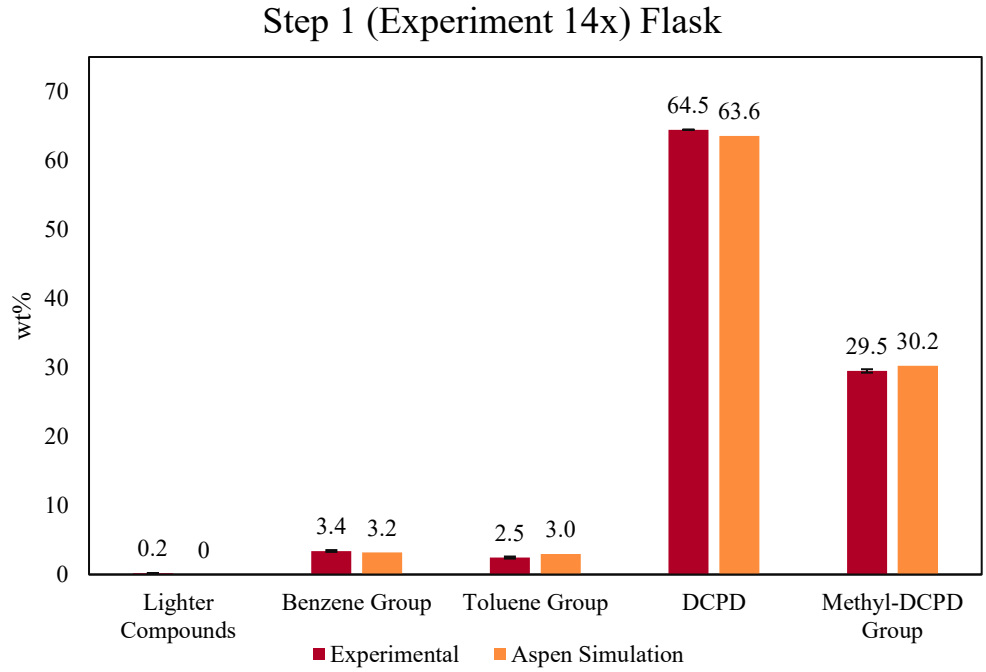


Figure 4.8: Comparison of experimental and simulation results for Step 1 (Experiment 14x) flask

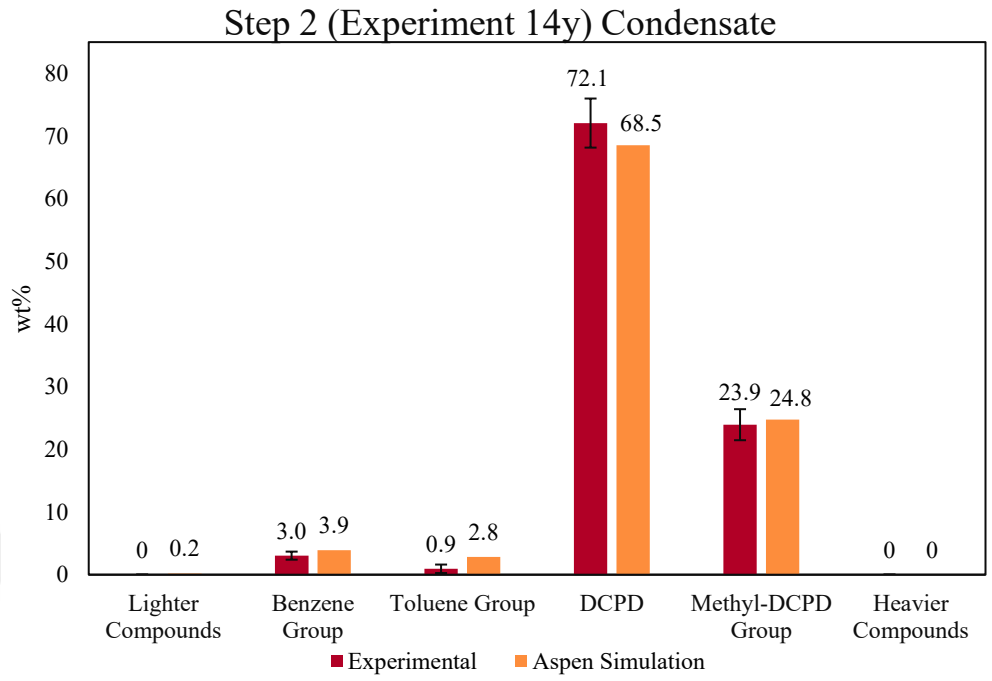


Figure 4.9: Comparison of experimental and simulation results for Step 2 (Experiment 14y) condensate

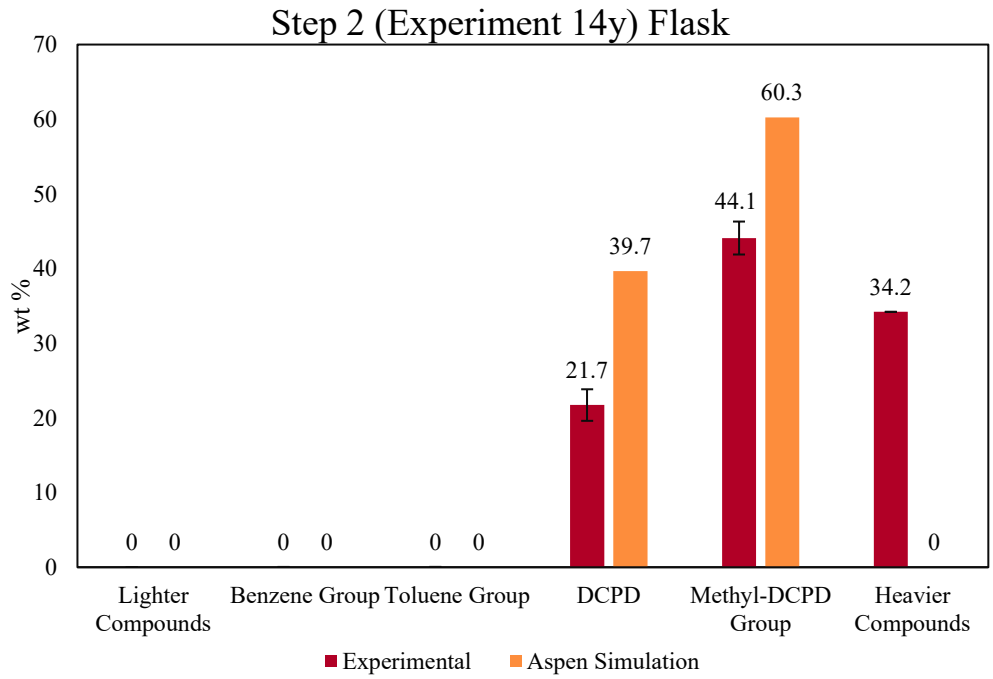


Figure 4.10: Comparison of experimental and simulation results for Step 2 (Experiment 14y) flask

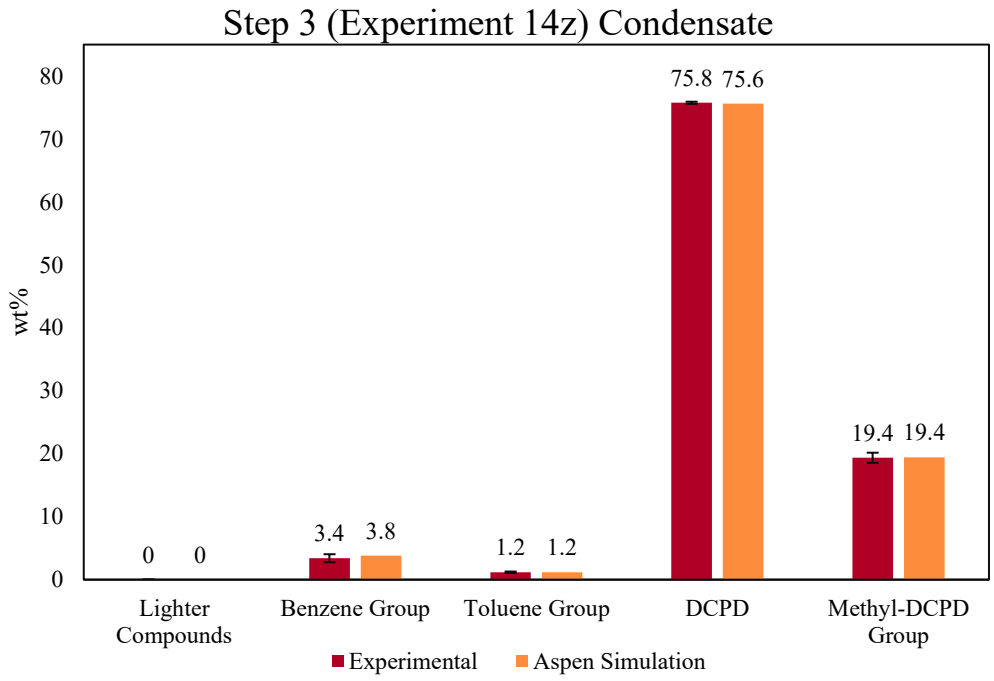


Figure 4.11: Comparison of experimental and simulation results for Step 3 (Experiment 14z) condensate

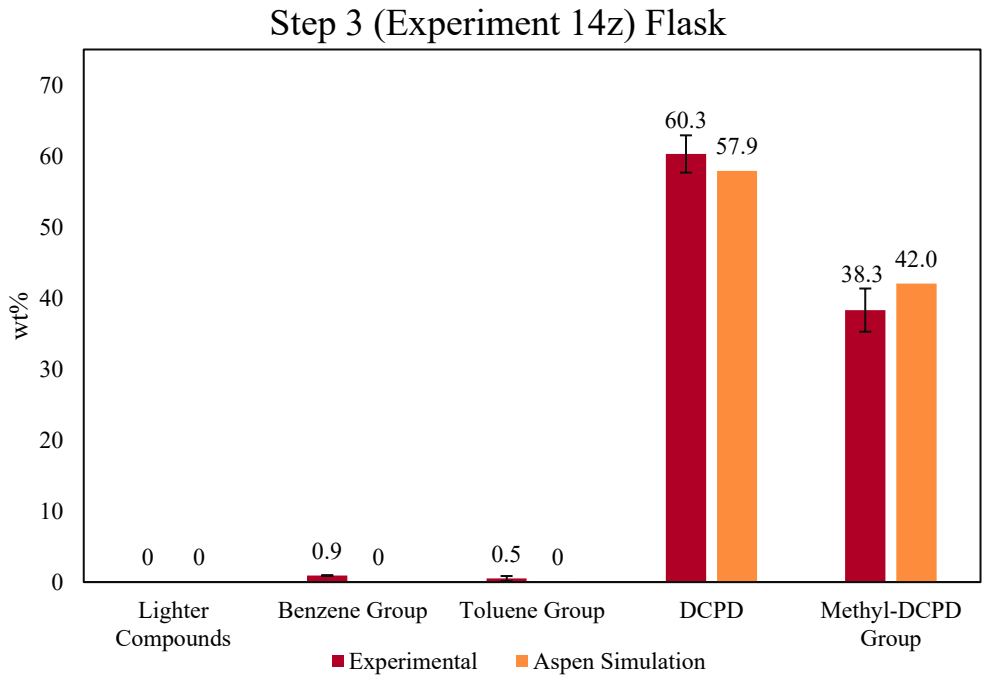


Figure 4.12: Comparison of experimental and simulation results for Step 3 (Experiment 14z) flask

Table 4.6: Aspen Plus inputs for the simulation of phase equilibrium experiments

Parameter	*Aspen Input*
Property Method	Peng Robinson
Equipment	BatchSep
Number of Stage	*2*
Heat Transfer-Specified Medium	
Temperature*	*80* °C^{x}/*125* °C^{y}/*110* °C^{z}
Pressure	*100 mbar*
Initial Conditions	*Empty*
Condenser Inlet Diameter	*2 cm*
Operating Steps	*Condenser Pressure 100 mbar*
Pot Volume	*8 L*
Condenser Temperature	*-10*°C

*x represents the "Benzene and Lighter Hydrocarbons Removal Step (Step 1)", y represents the "DCPD Removal Step from the Heavy Residue (Step 2)" and z represents the "DCPD Isolation Step (Step 3)".

4.3 Monomerization Reaction Kinetics and Modelling Results

Reaction kinetics of DCPD monomerization was studied by *in-situ* GC-MS experiments as stated in experimental part. Reaction kinetics data enabled us to simulate recative distillation of PYGAS by using more realistic data. The kinetic data, experimental and simulation results are compared with the recent kinetic data in literature (Xu et al., 2019).

4.3.1 GC-MS Reaction Experiment Results

The injection port liner of GC-MS (Agilent Technologies GC 7890B-MS 5977E) was used as reaction chamber where the reaction takes place under flash vaporization conditions. This approach is advantageous because of small sample size, negligible

heat effects, *in-situ* separation of the products and reactants, and the control of the reaction parameters such as temperature and pressure (Langer and Patton, 1972). DCPD monomerization reaction in a gas chromatographic reactor is also investigated in literature where GC column is used as a reactor (Griffith et al., 1987), (Langer and Patton, 1972). In this work, DCPD monomerization was also investigated in PYGAS mixture and the results are presented.

In this thesis, the GC-MS inlet liner with 990 μL volume was used as a differential reactor where the glass wool in the inlet liner which offer higher heat transfer rates. During the experiments, the column temperature was kept at 50°C, in order to prevent the reaction to proceed in the column. Injection port temperature and helium flow rates were adjusted to obtain various average residence times of sample vapor in injection port and the composition of sample was analysed by GC-MS. GC-MS reaction experiments were conducted by using diluted solutions of DCPD in hexane, heptane, and toluene. However, no significant change in the composition of reaction products was observed under the experimental conditions applied. Therefore solvent effect for the reversible reaction of DCPD monomerization is accepted as negligible. Table 4.7 represents the composition analyses under 10 mL/min carrirer gas flows (He) at the temperature range of 80°C to 350°C. The effect of temperature on the product stream composition when 0.2 μL DCPD in solvent (1:20 by volume) was injected is shown in Figure 4.13 for 10 mL/min and 20 mL/min Helium flow. GC-MS chromatograms and mass spectra obtained during the experiments along with GC-MS parameters such as carrier gas flow, oven gas flow, oven program are given in Appendix F and Appendix G. As no monomerization occurs on 80°C, the compositions represents the injected sample. As it can be seen in Figure 4.13, CPD weight fractions show similar trends between 80°C and 350°C for 10 and 20 mL/min He flows. No significant change in the concentration of CPD is observed at the temperature range of 80°C to 240°C due to lower reaction rates. DCPD monomerization significantly increases at 240°C and after 330°C, CPD concentration slightly increases until reaction goes to completion at 350°C. DCPD conversion is lower for 20 mL/min He flow when compared to 10 mL/min He flow

at the temperature range of 80°C to 330°C until monomerization completes at 350°C. For instance at 270°C, compositions are 33.14% wt CPD and 66.86% DCPD for 10 mL/min while 19.10% wt CPD and 80.93% DCPD for 20 mL/min He flow. This may result from the longer residence time spent in the GC injection port for 10 mL/min He flow when compared to 20 mL/min, therefore, longer reaction time.

Table 4.7: GC-MS reaction experiment sets and results for 10 mL/min He

GC-Run	*Inlet Temperature (°C)*	*Oven Temperature (°C)*	*%wt CPD*	*%wt DCPD*
1	80	50	0	100.00
2	240	50	6.19	93.34
3	250	50	13.25	86.75
4	270	50	33.14	66.86
5	290	50	70.13	29.87
6	310	50	96.15	3.85
7	330	50	99.19	0.82
8	350	50	100.00	0

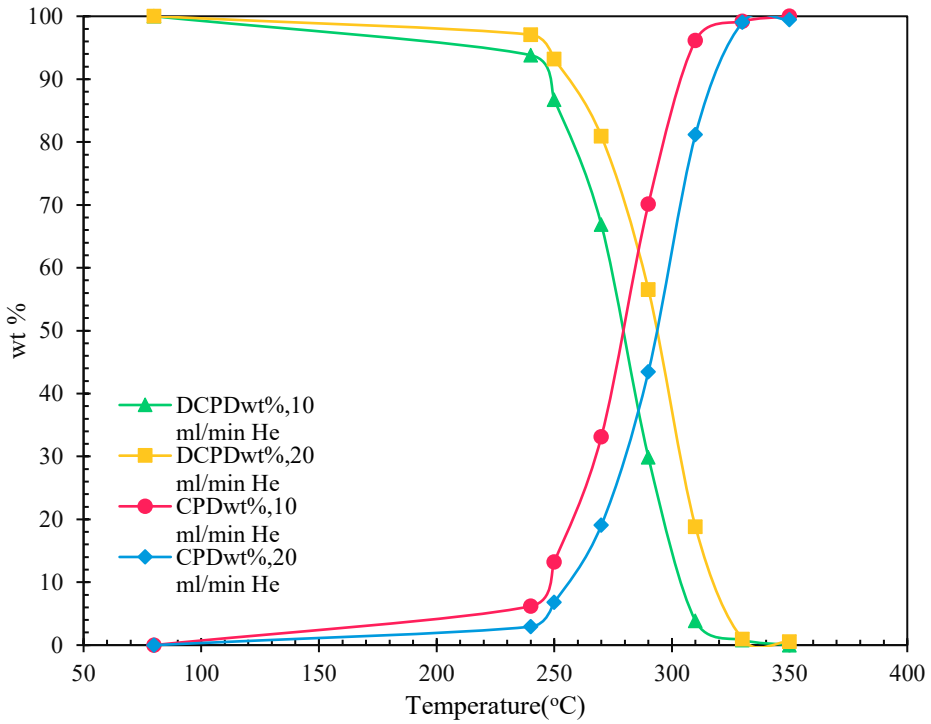


Figure 4.13: Effect of temperature on weight fraction of CPD and DCPD for 10 mL/min He and 20 mL/min He

In order to investigate the DCPD monomerization in the presence of other constituents in PYGAS such as benzene group, toluene group and Met-DCPD, GC-MS reaction experiments were also conducted by using PYGAS samples as feed. The composition of reaction mixture was reported in accordance with Table 4.5 in terms of representative compounds. The product composition of the monomerization reactions taking place in the injection port of the GC (which is indeed the reactor) are shown in Figure 4.14 and Figure 4.15 for Met-DCPD and DCPD, respectively.

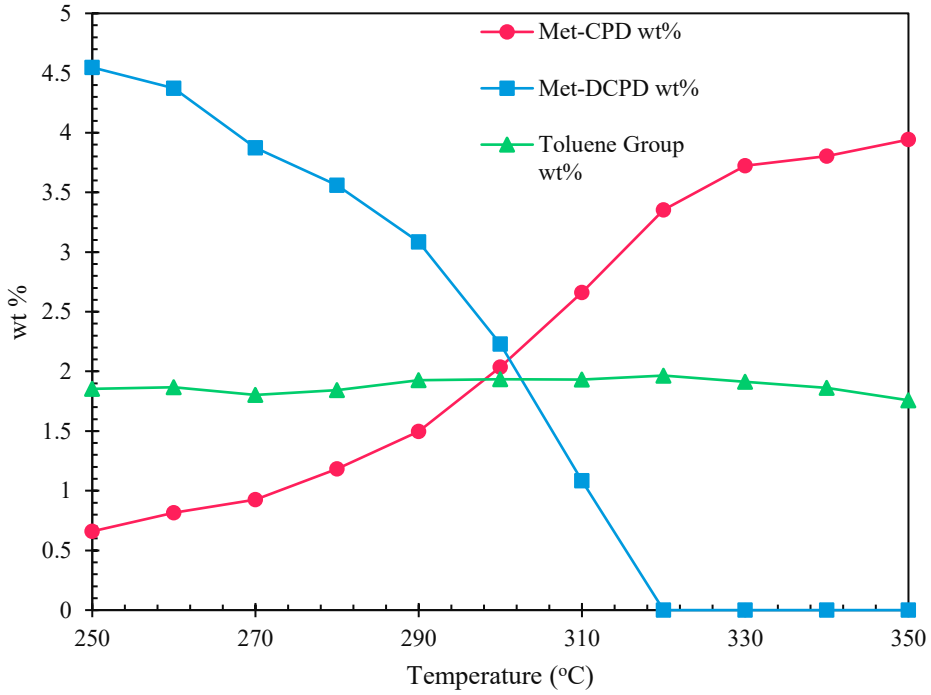


Figure 4.14: Effect of temperature on weight fraction of Met-CPD, Met-DCPD and toluene for 20 mL/min He

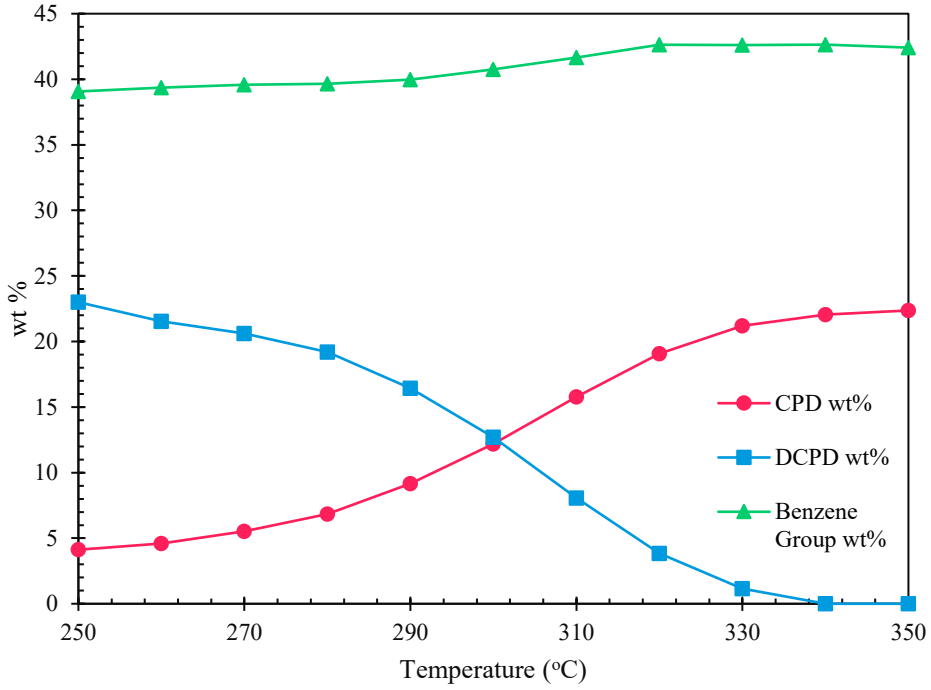


Figure 4.15: Effect of temperature on weight fraction of CPD, DCPD and benzene for 20 mL/min He

Both Figure 4.14 and Figure 4.15 indicate that the benzene and toluene groups were not affected by the reactor temperature. No substantial monomerization of DPCD and Met-DCPD was observed at temperatures below 270°C. However, nearly half of the DCPD was monomerized at 300°C, this ratio was sharply increased with temperature so that almost all DCPD and Met-DCPD completely monomerized to CPD at 330°C. It shold be noticed that monomerization of one mole of Met-DCPD also yields one mole CPD, which shows the contribution of Met-DCPD to CPD production. Detailed GC-MS chromatograms of PYGAS at various temperatures are given in Appendix H. Conversion of DCPD in its pure form and in PYGAS are compared in Figure 4.16.

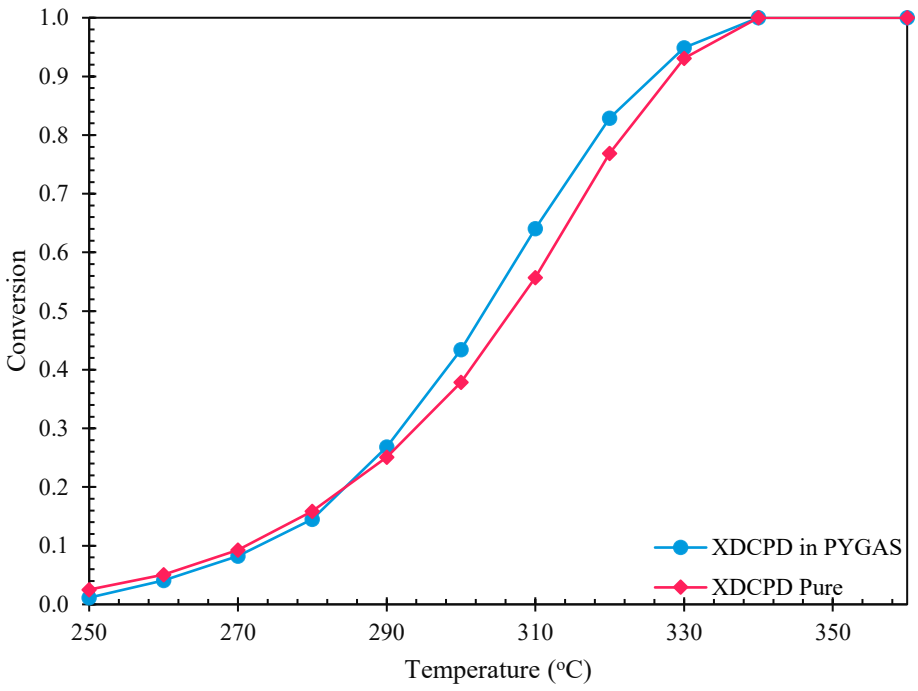


Figure 4.16: Temperature effect on conversion (XDCPD) for pure DCPD and DCPD in PYGAS

As it can be seen in Figure 4.16, the converison of DCPD in pure DCPD sample and PYGAS exhibit similar temperature course of reaction. Therefore, the reaction rate of DCPD does not affected by the presence of components exist in toluene, benzene group significantly. A slight increase in DCPD conversion is observed between the temperatures 310°C and 330°C in PYGAS. Therefore the kinetic data obtained can

be used to obtain reaction rate expression which represents the reversible monomerization reaction of DCPD in both pure DCPD and PYGAS with confidence.

At temperatures above 140°C, DCPD monomerizes to CPD by reversible reaction (Eqn 4.1) (Herndon et al., 1967).

$$DCPD \leftrightarrow 2\,CPD \tag{4.1}$$

The differential reactor can be modeled as a batch reactor. It was assumed that the reactor is perfectly mixed due to its small volume, therefore the reaction rate was considered to be uniform within the the reactor volume. The mass balance is given in Equation 4.2.

$$-r_{DCPD} = \frac{dX}{dt}\left(\frac{N_{A_0}}{V}\right) \tag{4.2}$$

And;

$$k_{0_{forward}} e^{\left(\frac{-E_{A_1}}{T}\right)}(1-X)^n - k_{0_{reverse}} e^{\left(\frac{-E_{A_2}}{T}\right)}(X)^2 = \frac{dX}{dt}\left(\frac{N_{A_0}}{V}\right) \tag{4.3}$$

Where N_{Ao} is the moles of DCPD initially fed to the reactor, V is the reactor volume, r_{DCPD} is the reaction rate of the DCPD, t is time, X is the temperature course of conversion and T is injection port temperature. X, N_{Ao}, V and T were used for nonlinear regression analysis to determine $k_{0forward}$ (forward reaction pre-exponential factor), E_{A1} (activation energy of the forward reaction), n (reaction order), $k_{0reverse}$ (reverse reaction pre-exponential factor) and E_{A2} (activation energy of the reverse reaction). Nonlinear regression analysis was conducted by using POLYMATH and the values of $k_{0forward}$, E_{A1}, n, $k_{0reverse}$ and E_{A2} were calculated. The expression used for model is given in Equation 4.4.

$$Y = A_1\, e^{\left(\frac{-E_1}{T}\right)}(1-X)^{A_2} - A_3 e^{\left(\frac{-E_2}{T}\right)}(X)^2 \tag{4.4}$$

Where Y is a dependent variable $\left(\frac{dX}{dt}\right)$, T and X are independent variables, A_1, E_1, A_2, A_3 and E_2 are model variables. Y values were obtained by calculating the conversion of DCPD from GC-MS analysis results and dividing by reaction time. Initial guess values were deduced from the literature and the non-linear regression

analysis results with a precision of R^2 =0.97 are given in Table 4.8. For the selected model, experimental Y values and the calculated Y values are compared in Table 4.9. The comparison between the parameters in literature and the experimental results were presented in Table 4.10.

Table 4.8: Regression analysis results of POLYMATH for reaction rate expression

Variable	*Initial Guess*	*Value*	*95% Confidence*
A1 (s^{-1})	$1.00x10^{16}$	$1.38x10^{16}$	$1.57x10^{15}$
E1 (k*J/K·mol*)$^{-1}$	$1.89x10^{4}$	$1.85x10^{4}$	65.70
A2	1.00	0.47	0.03
A3 *(L/mol)*s^{-1}	$2.00x10^{8}$	$2.02x10^{10}$	$1.51x10^{10}$
E2 (k*J/K·mol*)$^{-1}$	8600.00	$1.27x10^{4}$	444.90

Table 4.9: Comparison of regression analysis results and experimental results

$Y_{experimental}$	$Y_{calculated}$	ΔY	*Relative Error (%)*
3.16	2.86	0.30	9.49
6.76	5.49	1.27	18.79
17.07	17.79	-0.72	4.22
36.39	39.86	-3.47	9.54
50.23	43.10	7.13	14.19
52.15	55.10	-2.95	5.66

The kinetic parameters determined in this work deviate from the literature, especially for dimerization of CPD reaction. Pre-exponential factor and activation energy for CPD dimerization is determined as $2.02x10^{10}$ and 105.93 kJ/mol respectively which

are higher than the most of the results published in literature. In this study, DCPD monomerization reaction was conducted in GC-MS liner under constant pressure and flow conditions. The kinetic data obtained by determining monomerization kinetics in vapor-liquid mixture formed by flash vaporization is more realistic than the reaction kinetics pure liquid phase or vapor phase monomerization kinetics when the reactive distillation column conditions are considered. In fact, as presented in next part, Reactive Distillation Experiments and Modelling Results, simulation studies using the reaction rate expressions obtained in this study better fits to the experimental results when compared to the simulations carried out using the kinetic data from Xu et al. (2019).

Table 4.5: Comparison of the pre-exponential factors and activation energies of DCPD monomerization reaction

Comparison with Literature	*$k_0$forward s^{-1}*	*E_a forward (kJ/mol)*	*k_0 reverse $(L/mol)s^{-1}$*	*E_a reverse (kJ/mol)*
Herndon et al., 1967	$1.1x10^{13}$	142.1	NA	NA
Griffith et al., 1987	$4.0x10^{14}$	157.7	NA	NA
Langer and Patton, 1972	$5.0x10^{14}$	156.1	NA	NA
Palmova et al., 2001	$1.4x10^{14}$	157	$1.9x10^{7}$	75
Nurulinna et al., 2001	$2.6x10^{13}$	140.3	$1.2x10^{6}$	68.6
Xu et al., 2019	$1.2x10^{15}$	157.2	$1.4x10^{6}$	68.8
This Work	$1.4x10^{16}$	153.8	$2x10^{10}$	105.9

4.3.2 Reactive Distillation Experiments and Modelling Results

DCPD monomerization reaction is reversible, and reaction shifts towards to product side above 140°C where CPD is produced (Herndon et al., 1967). Therefore, in reactive distillation experiments, data was collected at the temperature range of 150°C-160°C to determine the vapor-liquid composition of DCPD and CPD in a reaction medium.

All reactive distillation experiments were performed by using pure DCPD as feedstock in the reaction flask initially. Then the reaction flask temperature was increased to the set value by an electric heater after the system was purged with nitrogen. The set temperature was altered and monitored from the electric heater. Reactive distillation experiments were conducted in two groups. In the first group, the system was operated at total reflux. In the total reflux experiments, condensate collection valve was held at close position and no condensate was collected over the duration of the experiments. In the second group of experiments, the vapor phase was collected as condensate on a graduated cylinder as shown in the Figure 3.3. Samples were collected from the reaction flask (liquid phase) and condensate (vapor phase) at specific time intervals throughout the experiments as given in Table 3.2. Samples collected in reactive distillation experiments were analyzed in GC-MS. The composition of CPD and DCPD in the vapor phase (condensate) and liquid phase (reaction flask) at the conclusion of experiment's duration are presented in Table 4.11. While both Experiment 27 and Experiment 29 were operated at total reflux and no condensate was collected, vapor phase samples were collected for Experiment 29. Condensate collection valve was opened once the experiment was started for experiments 31, 34, 36, 39 and 40.

Table 4.11: Reactive distillation experiments and results

Experiment Number	*Duration (h)*	*Temperature of Reaction Flask (°C)*	*%wt CPD in Liquid Phase*	*%wt CPD in VaporPhase*	*%wt DCPD in Liquid Phase*	*%wt DCPD in VaporPhase*	*CPD Volume in Condensate (mL)*
Experiment 27	3	160	1.32	Total Reflux	89.86	Total Reflux	Total Reflux
Experiment 29	1	160	1.14	71.35	98.57	25.67	Total Reflux
Experiment 31	1	160	1.31	88.52	98.39	11.49	80
Experiment 34	1	155	1.15	96.16	98.74	3.84	10
Experiment 36	2.5	150	0.89	94.77	99.11	5.23	8
Experiment 39	1	155	0.89	96.55	99.11	3.46	75
Experiment 40	1	150	1.28	97.20	98.72	2.80	24

Experiment 27 was conducted at total reflux conditions where the condensate valve was closed and monomerized CPD was not collected and recycled back to evaporating flask. It was observed from the GC-MS analysis that the CPD present in the reaction flask underwent side reactions and oligomerization product tricyclopentadiene (TCPD) formed after 50 minutes. The concentration of the TCPD increased up to 8.4% wt after 180 minutes of reaction at 160°C. Altough the DCPD concentration decreased over time, no significant change was observed in CPD concentration which is about 1.32 %wt. Detailed GC-MS chromatograms of Experiment 27 are given in Appendix I. DCPD, CPD and TCPD concentration change over time are shown in Figures 4.17 and Figure 4.18. Pure DCPD was present in the reaction flask initially and the time was recorded as the temperature of the system reached 160°C.

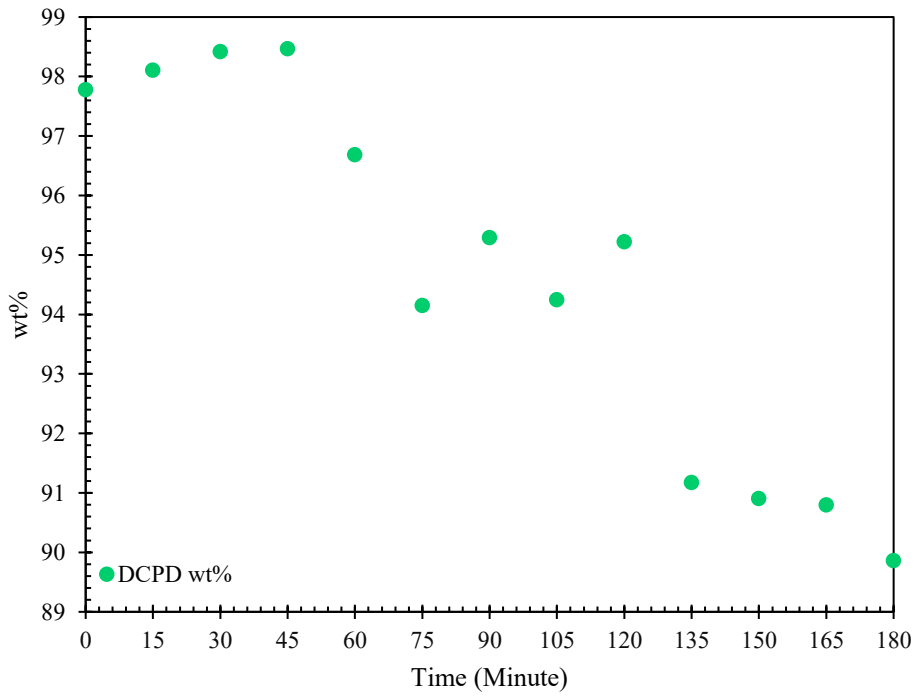


Figure 4.17: Weight percentage of DCPD over time at 160°C

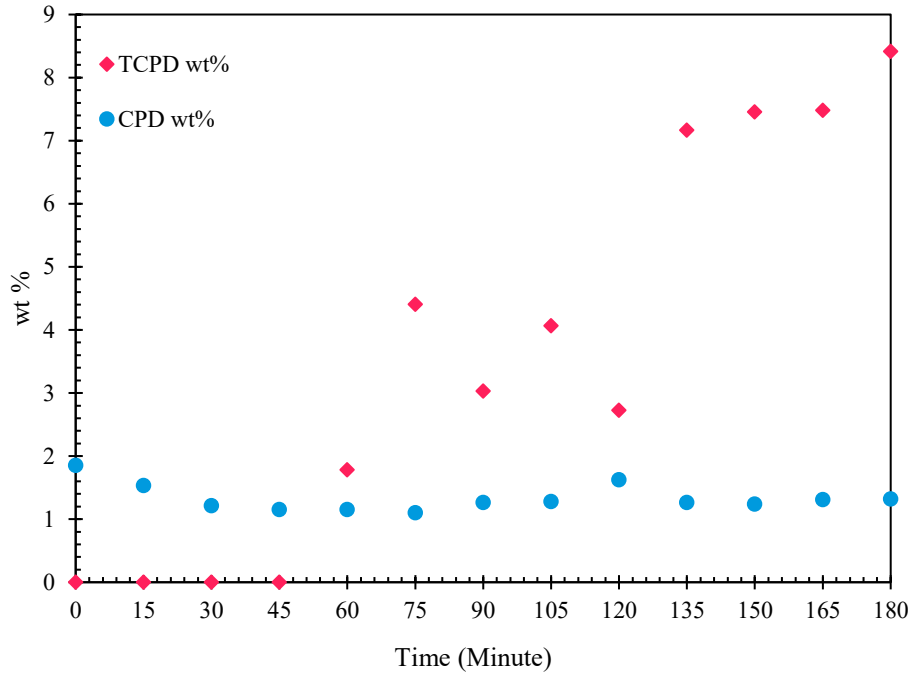


Figure 4.18: Weight percentages of CPD and TCPD over at 160°C

Therefore it was suggested that the monomerized CPD should be removed from the system in order to prevent the oligomerization reactions and the vapor phase was collected as condensate for experiments 31, 34, 36, 39 and 40. Experiments 31 and 36 were conducted with the condensate collection and the condensate valve was at an open position at 160°C for 1 hour and 150 °C for 2.5 hours respectively by starting with pure DCPD in the reaction flask initially. No oligomer formation was observed during these experiments. Therefore the CPD removal from the reaction medium eliminated the CPD loss due unwanted oligomerization reactions during the experiments. Condensate collection valve was opened at 155°C for 1 hour for Experiment 34 and 10 mL condensate was collected. When the set temperature changed to 160°C in Experiment 31, an increase in the volume of the collected condensate (80 mL) was observed. In Experiment 39, the set temperature was 155°C yet the condensate valve was opened at 20°C and 75 mL condensate was collected implying the monomerization starts before reaching 155°C. In Experiment 40, the set temperature was 150°C yet the condensate valve was opened at 20°C and 24 mL

condensate was collected. Results show that the DCPD monomerization is highly sensitive to temperature changes within the range of 150°C-160°C.

The experimental conditions and parameters of Experiment 39 were simulated in Aspen Plus by using 2 stage batch distillation column with reaction medium comprising only pot and condenser, similar to experimental set-up. Column dimentions were selected according to the dimentions of the laboratory apparatus. Set temperature of the electric heater was used for the heat transfer information in simulations. The parameters and data used in Aspen simulations are given in Table 4.12. The distillate mass flow rate was specified as 0.4 kg/min in agreement with the experimental results of Experiment 39**.** The kinetic parameters determined in this study were used in Aspen simulation, and the results are compared with experimental results. In addition, kinetic parameters published in literature were also tested by Aspen Simulation and the results are also compared with the experimental results obtained in this study as shown in Figure 4.19, 4.20, 4.21, 4.22 and 4.23.

Table 4.12: Aspen Plus inputs for the simulation of reactive distillation experiment

Parameter	*Aspen Input*
Property Method	Peng Robinson
Equipment	BatchSep
Number of Stage	*2*
Heat Transfer-Specified Medium Temperature	*155*°C
Pressure	*1 bar*
Initial Conditions	*Pad Gas Nitrogen*
Condenser Inlet Diameter	*2 cm*
Operating Steps	*Distillate Mass Flowrate*
	0.4 kg/min
Pot Volume	*5 L*
Condenser Temperature	*-20*°C

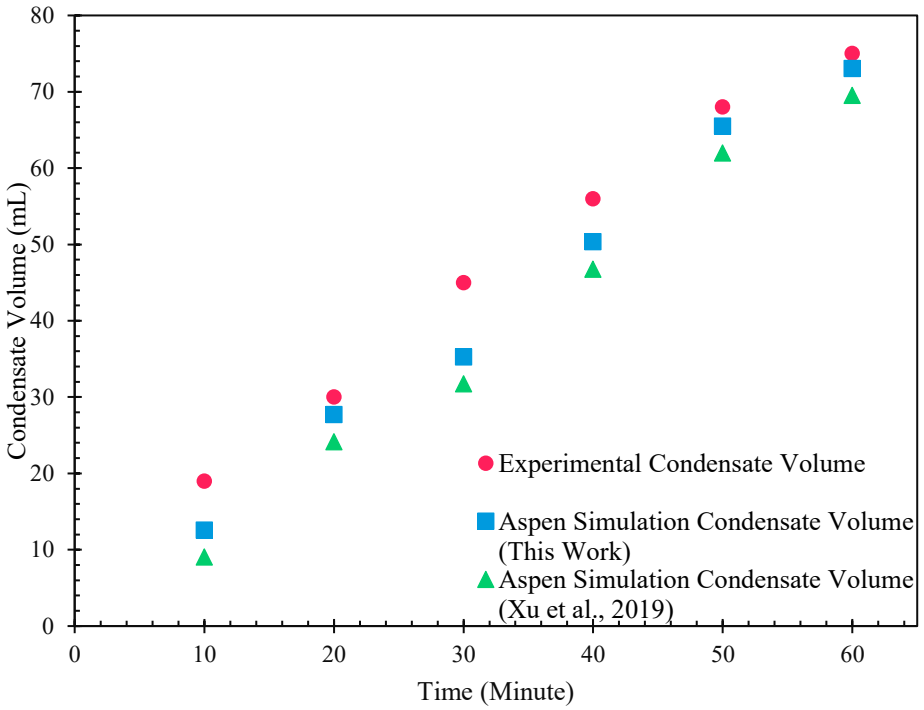


Figure 4.19: Condensate volume over time for experiments and model simulation

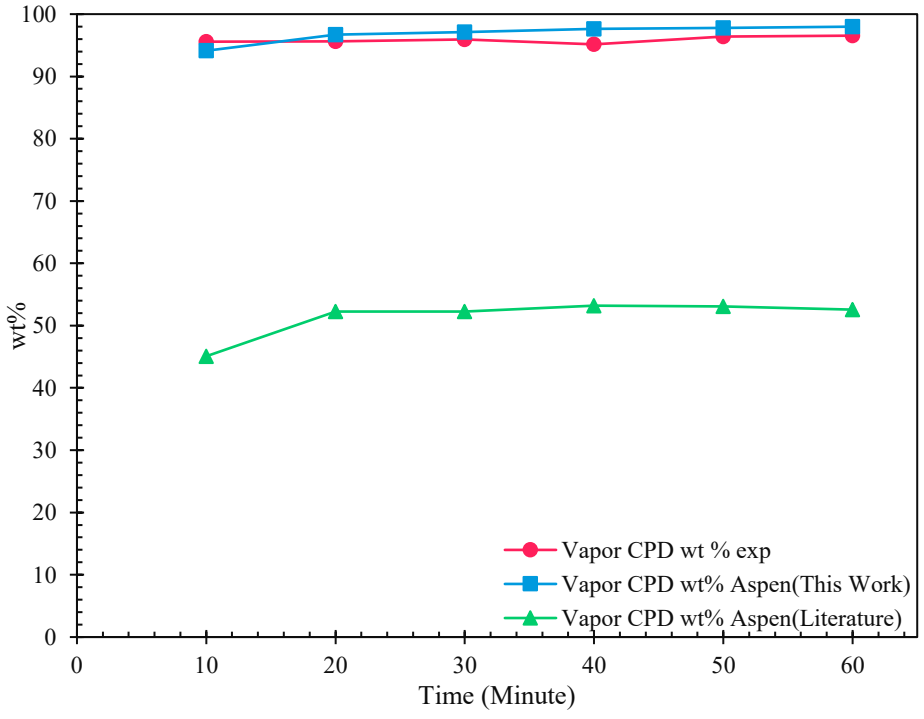


Figure 4.20: Model simulation for literature kinetics and the experimental kinetics for vapor phase (condensate) CPD's weight percentage

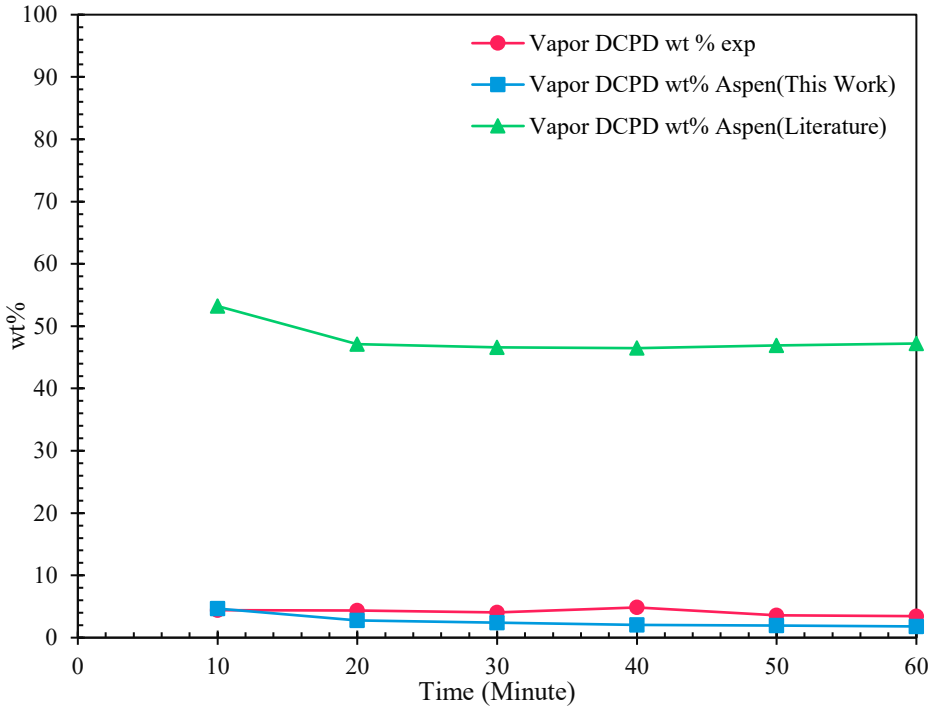


Figure 4.21: Model simulation for literature kinetics and the experimental kinetics for vapor phase (condensate) DCPD's weight percentage

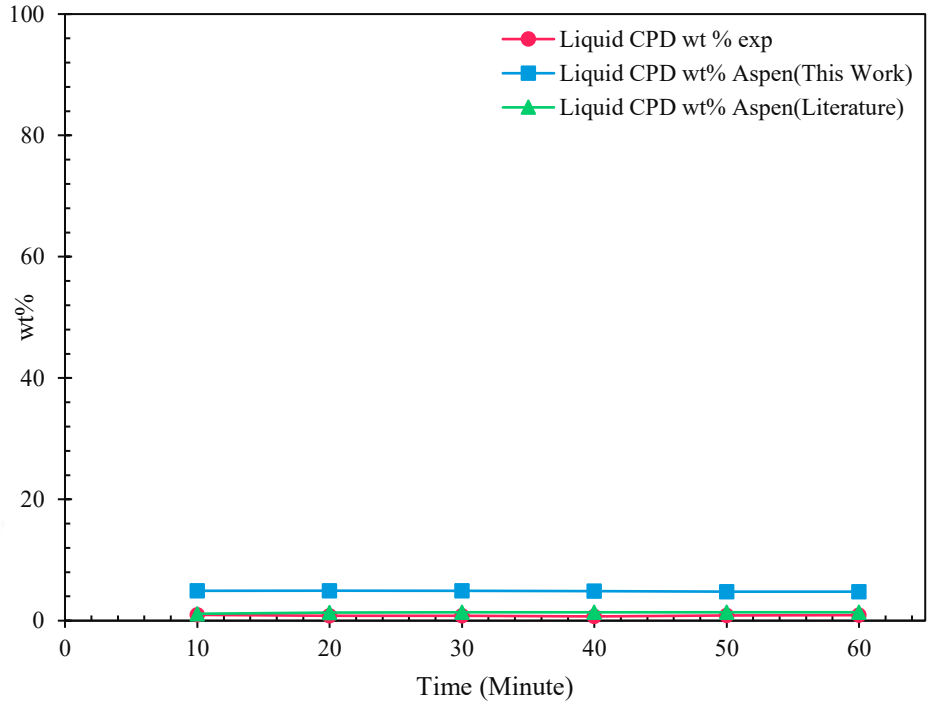


Figure 4.22: Model simulation for literature kinetics and the experimental kinetics for liquid phase (reaction flask) CPD's weight percentage

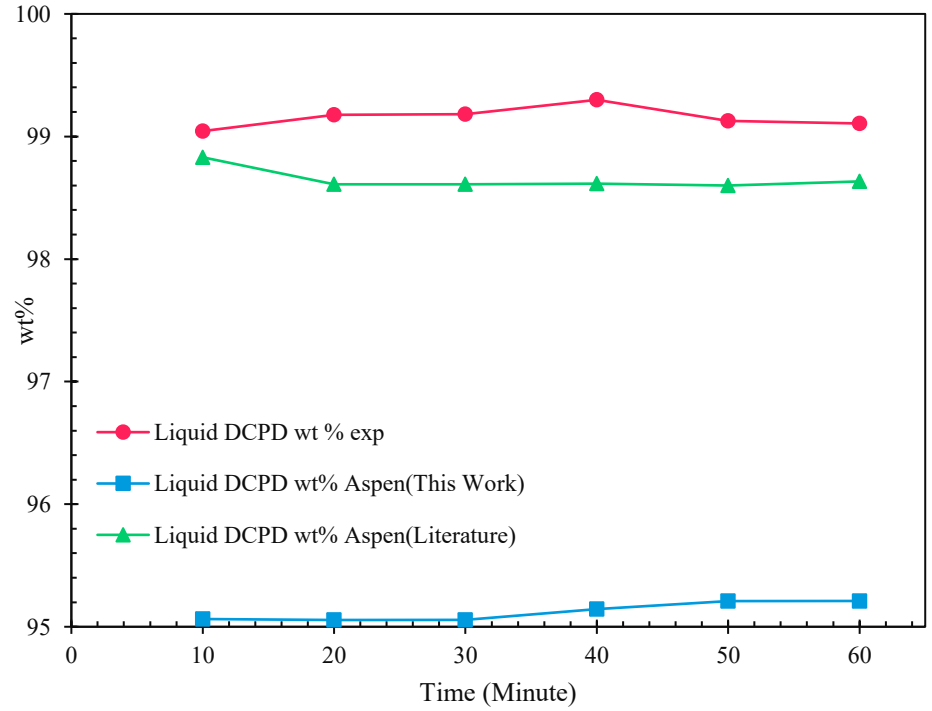


Figure 4.23: Model simulation for literature kinetics and the experimental kinetics for liquid phase (reaction flask) DCPD's weight percentage

Detailed GC-MS chromatograms of Experiment 39 are given in Appendix J. Figure 4.19 shows collected condensate volume over time for Experiment 39, and the both Aspen simulation results with kinetic parameters obtained in this work and literature. Condensate volume increases with time as reaction proceeds to produce CPD. Kinetic parameters determined in this study shows a better fit for the actual condensate volume collected in the experiment. Vapor phase samples were collected from the condensate while the liquid phase samples were collected from the reaction flask during the experiment. Compositions of CPD and DCPD in vapor phase (condensate) are shown in Figure 4.20 and Figure 4.21 while in liquid phase (reaction flask) are shown in Figure 4.22 and Figure 4.23 respectively. CPD can be obtained at a high purity in condensate. Low concentrations of CPD in reaction flask show the produced CPD can be separated from the reaction medium. Experimental kinetic data show a better fit for vapor phase (condensate) compositions. Slight deviations in the liquid phase compositions may result from the uncertainties coming from the VLE calculations of the chosen model.

4.4 Aspen Simulation of Seperation Sequence for the Production of CPD from PYGAS in an Industrial Scale

Our experimenal studies indicated that the benzene and lighter hydrocarbons can be separated from the PYGAS mixture while the DCPD separation requires more than one distillation step. Therefore, a distillation sequence was proposed for the separation of lighter hydrocarbons in the PYGAS mixture as the first step and then the reactive distillation of DCPD-rich mixture as second step. In second step, DCPD can be monomerized to CPD and CPD is separated *as distillate* from the remainings by a high boiling point difference. These two steps can be performed in the same distillation system for both batch and continuous operations.

In this thesis, two-step separation sequence of DCPD/CPD from PYGAS was simulated and examined in both batch and continuous industrial scale distillation systems by using Aspen Plus simulation software. As DCPD is a specialty chemical,

DCPD production capacity was kept at moderate level yet the scale of the production can be altered as needed. Since the consistency of VLE and reaction kinetics data were tested as shown in previous sections, large-scale simulation can be performed with confidence. As raw material, PYGAS can be obtained from SOCAR in Turkey and the PYGAS composition is accepted as not variant. However, the update on the simulation can be achieved easily for any changes in the composition of PYGAS.

Industrial scale production of CPD from PYGAS was simulated in two stages; removal of the benzene and lighter hydrocarbons from the PYGAS mixture and DCPD purification by reactive distillation system where CPD is collected at desired purity. CPD readily dimerizes into DCPD at or above room temperatures, therefore, no additional reactor for the dimerization is required. Dimerization of CPD to DCPD can be achieved by storing the distillate for a prolonged time under proper storing conditions.

For the first stage, the aim is to separate benzene and lighter hydrocarbons from the PYGAS mixture. Medium-pressure steam was selected as a utility for the pot heating with 175°C inlet and 173°C outlet temperature due its lower cost and availability to meet the heating requirements (Towler & Sinnot, 2013). The column pressure was selected below atmospheric pressure for both batch and continuous columns to prevent the unwanted reactions during separation at the first stage. Kinetic data was provided from the experimental studies as reaction information, yet the temperature was kept low by decreasing the pressure of the system to 0.6 bar in order to prevent reaction formation. Packed columns are preferred for the column diameters smaller than 76 cm due to lower cost of the equipment. Column height and the column diameter were determined by trials with the rule of thumb of column height/column diameter ratio should be smaller than 20. 16 mm metal rings as packing materials were selected according to the column diameter due to their low packing factor and to increase mass transfer (Wankat, 2016), (Douglas, 1988). Number of stages represents the Aspen Plus calculation nodes in the column therefore selected as 35. The bottom stream of the column was used as the feed for the second stage simulation. In the second stage, it was aimed to monomerize DCPD to CPD and

collect CPD at higher purity from condensate. Medium-pressure steam was selected as a utility for the pot heating with 175°C inlet and 173°C outlet temperature and the pressure was selected above atmospheric pressures to increase the reaction rate without increasing temperature and allowing the oligomer formation. The condenser temperature was fixed to -20°C to prevent dimerization of CPD to DCPD in the condenser. During the development of the model, only reversible reactions of the DCPD and Met-DCPD were considered by making the Met-DCPD as a representative component for other co-dimer as well. It was assumed that the vapor-liquid equilibrium was not disturbed by the reversible reaction of DCPD and Met-DCPD within the reactive distillation system. Due to the lack of kinetic information for the reversible Met-DCPD monomerization reaction in the literature, kinetic data obtained from the GC-MS reaction experiments for DCPD was used.

4.4.1 Batch Distillation Column Simulation

Two-step separation sequence of DCPD/CPD from PYGAS was simulated in both batch and continuous distillation systems for operational flexiblity by using Aspen Plus simulation software. In the first step, benzene and lighter hydrocarbon separation was simulated. In the second step, reactive distillation of DCPD was investigated in batch operating column simulation.

4.4.1.1 Benzene and Lighter Hydrocarbons Removal Batch Column Simulation

The first step of the proposed separation sequence is the removal of the benzene and lighter hydrocarbons. Simulations were conducted in Aspen Plus for batch operating column in BatchSep equipment and the inputs are given in Table 4.13. It was aimed to detain all DCPD content in the pot, while removing the benzene and lighter hydrocarbons from the PYGAS mixture. The acceptable DCPD loss from the initial mass in PYGAS mixture was determined as %5 wt, therefore, design specifications

were selected. Pot temperature and the composition change of DCPD, benzene and CPD in pot are given in Figure 4.24 and Figure 4.25 respectively.

Table 4.13: Aspen Plus inputs for the batch operating simulation of industrial scale removal of benzene and lighter hydrocarbons

Parameter	*Aspen Input*
Property Method	Peng Robinson
Equipment	BatchSep
Number of Stage	*35*
Reflux Ratio	*1*
Heat Transfer	Steam Heating
Steam Temperature	*175°C Maximum Duty*
Initial Conditions	*Total Initial Charge*
Packing Type	*Metal Pall Ring 16mm*
Column Diameter	*40 cm*
Column Height	*2 m*
Pressure	*0.6 bar*
Condenser Inlet Diameter	*45 cm*
Operating Steps	*Mass Fraction of DCPD in Pot ≥ 0.62*
Pot Volume	*1000 L*
Operating Time	*1 h*
Reaction	*Occur in All Stages*
Condenser Temperature	*Total Condenser*

Figure 4.24 indicates that the pot temperature increases as benzene and lighter hydrocarbons removed from the system. As it can be seen from the Figure 4.25, CPD mass fraction does not increase in pot as no CPD is produced by monomerization reaction at selected pressure and temperature. Benzene removal from the distillation column increases the DCPD mass fraction in pot at first step of the separation sequence. Effect of the column pressure on DCPD mass fraction, DCPD mass, the

benzene mass in pot and pot temperature are also investigated in Aspen Plus simulations. Simulation results are given in Figure 4.26, Figure 4.27, Figure 4.28 and Figure 4.29 respectively. It was concluded that the optimum column pressure can be selected as 0.6 bar for higher DCPD mass fraction and DCPD yield with low benzene residue. As pressure exceeds 0.6 bar, monomerization of the DCPD is observed due increasing temperatures of the pot. Optimization analysis was also conducted for the reflux ratio. Effect of the reflux ratio on DCPD mass fraction, DCPD mass, the benzene mass in pot and pot temperature are given in Figure 4.30, Figure 4.31, Figure 4.32 and Figure 4.33 respectively when the pressure was fixed to 0.6 bar. Both final mass fraction and the amount of DCPD in pot increases with reflux ratio, however, when the reflux ratio exceeds 1 DCPD mass fraction decreases due to increasing mass fractions of Met-DCPD group. Therefore optimum reflux ratio was selected as 1. It can also be concluded that the reflux ratio does not have a significant effect on pot temperature of the distillation column for the benzene and lighter hydrocarbon separation step (Figure 4.33).

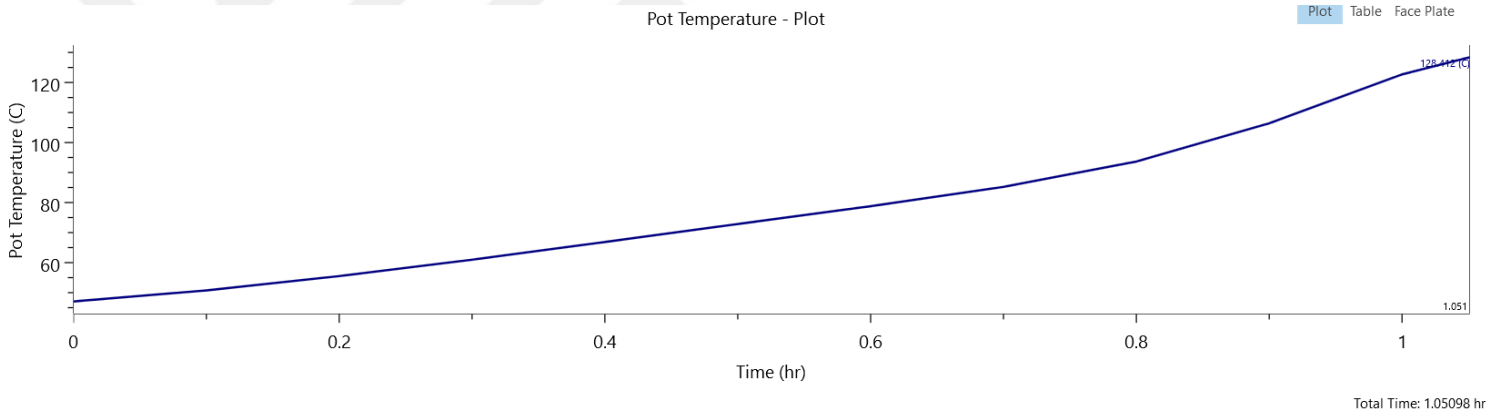


Figure 4.24: Pot temperature over time for lighter hydrocarbon separation simulation

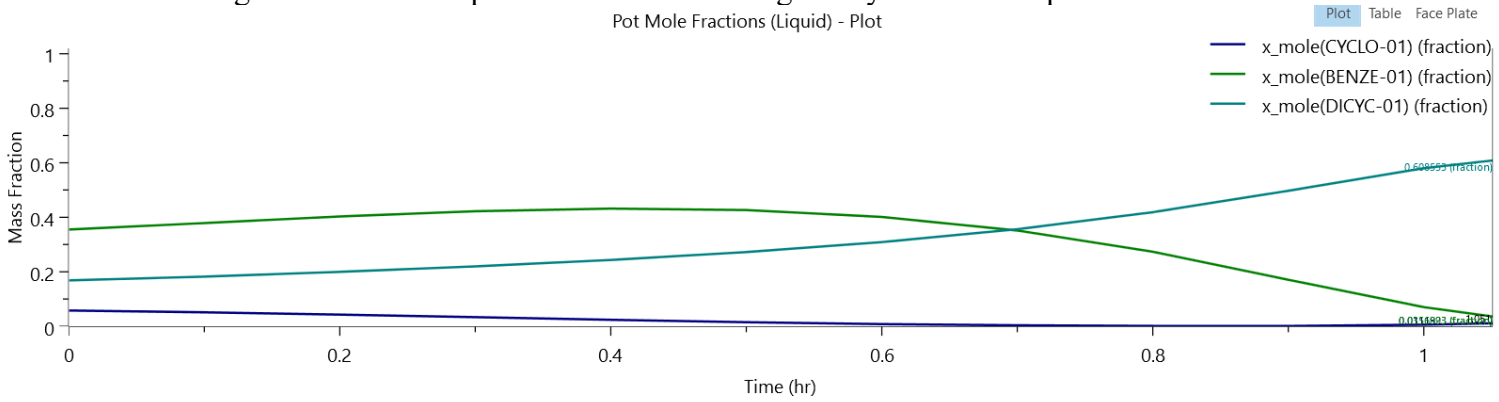


Figure 4.25: Pot composition of CPD, benzene and DCPD over time for lighter hydrocarbon separation simulation

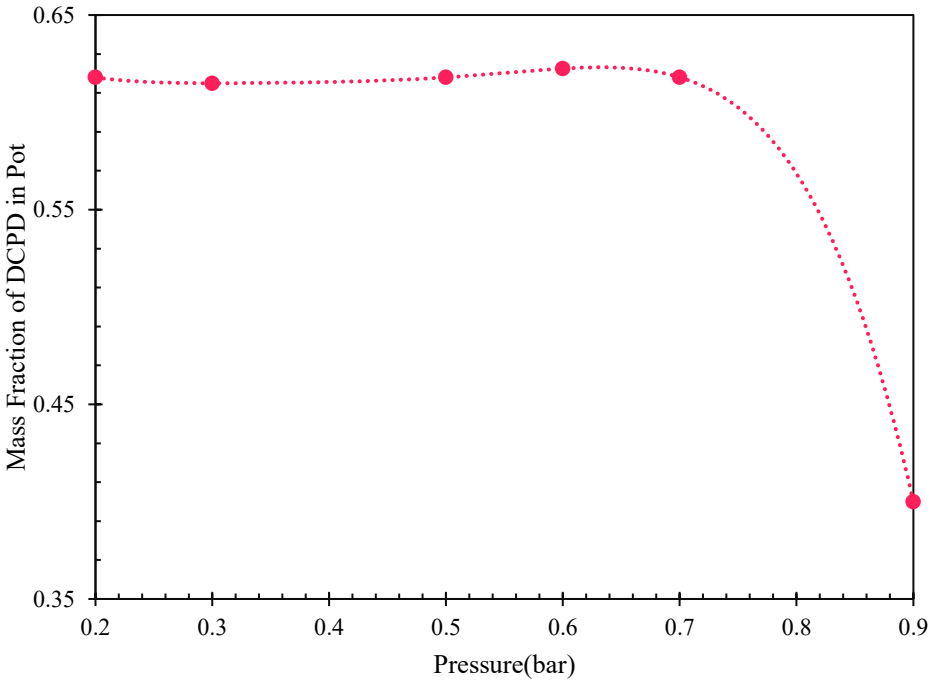


Figure 4.26: Effect of column pressure on mass fraction of DCPD in pot for lighter hydrocarbon separation simulations

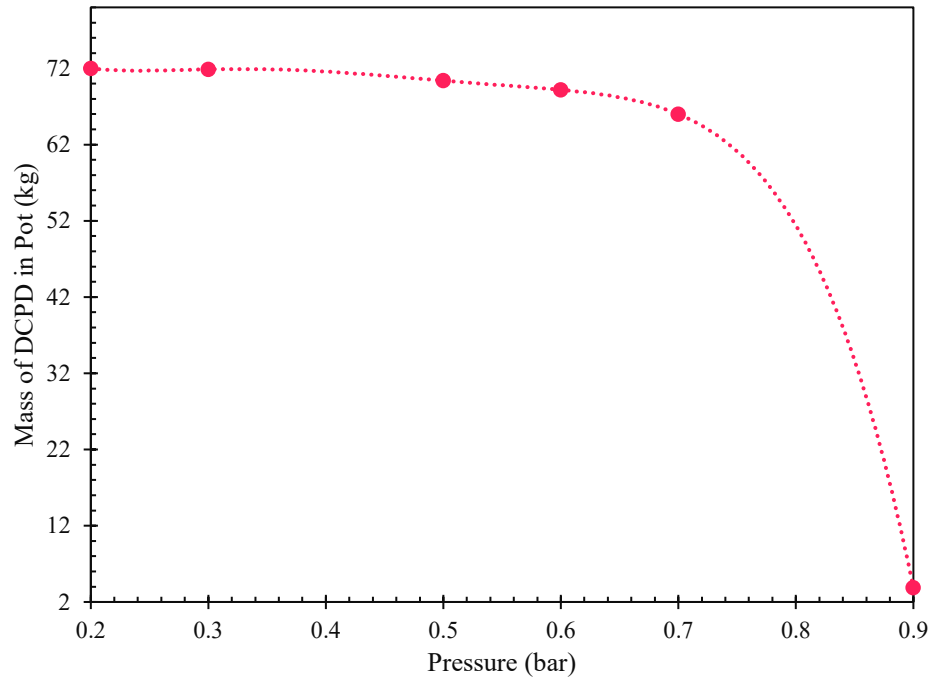


Figure 4.27: Effect of column pressure on DCPD mass in pot for lighter hydrocarbon separation simulations

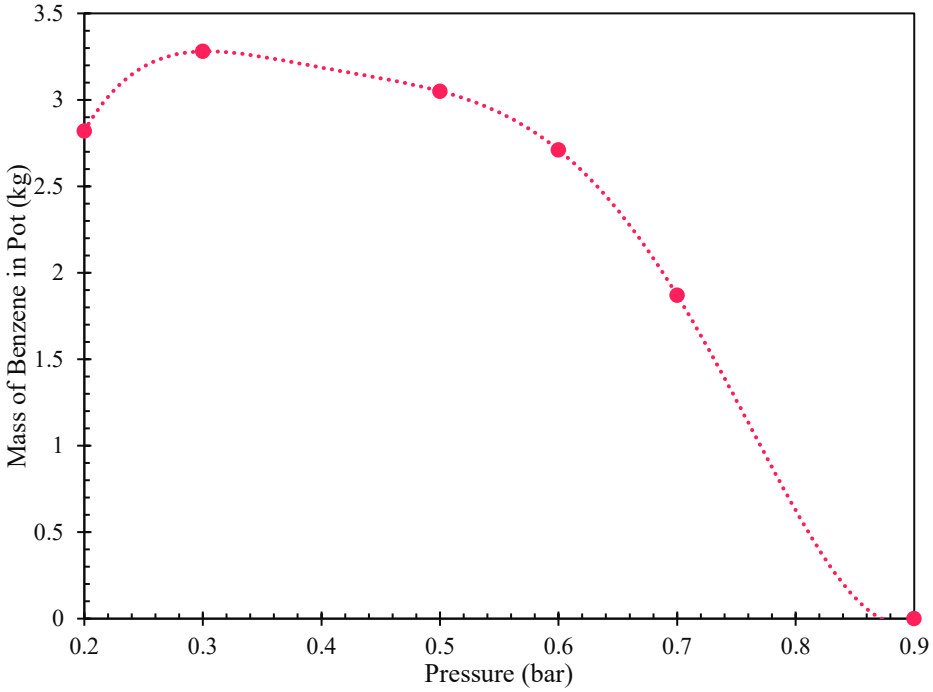


Figure 4.28: Effect of column pressure on benzene mass in pot for lighter hydrocarbon separation simulations

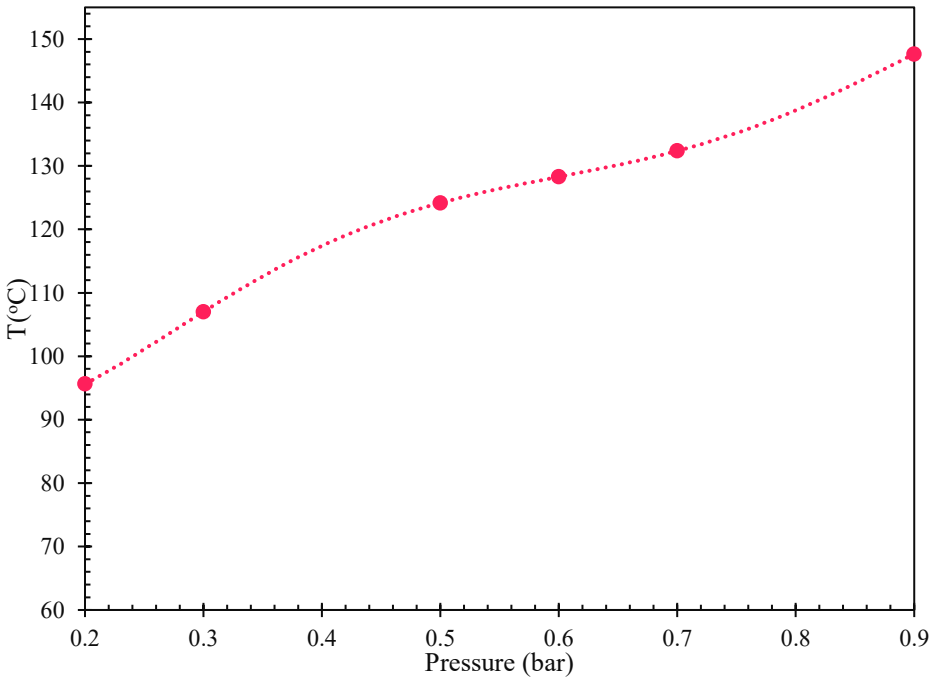


Figure 4.29: Effect of column pressure on pot temperature for lighter hydrocarbon separation simulations

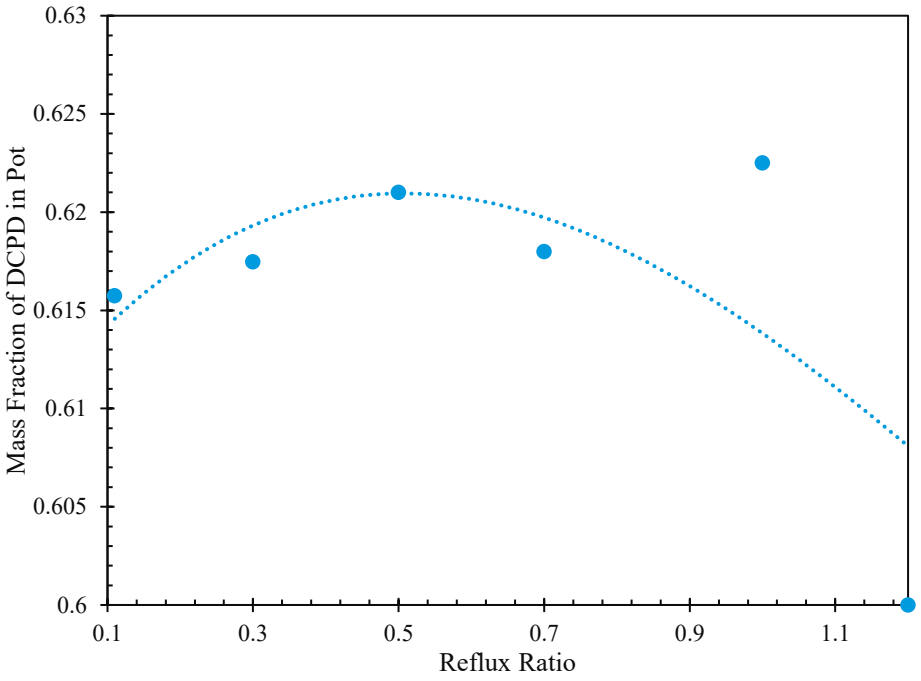


Figure 4.30: Effect of reflux ratio on mass fraction of DCPD in pot for lighter hydrocarbon separation simulations

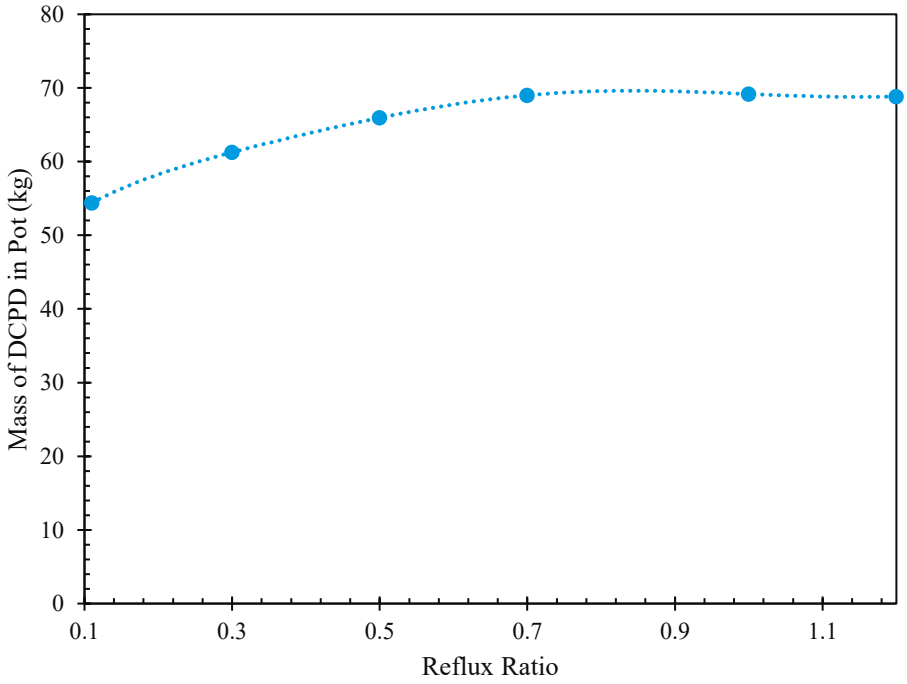


Figure 4.31: Effect of reflux ratio on DCPD mass in pot for lighter hydrocarbon separation simulations

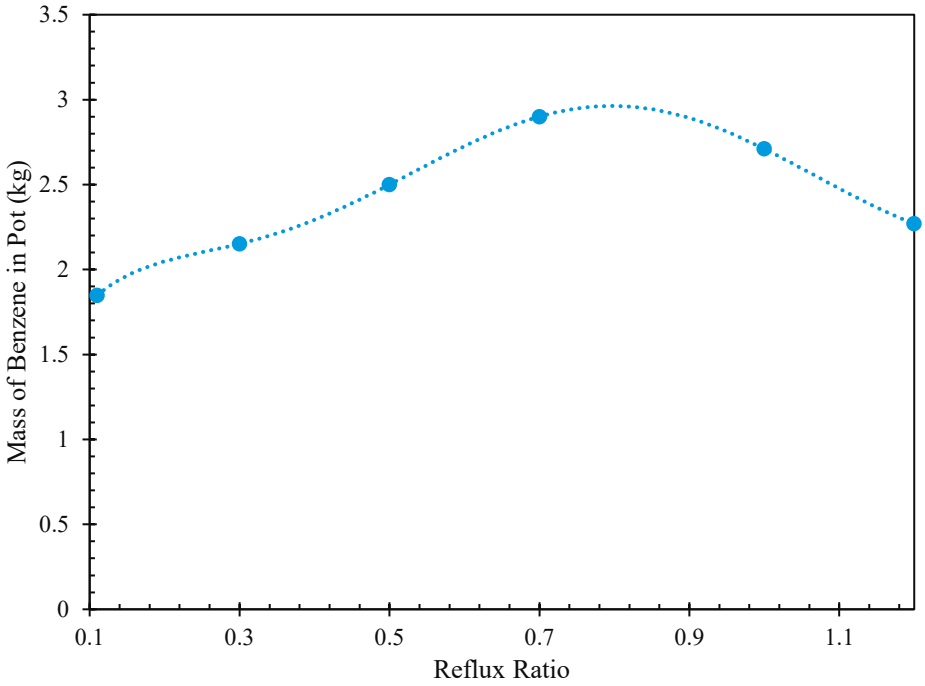


Figure 4.32: Effect of reflux ratio on benzene mass in pot for lighter hydrocarbon separation simulations

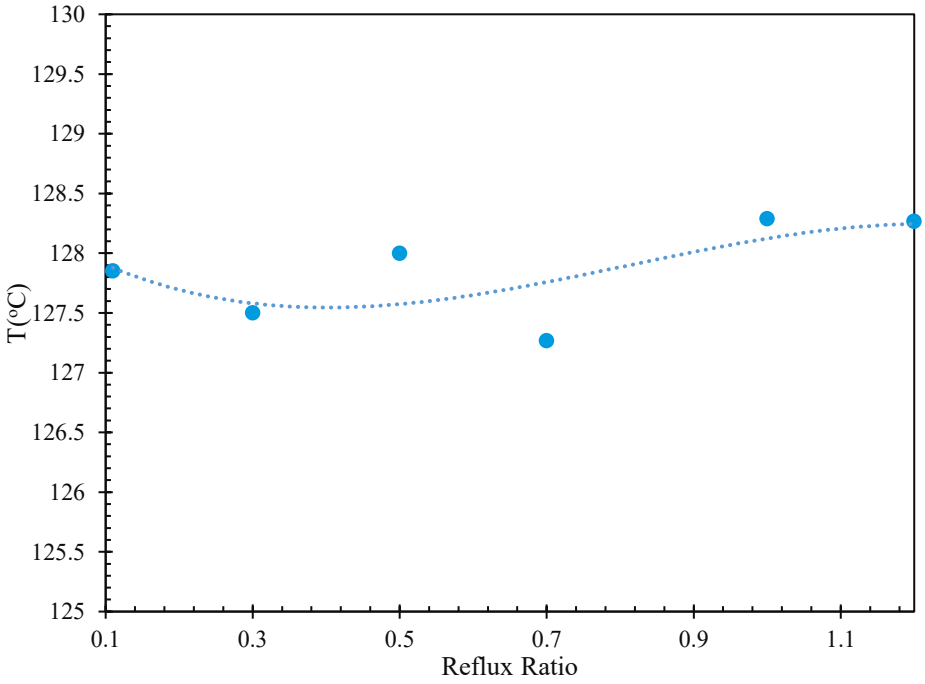


Figure 4.33: Effect of reflux ratio on pot temperature for lighter hydrocarbon separation simulations

4.4.1.2 Reactive Distillation Batch Column Simulation

The second step of the proposed separation sequence is reactive distillation where DCPD monomerizes to CPD and, CPD is separated from the remainings. Simulation studies were conducted in Aspen Plus and the inputs are given in Table 4.14. Pot temperature along with the CPD and DCPD composition change with time in distillate are given in Figure 4.34 and Figure 4.35 respectively. Reaction rates of CPD, DCPD, Met-CPD and Met-DCPD are given in Figure 4.36. It can be seen that the monomerization of DCPD in pot starts around 140°C and the CPD mass fraction gradually increases in distillate to a desired purity of ≥90% wt. Reaction rate of DCPD monomerization increases with pot temperature and decreases as the DCPD concentration decreases. Reaction rate of Met-DCPD is lower than that of DCPD, due to lower concentrations in the remaining PYGAS mixture since the same reaction information was used for both reactions. Pot compositions of CPD, DCPD, Met-CPD and Met-DCPD over time are given in Figure 4.37 where significant decrease in the mass fraction of DCPD is observed. Effect of the column pressure on CPD mass fraction in distillate, CPD mass in distillate, and the pot temperature are given in Figure 4.38, Figure 4.39 and Figure 4.40 respectively. As pressure increases, the amount of CPD collected in distillate increases however in order to decrease the operational and equipment costs, maximum operating pressure was selected as 1.5 bar. Effect of reflux ratio on CPD mass fraction in distillate, CPD mass in distillate, and the pot temperature are also shown in Figure 4.41, Figure 4.42 and Figure 4.43 respectively. A minimum reflux ratio of 2.5 is needed in second step in order to have CPD purity higher than %92 wt. When the reflux ratio is fixed to 2.5, 61.4 kg CPD can be retrieved in disttilate. In order to increase the CPD amount to 76.48 kg in distillate, reflux ratio can be increased up to 10 at the cost of increasing the operational costs. When the reflux ratio exceeds 10, CPD yield decreases due to lower distillat collection rates (Figure 4.42). Therefore reflux ratio should be selected between 4 and 10, optimum value was determined as 8 in this study. As can be seen

in Figure 4.43, temperature of the pot is higher for lower reflux ratios due to poor separation of DCPD from CPD in the reactive distillation system.

Table 4.14: Aspen Plus inputs for the batch operating simulation of industrial scale production of CPD

Parameter	*Aspen Input*
Property Method	Peng Robinson
Equipment	BatchSep
Number of Stage	*35*
Reflux Ratio	*8*
Heat Transfer	Steam Heating
Steam Temperature	*175°C Maximum Duty*
Initial Conditions	*Pad Gas Nitrogen*
Packing Type	*Metal Pall Ring 16mm*
Column Diameter	*40 cm*
Column Height	*2 m*
Pressure	*1.5bar*
Condenser Inlet Diameter	*45 cm*
Operating Steps	*Mass Fraction of CPD in Distillate ≥ 0.92*
Pot Volume	*1000 L*
Operating Time	*1 h*
Reaction	*Occur in All Stages*
Condenser Temperature	*-20°C*

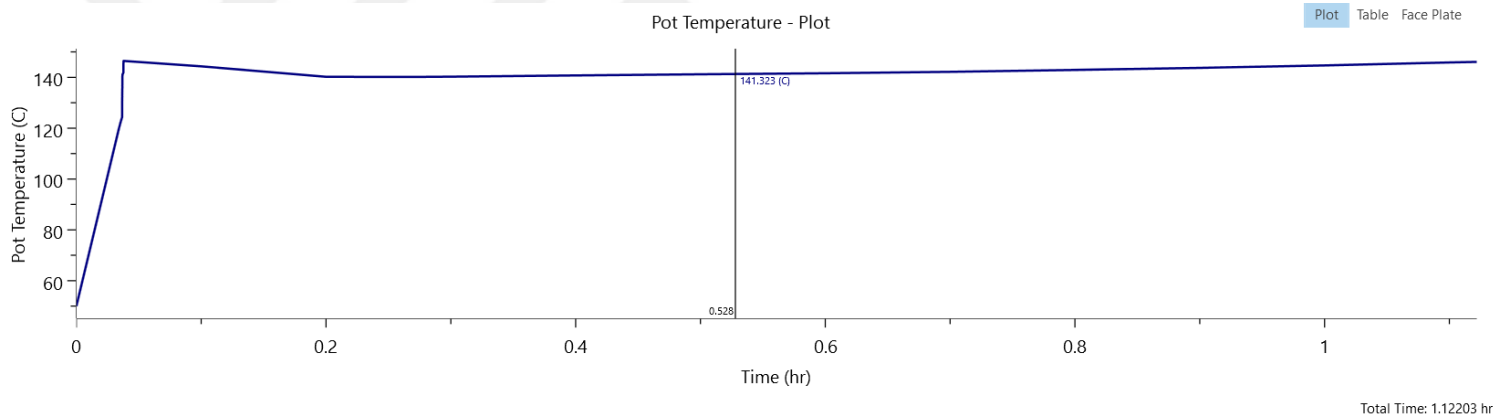


Figure 4.34: Pot temperature over time for reactive distillation simulation

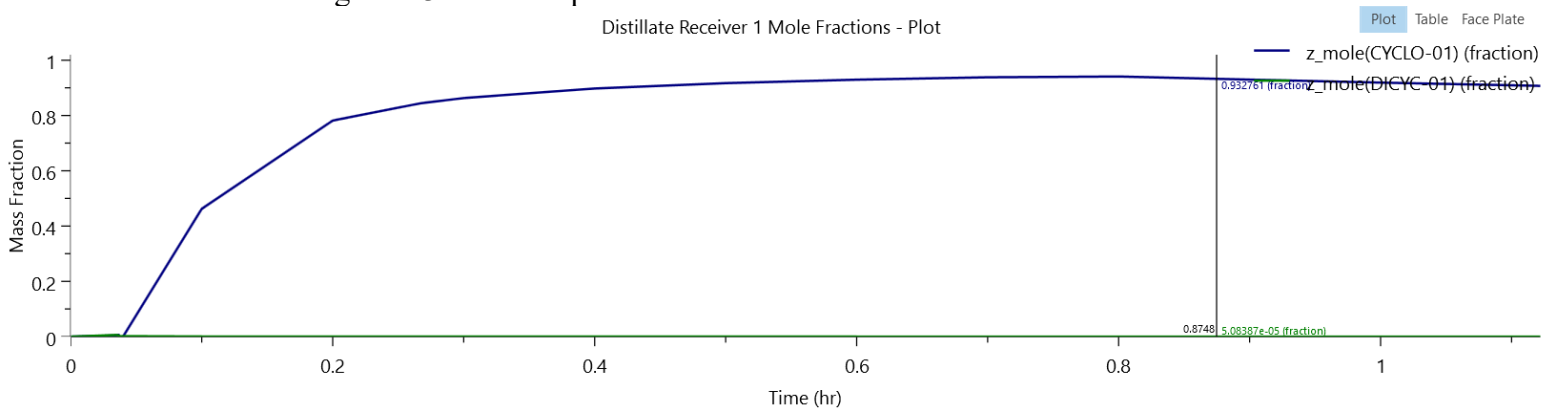


Figure 4.35: Distillate composition of CPD and DCPD over time for reactive distillation simulation

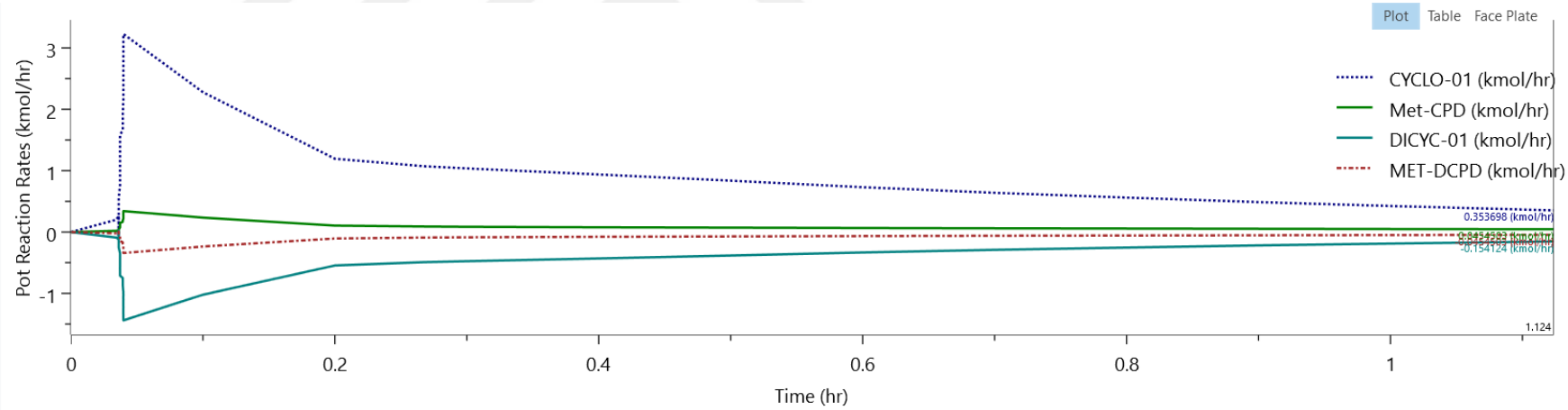


Figure 4.36: Reaction rates over time for CPD, DCPD, Met-CPD and Met-DCPD

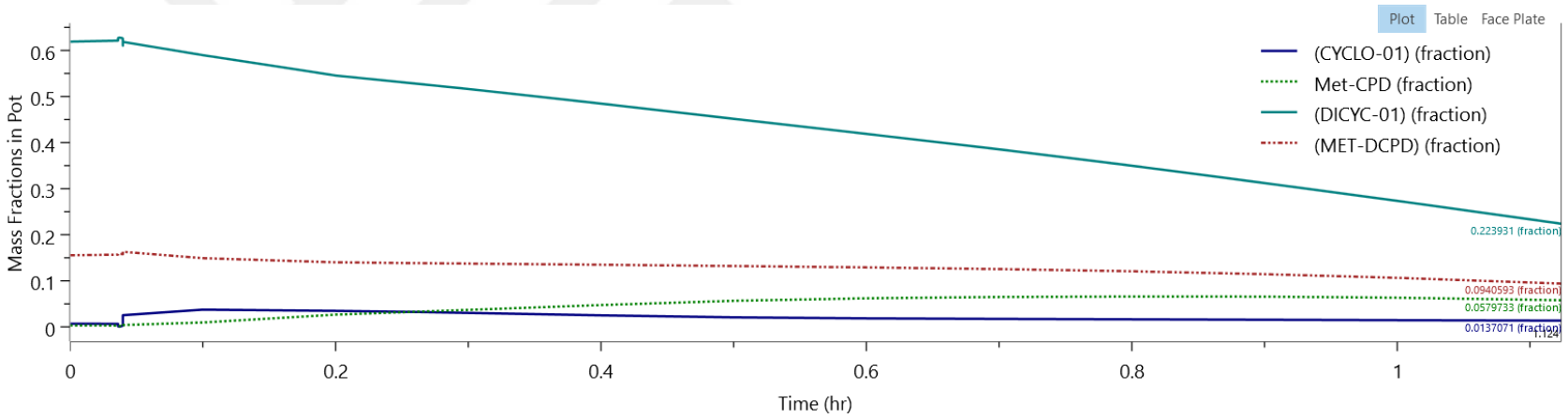


Figure 4.37: Compositions of CPD, DCPD, Met-CPD and Met-DCPD over time in pot

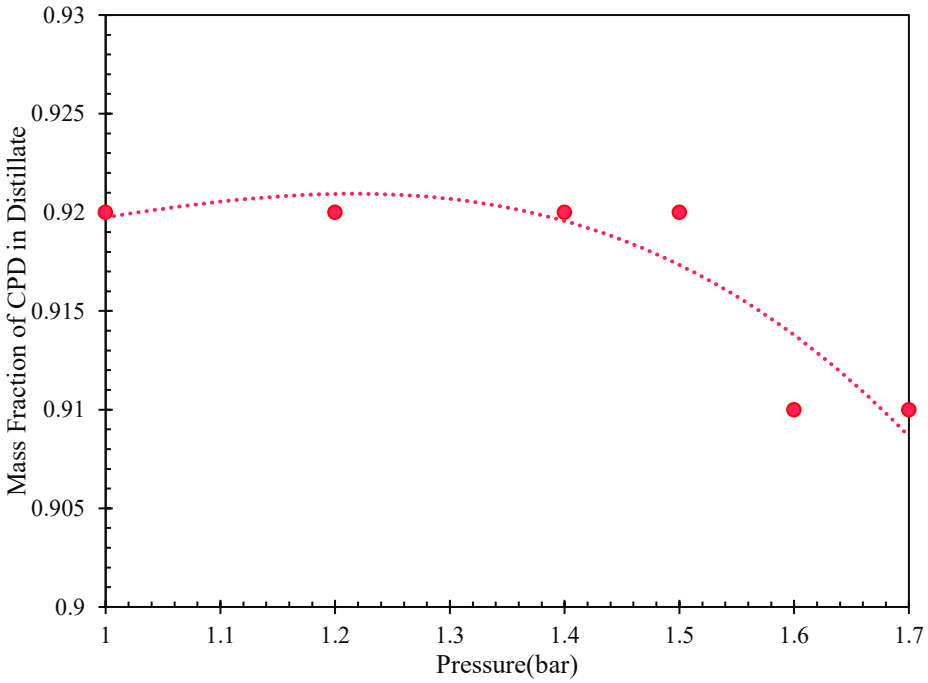


Figure 4.38: Effect of pressure on mass fraction of CPD in distillate for reactive distillation simulations

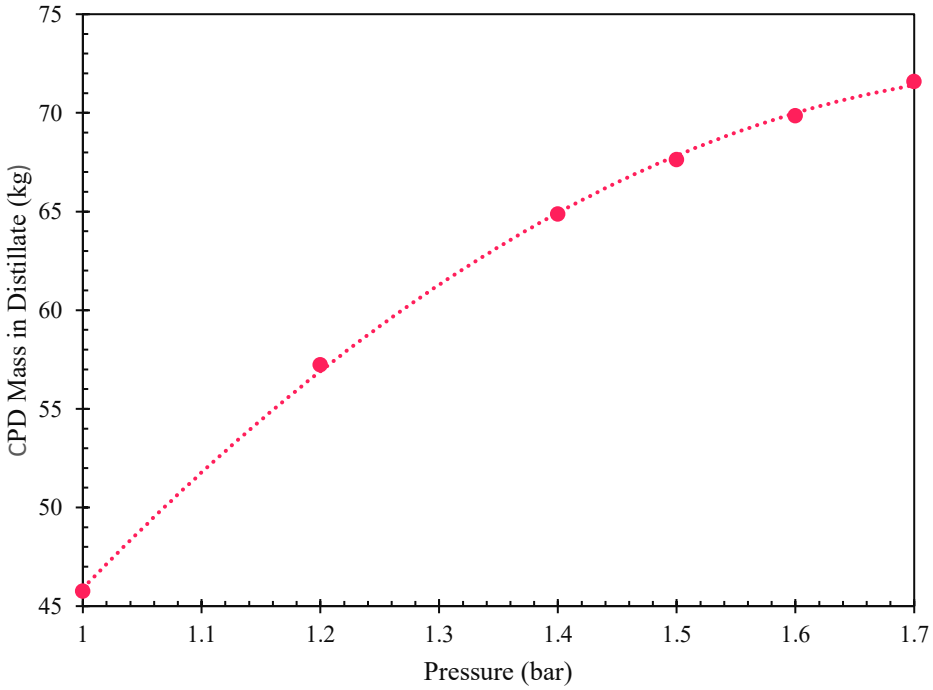


Figure 4.39: Effect of pressure on CPD mass in distillate for reactive distillation simulations

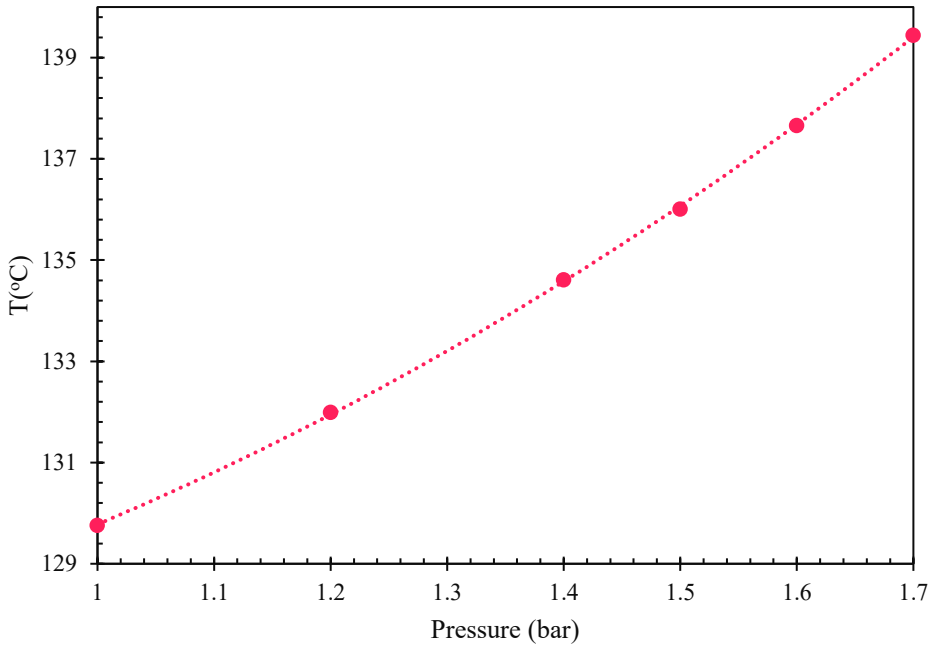


Figure 4.40: Effect of pressure on pot temperature for reactive distillation simulations

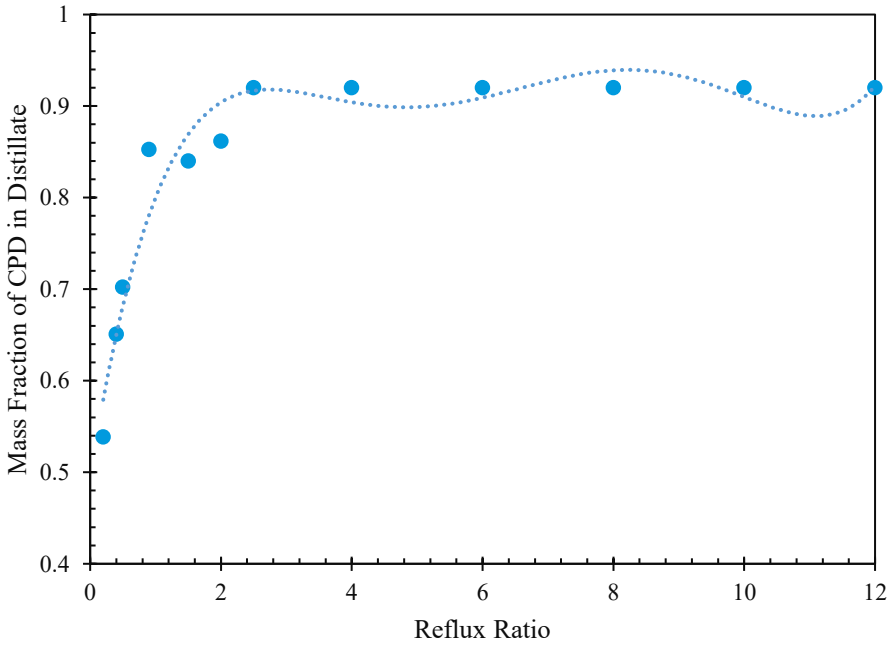


Figure 4.41: Effect of reflux ratio on mass fraction of CPD in distillate for reactive distillation simulations

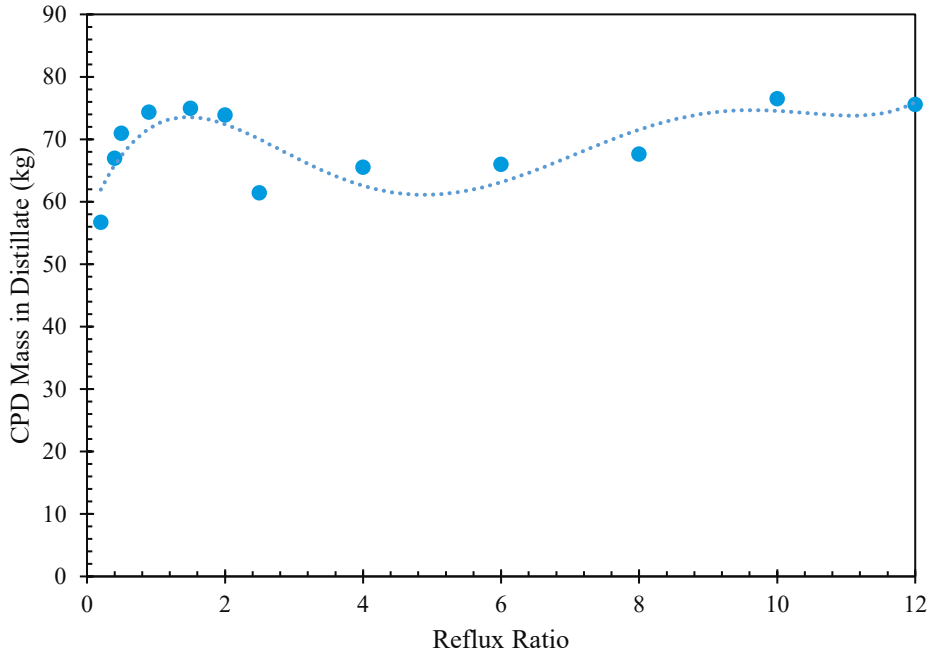


Figure 4.42: Effect of reflux ratio on CPD mass in distillate for reactive distillation simulations

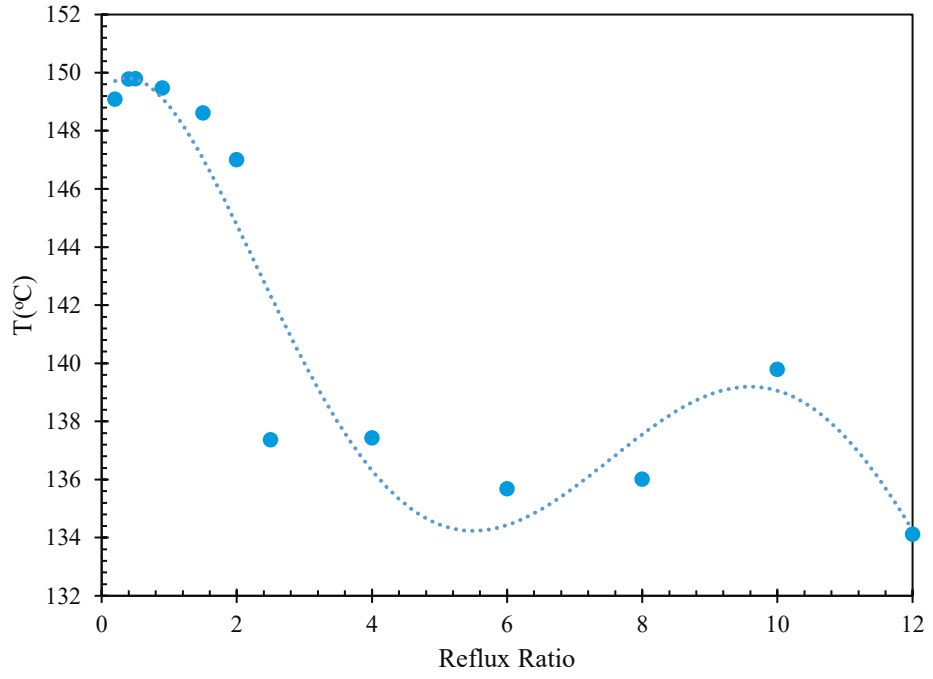


Figure 4.43: Effect of reflux ratio on pot temperature for reactive distillation simulations

4.4.2 Continuous Operating Column Simulation

Benzene and lighter hydrocarbon separation and the reactive distillation of DCPD is also examined in continuous operating column simulation.

4.4.2.1 Benzene and Lighter Hydrocarbons Removal Continuous Column Simulation

The first step of the proposed separation sequence for the removal of the benzene and lighter hydrocarbons were simulated in Aspen Plus for continuous operating column and the inputs are given in Table 4.15.

Table 4.15: Aspen Plus inputs for the continuous operating simulation of industrial scale removal of benzene and lighter hydrocarbons

Parameter	*Aspen Input*
Property Method	Peng Robinson
Equipment	RadFrac
Number of Stage	*35*
Reflux Ratio	*1*
Heat Transfer	Steam Heating
Steam Temperature	*175°C Medium Pressure Steam*
Packing Type	*Metal Pall Ring 16mm*
Column Diameter	*40 cm*
Column Height	*2 m*
Pressure	*0.6 bar*
Design Spesifications	*Mass Fraction of DCPD in Distillate ≥ 0.62*
Reaction	*Starting Stage:32* *Ending Stage:34*
Operation Time	*1 h*

4.4.2.2 Reactive Distillation Continuous Column Simulation

Separation sequence for the removal of CPD by the reactive distillation method was also studied in continuous operating column and the Aspen Plus simulation inputs are given in Table 4.16.

Table 4.16: Aspen Plus inputs for the continuous operating simulation of industrial scale production of CPD

Parameter	*Aspen Input*
Property Method	Peng Robinson
Equipment	RadFrac
Number of Stage	*35*
Reflux Ratio	*8*
Heat Transfer	Steam Heating
Steam Temperature	*175°C Medium Pressure Steam*
Packing Type	*Metal Pall Ring 16mm*
Column Diameter	*40 cm*
Column Height	*2 m*
Pressure	*1.5 bar*
Design Spesifications	*Mass Fraction of CPD in Distillate ≥ 0.92*
Reaction	*Starting Stage:32* *Ending Stage:34*
Operation Time	*1 h*

Temperature and composition profiles of continuous operating columns for lighter hydrocarbon separation and reactive distillation are given in Figure 4.44, Figure 4.45, Figure 4.46 and Figure 4.47 respectively. Stage 35 represents the reboiler while stage 1 represents the condenser where stages are the calculation nodes in packed column. DCPD and benzene can be removed in the first column as can be seen in Figure 4.46 and obtained as bottoms and distillate product respectively. In the second

column, monomerization of DCPD and subsequent separation of CPD allows high concentrations of CPD in distillate (Figure 4.47).

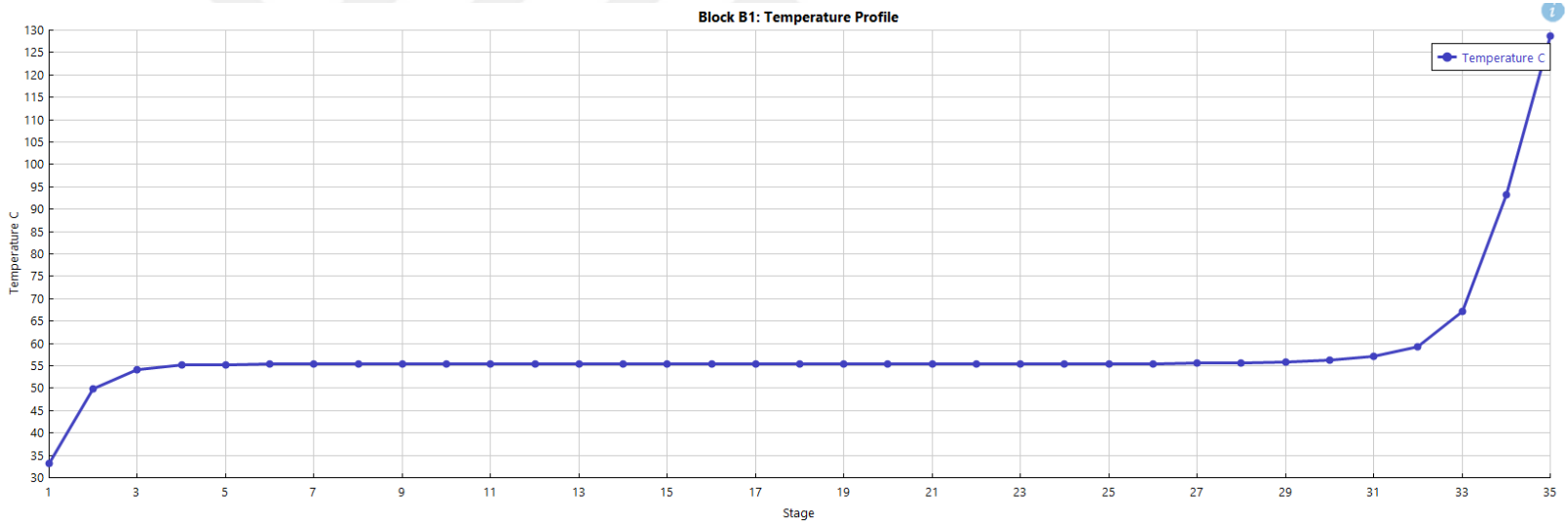


Figure 4.44: Temperature profile of continuous operating column for lighter hydrocarbon separation simulation

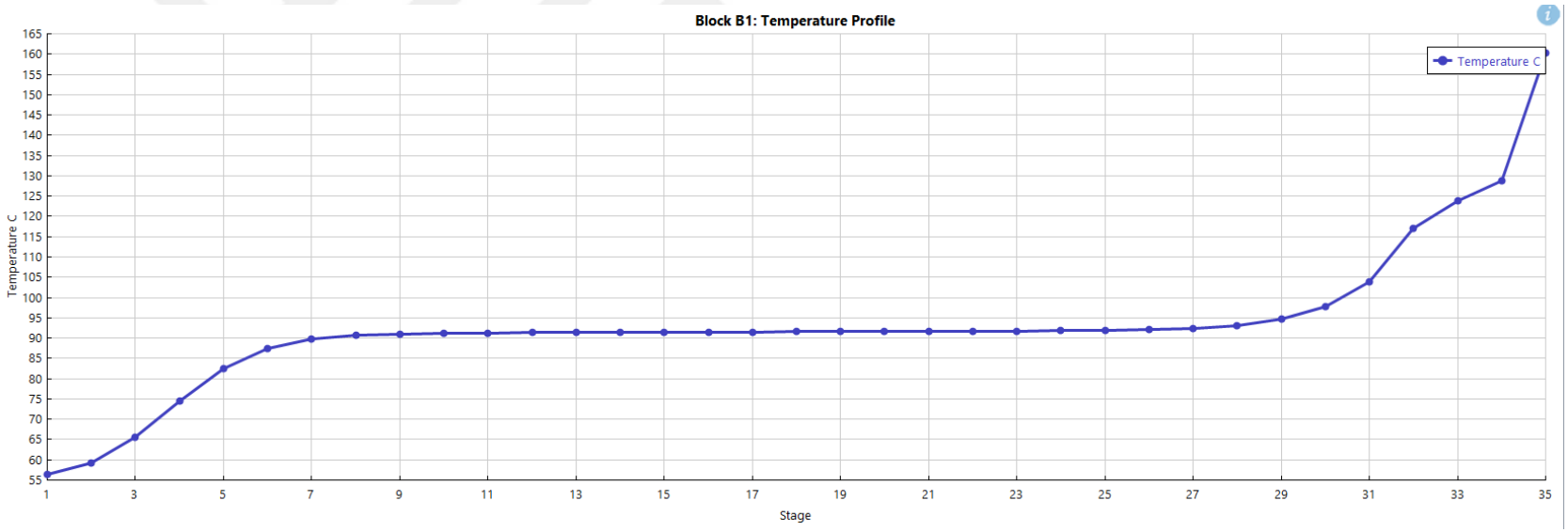


Figure 4.45: Temperature profile of continuous operating column for reactive distillation simulation

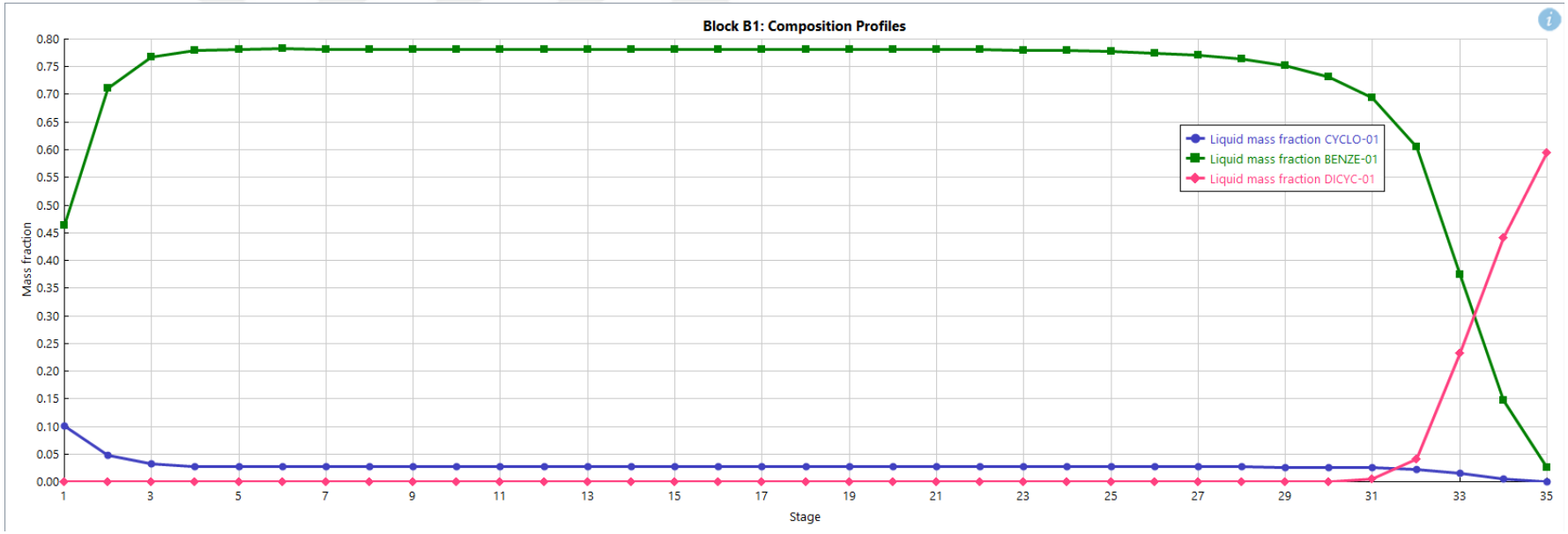


Figure 4.46: Composition profile of continuous operating column for lighter hydrocarbon separation simulation

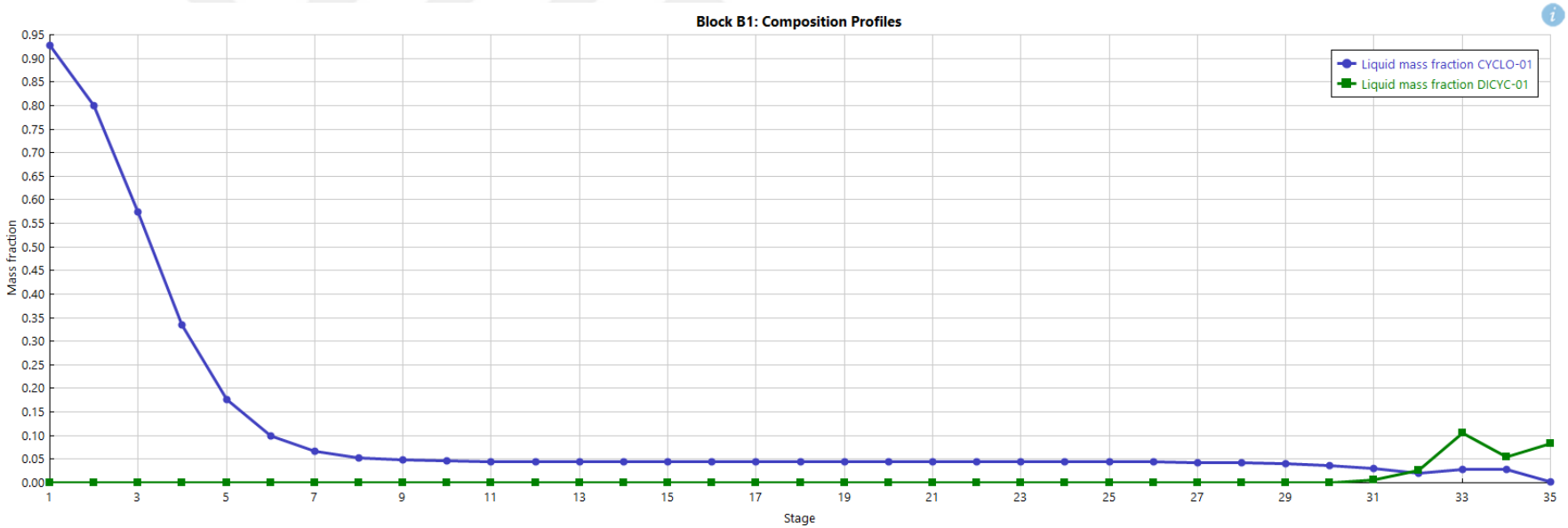


Figure 4.47: Composition profile of continuous operating column for reactive distillation simulation

4.4.3 Comparison of Batch and Continuous Operating Column Simulation Results

Simulation results for the removal of benzene and lighter hydrocarbons separation and the reactive distillation of CPD are presented and compared for batch and continuous operating columns.

4.4.3.1 Benzene and Lighter Hydrocarbons Removal Simulation Results

Simulation results for batch and continuous operating column for the removal of benzene and lighter hydrocarbons are compared in Table 4.17.

Table 4.17: Comparison of the Aspen Plus results for the batch and continuous operating simulation of benzene and lighter hydrocarbon removal stage

Parameter	*Batch Column*		*Continuous Column*
	Initial	*Final*	
Liquid Phase Temperature	*25.00°C*	*128.30°C*	*128.62°C*
CPD mass in Pot	12.60 kg	0.84 kg	0.04 kg
CPD mass fraction in Pot	0.04	0.01	0
Met-CPD mass in Pot	3.90 kg	0.36 kg	0.27 kg
Met-CPD mass fraction in Pot	0.013	0.003	0.002
DCPD mass in Pot	72.00 kg	69.18 kg	66.48 kg
DCPD mass fraction in Pot	0.24	0.62	0.60
Benzene mass in Pot	90.00 kg	2.71 kg	2.94 kg
Benzene mass fraction in Pot	0.30	0.02	0.03
Met-DCPD mass in Pot	18.00 kg	17.37 kg	16.19 kg
Met-DCPD mass fraction in Pot	0.06	0.15	0.15
Condenser Duty (kW/kg DCPD)	0.66	0.15	0.65
Reboiler Duty (kW/kg DCPD)	0.66	0.18	0.64

4.4.3.2 Reactive Distillation Simulation Results

Simulation results for batch and continuous operating column for industrial scale production of CPD are compared in Table 4.18.

Table 4.18: Comparison of the Aspen Plus results for the batch and continuous operating simulation of industrial scale production of CPD

Parameter	*Batch Column*		*Continuous Column*
	Initial	*Final*	
Liquid Phase Temperature	*25.00°C*	*136.01°C*	*160.29°C*
CPD production	0.84 kg	67.63 kg	64.92 kg
CPD mass fraction	0.01	0.92	0.93
Met-CPD mass	0.36 kg	2.38 kg	1.83 kg
Met-CPD mass fraction	0.003	0.03	0.03
DCPD mass in Distillate	69.18 kg	0.01 kg	0
DCPD mass fraction	0.62	0	0
Met-DCPD mass	17.37 kg	0.001 kg	0
Met-DCPD mass fraction	0.15	0	0
Condenser Duty (kW/kg CPD)	0.02	1.10	1.17
Reboiler Duty (kW/kg CPD)	1.54	1.12	1.61
Equipment Cost	NA*	NA*	65,100 USD

* BatchSep is not supported by Aspen Process Economic Analyzer Module

In this study, aim is to produce ≥ %90 purity CPD/DCPD. The simulation results represents the production of CPD and DCPD at 92% purity in a single equipment. DCPD can be retrieved from PYGAS with a yield of 94%. However, with reactive distillation method, purity of the CPD and DCPD can increase up to 99.9% with lower CPD/DCPD yields.

CHAPTER 5

CONCLUSION

In this study, the production of high purity dicyclopentadiene (≥ %90) from PYGAS obtained from SOCAR, Turkey is investigated. It is aimed to develop a process where benzene and lighter hydrocarbons are separated from the PYGAS mixture by distillation and the recovery of CPD from the remaining PYGAS mixture by reactive distillation system. After separation, DCPD can be produced by dimerization of CPD by storing, since CPD spontaneously dimerizes to its dimer at room temperature. PYGAS samples that are obtained from SOCAR, Turkey and DCPD samples are analyzed by using GC-MS to characterize compositions. Vapor-liquid equilibrium behavior of DCPD in PYGAS, and the chemical equilibrium between CPD and DCPD are investigated and the prominent experiments are simulated by using Aspen Plus. Results obtained from experimental studies are compared with the simulation results. It is concluded that the experimental studies with PYGAS separation and DCPD monomerization can be modeled by using Peng Robinson EOS with confidence. Therefore, the feed composition and selected Peng Robinson EOS model can be further used for the determination of the separation sequence of multicomponent distillation including reaction medium for the production of DCPD from PYGAS. The reversible monomerization kinetics of DCPD is investigated by *in-situ* GC-MS reaction experiments. The kinetic data obtained was analyzed and fitted to first order reaction kinetics by performing nonlinear regression analysis. Pre-exponential factors and activation energies are determined as $1.4x10^{16}$ s^{-1}, 53.8 kJ/mol respectively for DCPD monomerization and $2x10^{10}$ s^{-1}, 105.9 kJ/mol respectively for CPD dimerization reactions. The kinetic model obtained from the experiments is used for reaction information in reactive distillation simulations and fits the experimental studies with confidence, therefore, can be used in the simulation of industrial scale DCPD production from PYGAS. In this modeling study supported

by experimental data, a novel method for the production of DCPD with high purity (≥ 90%wt) by reactive distillation is proposed. The simulation results represents the production of CPD at 92% purity in a single equipment. DCPD can be retrieved from PYGAS with a yield of 94% decreasing the capital and the operational costs compared to conventional methods.

REFERENCES

Abushwireb, F., Elakrami, H., & Emtir, M. (2007). Recovery of aromatics from pyrolysis gasoline by conventional and energy-integrated extractive distillation. *17th European Symposium on Computer Aided Process Engineering – ESCAPE17*, 1071–1076. https://doi.org/10.1016/s1570-7946(07)80203-3

Alrefaai, M. M., Guerrero Peña, G. D. J., Raj, A., Stephen, S., Anjana, T., & Dindi, A. (2018). Impact of dicyclopentadiene addition to diesel on cetane number, sooting propensity, and soot characteristics. *Fuel*, *216*, 110–120. https://doi.org/10.1016/j.fuel.2017.11.145

am Ende, D. J., Whritenour, D. C., & Coe, J. W. (2007). Cyclopentadiene: The impact of storage conditions on thermal stability. Organic Process Research & Development, 11(6), 1141–1146. https://doi.org/10.1021/op6002727

Ayuso, M., Navarro, P., Moya, C., Moreno, D., Palomar, J., García, J., & Rodríguez, F. (2022). Extractive distillation with ionic liquids to separate benzene, toluene, and xylene from pyrolysis gasoline: Process design and techno-economic comparison with the Morphylane process. *Industrial & Engineering Chemistry Research*, *61*(6), 2511–2523. https://doi.org/10.1021/acs.iecr.1c04363

Bini, R., Chiappe, C., Mestre, V. L., Pomelli, C. S., & Welton, T. (2008). A rationalization of the solvent effect on the diels–alder reaction in ionic liquids using multiparameter linear solvation energy relationships. *Organic & Biomolecular Chemistry*, *6*, 2522–2529. https://doi.org/10.1039/b802194e

Bondaletov, V., Bondaletova, L., Van Thanh, N., & Baikova, N. (2015). Oxidation of petroleum resin based on dicyclopentadiene fraction. *Procedia Chemistry*, *15*, 103–108. https://doi.org/10.1016/j.proche.2015.10.016

Bělohlav, Z., Zámostný, P., Fulín, P., & Štěpánek, K. (2000). Kinetic model for dicyclopentadiene monomeration process. *Chemical and Biochemical Engineering Quarterly*.

Cai, Z., Shen, B., Xin, Z., Liu, W., & Ling, H. (2011). Gas-phase cracking dicyclopentadiene using hydrogen as a carrier gas. *Energy Sources, Part A: Recovery, Utilization, and Environmental Effects*, *33*, 594–603. https://doi.org/10.1080/15567030903161263

Cai, Zhi, Shen, B., Liu, W., Xin, Z., & Ling, H. (2009). Liquid-phase cracking of dicyclopentadiene by reactive distillation. *Energy &Fuels*, *23*(8), 4077–4081. https://doi.org/10.1021/ef900400w

Cao, K., Liu, X., Zhang, Y., Shi, J., Song, Y., & Yao, Z. (2015). Insights into the diels–alder reactions between cyclopentadiene and 1,3-butadiene with high temperature and high pressure. *Industrial & Engineering Chemistry Research*, *54*(31), 7565–7570. https://doi.org/10.1021/acs.iecr.5b01054

Cheung, T. T. P. (2000). Cyclopentadiene and dicyclopentadiene. *Kirk-Othmer Encyclopedia of Chemical Technology*, *8*, 219–235. https://doi.org/10.1002/0471238961.0325031211050514.a01.pub2

Chung, H. S., Chen, C. S., Kremer, R. A., Boulton, J. R., & Burdette, G. W. (1999). Recent developments in high-energy density liquid hydrocarbon fuels. *Energy & Fuels*, *13*(3), 641–649. https://doi.org/10.1021/ef980195k

Claus, M., Claus, E., Claus, P., Hönicke, D., Födisch, R., & Olson, M. (2016). Cyclopentadiene and Cyclopentene. *Ullmann's Encyclopedia of Industrial Chemistry*, 1–16. https://doi.org/10.1002/14356007.a08_227.pub2

Cuthbert, T. J., Li, T., & Wulff, J. E. (2019). Production and dynamic mechanical analysis of macro-scale functionalized polydicyclopentadiene objects facilitated by rational synthesis and reaction injection molding. *ACS Applied Polymer Materials*, *1*(9), 2460–2471. https://doi.org/10.1021/acsapm.9b00571

Douglas, J. M. (1988). *Conceptual design of Chemical Processes*. McGraw-Hill.

Dicyclopentadiene market share: Statistics report – 2030. Global Market Insights Inc. (n.d.). https://www.gminsights.com/industry-analysis/dicyclopentadiene-dcpd-market

Enache, D. I., Landon, P., Lok, C. M., Pollington, S. D., & Stitt, E. H. (2005). Direct comparison of a trickle bed and a monolith for hydrogenation of pyrolysis gasoline. *Industrial & Engineering Chemistry Research*, *44*(25), 9431–9439. https://doi.org/10.1021/ie0502180

Global Market Insights Inc. (2022). *Dicyclopentadiene market share: Statistics report – 2030*. Retriewed from https://www.gminsights.com/industry-analysis/dicyclopentadiene-dcpd-market

Griffith, T. D., Chu, A. H. T., & Langer, S. H. (1987). Multicolumn gas chromatographic reactor studies of the dissociation reactions of dicyclopentadiene and its methyl derivatives. *The Chemical Engineering Journal*, *36*(2), 73–91. https://doi.org/10.1016/0300-9467(87)80046-1

Gumerov, I. F., Yurasov, S. Yu., Shafigullin, L. N., Romanov, V. B., Romanova, N. V., Shafigullina, G. R., & Sokolova, Yu. A. (2018). Producing polydicyclopentadiene from lower-grade dicyclopentadiene. *Russian Engineering Research*, *38*(12), 1046–1048. https://doi.org/10.3103/s1068798x18120080

Guo, L., Wang, T., Li, D., & Wang, J. (2016). Intrinsic Kinetic Modeling of Thermal Dimerization of C5 Fraction. *China Petroleum Processing and Petrochemical Technology*, *18*, 92–99.

Guo, L., Wang, T., Li, D., & Wang, J. (2017). Liquid-holdup regions research of novel reactive distillation column for C5 fraction separation. *Chinese Journal of Chemical Engineering*, *25*(4), 433–441. https://doi.org/10.1016/j.cjche.2016.09.010

Han, H., Zou, J.-J., Zhang, X., Wang, L., & Wang, L. (2009). Endo- to exo-isomerization of dicyclopentadiene over zeolites. *Applied Catalysis A: General*, *367*(1–2), 84–88. https://doi.org/10.1016/j.apcata.2009.07.035

Herink, T., Fulín, P., Krupka, J., & Pašek, J. (2022). New Technology for production of dicyclopentadiene and methyl-dicyklopentadiene. *Polymers*, *14*, 667. https://doi.org/10.3390/polym14040667

Herndon, W. C., Grayson, C. R., & Manion, J. M. (1967a). Retro-diels-alder reactions. III. kinetics of the thermal decompositions of exo- and Endo-Dicyclopentadiene. *The Journal of Organic Chemistry*, *32*(3), 526–529. https://doi.org/10.1021/jo01278a003

Herndon, W. C., Grayson, C. R., & Manion, J. M. (1967b). Retro-Diels-Alder Reactions. III. Kinetics of the Thermal Decompositions of exo- and endo-Dicyclopentadiene. *The Journal of Organic Chemistry*, *32*(3), 526–529. https://doi.org/10.1021/jo01278a003

Herrera, M., Murgia, E., de Hazos, M., & Lubkowitz, J. (1981). Separation, identification, and quantitation of pyrolysis gasolines. *Journal of High Resolution Chromatography*, *4*(6), 297–299. https://doi.org/10.1002/jhrc.1240040613

Hsu, Haiso-Ching, Wang, S.-J., Ou, J. D., & Wong, D. S. (2017). Plant-wide design and control of C5 Separation Processes. *2017 6th International Symposium on Advanced Control of Industrial Processes (AdCONIP)*. https://doi.org/10.1109/adconip.2017.7983806

Hsu, Hsiao-Ching, Wang, S.-J., Ou, J. D.-Y., & Wong, D. S. (2015). Simplification and intensification of a C5 separation process. *Industrial & Engineering*

Chemistry Research, *54*(40), 9798–9804. https://doi.org/10.1021/acs.iecr.5b01705

Hwang, H.-J., Lin, C.-Y., & Wang, C.-S. (2008). Flame retardancy and dielectric properties of dicyclopentadiene-based benzoxazine cured with a phosphorus-containing phenolic resin. *Journal of Applied Polymer Science*, *110*(4), 2413–2423. https://doi.org/10.1002/app.28787

Jamróz, M. E., Gałka, S., & Dobrowolski, J. C. (2003). On dicyclopentadiene isomers. *Journal of Molecular Structure: THEOCHEM*, *634*(1–3), 225–233. https://doi.org/10.1016/s0166-1280(03)00348-8

Khan, A., Ali, S. S., Chodimella, V. P., Farooqui, S. A., Anand, M., & Sinha, A. K. (2021). Catalytic conversion of dicyclopentadiene into high energy density fuel: A brief review. *Industrial & Engineering Chemistry Research*, *60*(5), 1977–1988. https://doi.org/10.1021/acs.iecr.0c06168

Kim, H.-G., Lee, H. R., Lim, C.-S., & Seo, B. (2019). Separation of dicyclopentaidene in a C5 stream using a tetraethoxydimethyl disiloxane-derived silica composite membrane. *Journal of Industrial and Engineering Chemistry*, *79*, 79–86. https://doi.org/10.1016/j.jiec.2019.05.016

Krupka, Jiri, & Kolena, J. (2012). Gas chromatographic data and identification of isomeric products of cycloaddition reactions of conjugated C5 dienes. *Petroleum & Coal*, *54*, 385–396.

Krupka, Jiri, Pasek, J., Fila, V., Patera, J., & Severa, Z. (2005). Technology Aspects of the Hydrogenation of Cyclopentadiene to Cyclopentene. *Petroleum & Coal*, *47*, 22–32.

Krupka, Jiří, Pašek, J., Lederer, J., & Bílková, D. (2014). Kinetics of cycloaddition reactions of conjugated C5 dienes. *Petroleum & Coal*, *56*, 428–441.

Krupka, Jiří. (2010). Kinetics of thermal dimerizations of cyclopentadiene and methylcyclopentadienes and their codimerization. *Petroleum & Coal*, *52*(4), 290–306.

Krupka, Jiří. (2011). Rearrangement of 4-methyldicyclopentadiene to 2-methyldicyclopentadiene. *Petroleum & Coal*, *53*, 233–237.

Kumar, A., & Pawar, S. S. (2004). Alcl3-catalysed dimerization of 1,3-cyclopentadiene in the chloroaluminate room temperature ionic liquid. *Journal of Molecular Catalysis A: Chemical*, *208*(1–2), 33–37. https://doi.org/10.1016/s1381-1169(03)00510-7

Langer, S. H., & Patton, J. E. (1972). Gas-chromatographic reactor study of the kinetics of dicyclopentadiene dissociation. *The Journal of Physical Chemistry*, *76*(15), 2159–2170. https://doi.org/10.1021/j100659a017

Larriba, M., Navarro, P., Delgado-Mellado, N., Stanisci, V., García, J., & Rodríguez, F. (2017). Extraction of aromatic hydrocarbons from pyrolysis gasoline using tetrathiocyanatocobaltate-based ionic liquids: Experimental Study and Simulation. *Fuel Processing Technology*, *159*, 96–110. https://doi.org/10.1016/j.fuproc.2017.01.027

Larriba, M., Navarro, P., González, E. J., García, J., & Rodríguez, F. (2015). Dearomatization of pyrolysis gasolines from mild and severe cracking by liquid–liquid extraction using a binary mixture of [4empy][tf2n] and [emim][dca] ionic liquids. *Fuel Processing Technology*, *137*, 269–282. https://doi.org/10.1016/j.fuproc.2015.03.009

Li, L., Shen, B. X., & Ling, H. (2013). Gas phase cracking of dicyclopentadiene to produce cyclopentadiene. *Petroleum Science and Technology*, *31*(13), 1346–1352. https://doi.org/10.1080/10916466.2010.535087

Li, Y., Zou, J.-J., Zhang, X., Wang, L., & Mi, Z. (2010). Product distribution of tricyclopentadiene from cycloaddition of dicyclopentadiene and cyclopentadiene: A theoretical and experimental study. *Fuel*, *89*(9), 2522–2527. https://doi.org/10.1016/j.fuel.2009.11.020

Mauldin, T. C., Rule, J. D., Sottos, N. R., White, S. R., & Moore, J. S. (2007). Self-healing kinetics and the stereoisomers of dicyclopentadiene. *Journal of The Royal Society Interface*, *4*(13), 389–393. https://doi.org/10.1098/rsif.2006.0200

Medeiros, J. L., Araújo, O. Q., Gaspar, A. B., Silva, M. A., & Britto, J. M. (2007). A kinetic model for the first stage of pygas upgrading. *Brazilian Journal of Chemical Engineering*, *24*(1), 119–133. https://doi.org/10.1590/s0104-66322007000100011

Miki, H. (2019). Development of process for production of highly valuable chemicals derived from dicyclopentadiene for comprehensive utilization of C5 Chemicals. *Journal of the Japan Petroleum Institute*, *62*(6), 245–254. https://doi.org/10.1627/jpi.62.245

Monson, R. S. (1971). 8. The Diels-Alder Reaction. In *Advanced Organic Synthesis: Methods and Techniques* (pp. 71–79). essay, Academic Press.

Narayan, A., Wang, B., Nava Medina, I. B., Mannan, M. S., Cheng, Z., & Wang, Q. (2016). Prediction of heat of formation for exo -Dicyclopentadiene.

Journal of Loss Prevention in the Process Industries, *44*, 433–439. https://doi.org/10.1016/j.jlp.2016.10.015

Nurullina, E. V., Solov'eva, N. B., Liakumovich, A. G., & Samuilov, Ya. D. (2001). Production of High-Purity Dicyclopentadiene from the C5 Fraction of Hydrocarbon Pyrolysis. *Russian Journal of Applied Chemistry*, *74*(9), 1590–1593.

Palmová, I., Kosek, J., Schöngut, J., Marek, M., & Štěpánek, K. (2001). Experimental and modeling studies of oligomerization and copolymerization of dicyclopentadiene. *Chemical Engineering Science*, *56*, 927–935. https://doi.org/10.1016/s0009-2509(00)00307-9

Park, E., Kim, J., Yim, J.-H., Han, J., Kwon, T. S., Park, Y. K., & Jeon, J.-K. (2016). Synthesis of dicyclopentadiene oligomer over nanoporous al-Mcm-41 catalysts. *Journal of Nanoscience and Nanotechnology*, *16*(5), 4512–4515. https://doi.org/10.1166/jnn.2016.11005

Perrot, A., Hyršl, J., Bandžuch, J., Waňousová, S., Hájek, J., Jenčík, J., & Herink, T. (2021). Use of dicyclopentadiene and methyl dicyclopentadiene for the synthesis of unsaturated polyester resins. *Polymers*, *13*(18). https://doi.org/10.3390/polym13183135

Perrot, A., Hyršl, J., Bandžuch, J., Waňousová, S., Hájek, J., Jenčík, J., & Herink, T. (2023). A comparative study of a modified unsaturated polyester resin with dicyclopentadiene and methyl dicyclopentadiene blends. *Polymer*, *267*. https://doi.org/10.1016/j.polymer.2022.125639

Rahmatpour, A., & Ghasemi Meymandi, M. (2021). Large-scale production of C9 aromatic hydrocarbon resin from the cracked-petroleum-derived C9 fraction: Chemistry, scalability, and techno-economic analysis. *Organic Process Research & Development*, *25*(1), 120–135. https://doi.org/10.1021/acs.oprd.0c00474

Shan, W., & Mei, Y. (2013). Copolymers of dicyclopentadiene and tricyclopentadiene. *Polymer Science Series B*, *55*(5–6), 344–348. https://doi.org/10.1134/s1560090413060092

Sharma, A., Pandey, A., Shukla, D. K., & Pandey, K. N. (2018). Effect of self-healing dicyclopentadiene microcapsules on fracture toughness of epoxy. *Materials Today: Proceedings*, *5*, 21256–21262. https://doi.org/10.1016/j.matpr.2018.06.526

Sheehan, M., & Sharratt, P. (1999). An experimental study of the solvent effect on rate and selectivity in a concentrated diels−alder reaction. *Organic Process Research & Development*, *3*, 471–475. https://doi.org/10.1021/op990050s

Towler, G., & Sinnott, R. K. (2013). *Chemical engineering design: Principles, practice and economics of plant and process design, second edition* (2nd ed.). Butterworth-Heinemann.

SOCAR. (2020). *PYGAS Technical Data Sheet*

SOCAR. (2019). *PYGAS Safety Data Sheet*

Sottos, N., White, S., & Bond, I. (2007). Introduction: Self-healing polymers and composites. *Journal of The Royal Society Interface*, *4*, 347–348. https://doi.org/10.1098/rsif.2006.0205

Szekeres, G., Siklos, P., Nagy, L., & Jelinek, L. (1977). Thermal dimerization of cyclopentadiene and its reaction with isoprene. *Chemischer Informationsdienst*, *8*(50). https://doi.org/10.1002/chin.197750166

Toplosky, V. J., & Walsh, R. P. (2006). Thermal and mechanical properties of poly-dicyclopentadiene (DCPD) at cryogenic temperatures. *AIP Conference Proceedings*. https://doi.org/10.1063/1.2192354

Touazi, A. A., Didaoui, S., Khimeche, K., & Benziane, M. (2020). Measurement and prediction of thermophysical properties of binary mixtures of dicyclopentadiene with methylcyclohexane, toluene, and p-xylene. *Thermochimica Acta*, *685*. https://doi.org/10.1016/j.tca.2020.178536

Vintila, I. S., Iovu, H., Alcea, A., Cucuruz, A., Mandoc, A. C., & Vasile, B. S. (2020). The synthetization and analysis of dicyclopentadiene and Ethylidene-norbornene Microcapsule systems. *Polymers*, *12*. https://doi.org/10.3390/polym12051052

Wankat, P. C. (2016). *Separation Process Engineering: Includes Mass transfer Analysis* (4th ed.). Pearson Education.

Wang, B., Zhang, Z., Pei, Z., Qiu, J., & Wang, S. (2020). Current progress on the 3D printing of Thermosets. *Advanced Composites and Hybrid Materials*, *3*, 462–472. https://doi.org/10.1007/s42114-020-00183-z

Wang, Y. (2014). Optimization of C5 separation and production process. *Advances in Social Science, Education and Humanities Research*. https://doi.org/10.2991/emss-14.2014.41

Wilson, P. J., & Wells, J. H. (1944). The chemistry and utilization of cyclopentadiene. *Chemical Reviews*, *34*(1), 1–50. https://doi.org/10.1021/cr60107a001

Wittcoff, H. A., Reuben, B. G., & Plotkin, J. S. (2013). 5. Chemicals and Polymers from Ethylene, 8. Chemicals from the C5 Stream. In *Industrial Organic Chemicals* (3rd ed., pp. 139–321). essay, Wiley.

Xu, C., Al Shoaibi, A. S., Wang, C., Carstensen, H.-H., & Dean, A. M. (2011). Kinetic modeling of ethane pyrolysis at high conversion. *The Journal of Physical Chemistry A*, *115*(38), 10470–10490. https://doi.org/10.1021/jp206503d

Xu, R., Jocz, J. N., Wiest, L. K., Sarngadharan, S. C., Milina, M., Coleman, J. S., Iaccino, L. L., Pollet, P., Sievers, C., & Liotta, C. L. (2019). Cyclopentadiene dimerization kinetics in the presence of C5 alkenes and alkadienes. *Industrial & Engineering Chemistry Research*, *58*(50), 22516–22525. https://doi.org/10.1021/acs.iecr.9b04018

Yao, Z., Xu, X., Dong, Y., Liu, X., Yuan, B., Wang, K., Cao, K., & Luo, G. (2020). Kinetics on thermal dissociation and oligomerization of dicyclopentadiene in a high temperature & pressure Microreactor. *Chemical Engineering Science*, *228*. https://doi.org/10.1016/j.ces.2020.115892

Zhang, X. W., Jiang, K., Jiang, Q., Zou, J. J., Wang, L., & Mi, Z. T. (2007). Novel endo- to exo-isomerization of dicyclopentadiene. *Chinese Chemical Letters*, *18*(6), 673–676. https://doi.org/10.1016/j.cclet.2007.03.005

Zhang, X., Jiang, Q., Xiong, Z., Zou, J., Wang, L., & Mi, Z. (2008). Diels-Alder addition of dicyclopentadiene with cyclopentadiene in polar solvents. *Chemical Research in Chinese Universities*, *24*(2), 175–179. https://doi.org/10.1016/s1005-9040(08)60036-7

Zou, J.-J., Xu, Y., Zhang, X., & Wang, L. (2012). Isomerization of endo-dicyclopentadiene using al-grafted MCM-41. *Applied Catalysis A: General*, *421–422*, 79–85. https://doi.org/10.1016/j.apcata.2012.01.035

APPENDICES

A. Sample Chromatogram for PYGAS

PYGAS constituents were analyzed by GC-MS. Chromatographic grade heptane was used as a dilution solvent. Abundance at corresponding retention times (RTmin) are given in Figure A1 where peaks at 3.7 through 4.8 RTmin are solvent peaks for heptane. The magnified chromatograms are given in Figure A2, Figure A3, Figure A4, Figure A5, and Figure A6 while the method parameters are given in Table A1.

Table A 1: Method information for characterization of PYGAS

GC-MS Parameters	*Value*
Column	HP-5 ms
Inlet Type	Split (50:1)
Inlet Temperature	250°C
Injection Volume	0.2 µL
Inlet Gas Flow	He, 24 mL/min
Column Gas Flow	1.2 mL/min
Inlet Pressure	1.1 bar
Oven Program	50°C for 60 min
MS Gain Factor	2
Acquisition Type	Scan
Frequency	3.9 scans/sec
MS Step Size	0.1 m/z
MS Scan Range	30-500

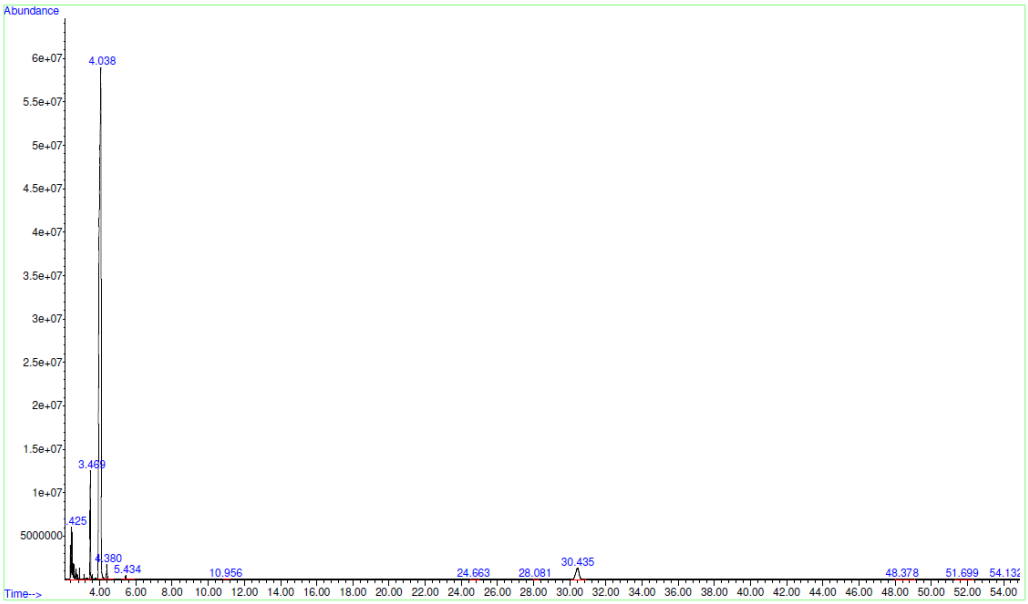


Figure A 1: Sample chromatogram for PYGAS in heptane

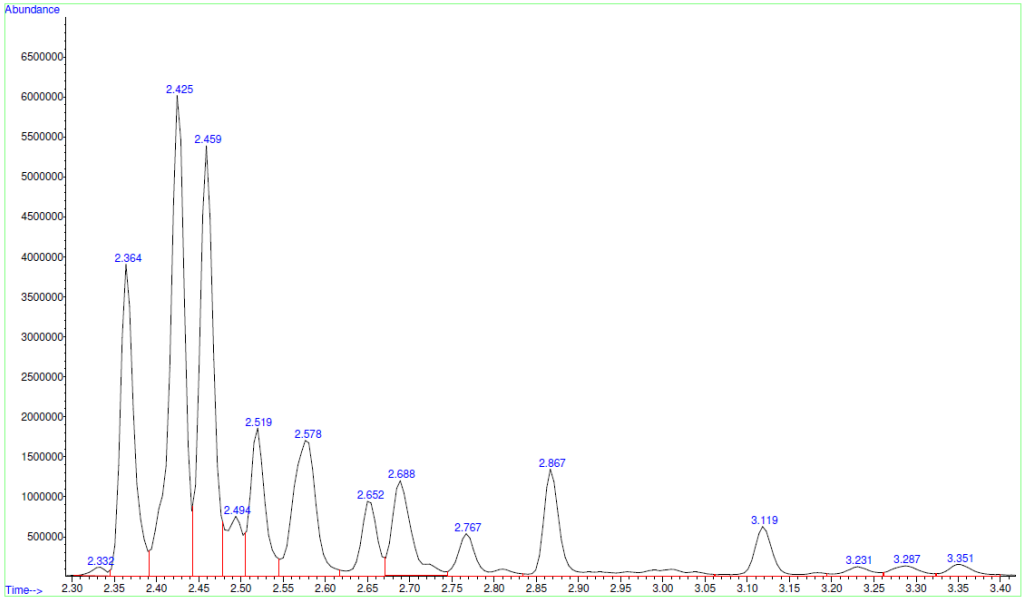


Figure A 2: Sample chromatogram for PYGAS constituents between 2.3 RTmin and 3.4 RTmin

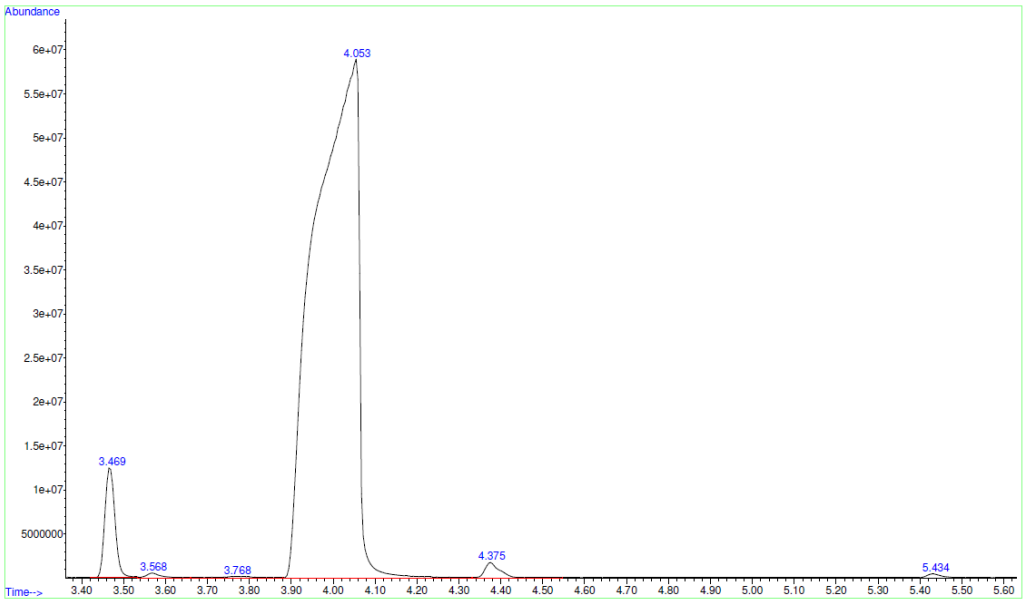


Figure A 3: Sample chromatogram for PYGAS constituents between 3.4 RTmin and 5.6 RTmin

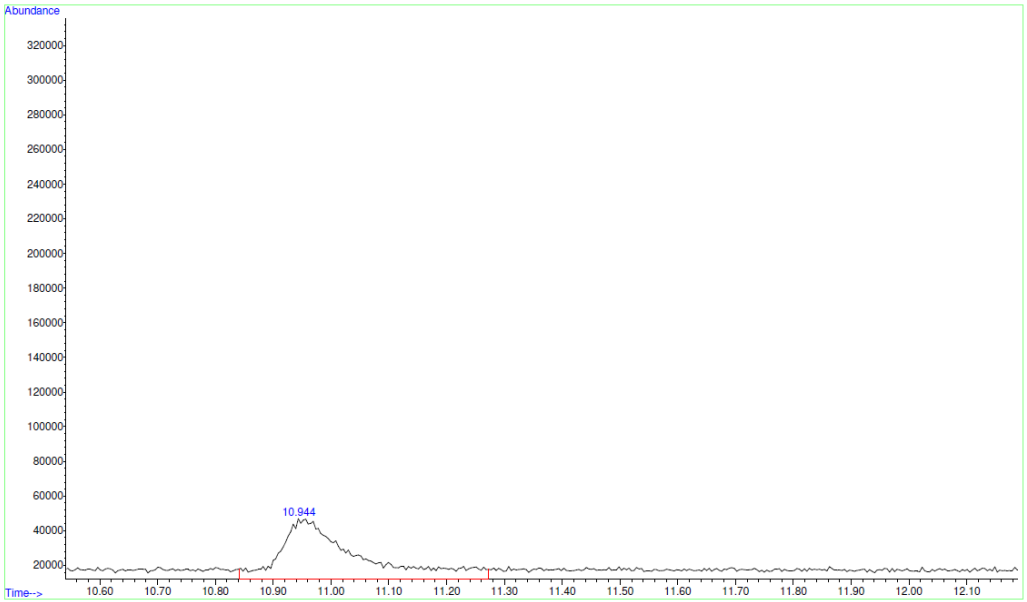


Figure A 4: Sample chromatogram for PYGAS constituents between 10.6 RTmin and 12.1 RTmin



Figure A 5: Sample chromatogram for PYGAS constituents between 24.6 RTmin and 30.8 RTmin

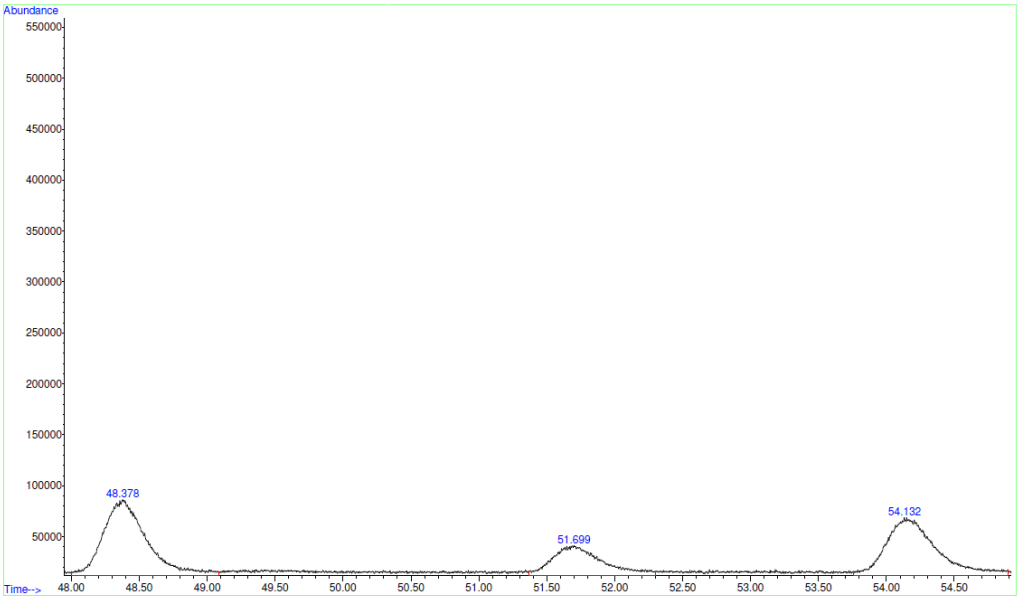


Figure A 6: Sample chromatogram for PYGAS constituents between 48 RTmin and 54.5 RTmin

Mass spectrums of the peaks are given Figure A7 through A33.

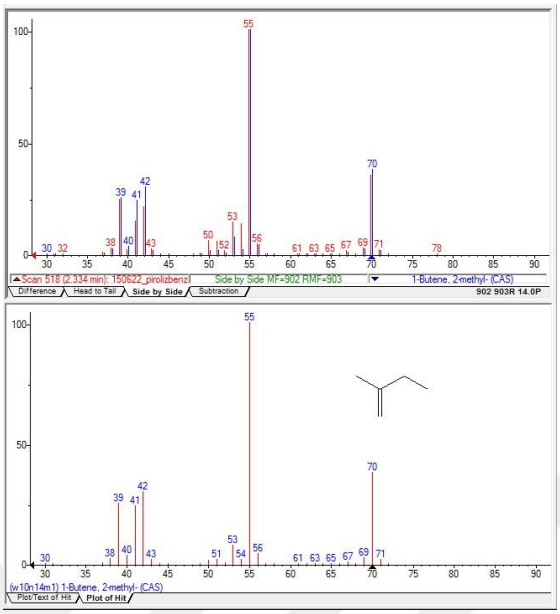


Figure A 7: Mass spectra and library match for peak at 2.33 RTmin

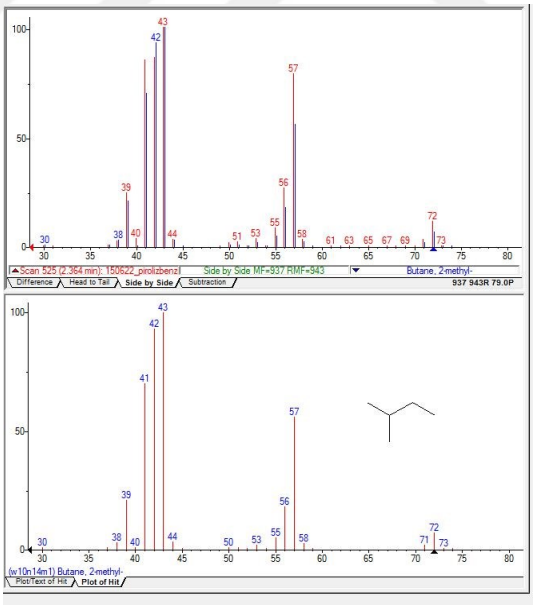


Figure A 8: Mass spectra and library match for peak at 2.36 RTmin

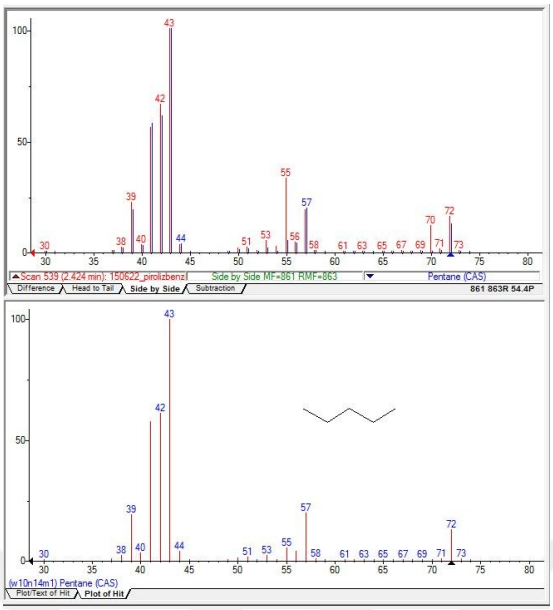


Figure A 9: Mass spectra and library match for peak at 2.43 RTmin

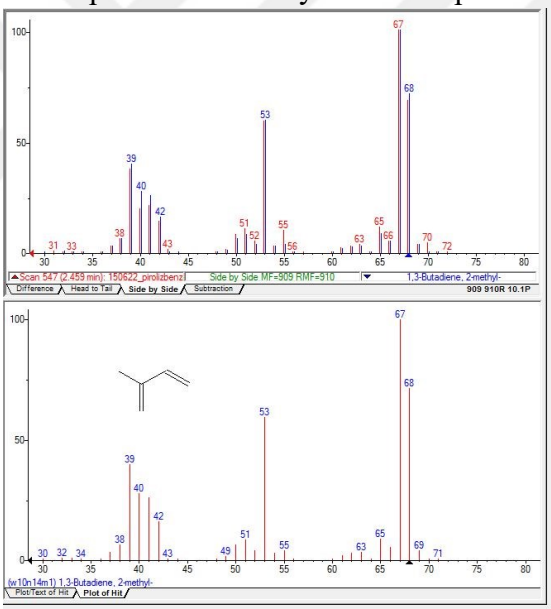


Figure A 10: Mass spectra and library match for peak at 2.46 RTmin

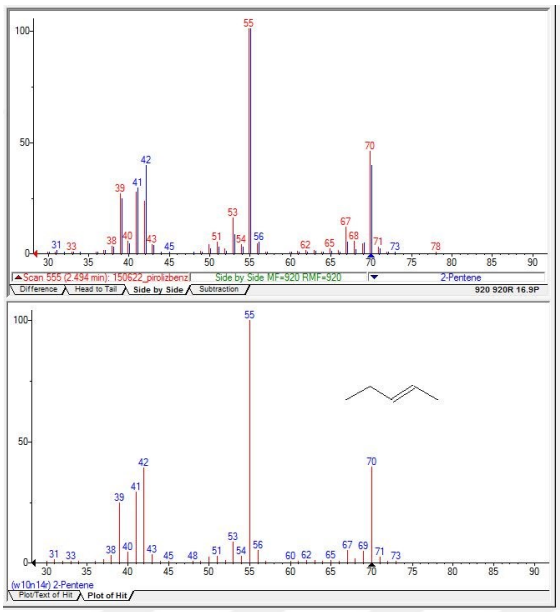


Figure A 11: Mass spectra and library match for peak at 2.49 RTmin

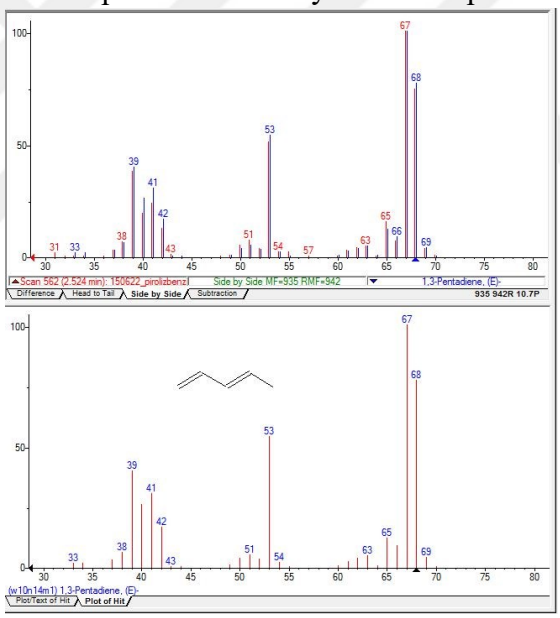


Figure A 12: Mass spectra and library match for peak at 2.52 RTmin

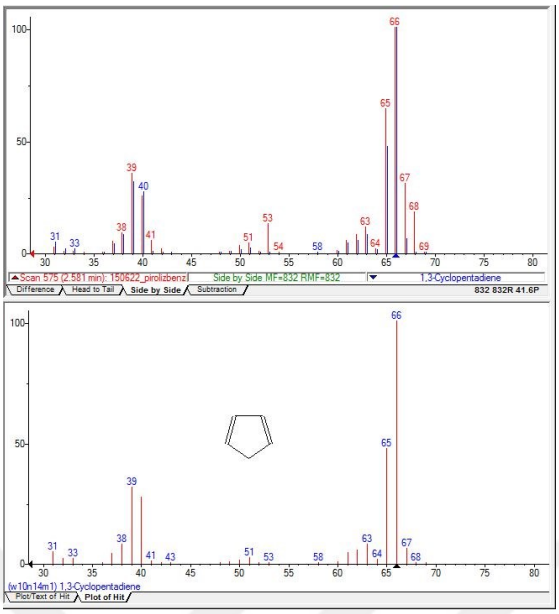


Figure A 13: Mass spectra and library match for peak at 2.58 RTmin

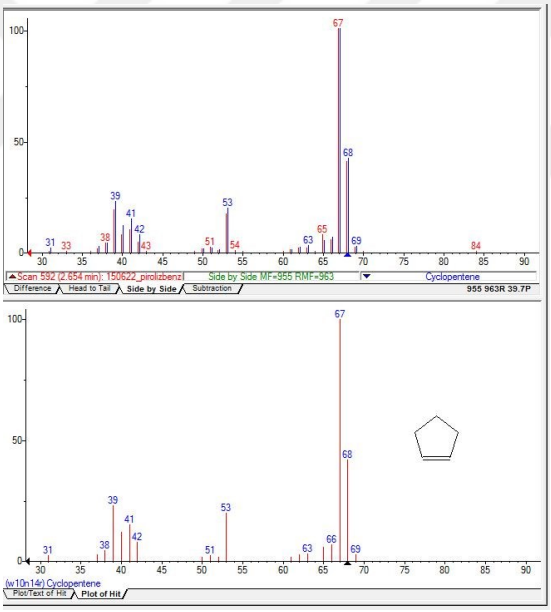


Figure A 14: Mass spectra and library match for peak at 2.65 RTmin

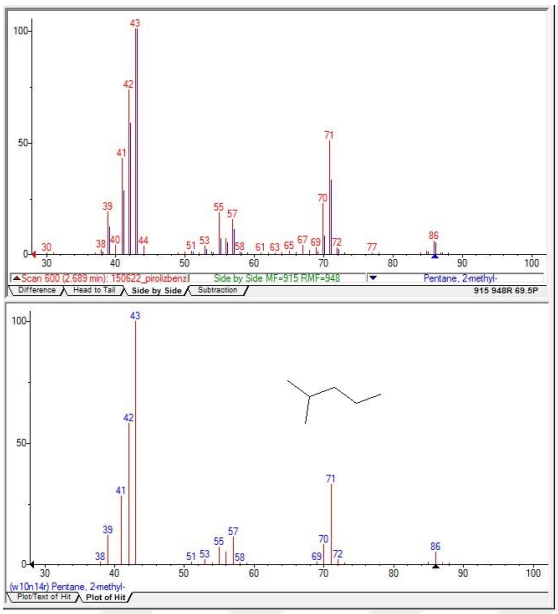


Figure A 15: Mass spectra and library match for peak at 2.69 RTmin

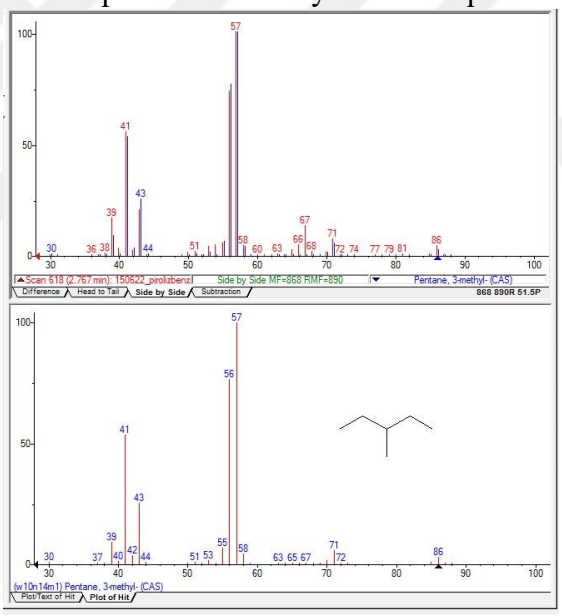


Figure A 16: Mass spectra and library match for peak at 2.77 RTmin

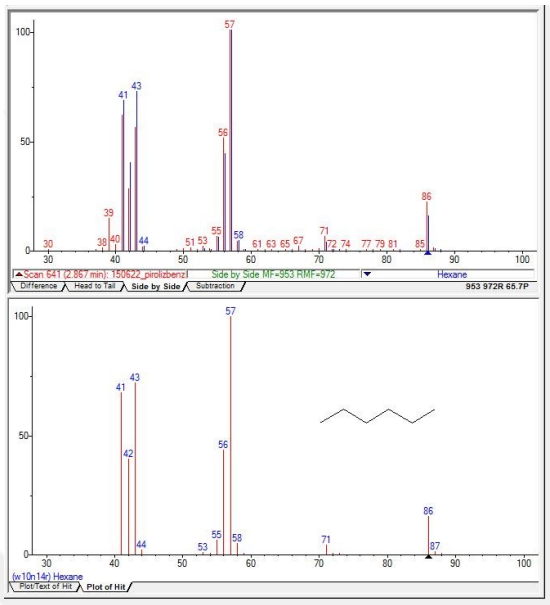


Figure A 17: Mass spectra and library match for peak at 2.87 RTmin

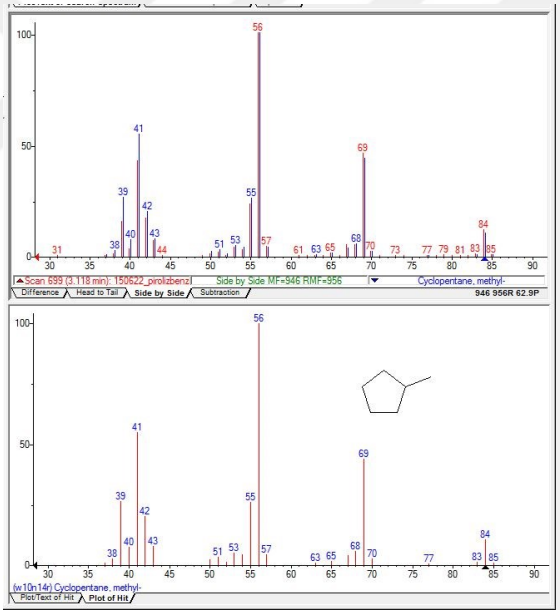


Figure A 18: Mass spectra and library match for peak at 3.12 RTmin

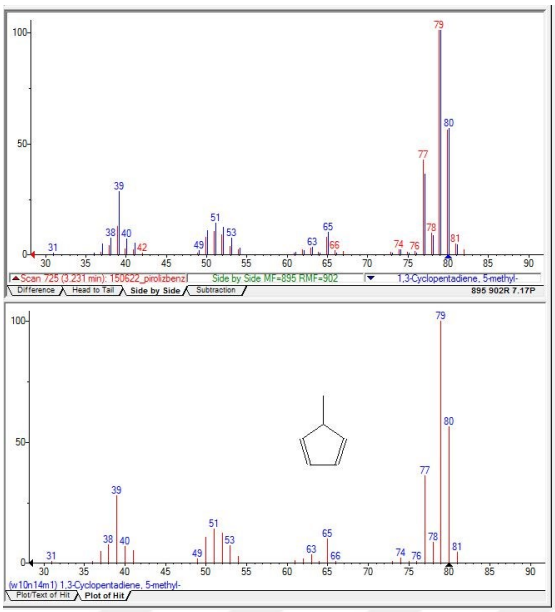


Figure A 19: Mass spectra and library match for peak at 3.23 RTmin

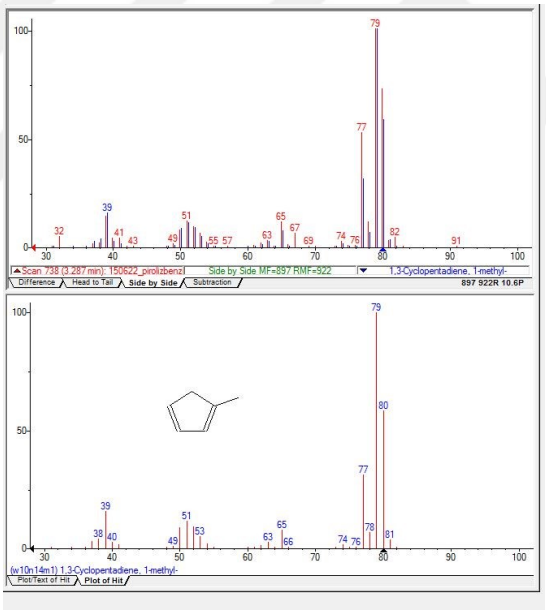


Figure A 20: Mass spectra and library match for peak at 3.29 RTmin

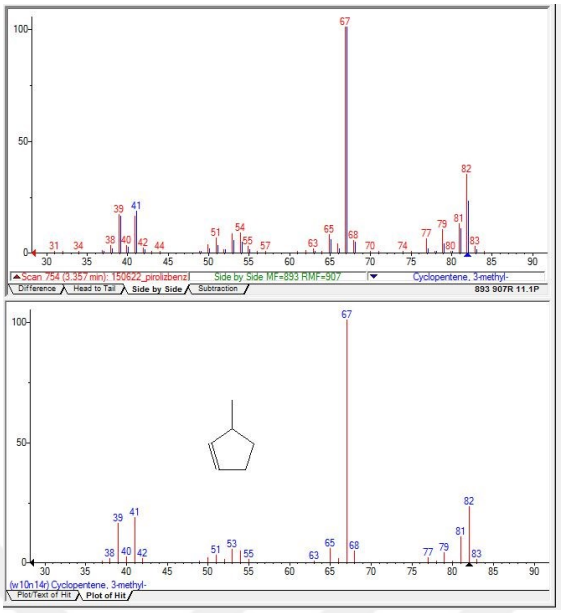


Figure A 21: Mass spectra and library match for peak at 3.36 RTmin

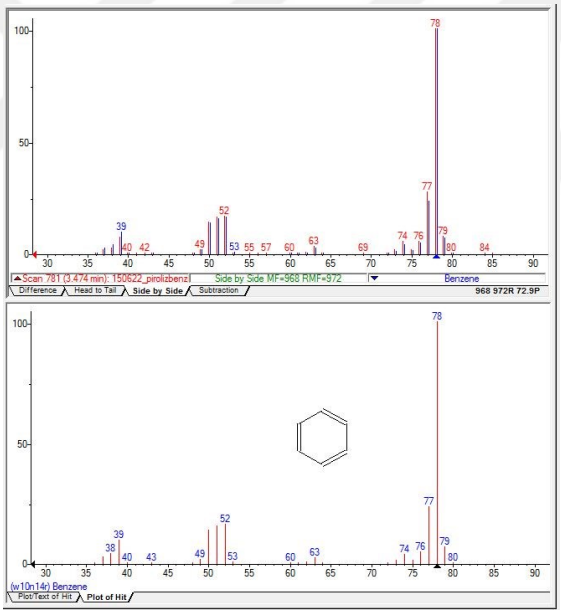


Figure A 22: Mass spectra and library match for peak at 3.48 RTmin

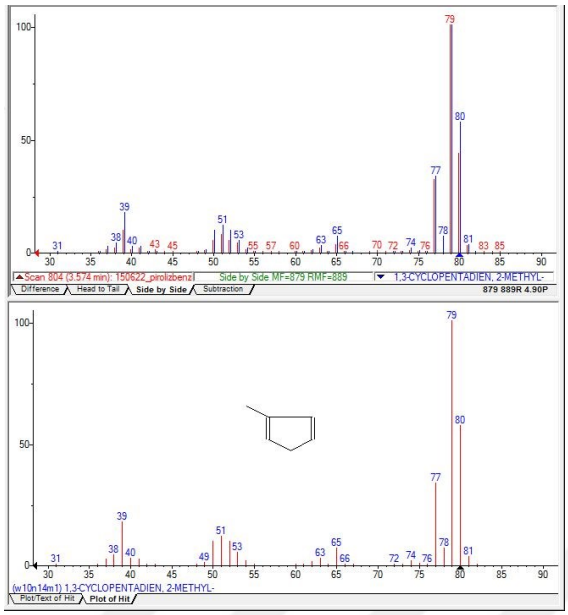


Figure A 23: Mass spectra and library match for peak at 3.57 RTmin

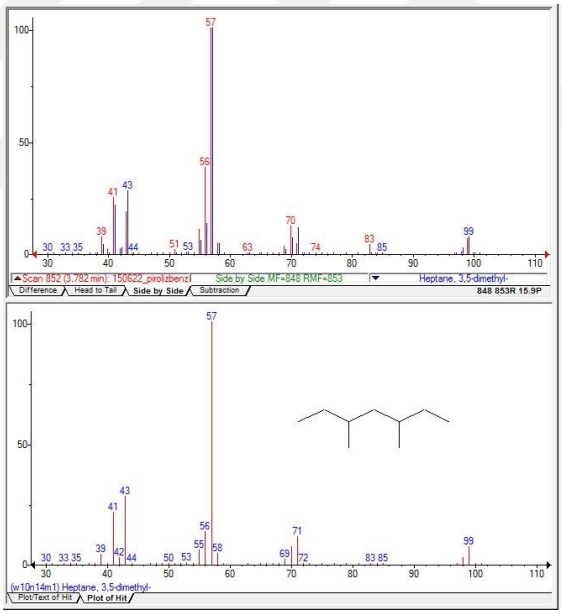


Figure A 24: Mass spectra and library match for peak at 3.78 RTmin

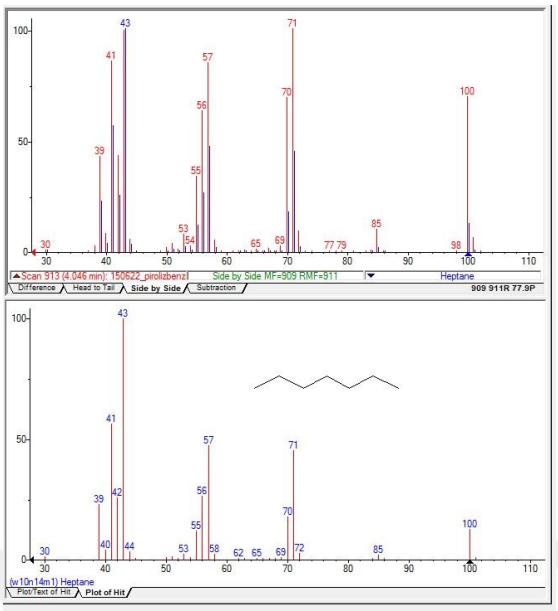


Figure A 25: Mass spectra and library match for peak at 4.05 RTmin

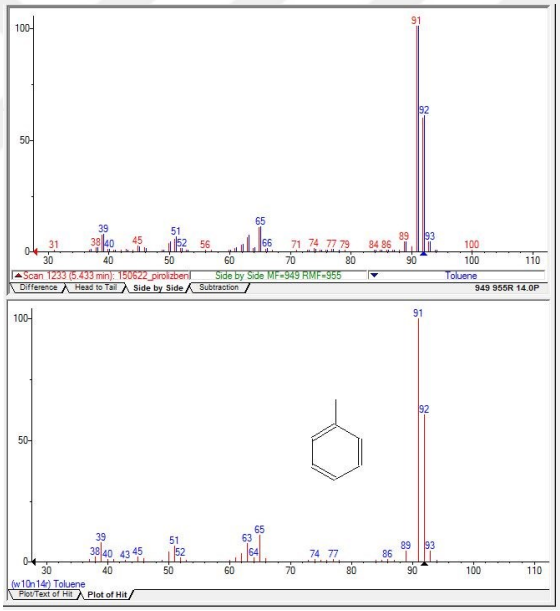


Figure A 26: Mass spectra and library match for peak at 5.43 RTmin

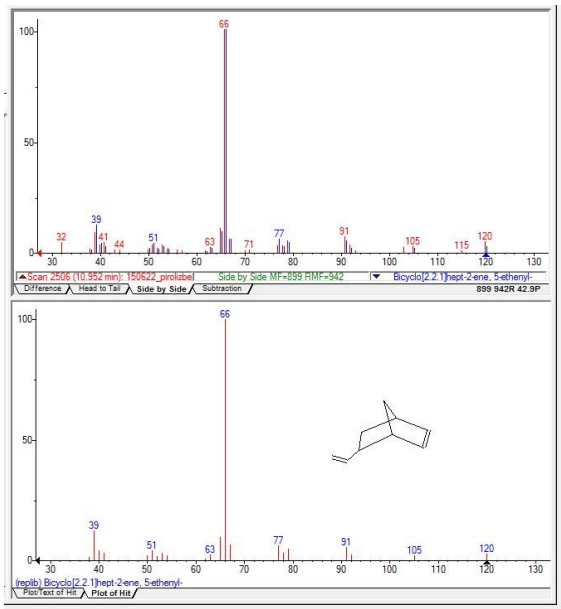


Figure A 27: Mass spectra and library match for peak at 10.95 RTmin

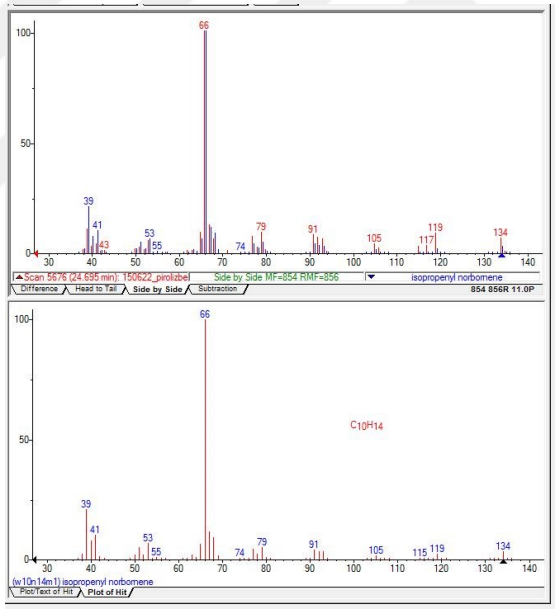


Figure A 28: Mass spectra and library match for peak at 24.69 RTmin

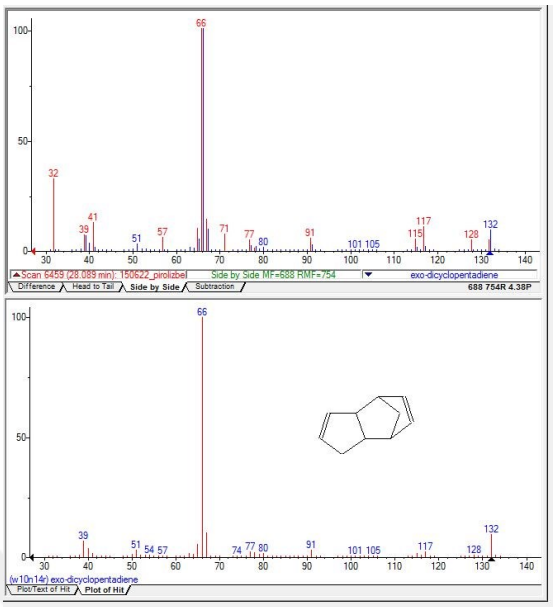


Figure A 29: Mass spectra and library match for peak at 28.09 RTmin

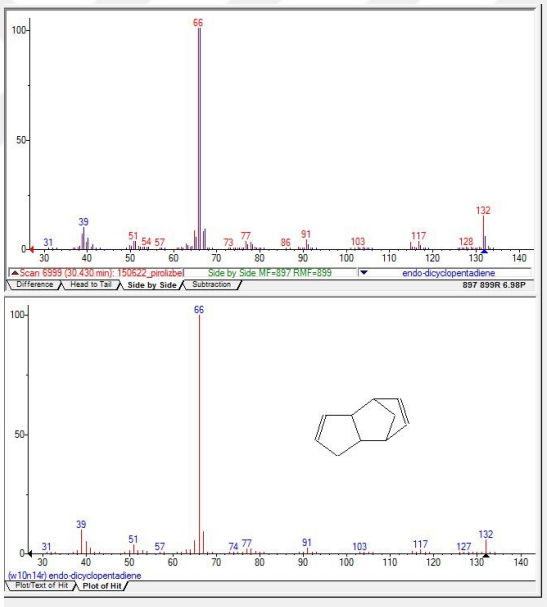


Figure A 30: Mass spectra and library match for peak at 30.43 RTmin

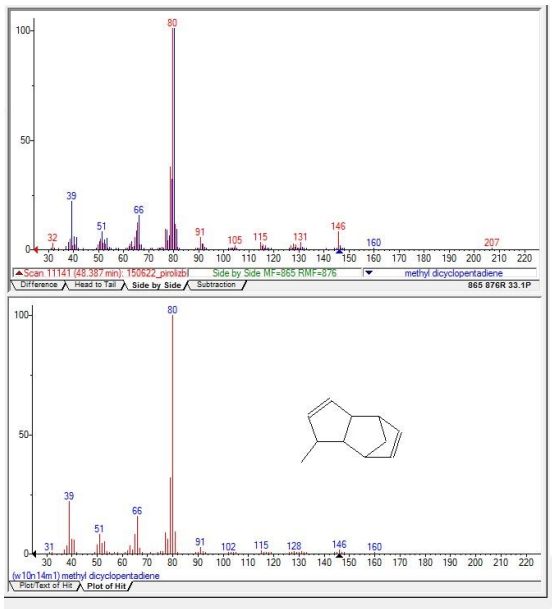


Figure A 31: Mass spectra and library match for peak at 48.39 RTmin

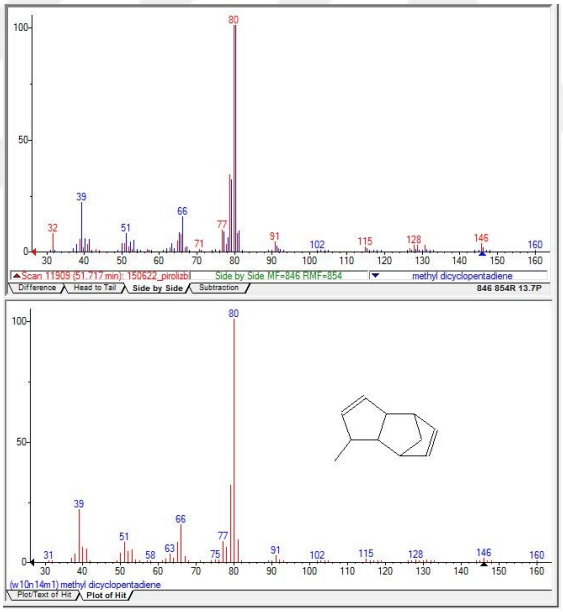


Figure A 32: Mass spectra and library match for peak at 51.72 RTmin

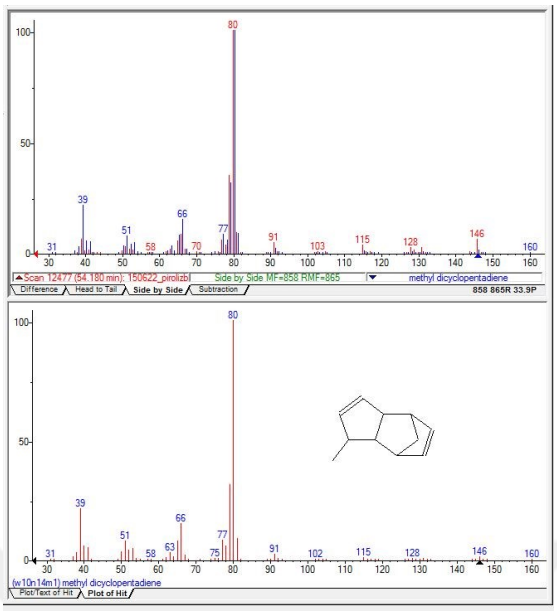


Figure A 33: Mass spectra and library match for peak at 54.18 RTmin

B. Sample Chromatogram for DCPD

DCPD constituents were analyzed by GC-MS. Chromatographic grade toluene was used as a dilution solvent. Abundance at corresponding retention times (RTmin) is given in Figure B1 where the peak at 3.315 is the solvent peak for Toluene. The magnified chromatogram is given in Figure B2, while the method parameters are given in Table B1.

Table B 1: Method information for characterization of DCPD

GC-MS Parameters	*Value*
Column	HP-5 ms
Inlet Type	Split (15:1)
Inlet Temperature	160°C
Injection Volume	0.2 µL
Inlet Gas Flow	He, 20 mL/min
Column Gas Flow	1.2 mL/min
Column Pressure	1.1 bar
Oven Program	50°C for 40 min
MS Gain Factor	2
Acquisition Type	Scan
Frequency	3.9 scans/sec
MS Step Size	0.1 m/z
MS Scan Range	30-500

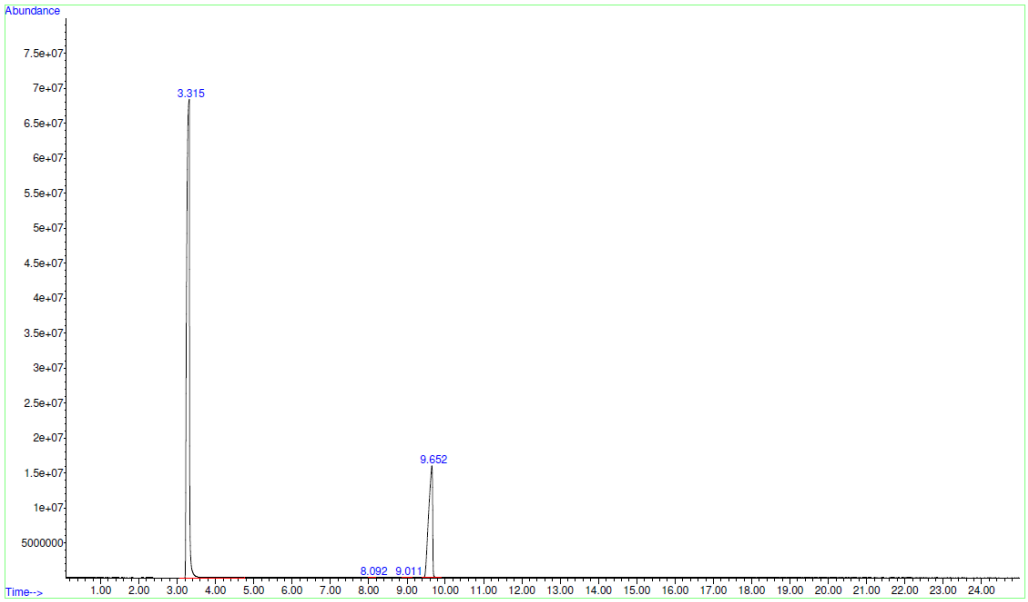


Figure B 1: Sample chromatogram for DCPD constituents in toluene

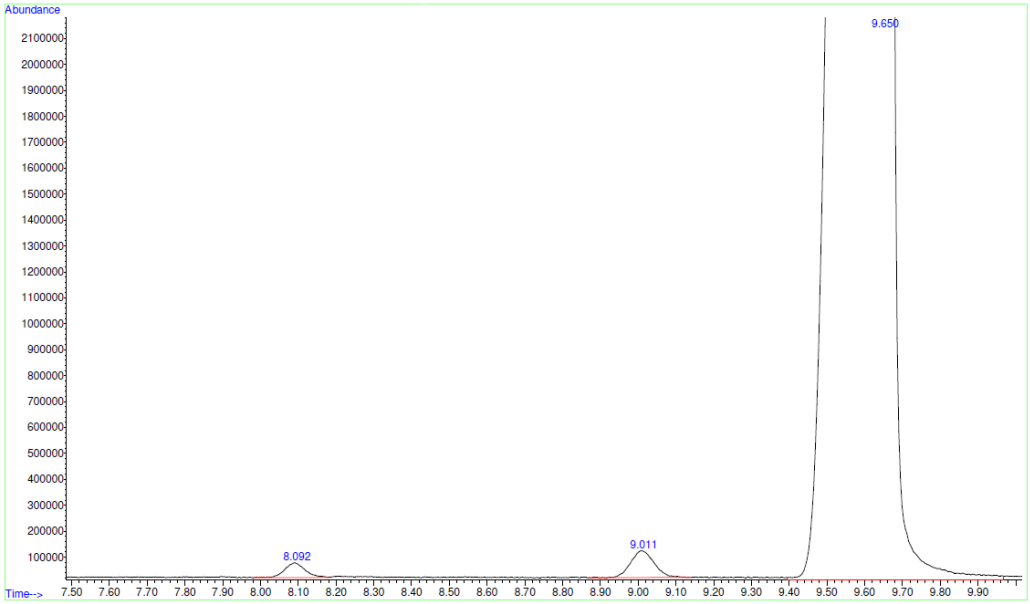


Figure B 2: Sample chromatogram for DCPD constituents between 7.5 RTmin and 9.9 RTmin

Mass spectras for the peaks are given in Figure B3, B4, B5 and B6.

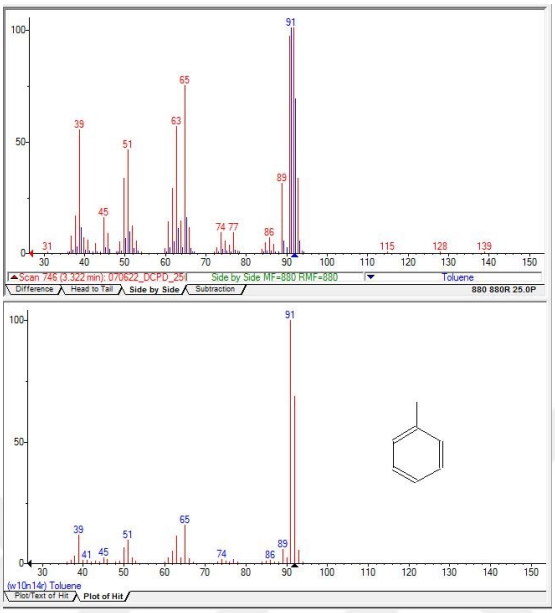


Figure B 3: Mass spectra and library match for peak at 3.32 RTmin

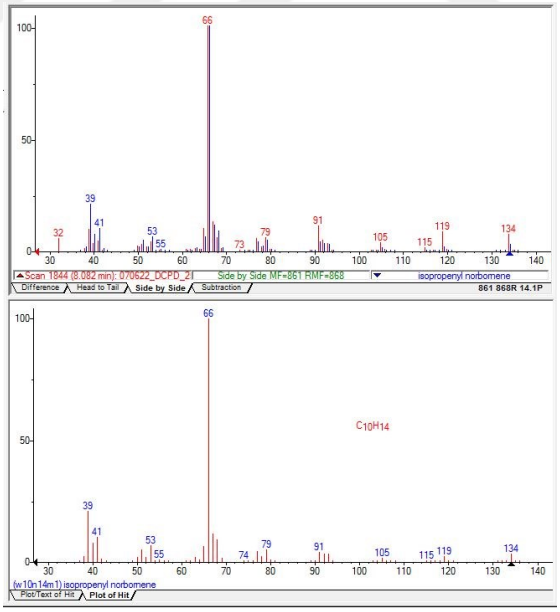


Figure B 4: Mass spectra and library match for peak at 8.08 RTmin

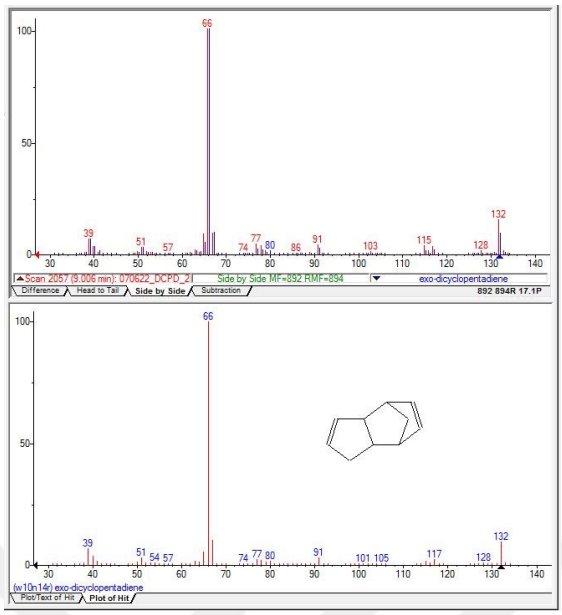


Figure B 5: Mass spectra and library match for peak at 9.01 RTmin

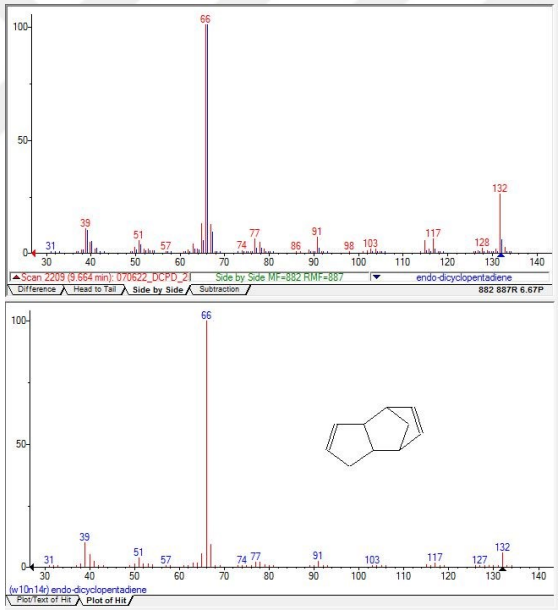


Figure B 6: Mass spectra and library match for peak at 9.66 RTmin

C. Experimental Procedure for Phase Equilibrium Experiment 14

1. Weigh 485 g PYGAS(SOCAR) in Mettler Toledo XS6002S Precision Balance, and note the weighed amount in the laboratory notebook.
2. Transfer weighed PYGAS into the evaporating flask.
3. Connect the evaporating flask to the rotary evaporator system.
4. Set the vacuum control system to 100 mbar.
5. For the first step, set the heating bath to 80°C allowing the benzene and lighter organic compounds to be fractionated.
6. Wait for 15 minutes.
7. After 15 minutes, detach the receiving flask from the rotary evaporator system.
8. Weigh the constituents of receiving flask.
9. Transfer the constituents of receiving flask into a sealed glass container after weighing, and note the weighed amount in the laboratory notebook.
10. Assemble the receiving flask back into the rotary evaporator system.
11. Set the heating bath to 125°C and the vacuum to 100 mbar allowing the DCPD-rich fraction to be separated from the heavy residue at the second step.
12. Continue on operation until no vapor or liquid droplets were observed in the rotary evaporator system,
13. Weigh the condensate and the evaporating flask and note the weighed amount in the laboratory notebook.
14. Transfer the constituents of the evaporating flask into sealed glass containers.
15. For the third step of the phase equilibrium experiment, transfer the collected mixture from the receiving flask to the evaporating flask.
16. Set the temperature to 110°C and the vacuum to 100 mbar for the isolation of DCPD
17. Continue on operation until no vapor or liquid droplets were observed in the rotary evaporator system,

18. Weigh the condensate and the evaporating flask and note the weighed amount in the laboratory notebook.

D. Experimental Procedure for Reactive Distillation Experiment 39

1. Weigh Dicyclopentadiene (≥99%wt, ZET) and note the weighed amount in the laboratory notebook.
2. Put the weighed DCPD in the flask.
3. Purged the system with nitrogen for 20 minutes.
4. After 20 minutes, set the electric heater to 20°C.
5. Run the mixer to 250 rpm.
6. Set the chiller that is connected to the condenser to -20°C
7. Add liquid nitrogen to the trap.
8. Put the graduated cylinder into an ice bath to prevent a re-dimerization reaction at room temperature.
9. Set the electric heater to 155°C and monitor the temperature increase by using both the electronic heaters temperature controller and thermometer.
10. As the temperature of the system reaches 155°C, record the time.
11. Collect samples from both flask and the condensate for 10-minute intervals.
12. Store the samples in an ice bath.
13. Prepare the GC-MS samples with cooled GC grade solvent in an ice bath and keep the samples in refrigerator during analyses.

E. Sample Chromatogram for Phase Equilibrium Experiment 14 Steps

Fractionated PYGAS constituents taken from condensate and flask of phase equilibrium experiment 14 Step 1, Step 2, and Step 3 were analyzed by GC-MS. Chromatograms are given in Figure E1 through E26. Chromatographic grade hexane was used as a dilution solvent. Abundance at corresponding retention times (RTmin) are given in Figure E1 where peaks at 2.3 through 2.6 RTmin are solvent peaks for hexane. Lighter hydrocarbons were characterized as a single peak at 2.236 RTmin. The method parameters are given in Table E1. Mass spectra are given in Figure E27 through E40.

Table E 1: Method information for phase equilibrium experiment samples

GC-MS Parameters	*Value*
Column	HP-5 ms
Inlet Type	Split (50:1)
Inlet Temperature	180°C
Injection Volume	0.2 µL
Inlet Gas Flow	He, 25 mL/min
Column Gas Flow	1.2 mL/min
Column Pressure	1.1 bar
Oven Program	50°C for 60 min
MS Gain Factor	2
Acquisition Type	Scan
Frequency	3.9 scans/sec
MS Step Size	0.1 m/z
MS Scan Range	30-500



Figure E 1: Sample chromatogram for Step 1 condensate constituents between 2 RTmin and 15.5 RTmin

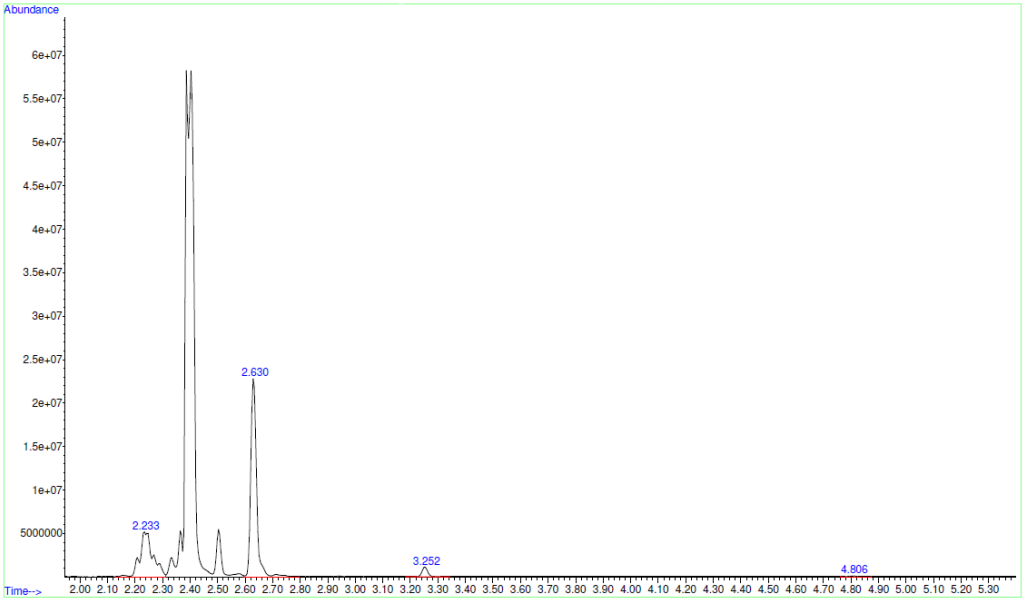


Figure E 2: Sample chromatogram for Step 1 condensate constituents between 2 RTmin and 5.3 RTmin

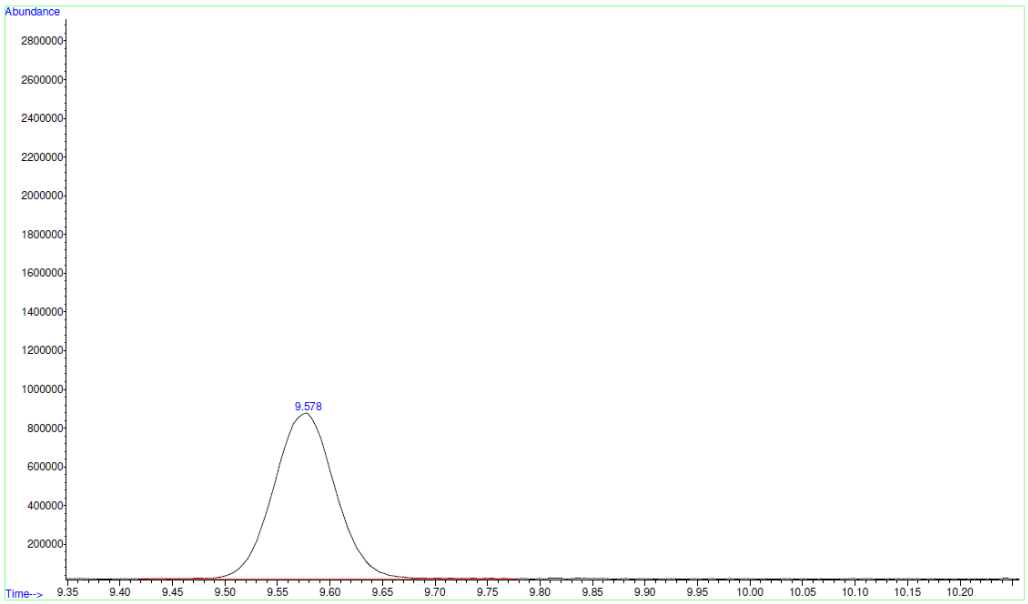


Figure E 3: Sample chromatogram for Step 1 condensate constituents between 9.35 RTmin and 10.2 RTmin

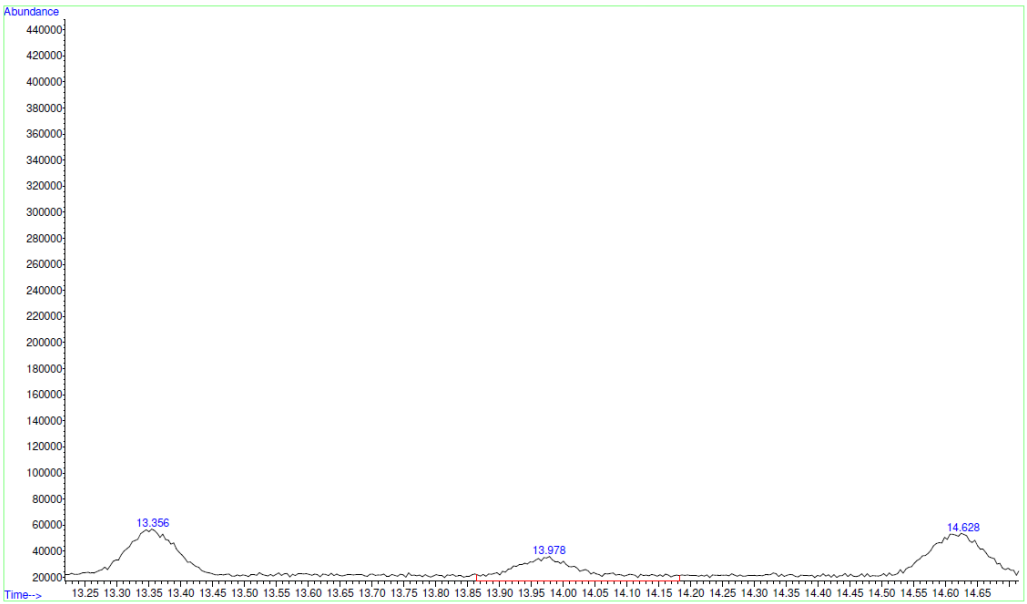


Figure E 4: Sample chromatogram for Step 1 condensate constituents between 13.25 RTmin and 15.65 RTmin

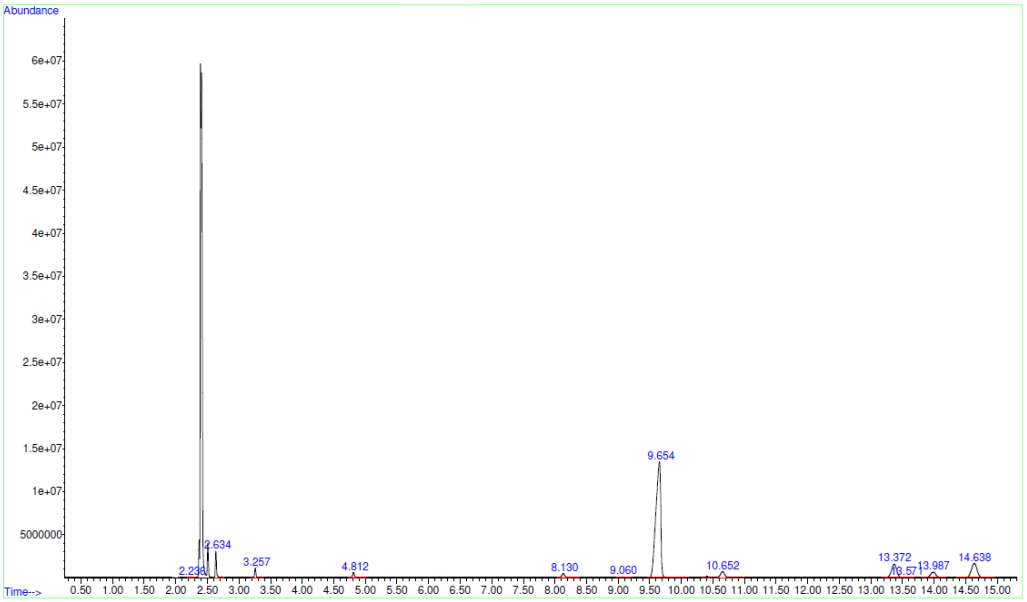


Figure E 5: Sample chromatogram for Step 1 flask constituents between 0.5 RTmin and 15 RTmin

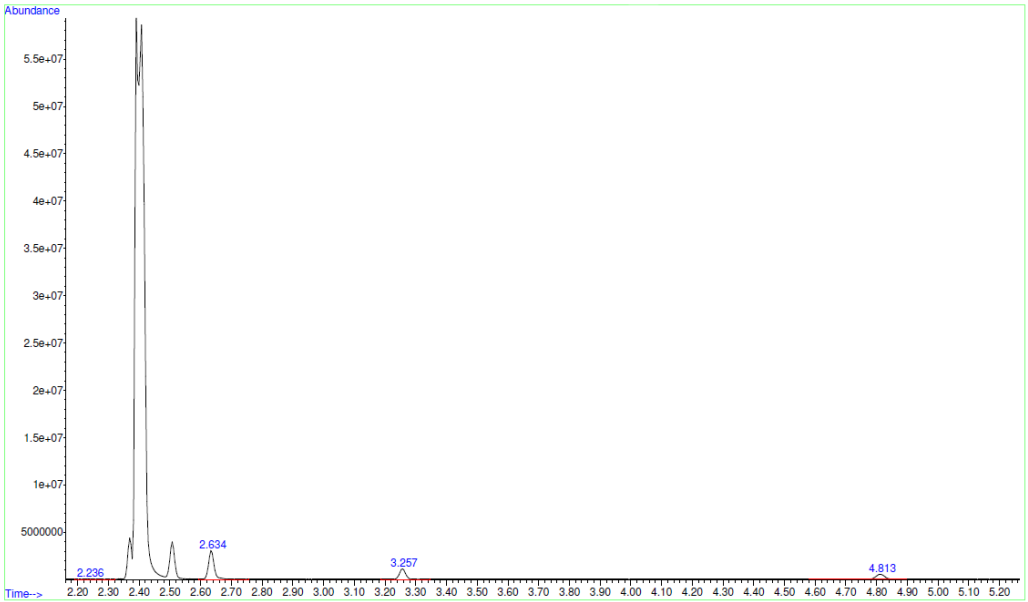


Figure E 6: Sample Chromatogram for Step 1 flask Constituents between 2.2 RTmin and 5.2 RTmin

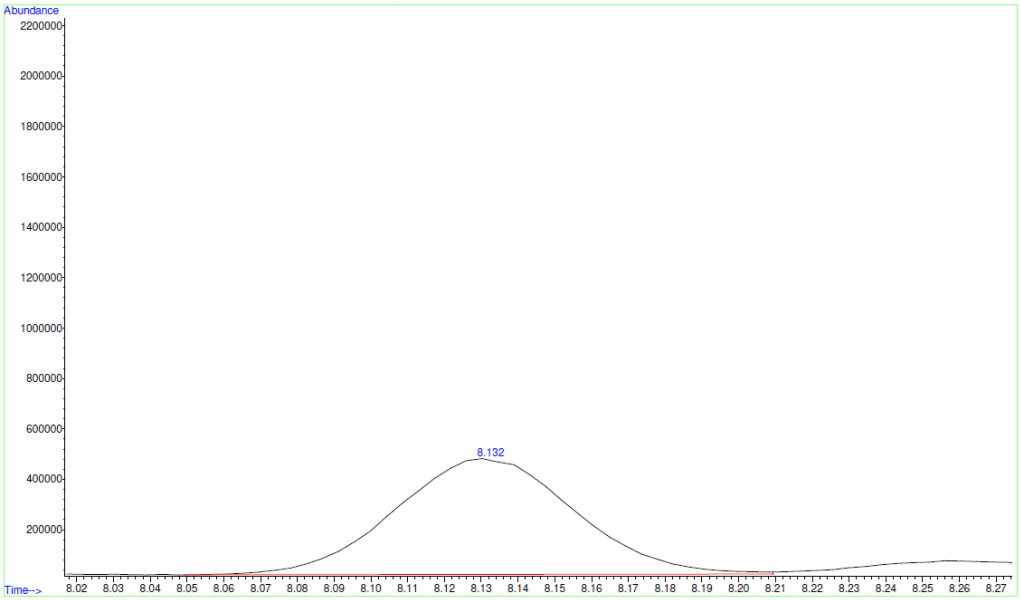


Figure E 7: Sample chromatogram for Step 1 flask constituents between 8 RTmin and 8.27 RTmin

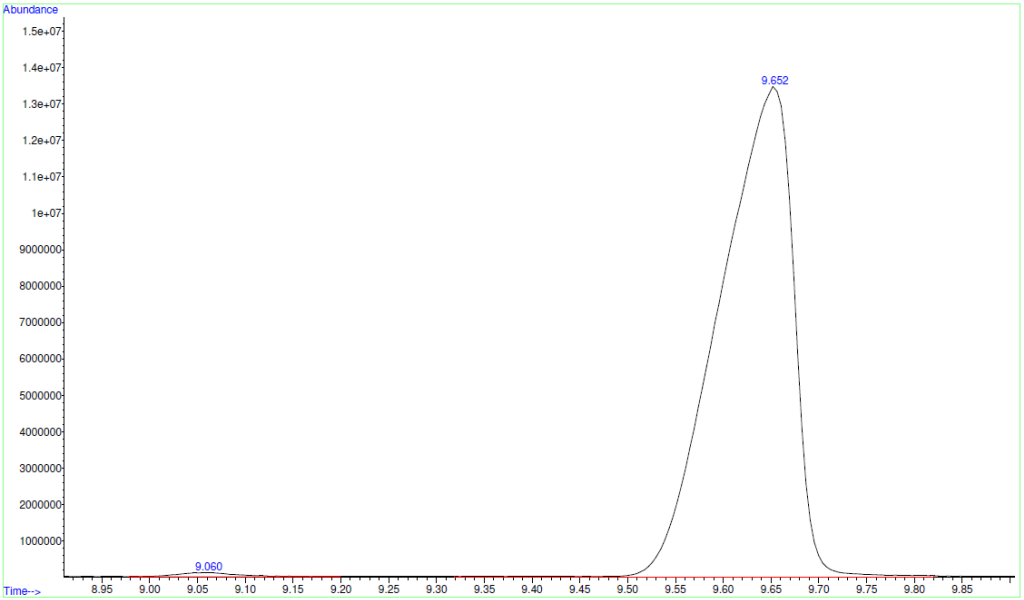


Figure E 8: Sample chromatogram for Step 1 flask constituents between 8.95 RTmin and 9.85 RTmin

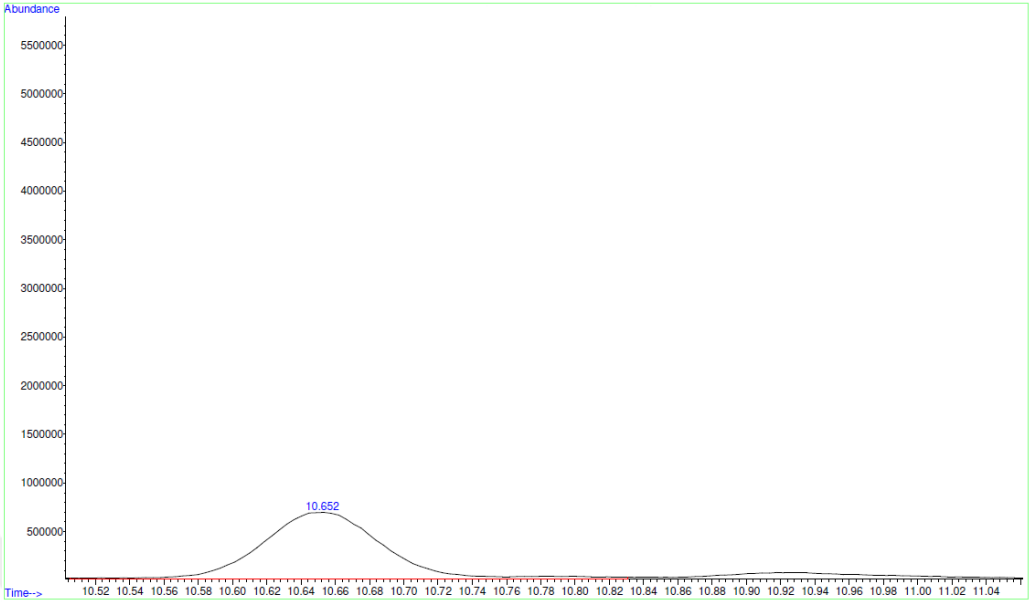


Figure E 9: Sample chromatogram for Step 1 flask constituents between 10.5 RTmin and 11 RTmin

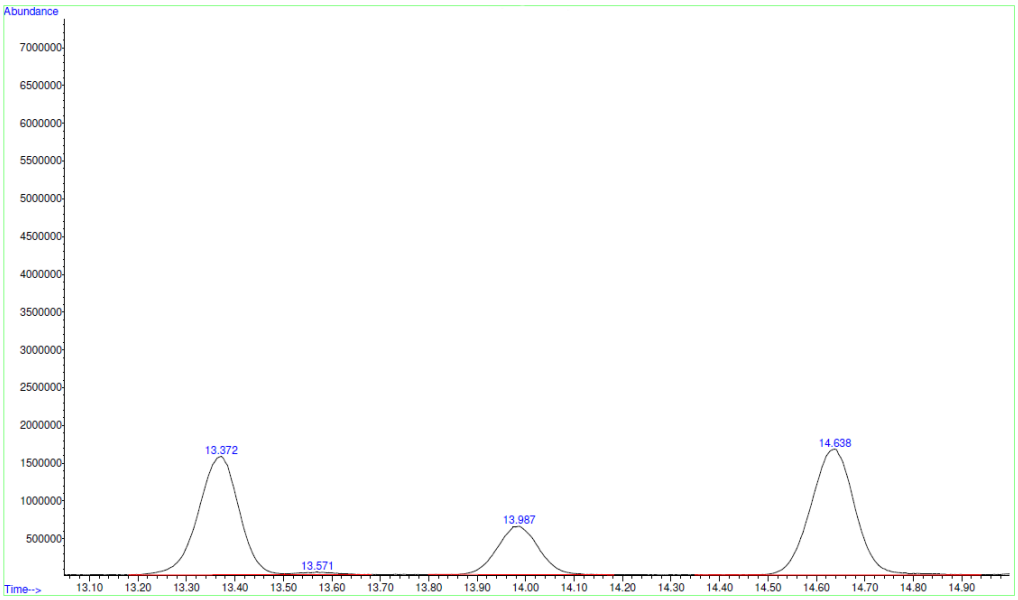


Figure E 10: Sample chromatogram for Step 1 flask constituents between 13 RTmin and 15 RTmin

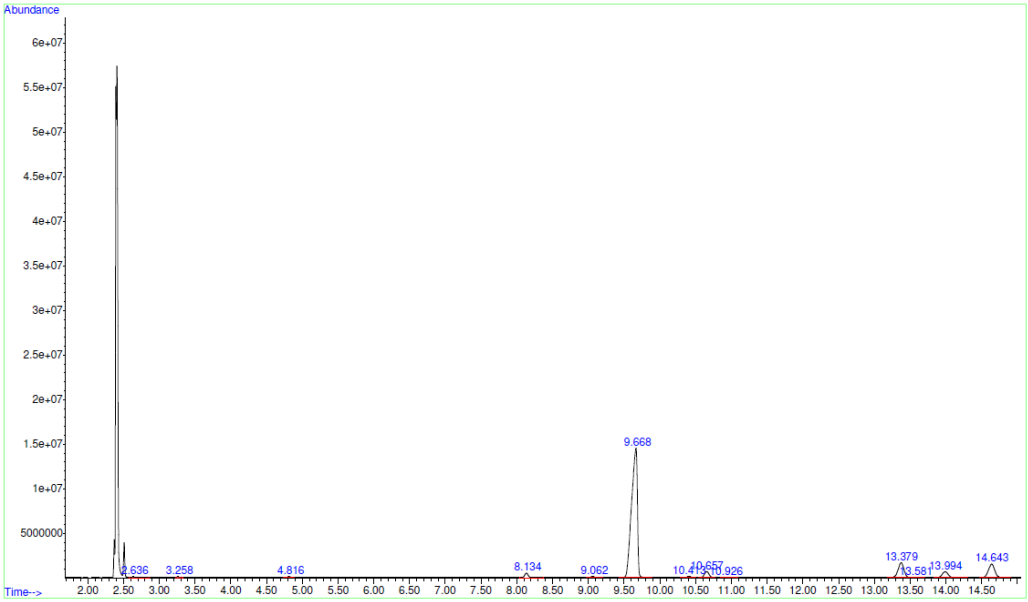


Figure E 11: Sample chromatogram for Step 2 condensate constituents between 2 RTmin and 15 RTmin

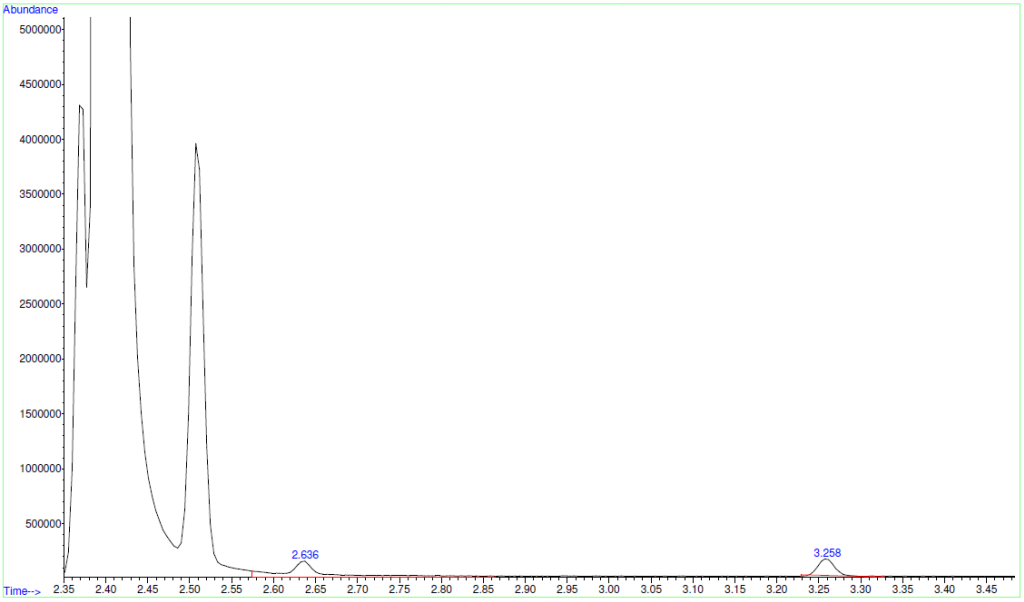


Figure E 12: Sample chromatogram for Step 2 condensate constituents between 2.35 RTmin and 3.45 RTmin

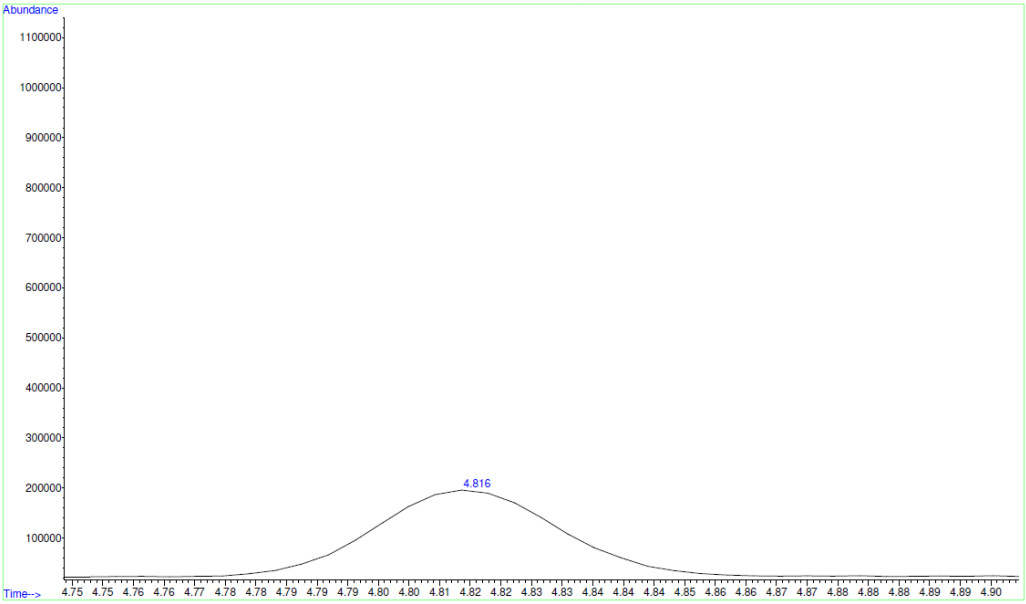


Figure E 13: Sample chromatogram for Step 2 condensate constituents between 4.75 RTmin and 4.90 RTmin

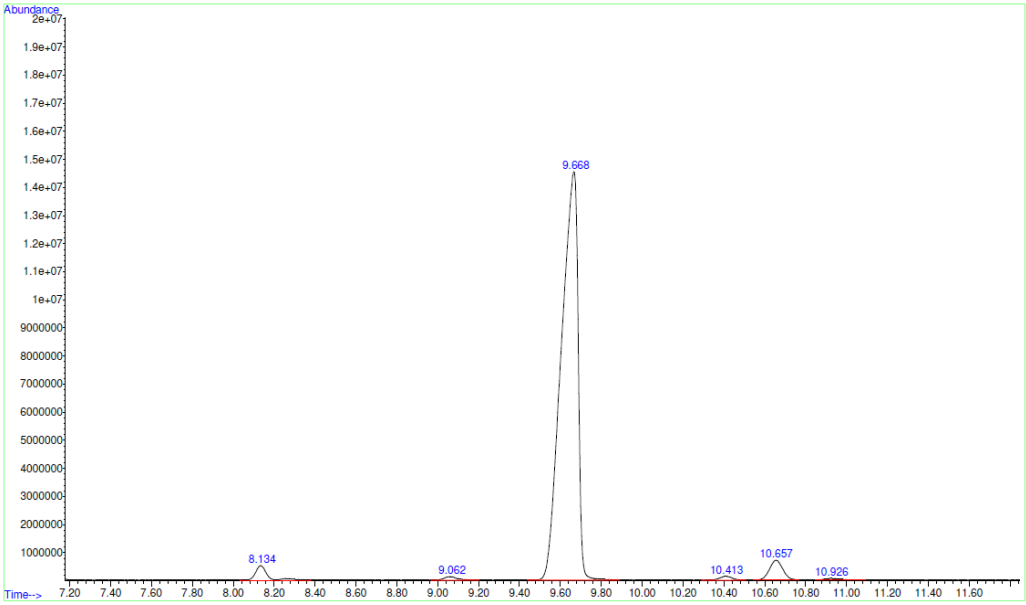


Figure E 14: Sample chromatogram for Step 2 condensate constituents between 7.2 RTmin and 11.60 RTmin

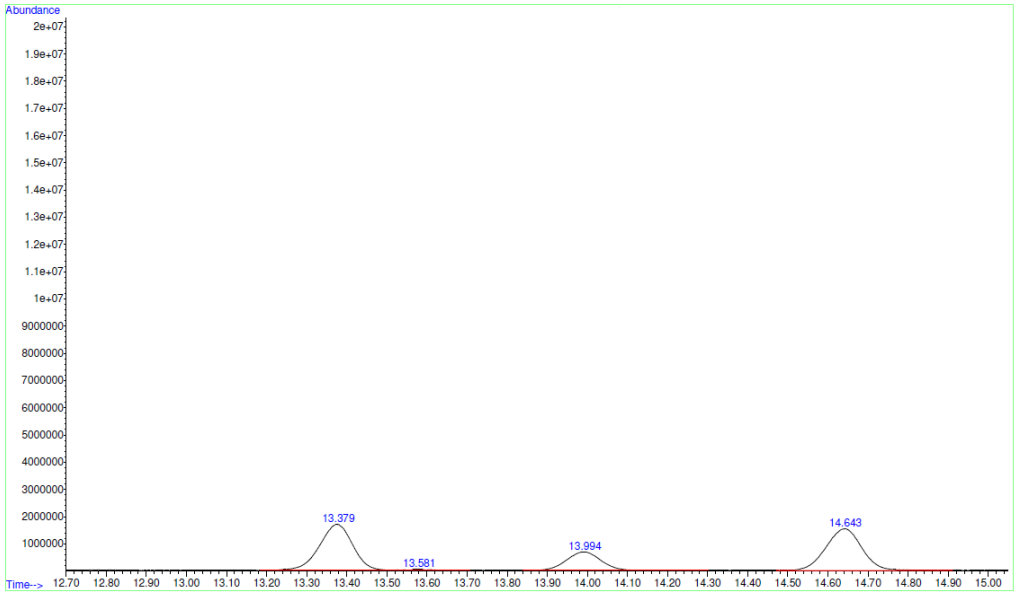


Figure E 15: Sample chromatogram for Step 2 condensate constituents between 12.70 RTmin and 15 RTmin

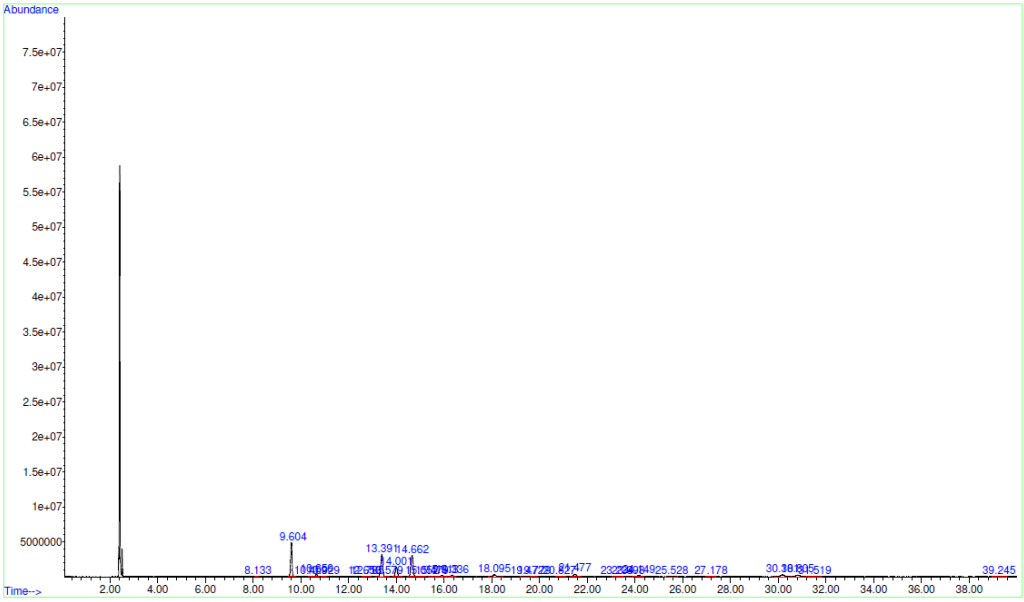


Figure E 16: Sample chromatogram for Step 2 flask constituents between 2 RTmin and 39.3 RTmin

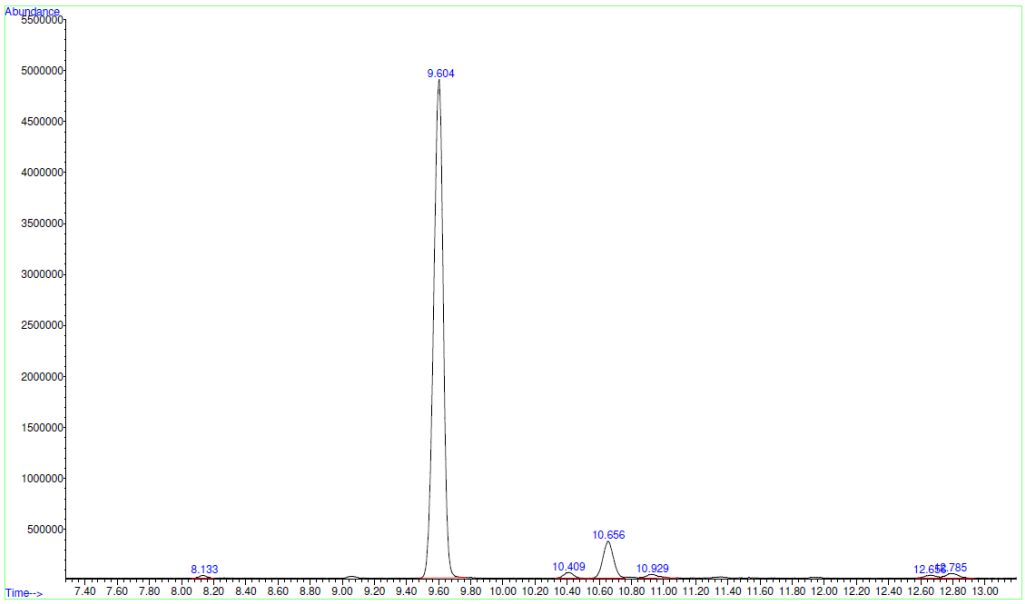


Figure E 17: Sample chromatogram for Step 2 flask constituents between 7.4 RTmin and 13 RTmin

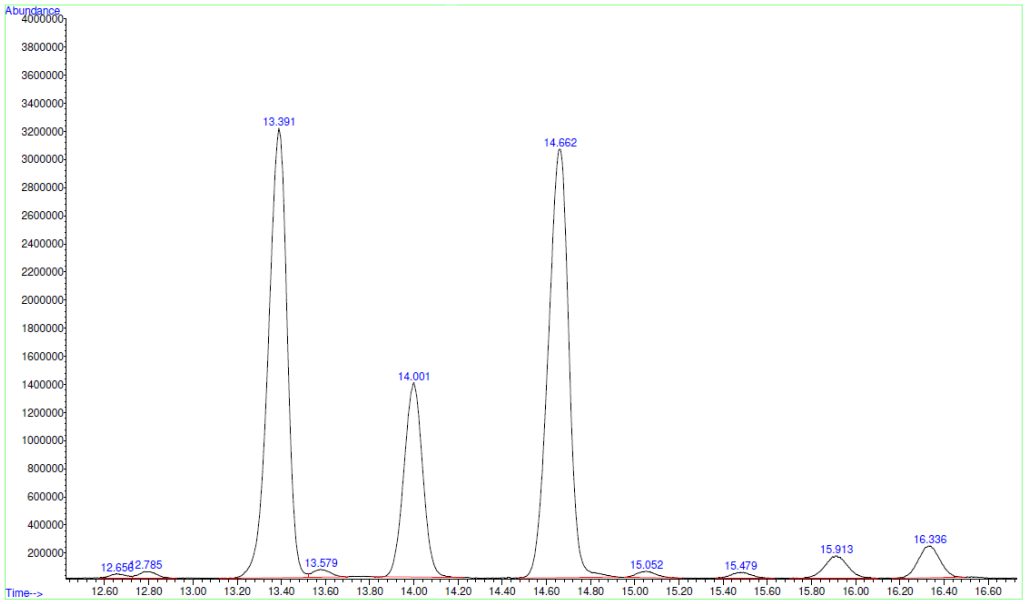


Figure E 18: Sample chromatogram for Step 2 flask constituents between 12.6 RTmin and 16.6 RTmin

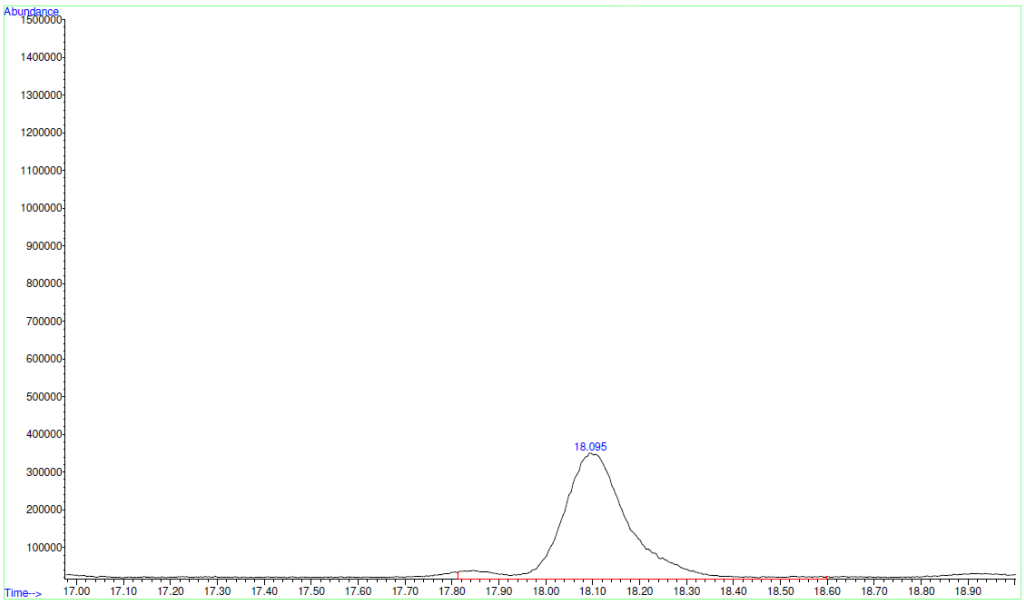


Figure E 19: Sample chromatogram for Step 2 flask constituents between 17 RTmin and 18.9 RTmin

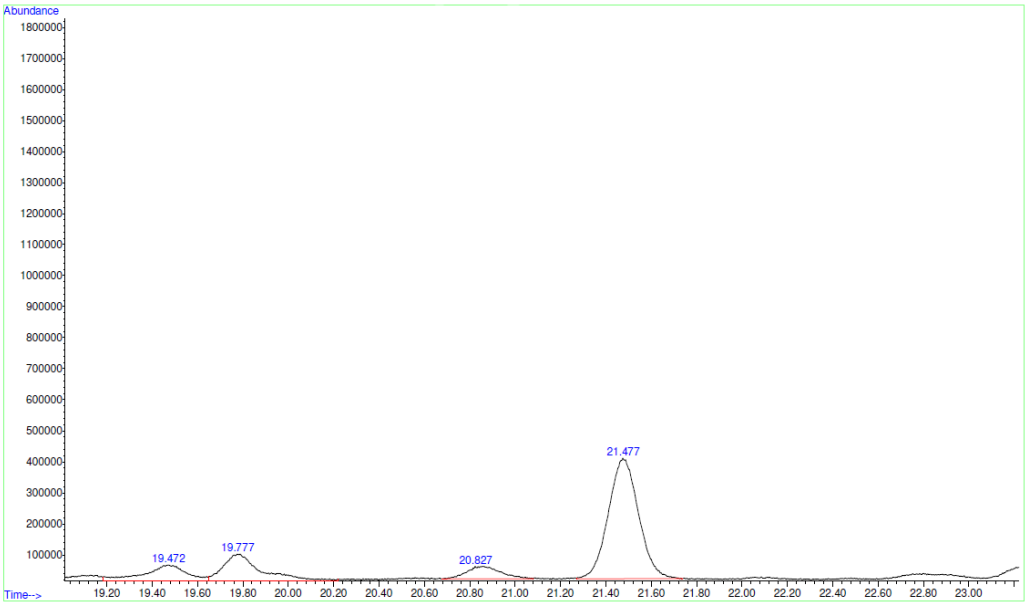


Figure E 20: Sample chromatogram for Step 2 flask constituents between 19.20 RTmin and 23.00 RTmin

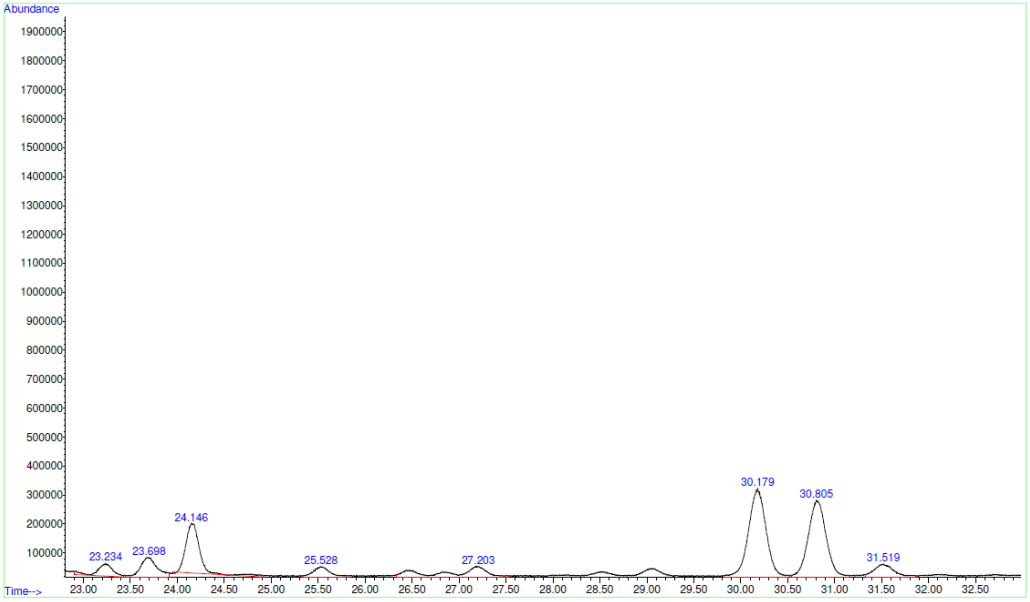


Figure E 21: Sample chromatogram for Step 2 flask constituents between 23 RTmin and 32.5 RTmin

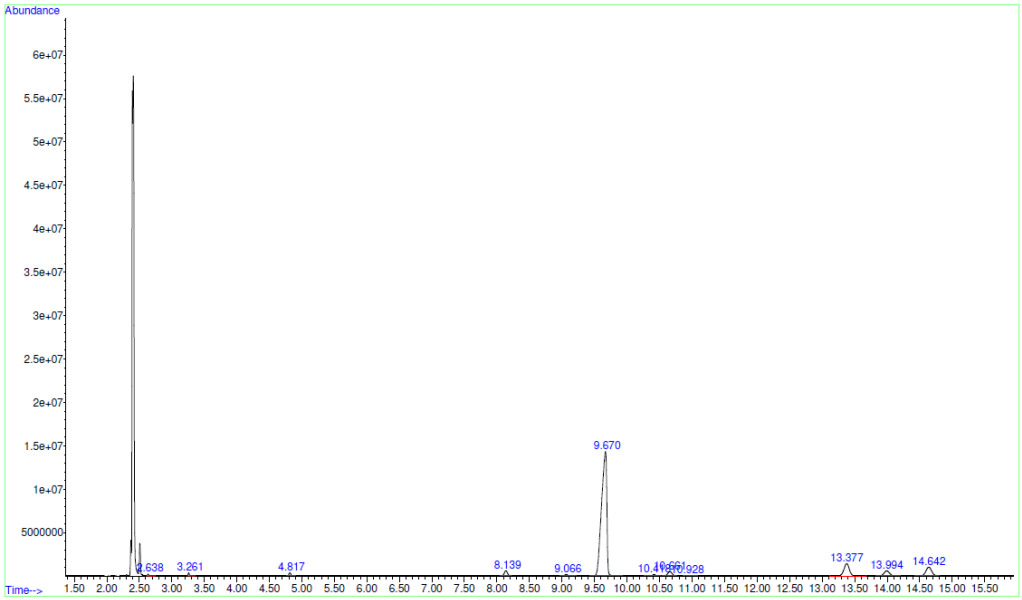


Figure E 22: Sample chromatogram for Step 3 condensate constituents between 1.5 RTmin and 15.5 RTmin

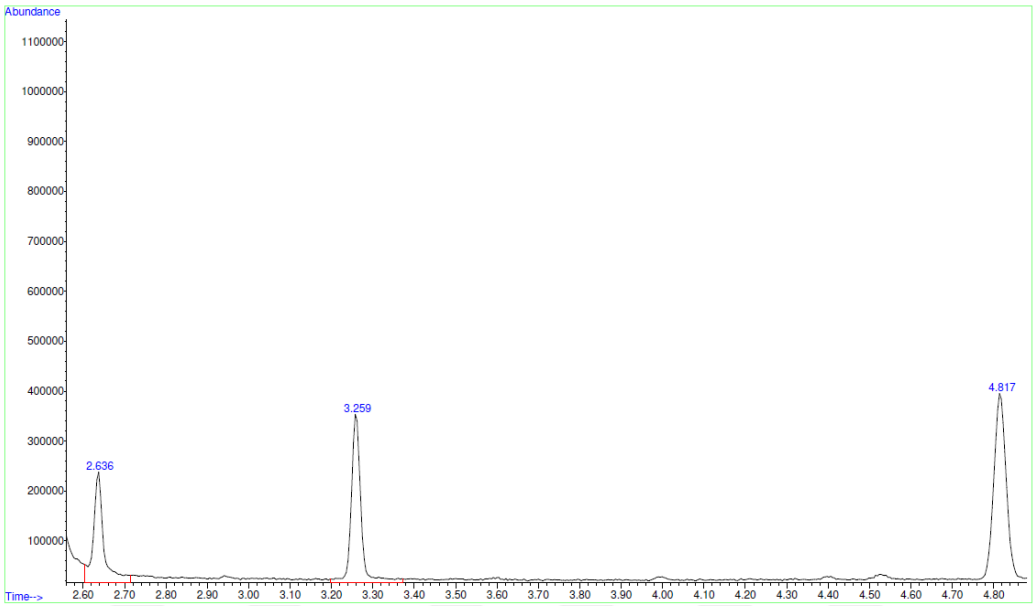


Figure E 23: Sample chromatogram for Step 3 condensate constituents between 2.6 RTmin and 4.8 RTmin

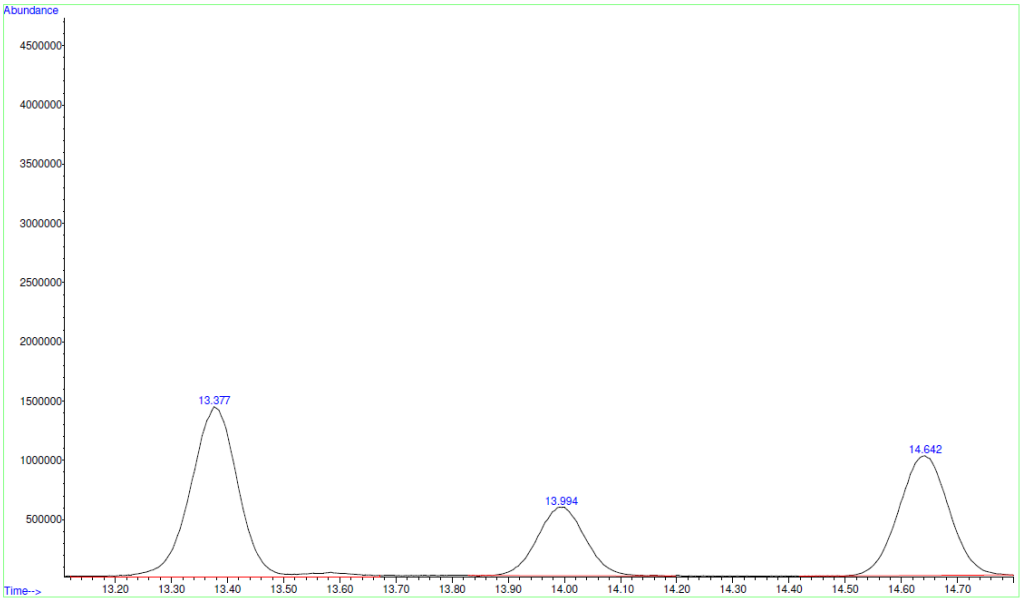


Figure E 24 : Sample chromatogram for Step 3 condensate constituents between 13.20 RTmin and 14.7 RTmin

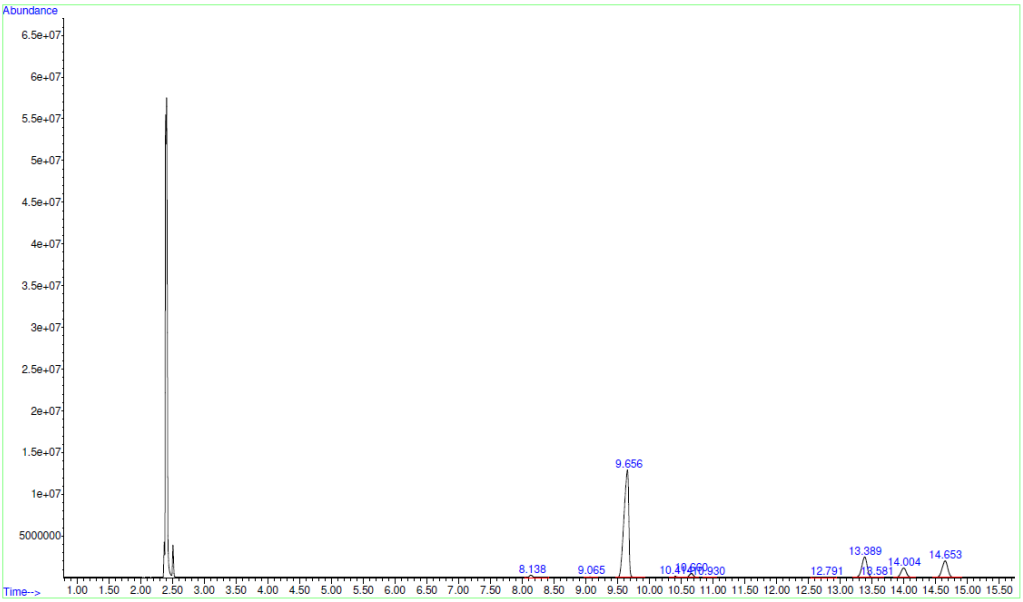


Figure E 25: Sample chromatogram for Step 3 flask constituents between 1 RTmin and 15.5 RTmin

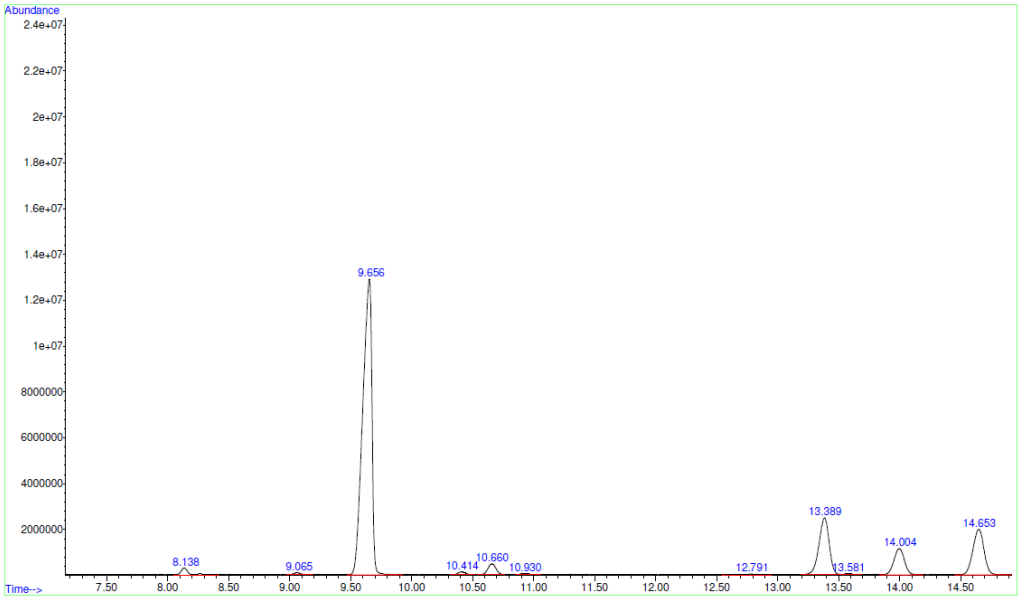


Figure E 26 : Sample chromatogram for Step 3 condensate constituents between 7.5 RTmin and 14.5 RTmin

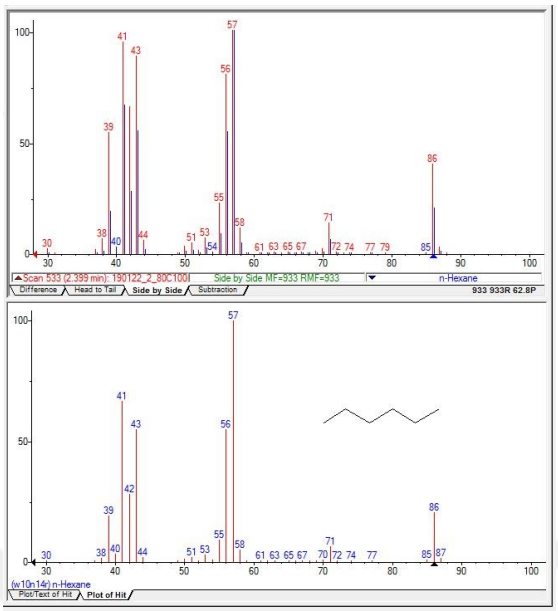


Figure E 27: Mass spectra and library match for peak at 2.40 RTmin

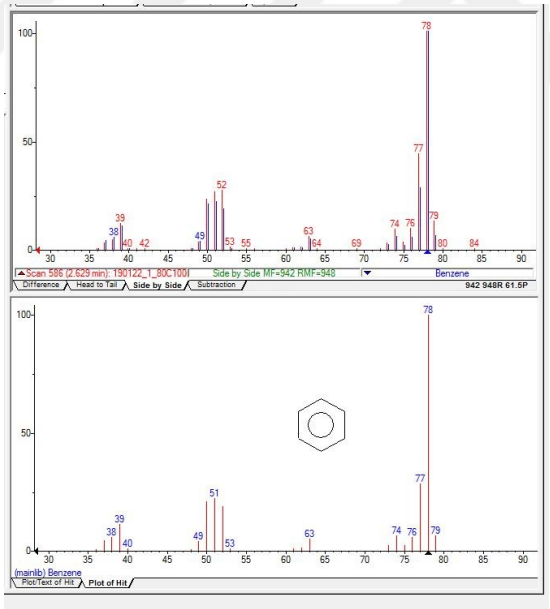


Figure E 28:Mass spectra and library match for peak at 2.62 RTmin

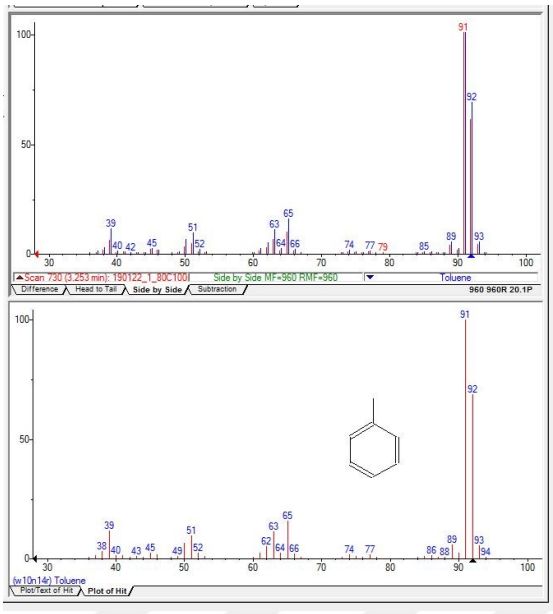


Figure E 29: Mass spectra and library match for peak at 3.25 RTmin

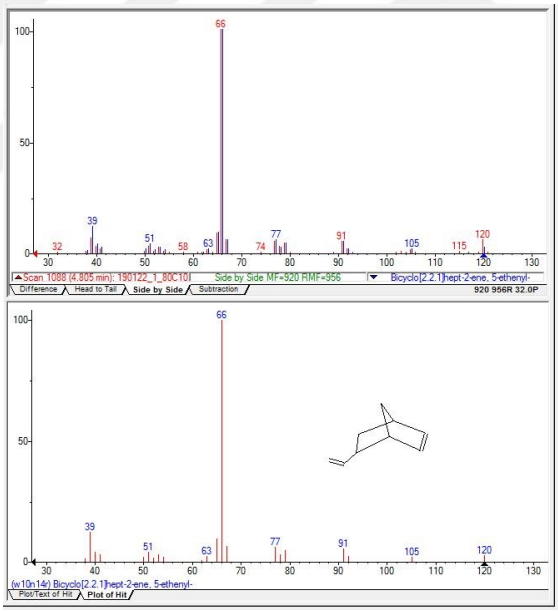


Figure E 30: Mass spectra and library match for peak at 4.81 RTmin

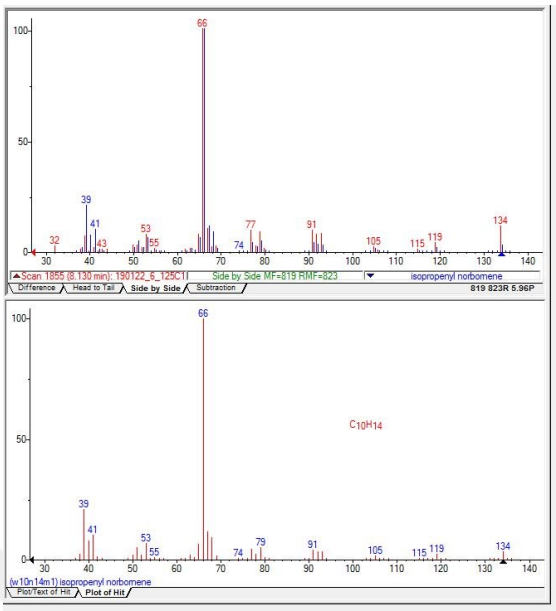


Figure E 31: Mass spectra and library match for peak at 8.13 RTmin

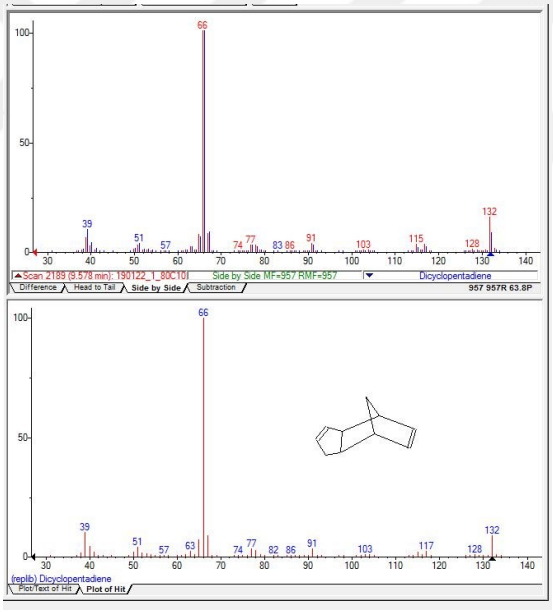


Figure E 32: Mass spectra and library match for peak at 9.58 RTmin

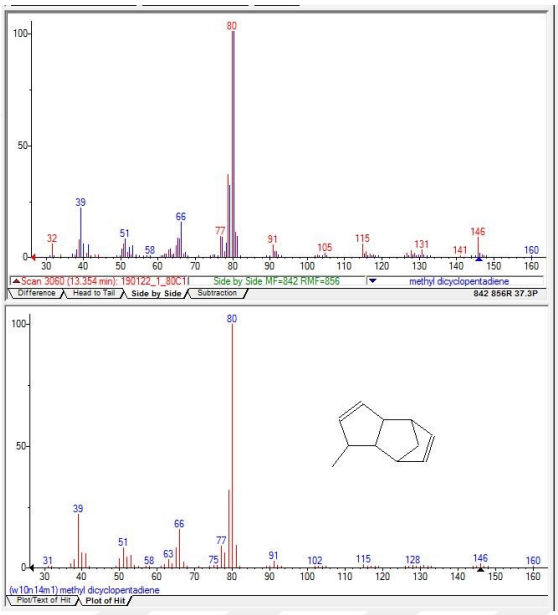


Figure E 33: Mass spectra and library match for peak at 13.35 RTmin

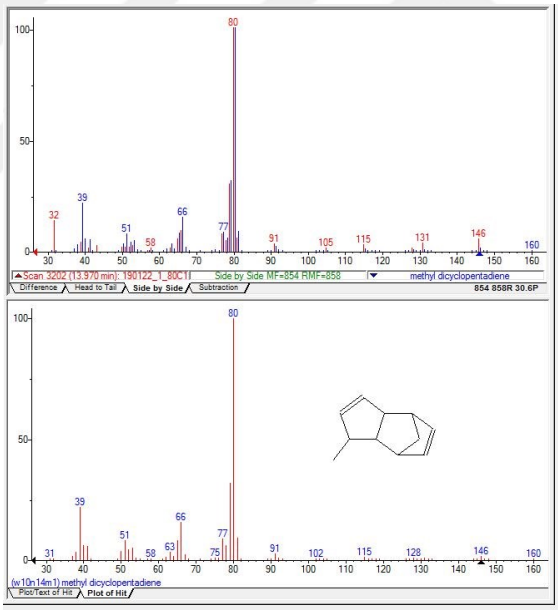


Figure E 34:Mass spectra and library match for peak at 13.97 RTmin

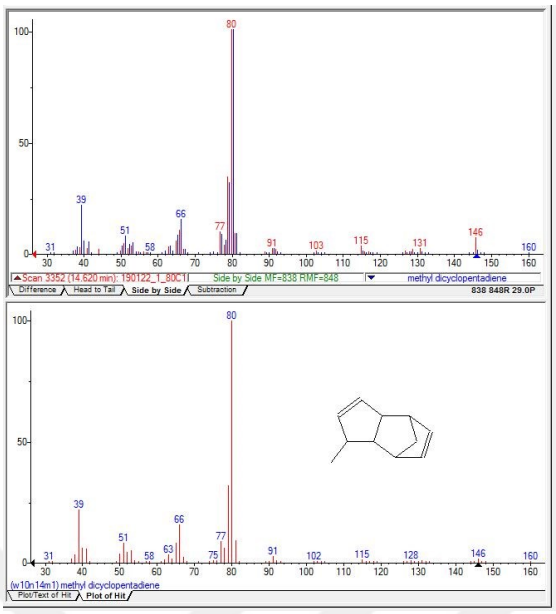


Figure E 35:Mass spectra and library match for peak at 14.62 RTmin

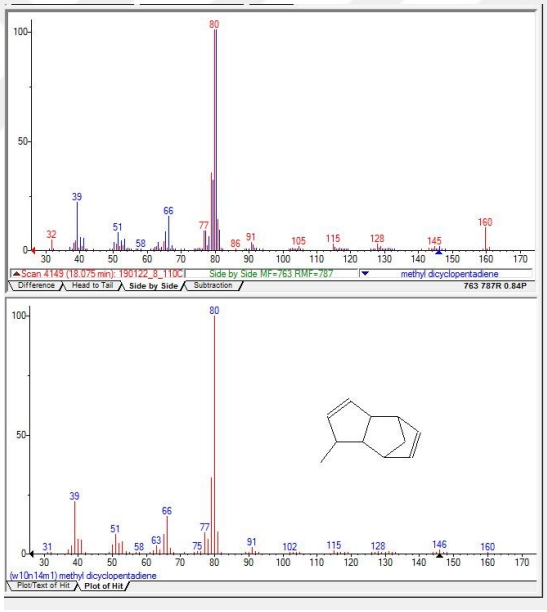


Figure E 36:Mass spectra and library match for peak at 18.10 RTmin

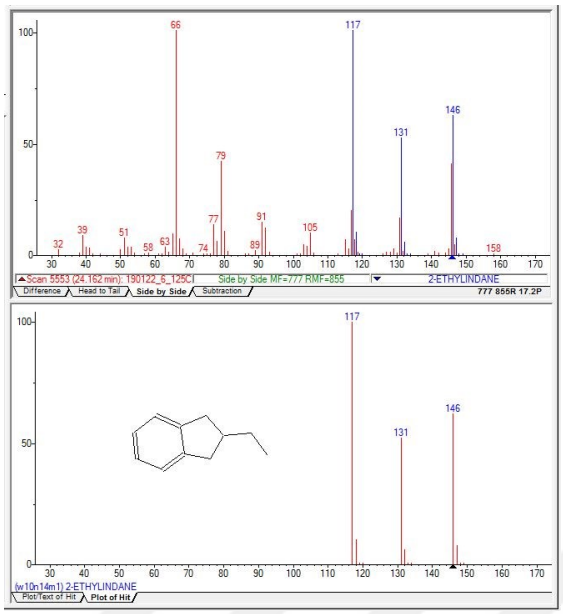


Figure E 37. Mass spectra and library match for peak at 24.16 RTmin

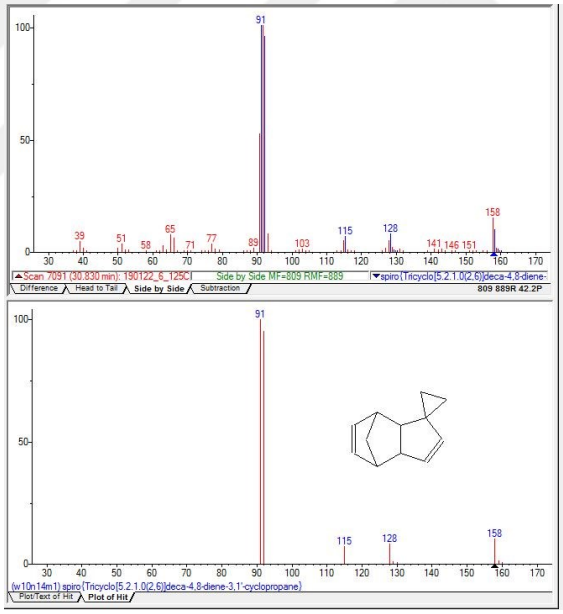


Figure E 38: Mass spectra and library match for peak at 30.83 RTmin

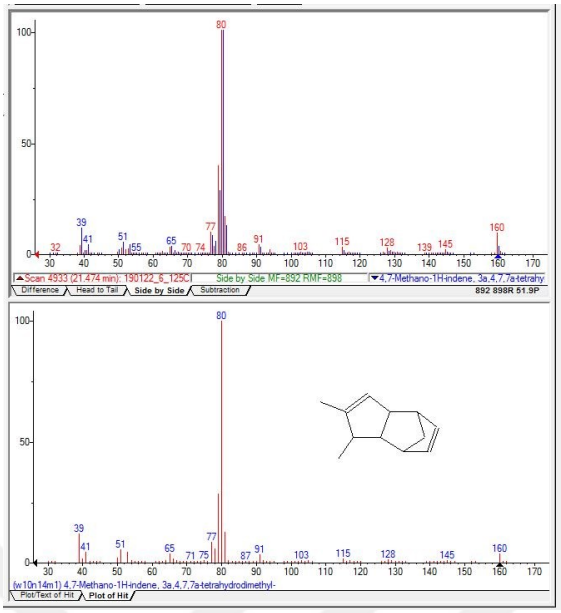


Figure E 39: Mass spectra and library match for peak at 21.47 RTmin

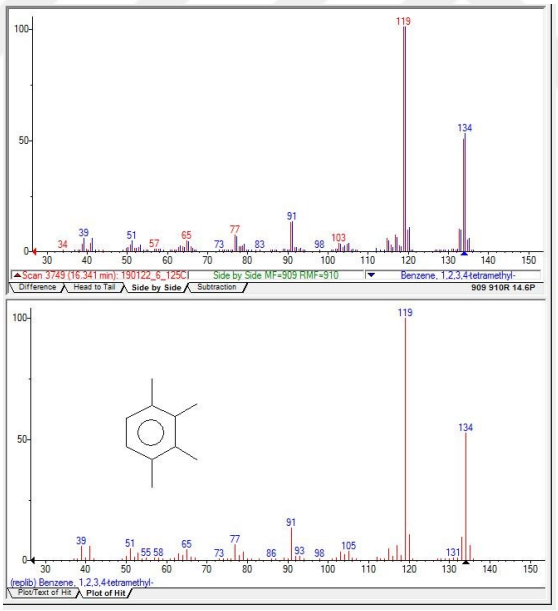


Figure E 40: Mass spectra and library match for peak at 16.34 RTmin

F. Sample Chromatogram for GC-MS Reaction Experiment of DCPD in Heptane

DCPD reaction experiments were conducted in GC-MS. Chromatographic grade heptane was used as a dilution solvent. Abundance at corresponding retention times (RTmin) are given in Figure F1 where peaks at 4.17 through 4.49 are solvent peaks for heptane. The chromatograms and spectras are given in Figure F1 through F25 while the method parameters are given in Table F1.

Table F 1: Method information for DCPD reaction in GC-MS in heptane

GC-MS Parameters	*Value*
Column	HP-5 ms
Inlet Type	Split (50:1)
Inlet Temperature	80-350°C
Injection Volume	0.2 µL
Inlet Gas Flow	He, 10-20 mL/min
Column Gas Flow	1.2 mL/min
Column Pressure	1.1 bar
Oven Program	50°C for 40 min
MS Gain Factor	2
Acquisition Type	Scan
Frequency	3.9 scans/sec
MS Step Size	0.1 m/z
MS Scan Range	30-500

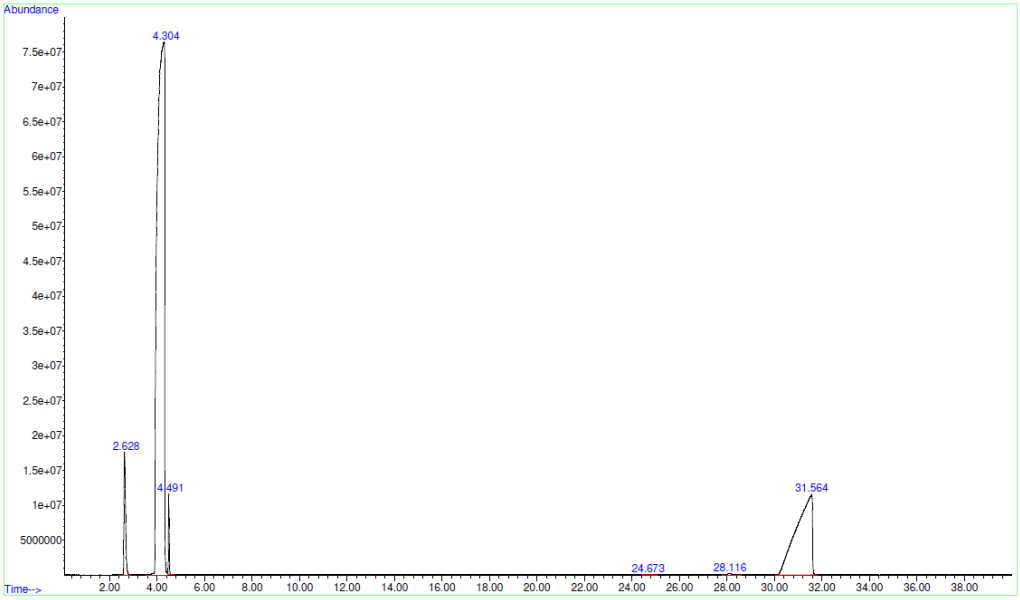


Figure F 1: Sample chromatogram for GC-MS reaction experiment constituents between 2 RTmin and 38 RTmin at 250°C and 10 mL/min Helium flow

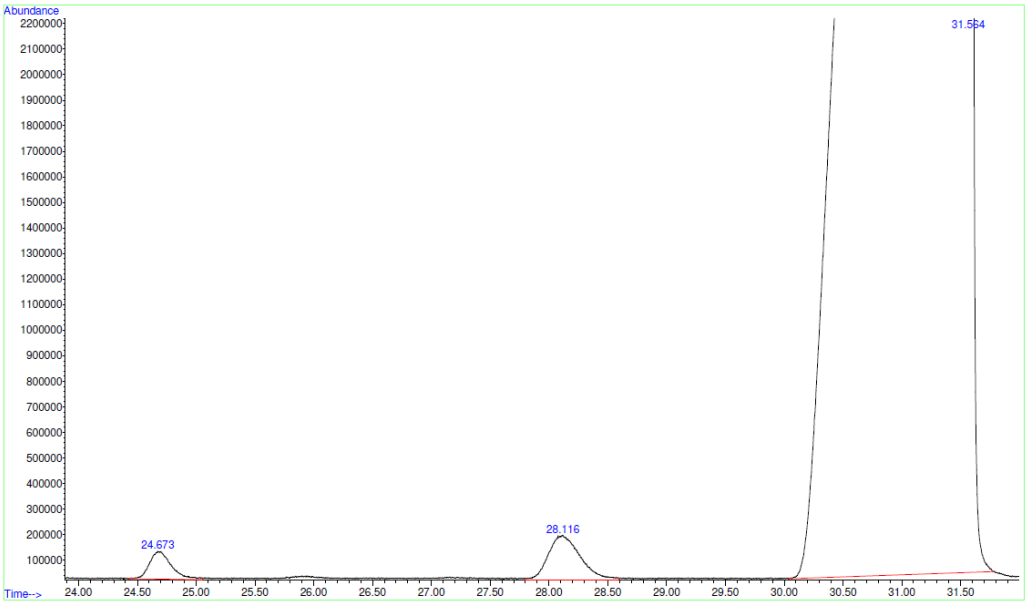


Figure F 2: Sample chromatogram for GC-MS reaction experiment constituents between 24 RTmin and 31.5 RTmin at 250°C and 10 mL/min Helium flow

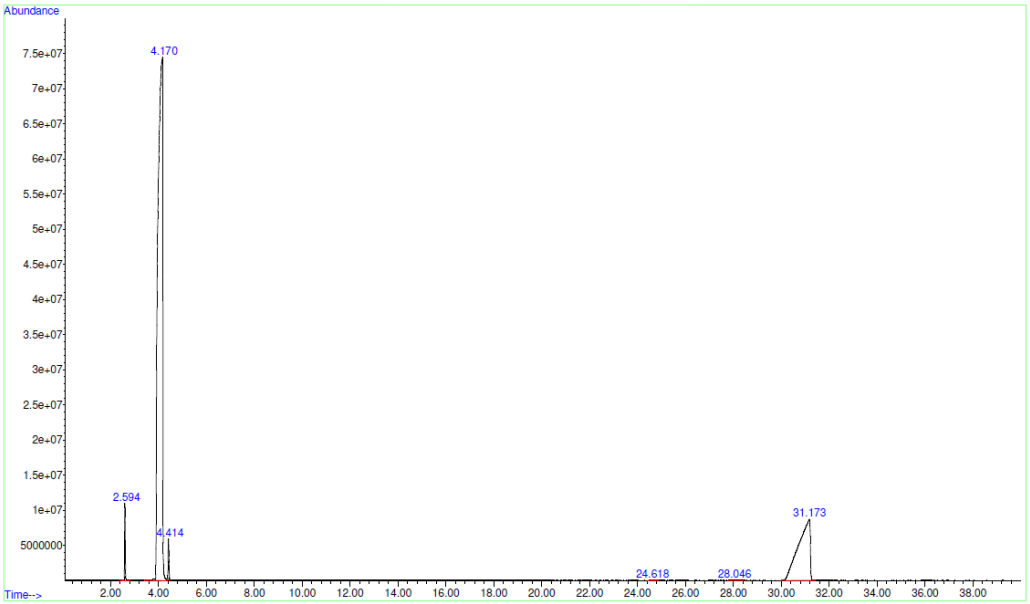


Figure F 3: Sample Chromatogram for GC-MS reaction experiment constituents between 2 RTmin and 38 RTmin at 250°C and 20 mL/min Helium flow

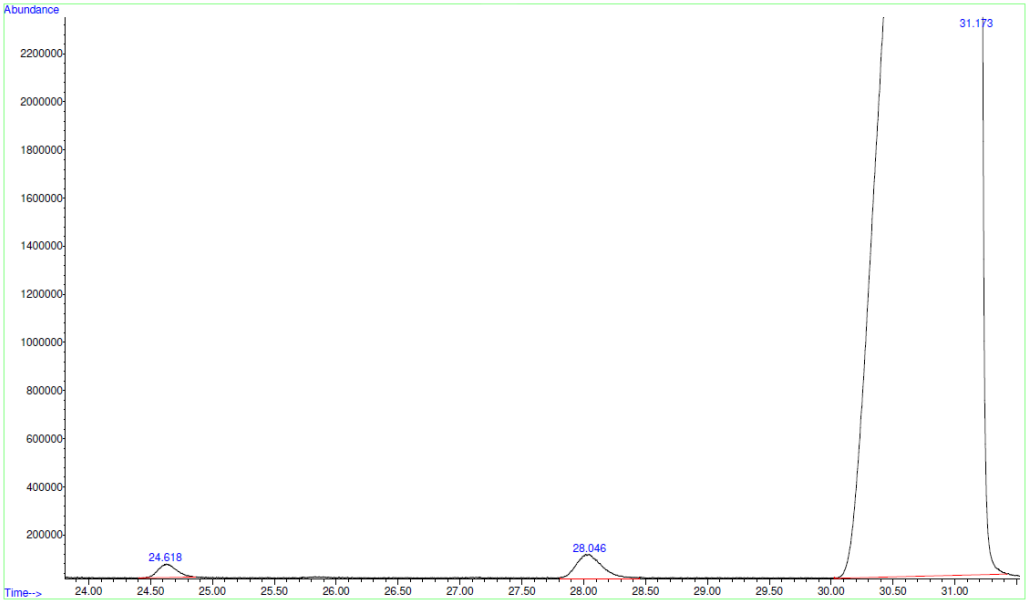


Figure F 4: Sample chromatogram for GC-MS reaction experiment constituents between 24 RTmin and 31 RTmin at 250°C and 20 mL/min Helium flow

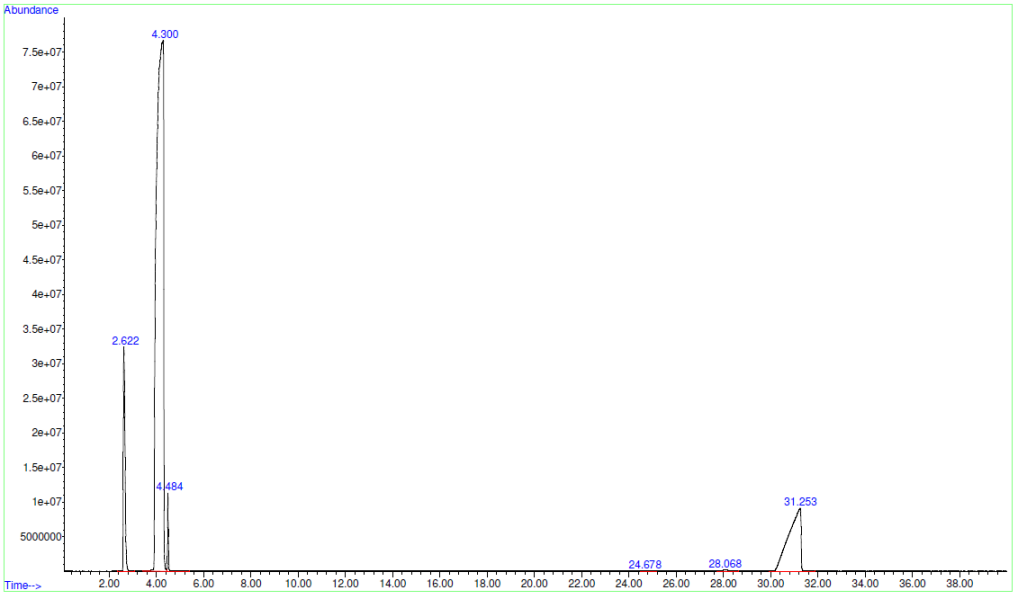


Figure F 5: Sample chromatogram for GC-MS reaction experiment constituents between 2 RTmin and 38 RTmin at 270°C and 10 mL/min Helium flow

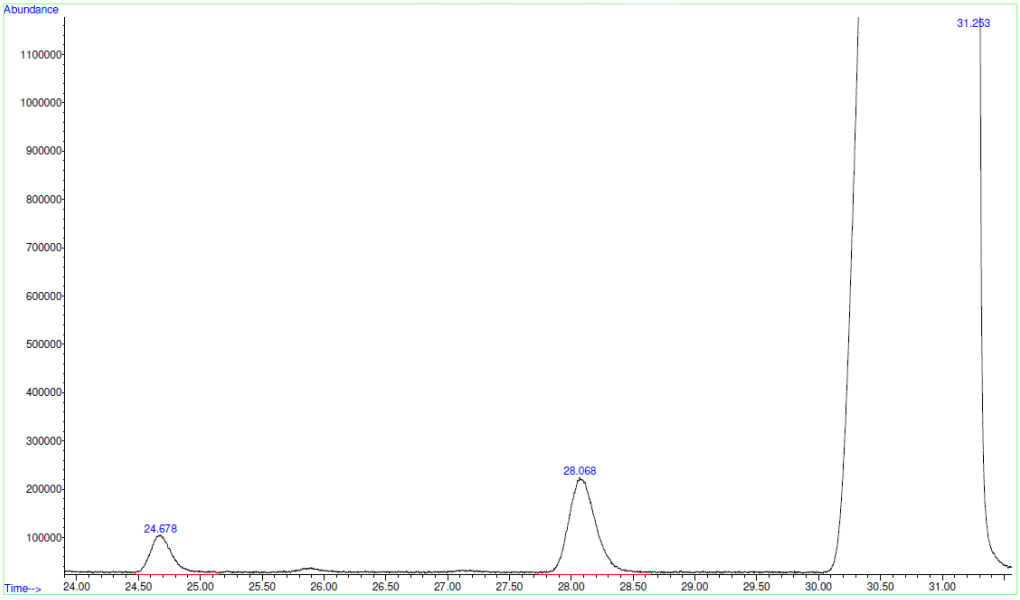


Figure F 6: Sample chromatogram for GC-MS reaction experiment constituents between 24 RTmin and 32 RTmin at 270°C and 10 mL/min Helium flow

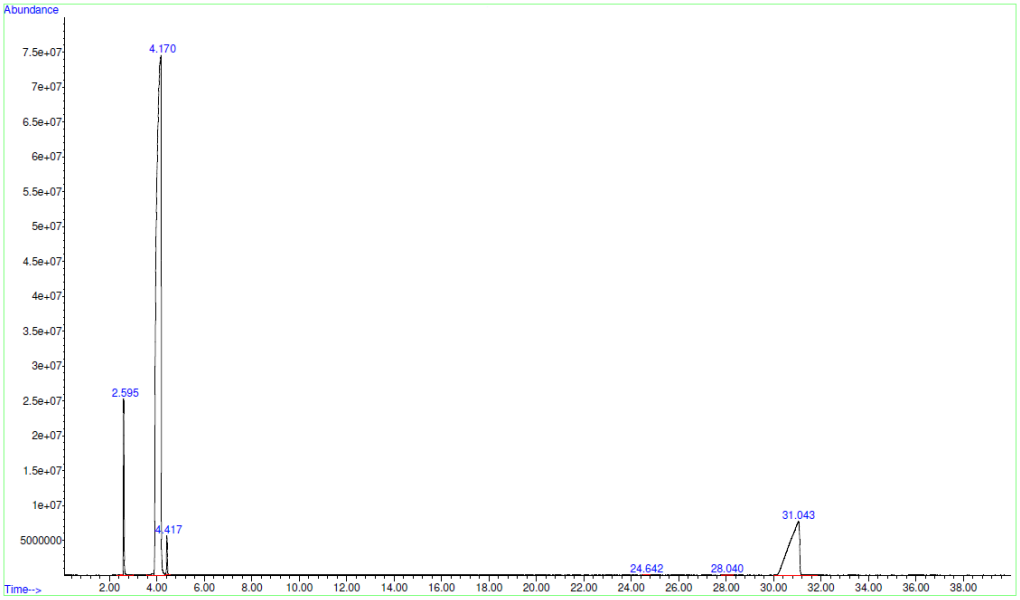


Figure F 7: Sample chromatogram for GC-MS reaction experiment constituents between 2 RTmin and 38 RTmin at 270°C and 20 mL/min Helium flow

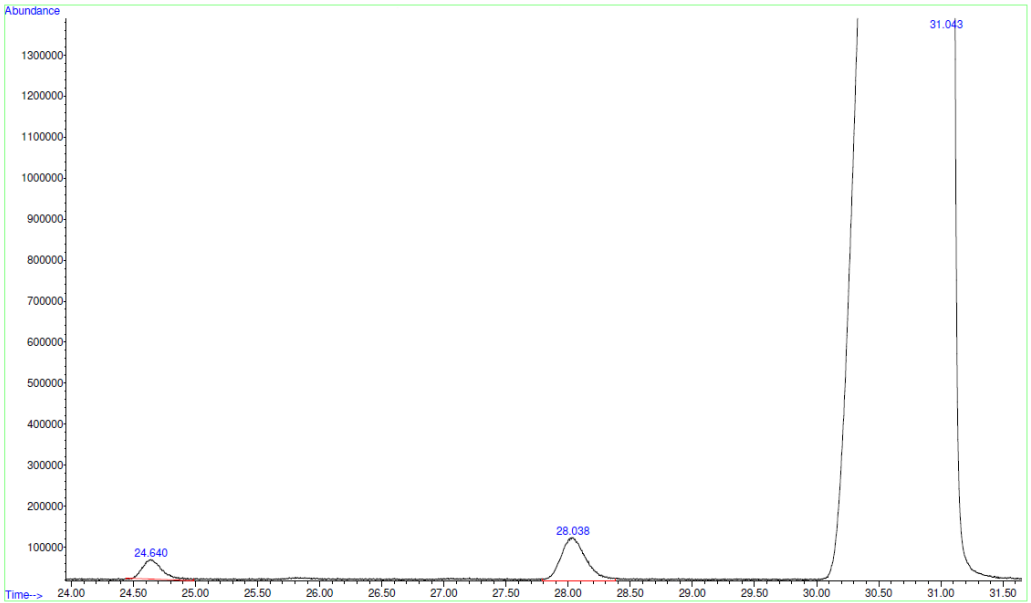


Figure F 8: Sample chromatogram for GC-MS reaction experiment constituents between 24 RTmin and 31.5 RTmin at 270°C and 20 mL/min Helium flow

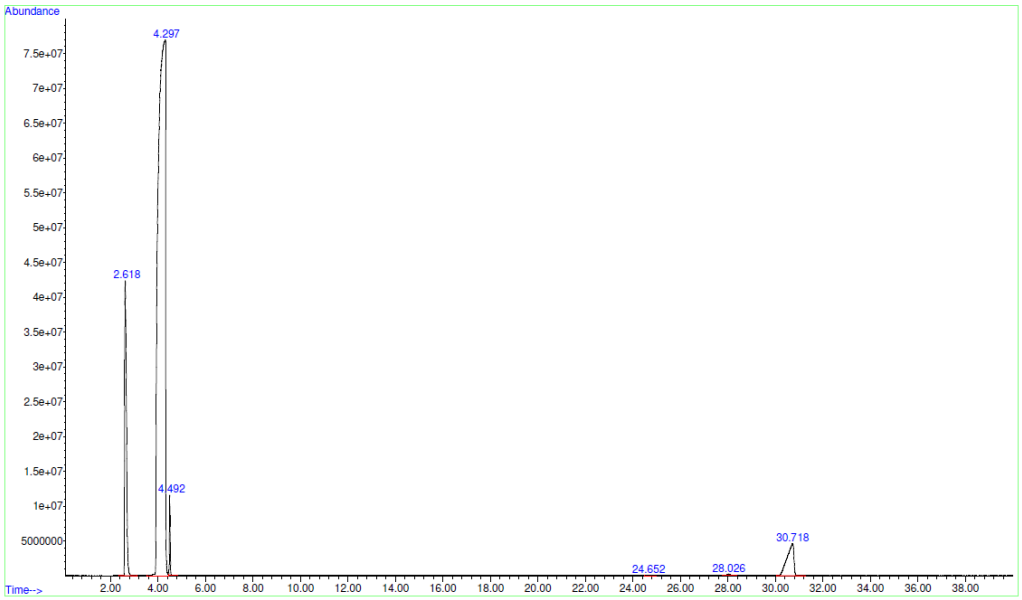


Figure F 9: Sample chromatogram for GC-MS reaction experiment constituents between 2 RTmin and 38 RTmin at 290°C and 10 mL/min Helium flow

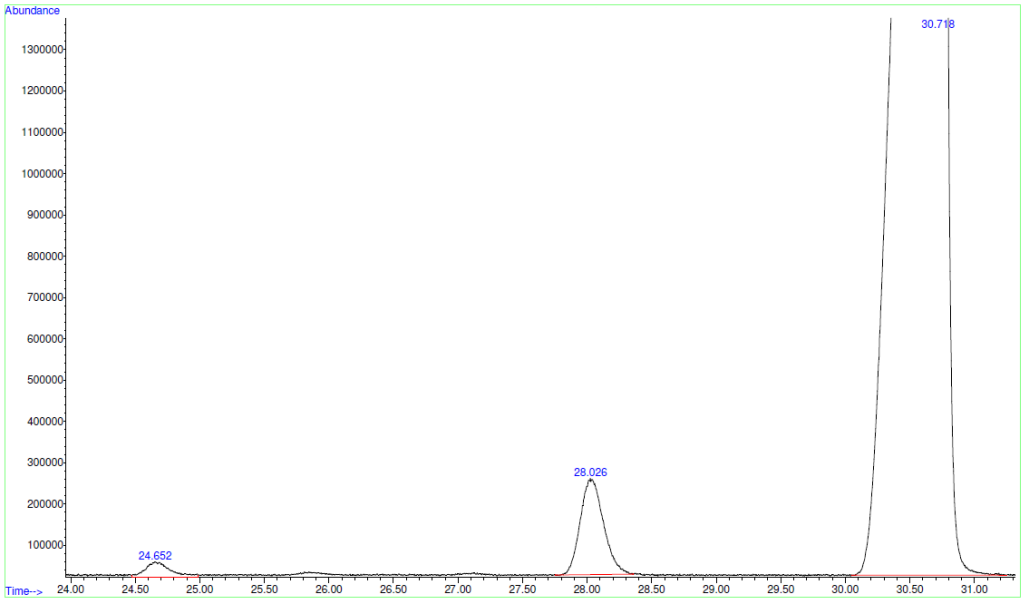


Figure F 10: Sample chromatogram for GC-MS reaction experiment constituents between 24 RTmin and 31 RTmin at 290°C and 10 mL/min Helium flow

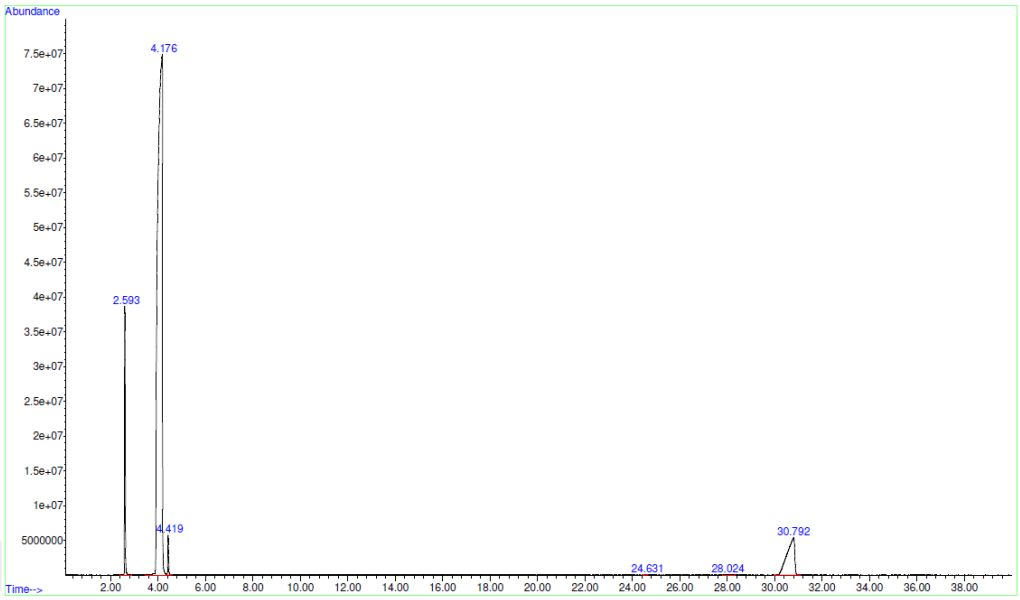


Figure F 11: Sample chromatogram for GC-MS reaction experiment constituents between 2 RTmin and 38 RTmin at 290°C and 20 mL/min Helium flow

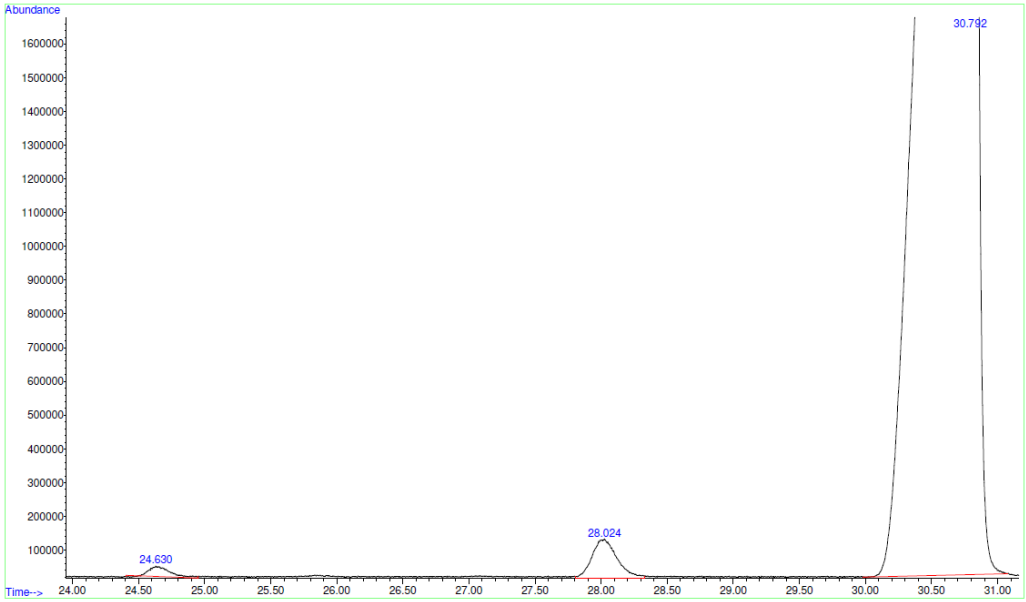


Figure F 12: Sample chromatogram for GC-MS reaction experiment constituents between 24 RTmin and 31 RTmin at 290°C and 20 mL/min Helium flow



Figure F 13: Sample chromatogram for GC-MS reaction experiment constituents between 2 RTmin and 38 RTmin at 330°C and 10 mL/min Helium flow

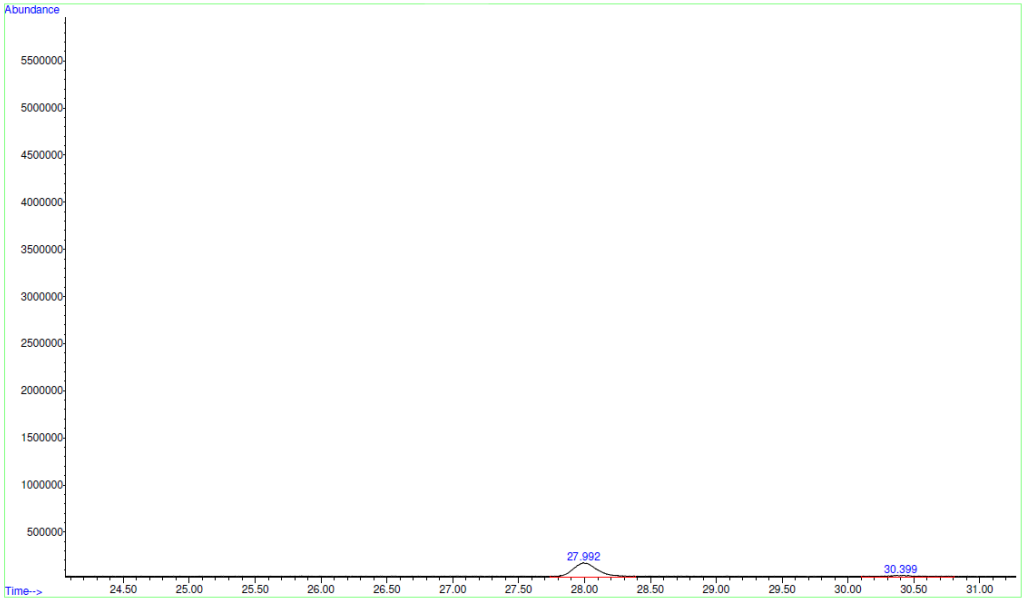


Figure F 14: Sample chromatogram for GC-MS reaction experiment constituents between 24 RTmin and 31 RTmin at 330°C and 10 mL/min Helium flow



Figure F 15: Sample chromatogram for GC-MS reaction experiment constituents between 2 RTmin and 38 RTmin at 330°C and 20 mL/min Helium flow



Figure F 16:Sample chromatogram for GC-MS reaction experiment constituents between 24 RTmin and 31 RTmin at 330°C and 20 mL/min Helium flow

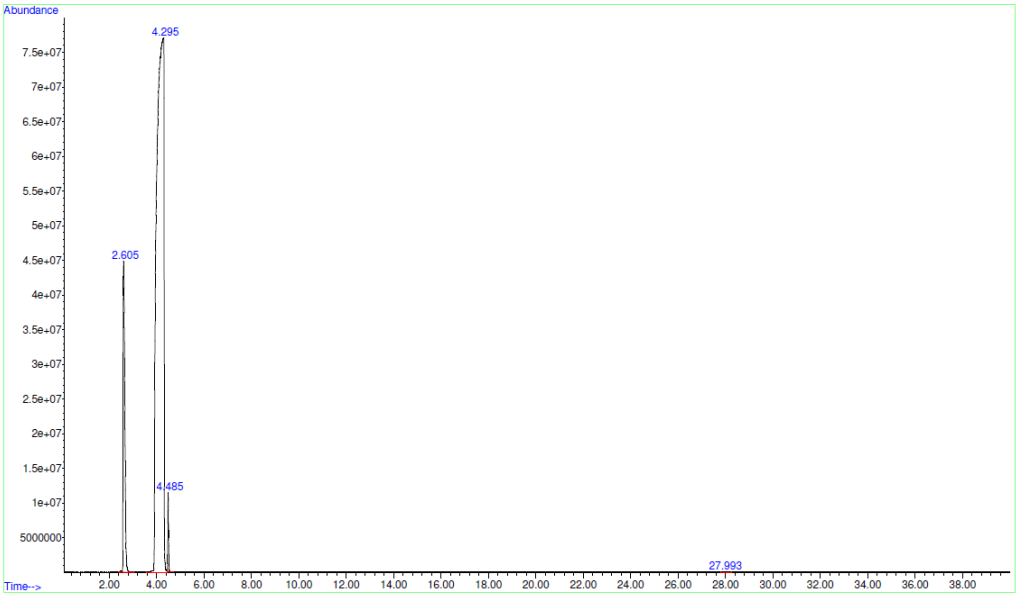


Figure F 17: Sample chromatogram for GC-MS reaction experiment constituents between 2 RTmin and 38 RTmin at 350°C and 10 mL/min Helium flow

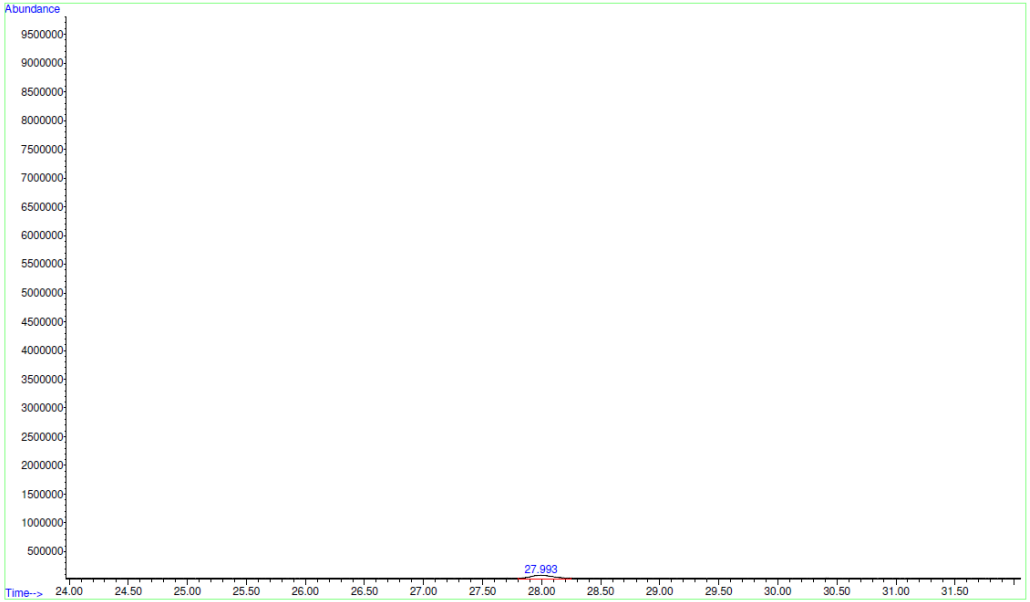


Figure F 18: Sample chromatogram for GC-MS reaction experiment constituents between 24 RTmin and 31.5 RTmin at 350°C and 10 mL/min Helium flow

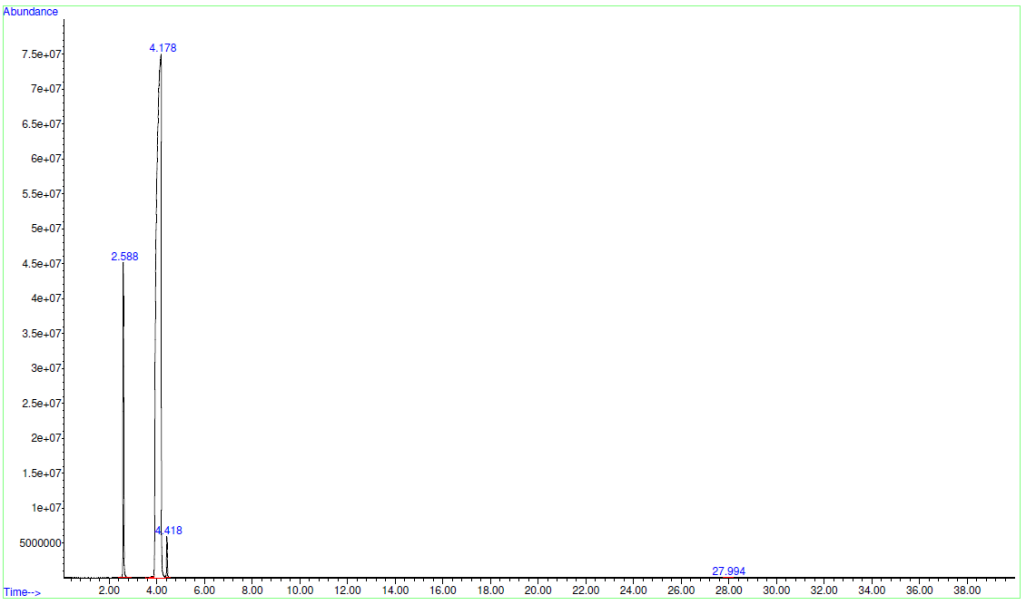


Figure F 19: Sample chromatogram for GC-MS reaction experiment constituents between 2 RTmin and 38 RTmin at 350°C and 20 mL/min Helium flow

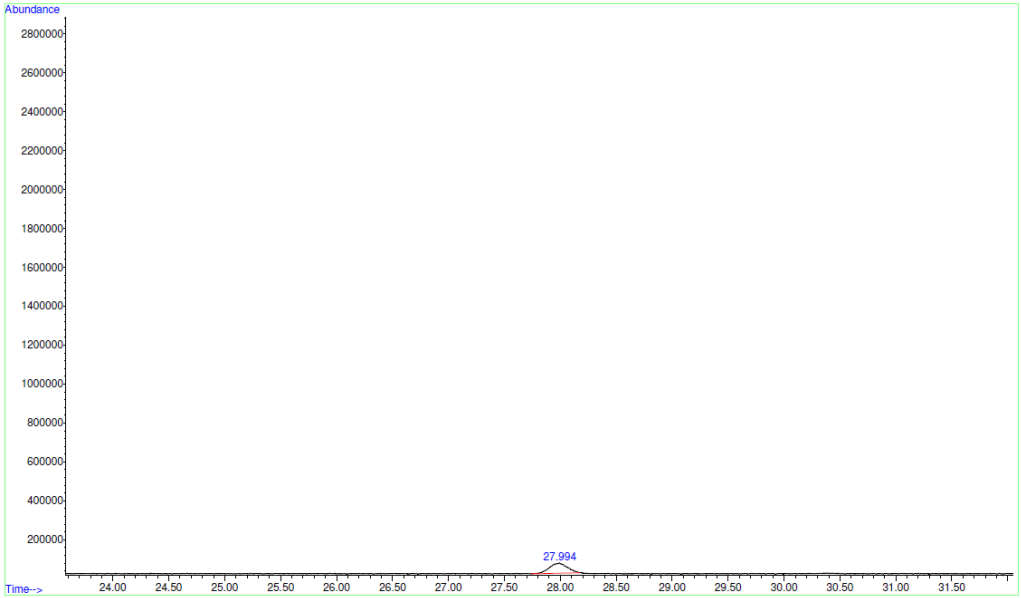


Figure F 20: Sample chromatogram for GC-MS reaction experiment constituents between 24 RTmin and 31.5 RTmin at 350°C and 20 mL/min Helium flow

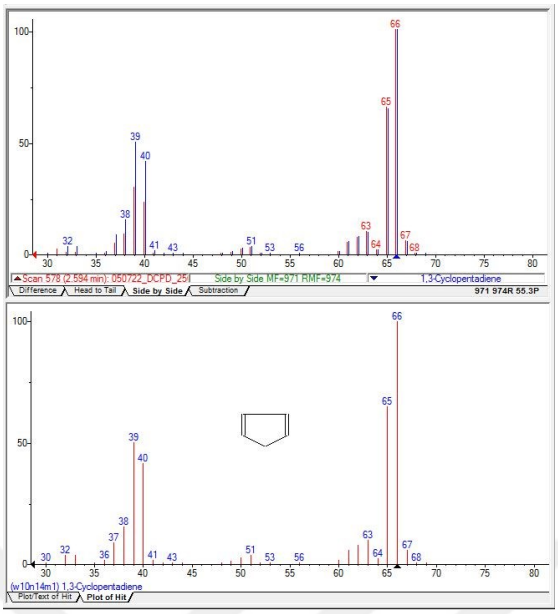


Figure F 21: Mass spectra and library match for peak at 2.59 RTmin

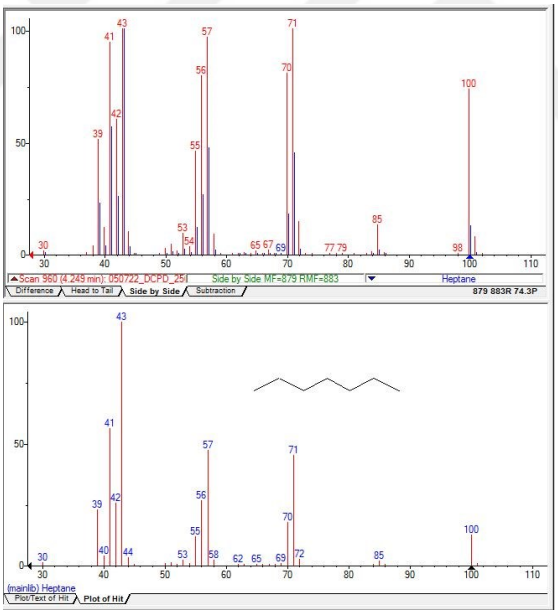


Figure F 22: Mass spectra and library match for peak at 4.25 RTmin

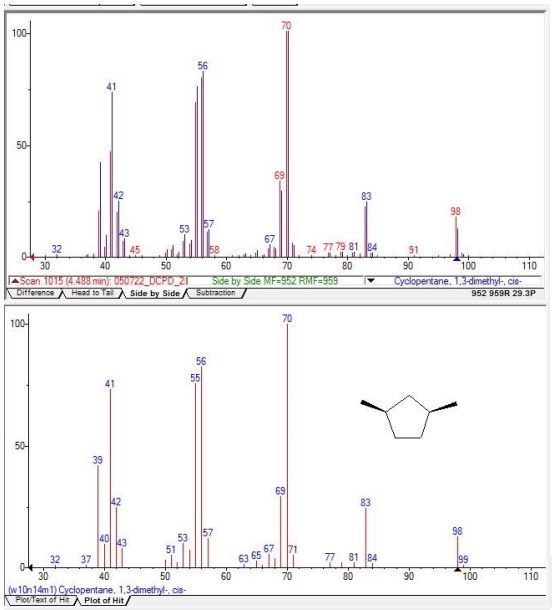


Figure F 23: Mass spectra and library match for peak at 4.49 RTmin

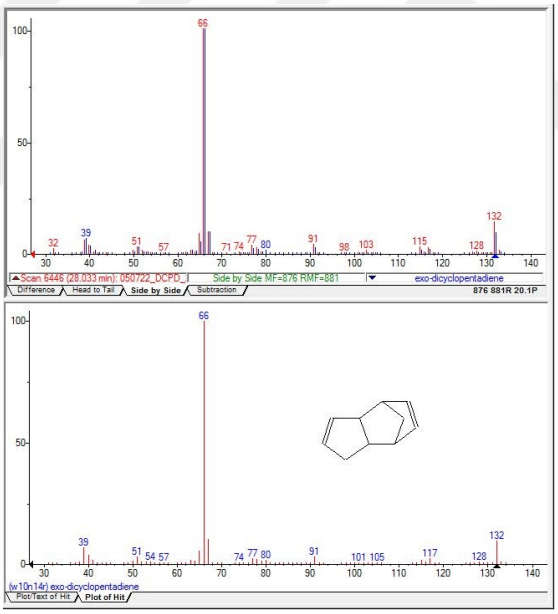


Figure F 24: Mass spectra and library match for peak at 28.03 RTmin

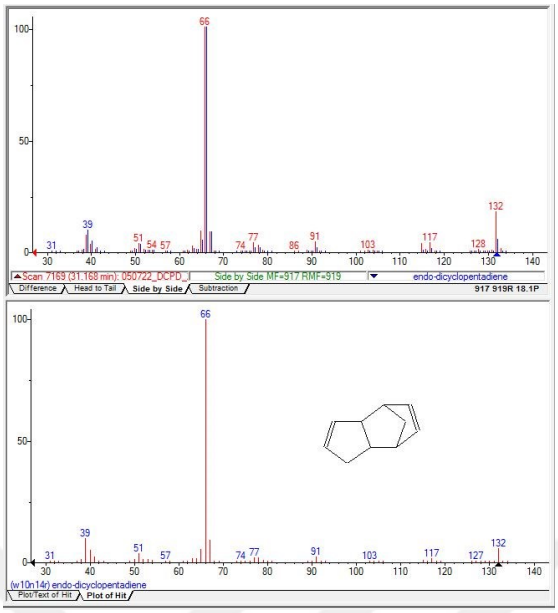


Figure F 25: Mass spectra and library match for peak at 31.17 RTmin

G. Sample Chromatogram for GC-MS Reaction Experiments of DCPD in Toluene

DCPD reaction experiments were conducted in GC-MS. Chromatographic grade toluene was also used as a dilution solvent. Abundance at corresponding retention time (RTmin) are given in Figure G1 where peak at 3.315 is solvent peak for toluene. The method parameters are given in Table G1.

Table G 1: Method information for DCPD reaction in GC-MS in toluene

GC-MS Parameters	*Value*
Column	HP-5 ms
Inlet Type	Split (50:1)
Inlet Temperature	80-350°C
Injection Volume	0.2 µL
Inlet Gas Flow	He, 20 mL/min
Column Gas Flow	1.2 mL/min
Column Pressure	1.1 bar
Oven Program	50°C for 25 min
MS Gain Factor	2
Acquisition Type	Scan
Frequency	3.9 scans/sec
MS Step Size	0.1 m/z
MS Scan Range	30-500

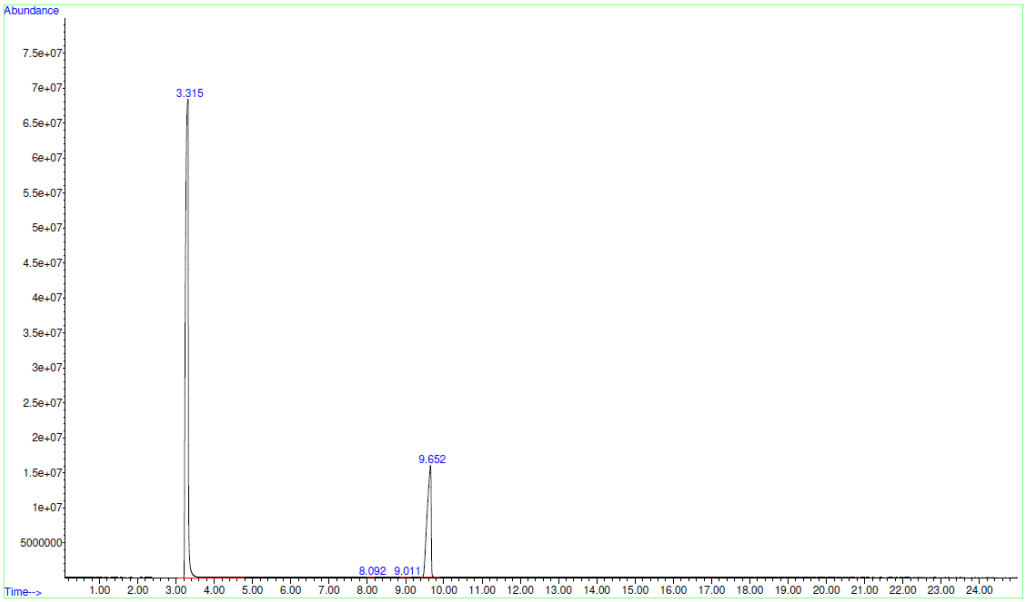


Figure G 1: Sample chromatogram for GC-MS reaction experiment constituents between 1 RTmin and 24 RTmin at 80°C in toluene

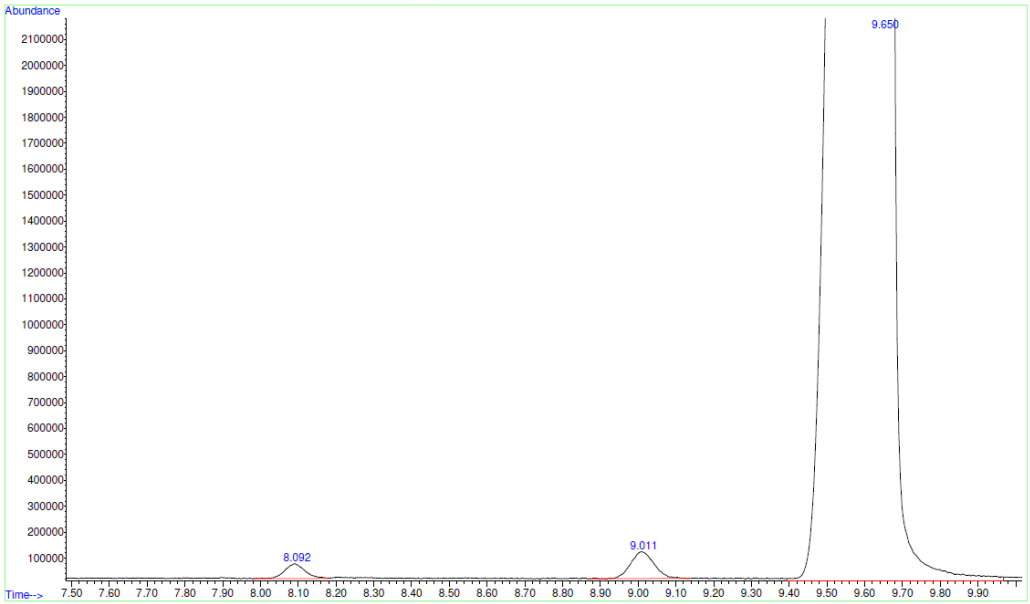


Figure G 2: Sample chromatogram for GC-MS reaction experiment constituents between 7.5 RTmin and 10 RTmin at 80°C in toluene

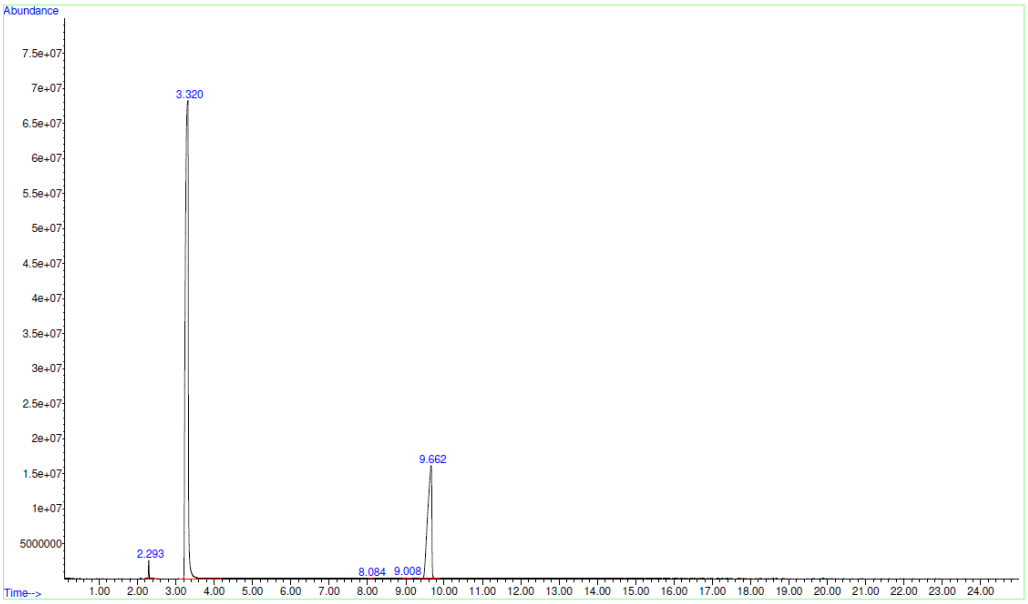


Figure G 3: Sample Chromatogram for GC-MS Reaction Experiment Constituents between 1 RTmin and 24 RTmin at 250°C in toluene

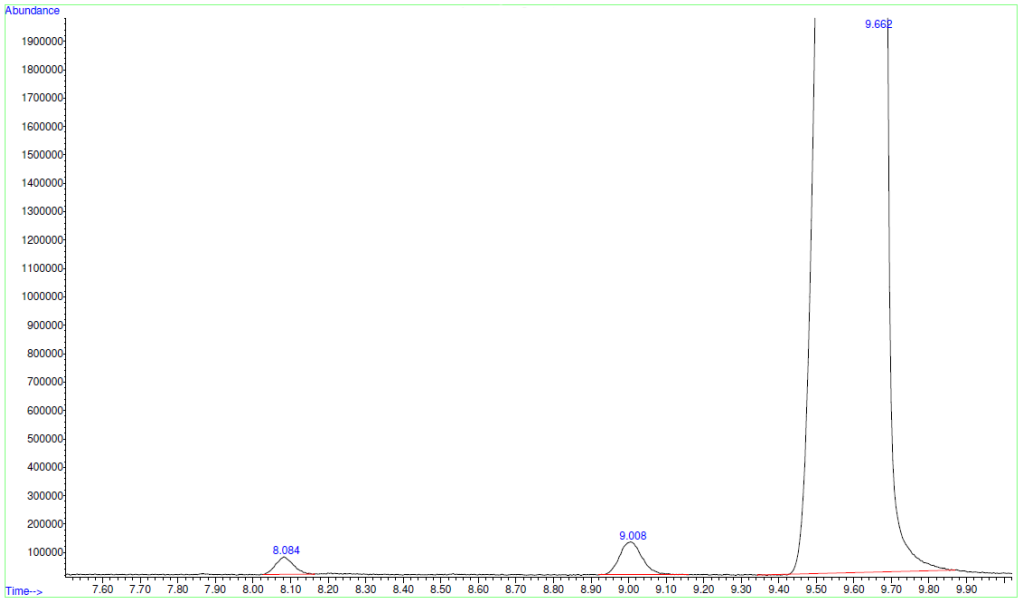


Figure G 4: Sample chromatogram for GC-MS reaction experiment constituents between 7.6 RTmin and 9.9 RTmin at 250°C in toluene

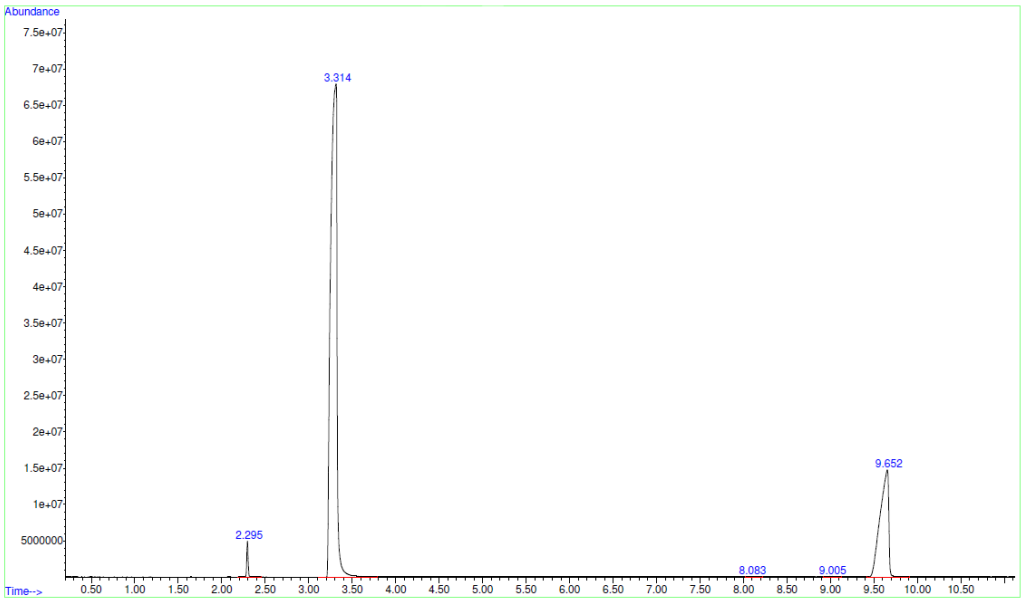


Figure G 5: Sample chromatogram for GC-MS reaction experiment constituents between 0.5 RTmin and 10.5 RTmin at 260°C in toluene

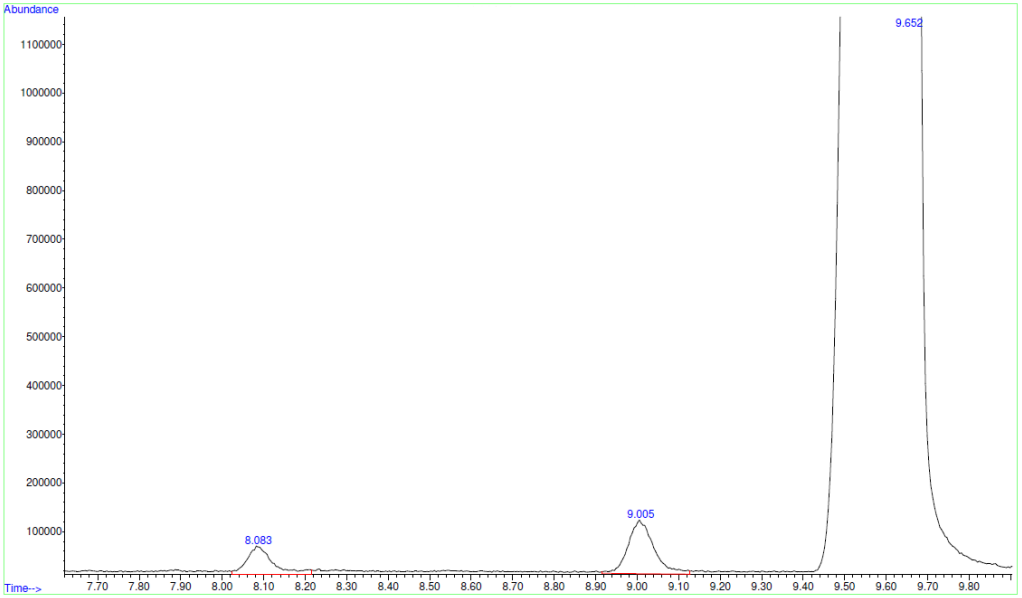


Figure G 6: Sample chromatogram for GC-MS reaction experiment constituents between 7.7 RTmin and 9.8 RTmin at 260°C in toluene

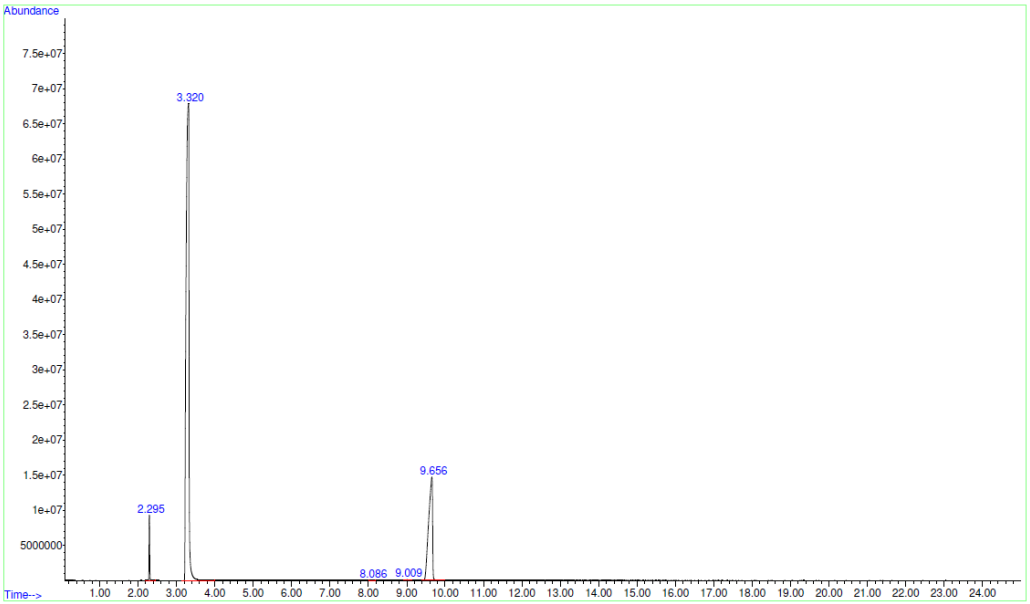


Figure G 7: Sample chromatogram for GC-MS reaction experiment constituents between 1 RTmin and 24 RTmin at 270°C in toluene

8

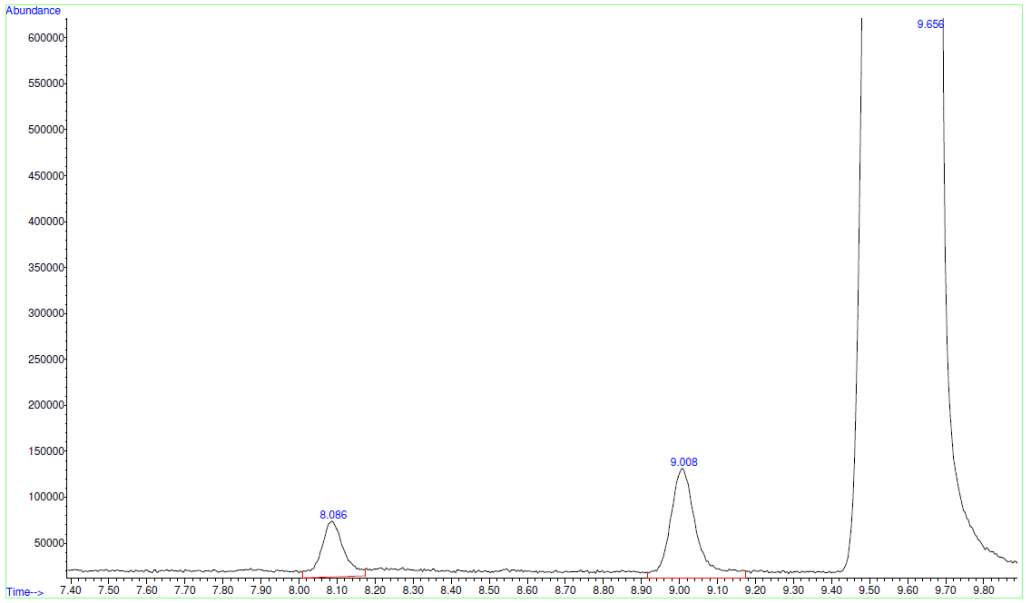


Figure G 8: Sample chromatogram for GC-MS reaction experiment constituents between 7.4 RTmin and 9.8 RTmin at 270°C in toluene

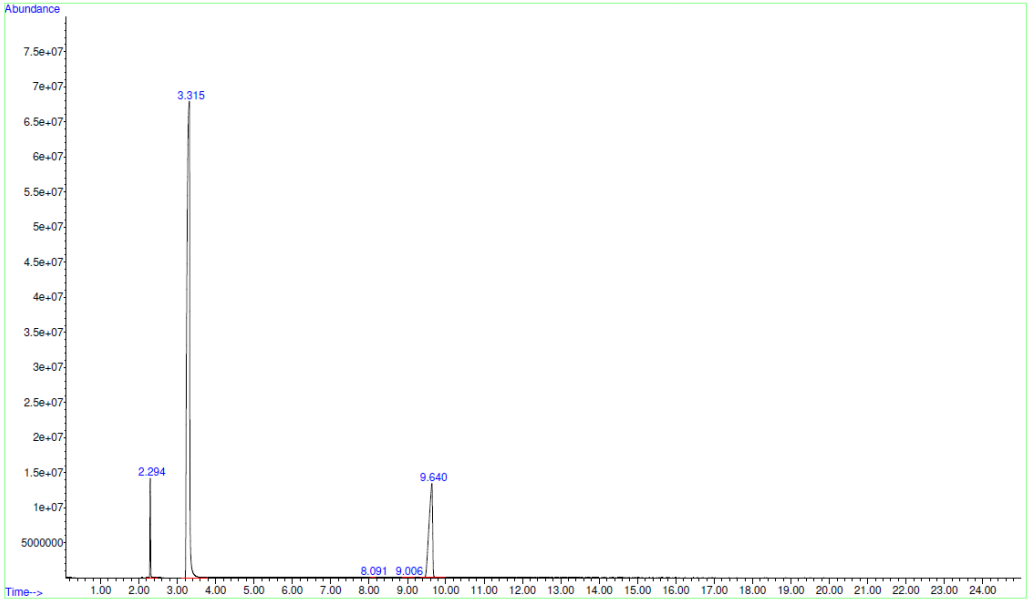


Figure G 9: Sample chromatogram for GC-MS reaction experiment constituents between 1 RTmin and 24 RTmin at 280°C in toluene

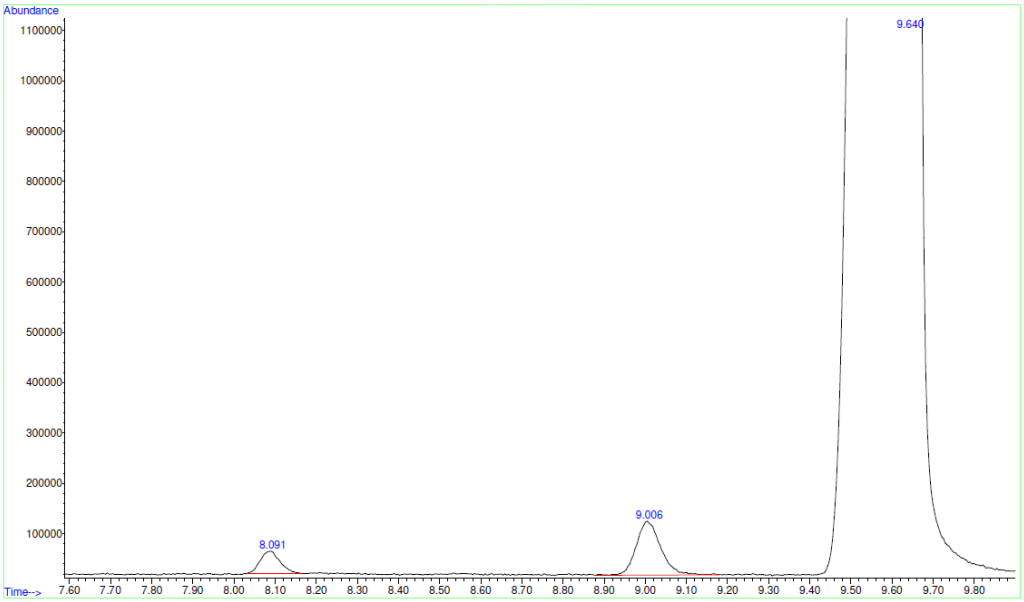


Figure G 10: Sample chromatogram for GC-MS reaction experiment constituents between 7.7 RTmin and 9.8 RTmin at 280°C in toluene

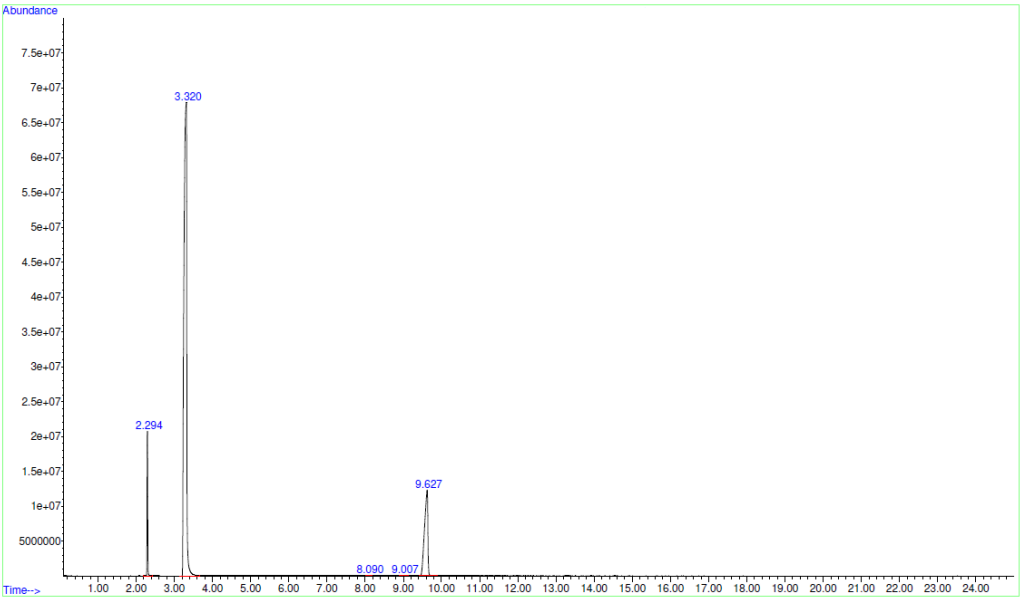


Figure G 11: Sample chromatogram for GC-MS reaction experiment constituents between 1 RTmin and 24 RTmin at 290°C in toluene

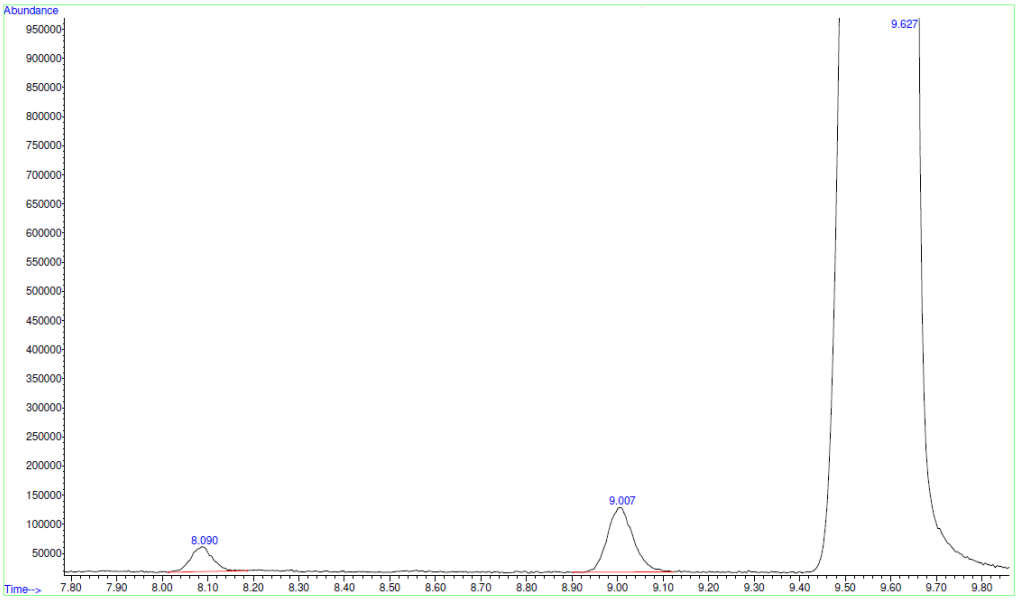


Figure G 12: Sample chromatogram for GC-MS reaction experiment constituents between 7.8 RTmin and 9.8 RTmin at 290°C in toluene



Figure G 13: Sample chromatogram for GC-MS reaction experiment constituents between 1 RTmin and 24 RTmin at 300°C in toluene

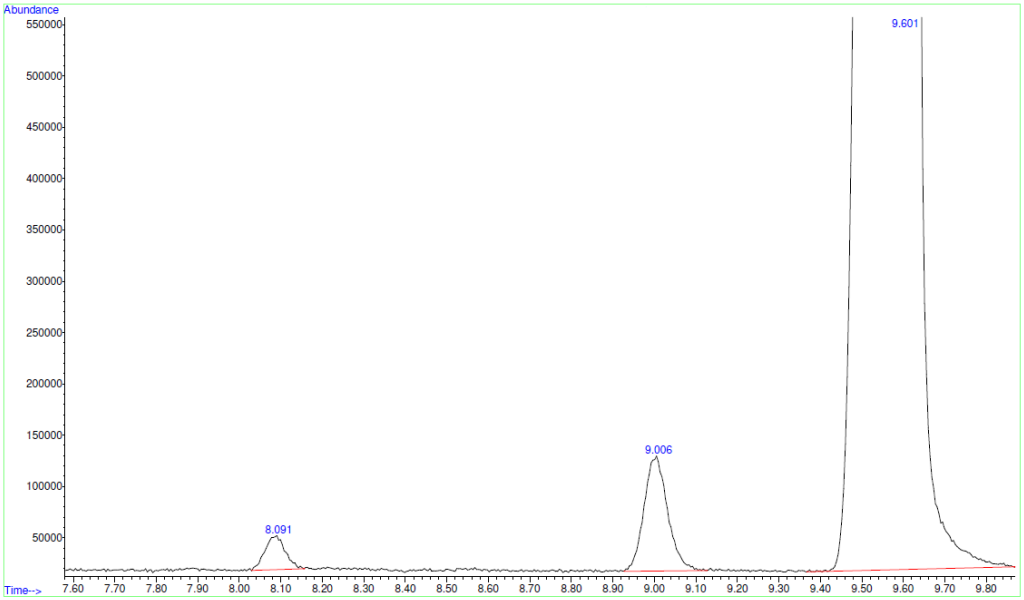


Figure G 14: Sample chromatogram for GC-MS reaction experiment constituents between 7.7 RTmin and 9.8 RTmin at 300°C in toluene

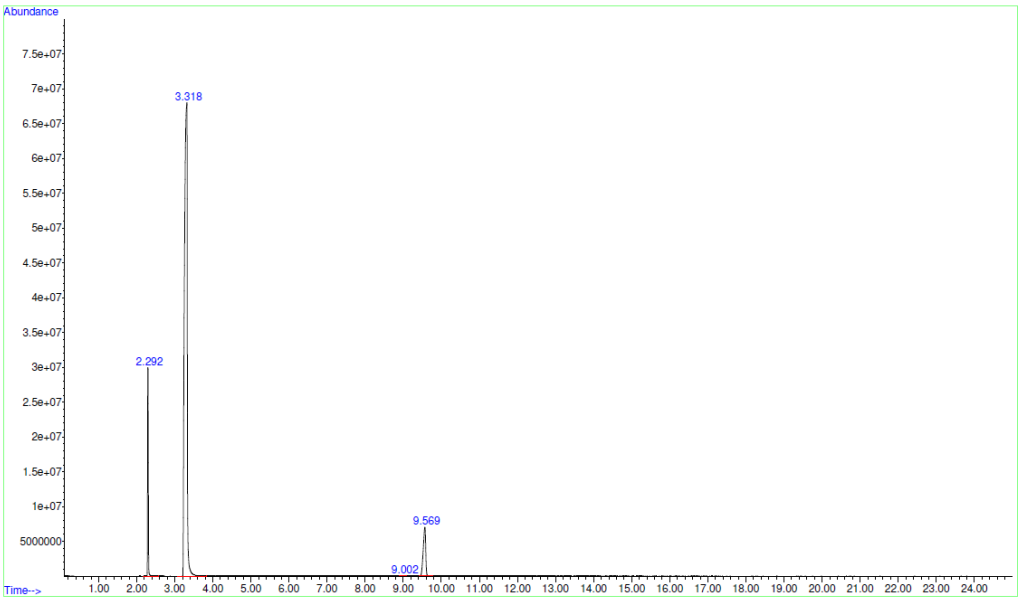


Figure G 15: Sample chromatogram for GC-MS reaction experiment constituents between 1 RTmin and 24 RTmin at 310°C in toluene

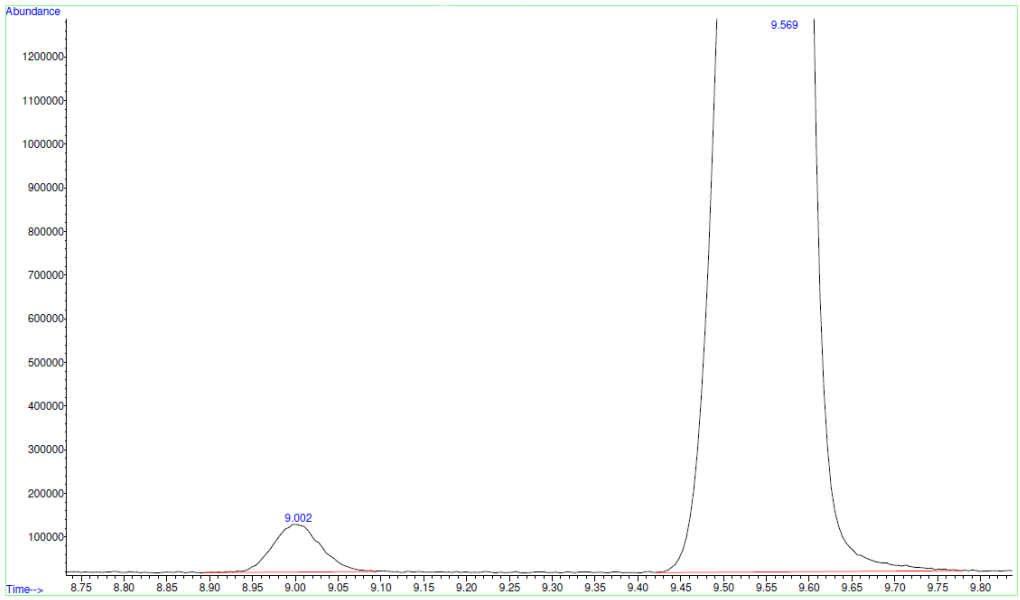


Figure G 16: Sample chromatogram for GC-MS reaction experiment constituents between 8.7 RTmin and 9.8 RTmin at 310°C in toluene

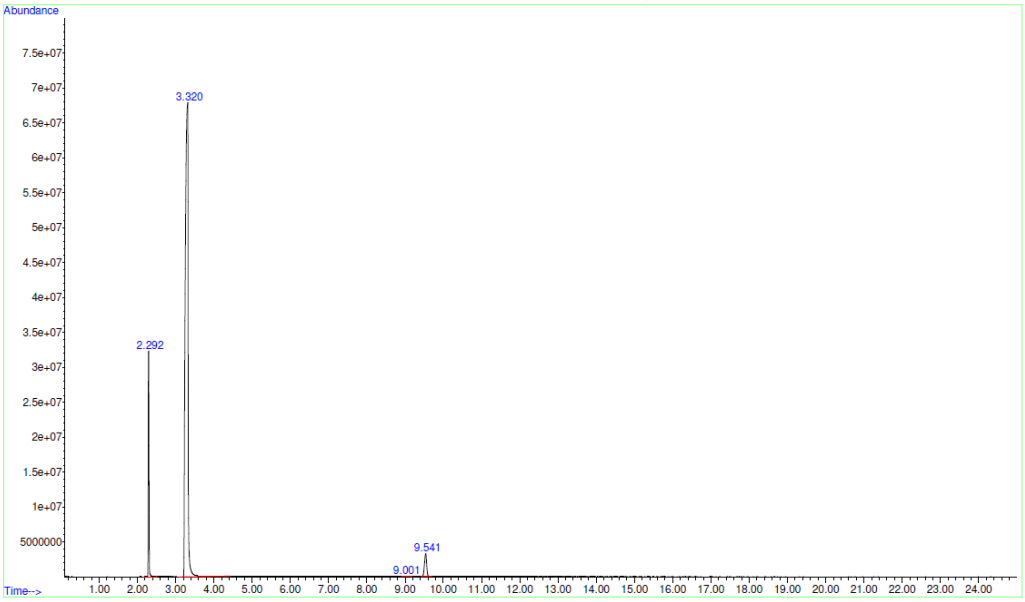


Figure G 17: Sample chromatogram for GC-MS reaction experiment constituents between 1 RTmin and 24 RTmin at 320°C in toluene

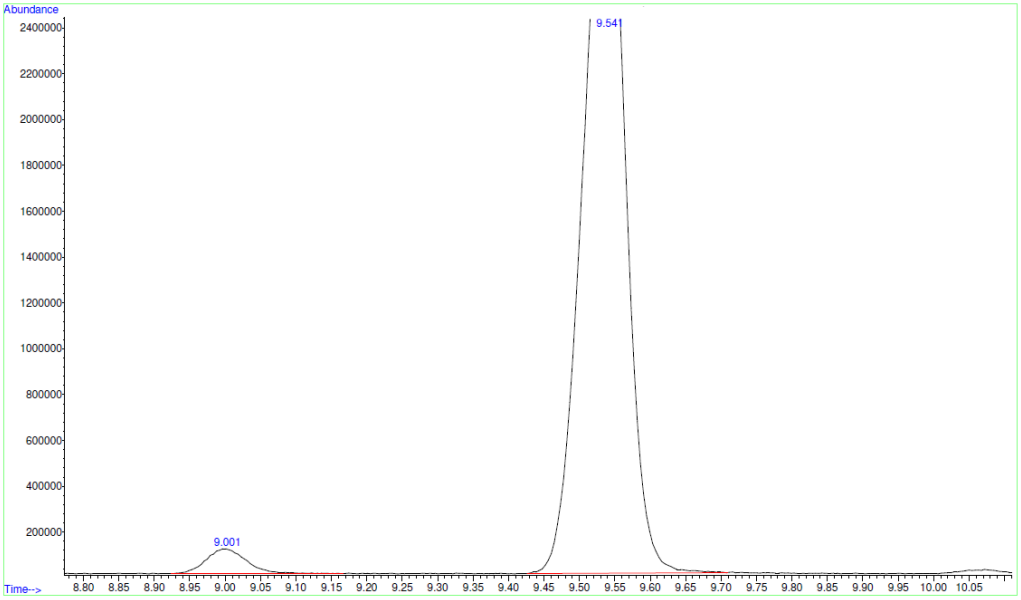


Figure G 18: Sample chromatogram for GC-MS reaction experiment constituents between 7.7 RTmin and 9.8 RTmin at 320°C in toluene



Figure G 19: Sample chromatogram for GC-MS reaction experiment constituents between 1 RTmin and 24 RTmin at 330°C in toluene

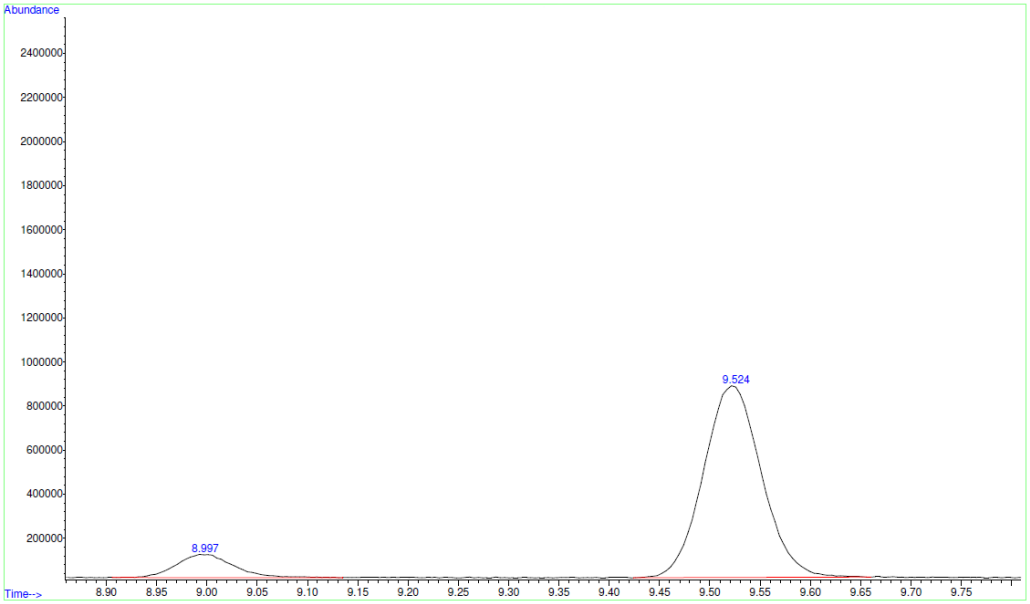


Figure G 20: Sample chromatogram for GC-MS reaction experiment constituents between 8.9 RTmin and 9.8 RTmin at 330°C in toluene



Figure G 21: Sample chromatogram for GC-MS reaction experiment constituents between 1 RTmin and 24 RTmin at 340°C in toluene

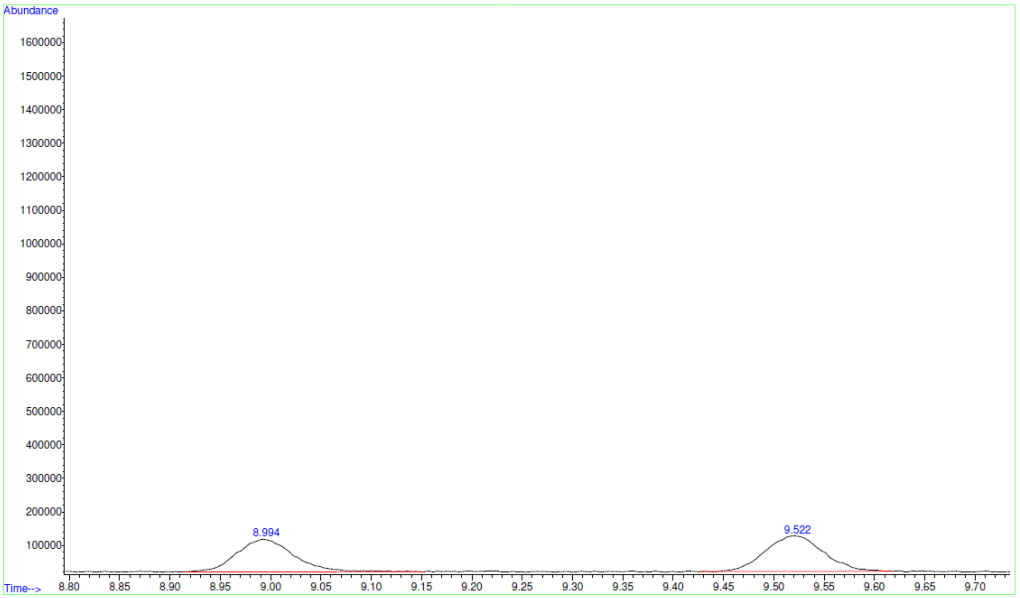


Figure G 22: Sample chromatogram for GC-MS reaction experiment constituents between 8.8 RTmin and 9.8 RTmin at 340°C in Toluene



Figure G 23: Sample chromatogram for GC-MS reaction experiment constituents between 1 RTmin and 24 RTmin at 350°C in toluene

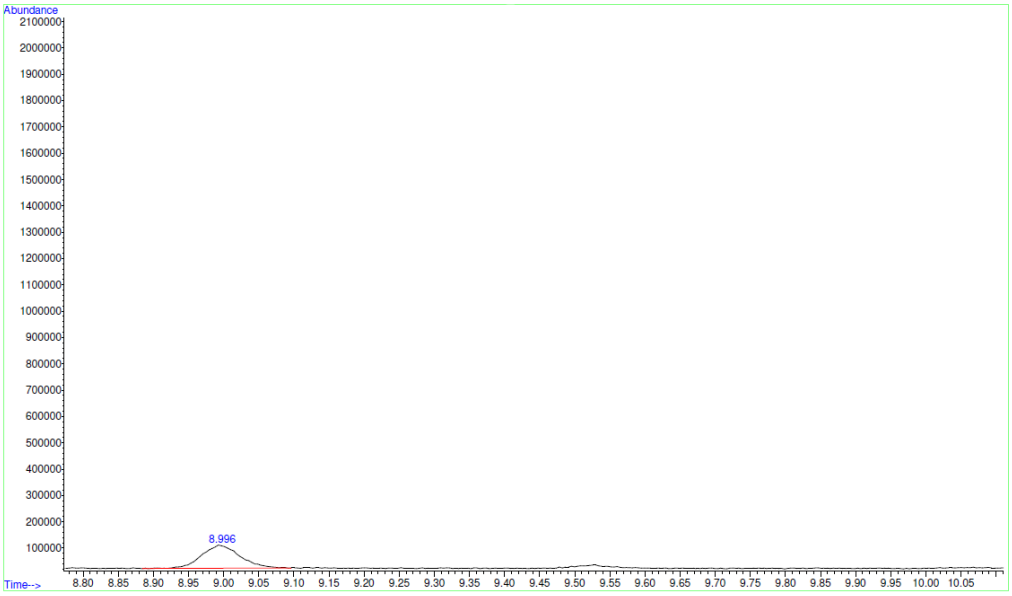


Figure G 24: Sample chromatogram for GC-MS reaction experiment constituents between 8.8 RTmin and 10.05 RTmin at 350°C in toluene

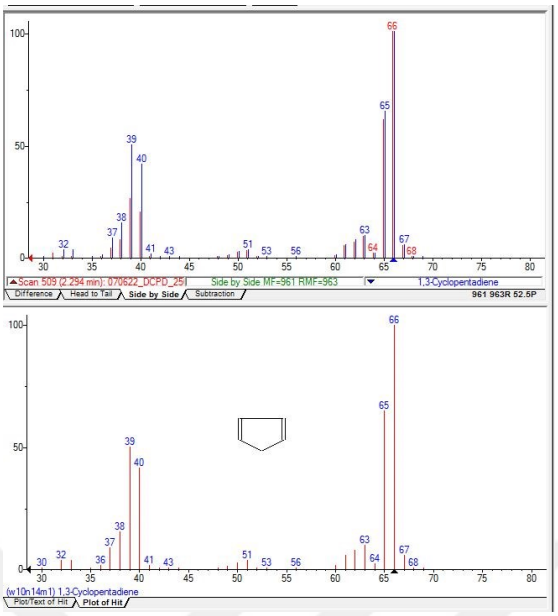


Figure G 25: Mass spectra and library match for peak at 2.29 RTmin

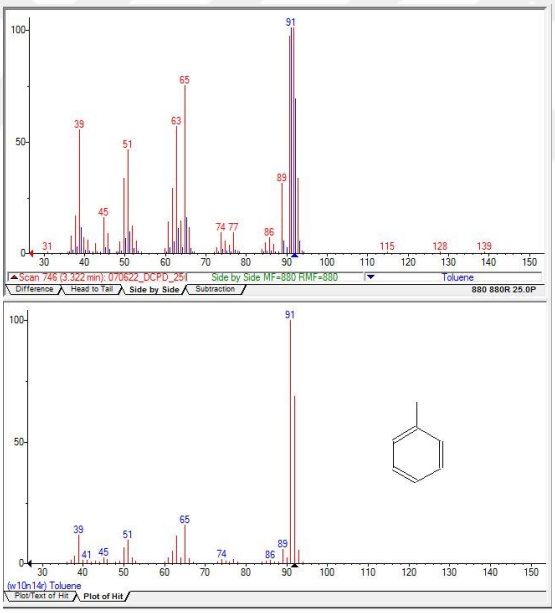


Figure G 26: Mass spectra and library match for peak at 3.32 RTmin

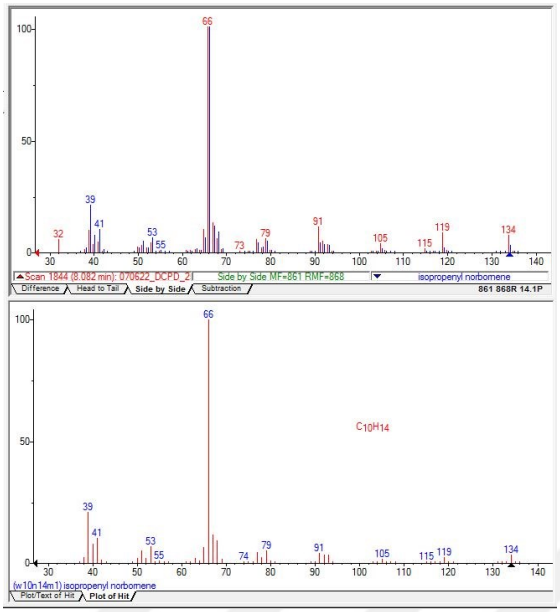


Figure G 27: Mass spectra and library match for peak at 8.10 RTmin

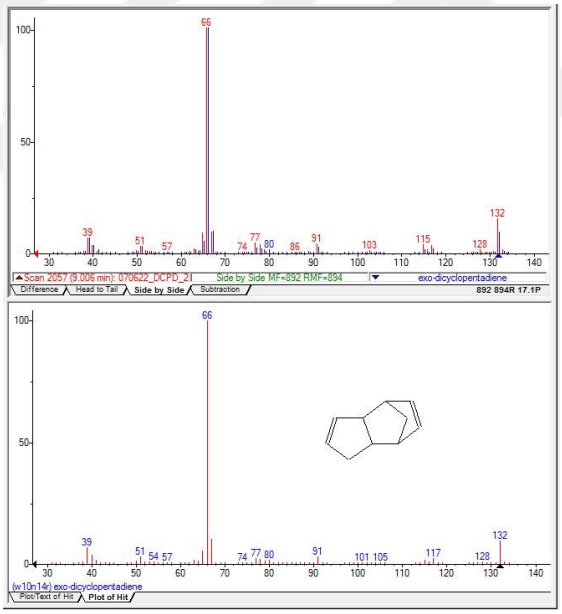


Figure G 28: Mass spectra and library match for peak at 9.01 RTmin

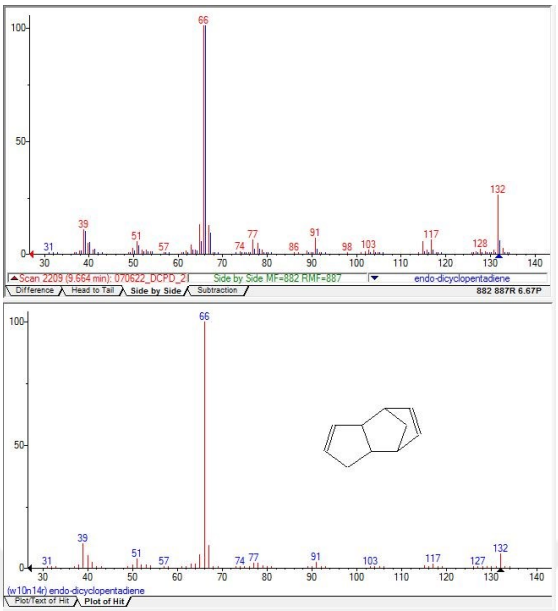


Figure G 29: Mass spectra and library match for peak at 9.66 RTmin

H. Sample Chromatograms for GC-MS Reaction Experiments of PYGAS in Heptane

PYGAS reaction experiments were conducted in GC-MS. Chromatographic grade toluene was also used as a dilution solvent. Abundance at corresponding retention time (RTmin) are given in Figure H1 where peaks at 4.0 through 4.3 are solvent peaks for heptane. The chromatograms are given in Figure H1 through H22 while the method parameters are given in Table H1.

Table H 1: Method information for PYGAS reaction in GC-MS in heptane

GC-MS Parameters	*Value*
Column	HP-5 ms
Inlet Type	Split (50:1)
Inlet Temperature	80-350°C
Injection Volume	0.2 µL
Inlet Gas Flow	He, 20 mL/min
Column Gas Flow	1.2 mL/min
Column Pressure	1.1 bar
Oven Program	50°C for 60 min
MS Gain Factor	2
Acquisition Type	Scan
Frequency	3.9 scans/sec
MS Step Size	0.1 m/z
MS Scan Range	30-500



Figure H 1: Sample chromatogram for PYGAS GC-MS reaction experiment constituents between 2 RTmin and 58 RTmin at 260°C in heptane

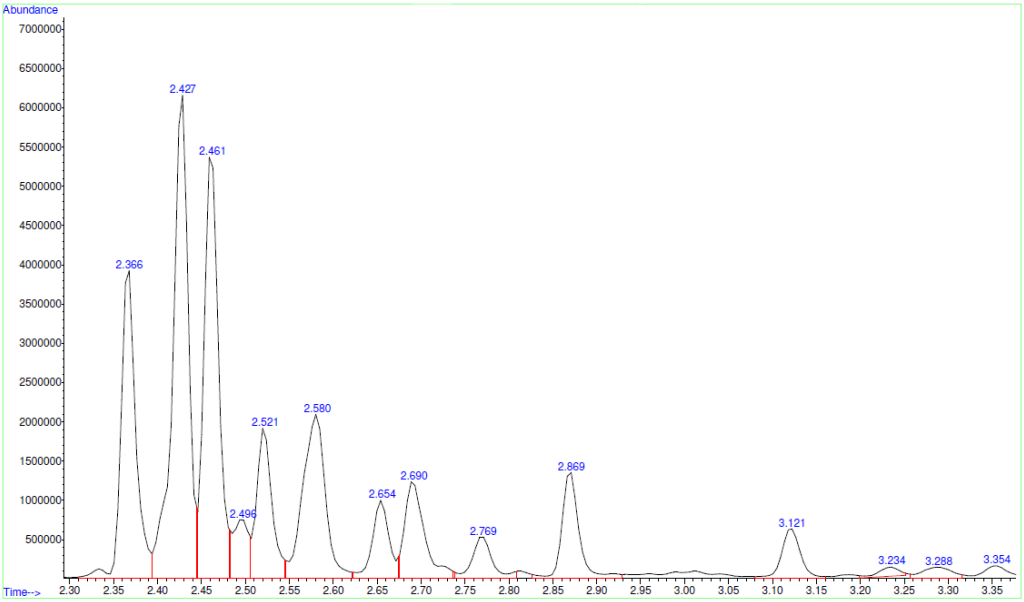


Figure H 2: Sample chromatogram for PYGAS GC-MS reaction experiment constituents between 2.2 RTmin and 3.35 RTmin at 260°C in heptane

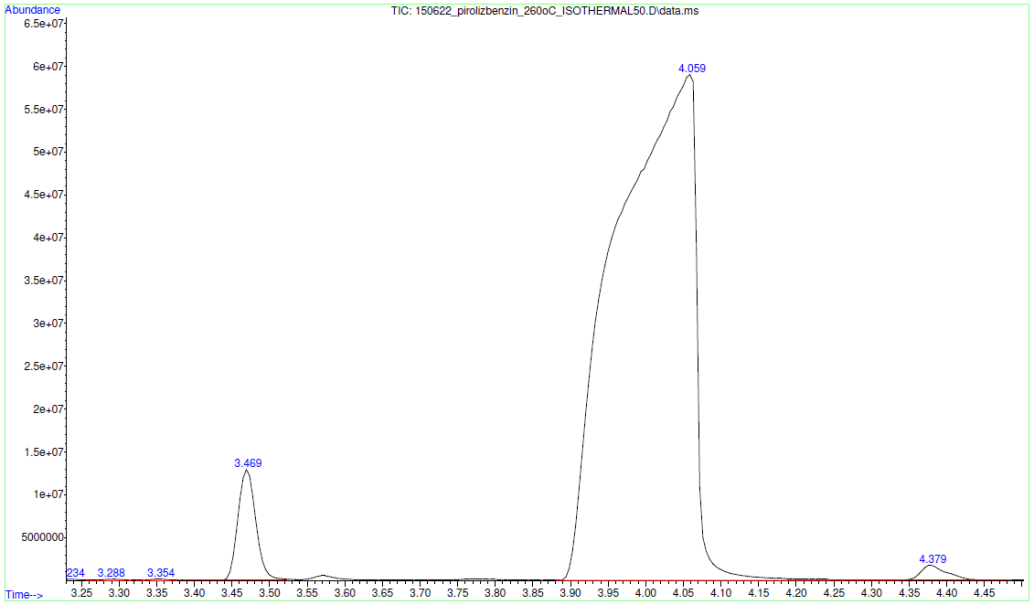


Figure H 3: Sample chromatogram for PYGAS GC-MS reaction experiment constituents between 3.25 RTmin and 4.45 RTmin at 260°C in heptane

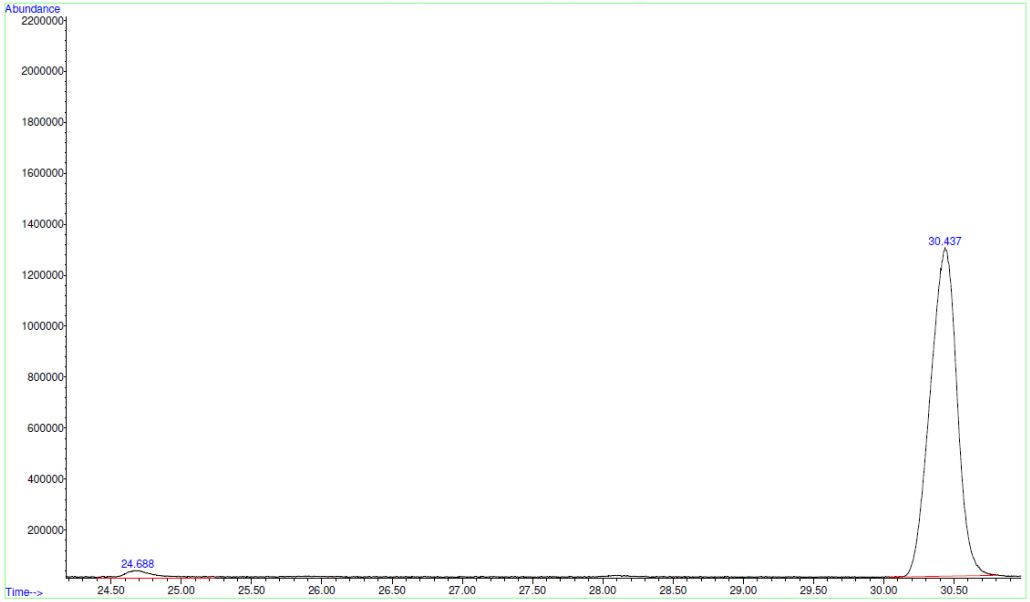


Figure H 4: Sample chromatogram for PYGAS GC-MS reaction experiment constituents between 24.668 RTmin and 30.5 RTmin at 260°C in heptane



Figure H 5: Sample chromatogram for PYGAS GC-MS reaction experiment constituents between 48 RTmin and 54.50 RTmin at 260°C in heptane

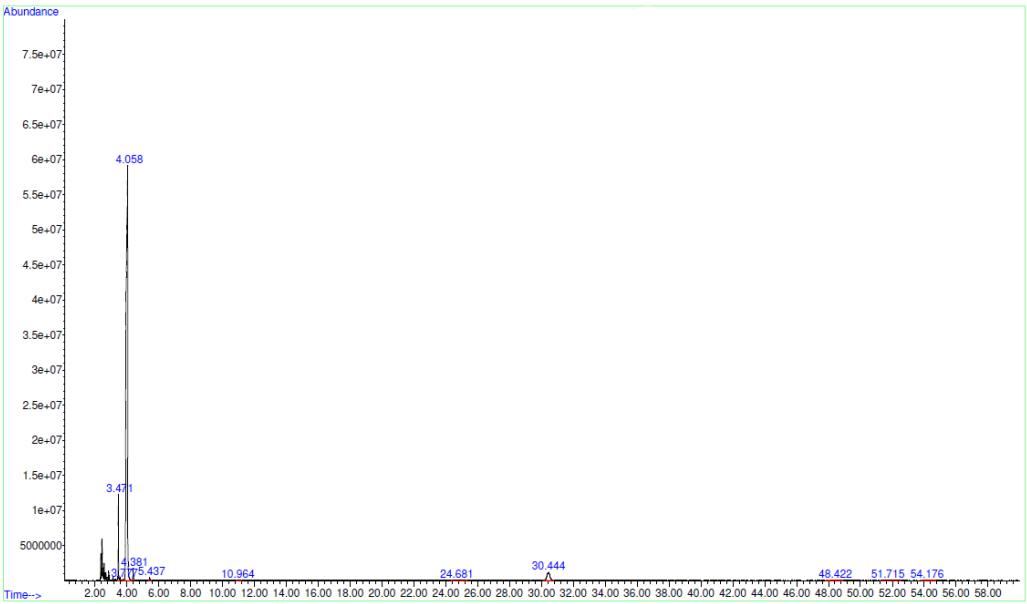


Figure H 6: Sample chromatogram for PYGAS GC-MS reaction experiment constituents between 2 RTmin and 58 RTmin at 270°C in heptane

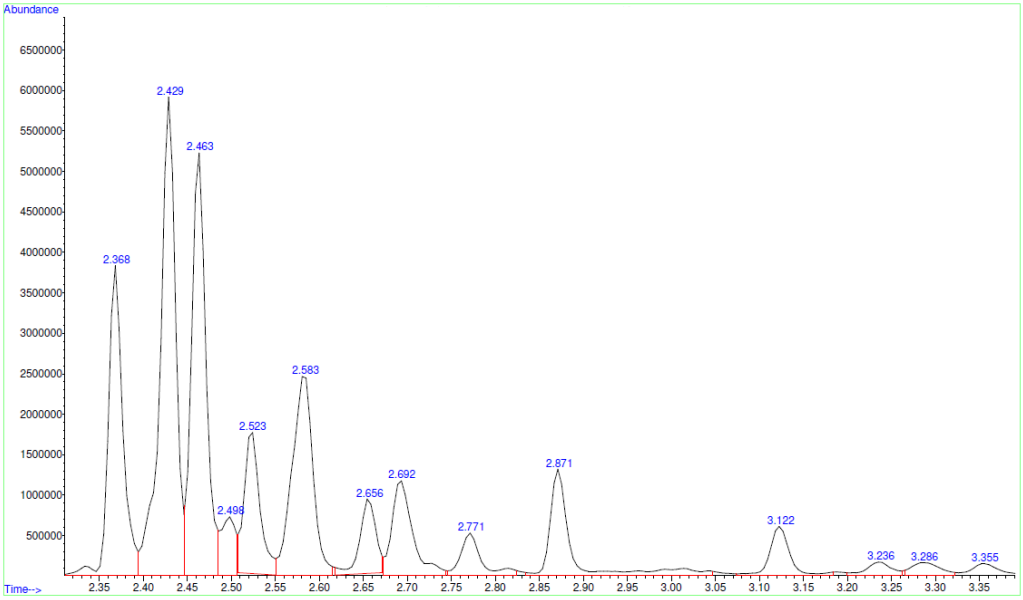


Figure H 7: Sample chromatogram for PYGAS GC-MS reaction experiment constituents between 2.35 RTmin and 3.25 RTmin at 270°C in heptane

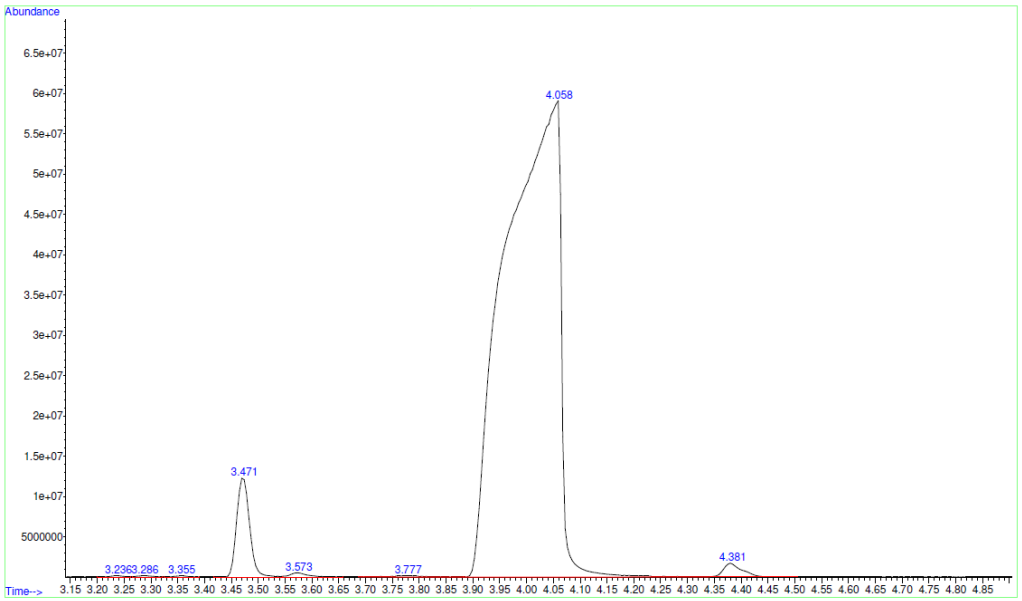


Figure H 8: Sample chromatogram for PYGAS GC-MS reaction experiment constituents between 3.15 RTmin and 4.85 RTmin at 270°C in heptane

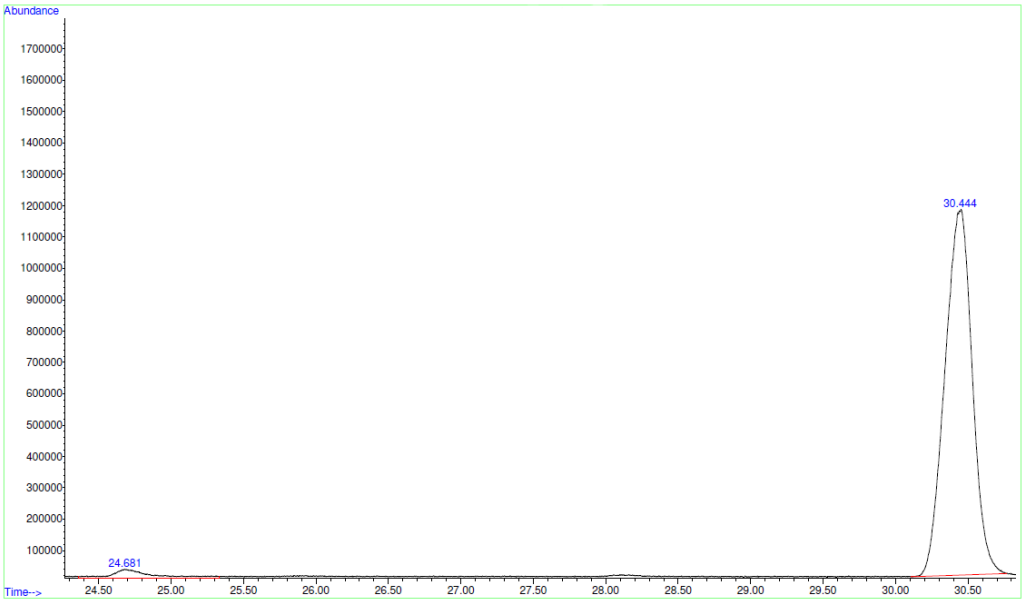


Figure H 9: Sample chromatogram for PYGAS GC-MS reaction experiment constituents between 24.5 RTmin and 30.5 RTmin at 270°C in heptane

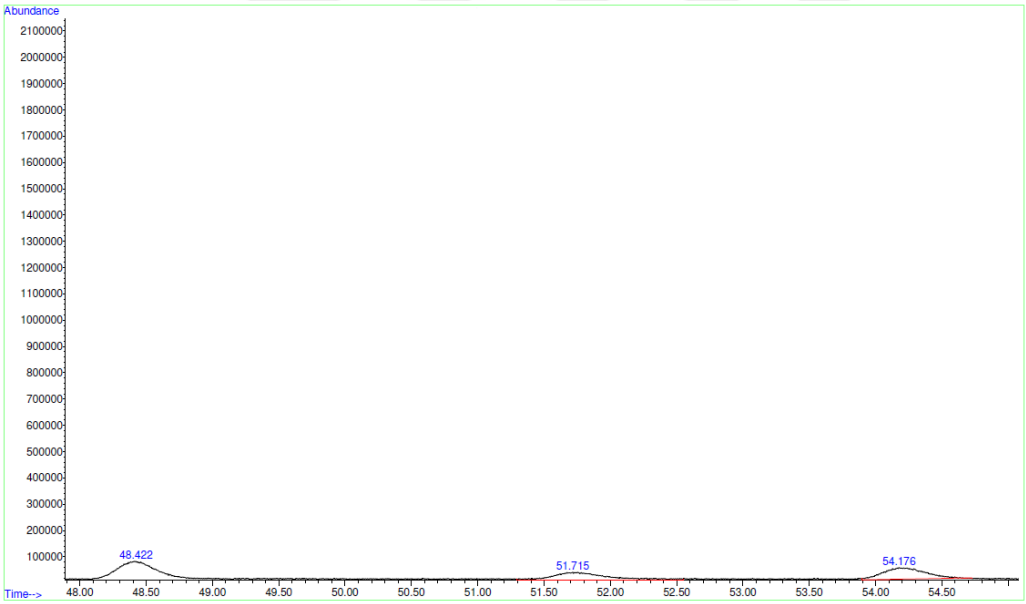


Figure H 10: Sample chromatogram for PYGAS GC-MS reaction experiment constituents between 48 RTmin and 54.5 RTmin at 270°C in heptane



Figure H 11: Sample chromatogram for PYGAS GC-MS reaction experiment constituents between 2 RTmin and 58 RTmin at 300°C in heptane

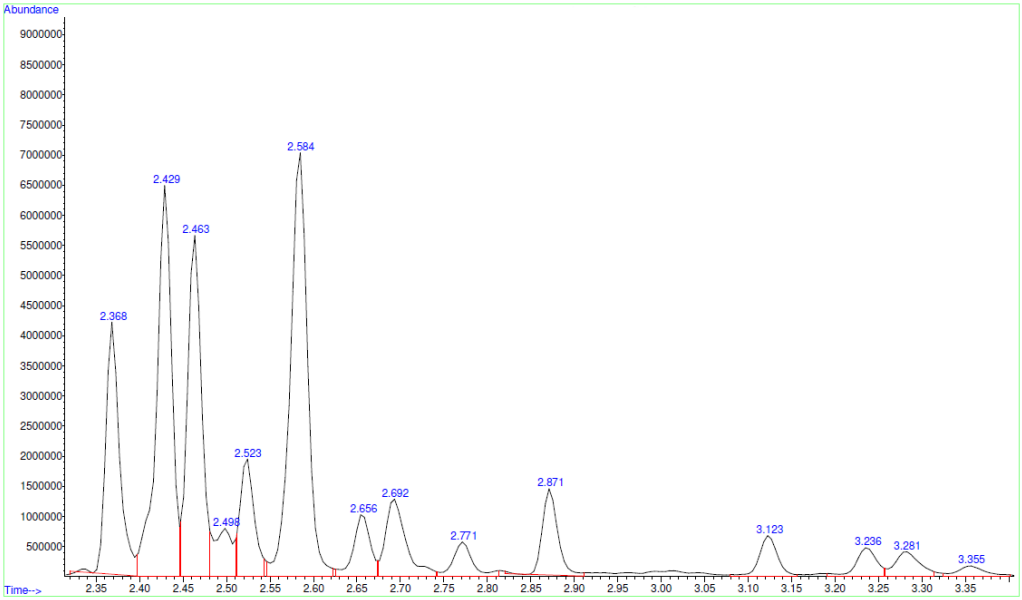


Figure H 12: Sample chromatogram for PYGAS GC-MS reaction experiment constituents between 2.35 RTmin and 3.35 RTmin at 300°C in heptane

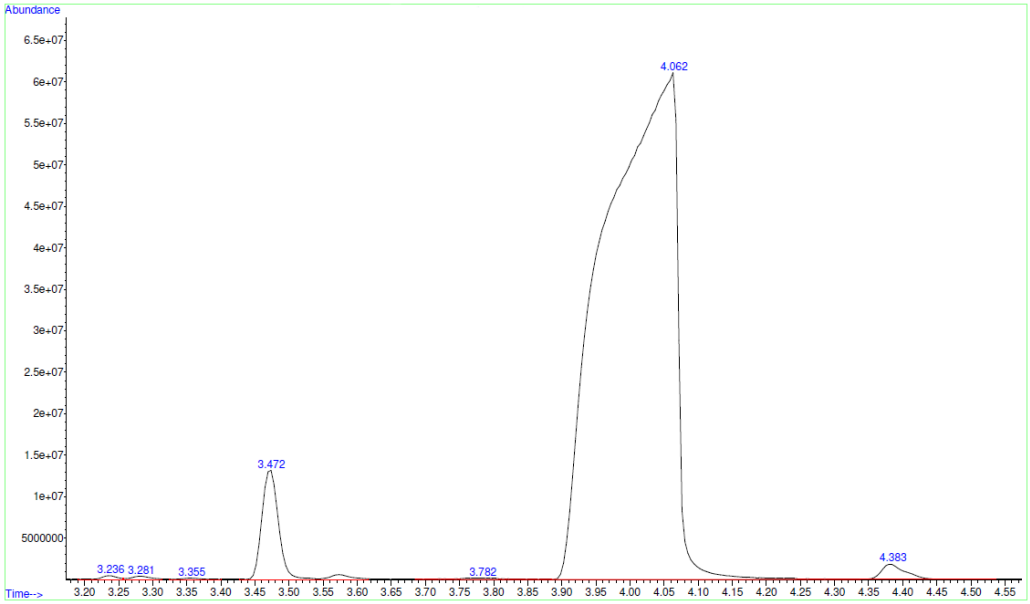


Figure H 13: Sample chromatogram for PYGAS GC-MS reaction experiment constituents between 3.2 RTmin and 4.55 RTmin at 300°C in heptane



Figure H 14: Sample chromatogram for PYGAS GC-MS reaction experiment constituents between 24.5 RTmin and 30.5 RTmin at 300°C in heptane



Figure H 15: Sample chromatogram for PYGAS GC-MS reaction experiment constituents between 48.2 RTmin and 54.4 RTmin at 300°C in heptane

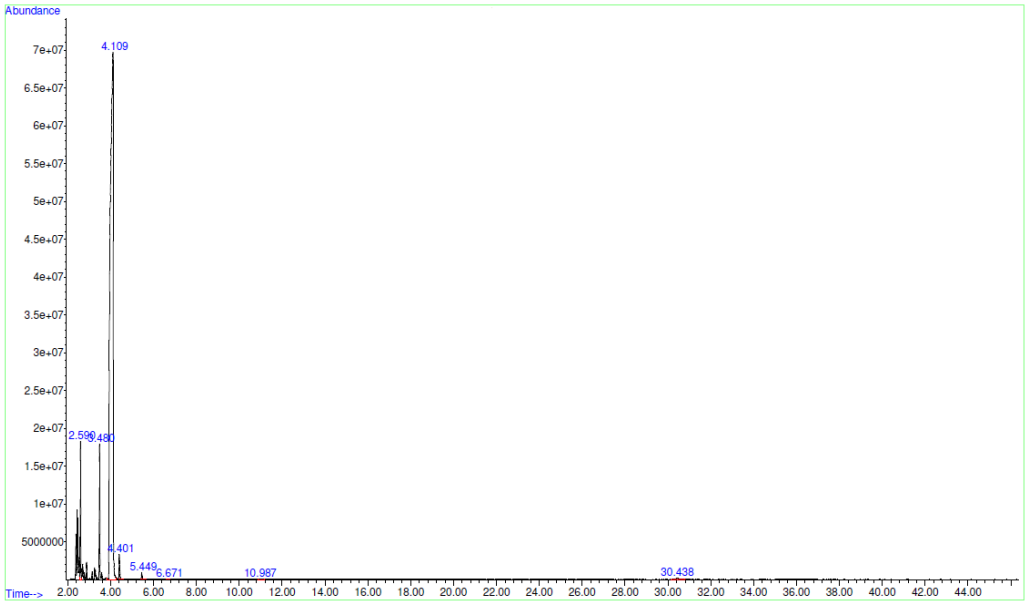


Figure H 16: Sample chromatogram for PYGAS GC-MS reaction experiment constituents between 2 RTmin and 58 RTmin at 320°C in heptane

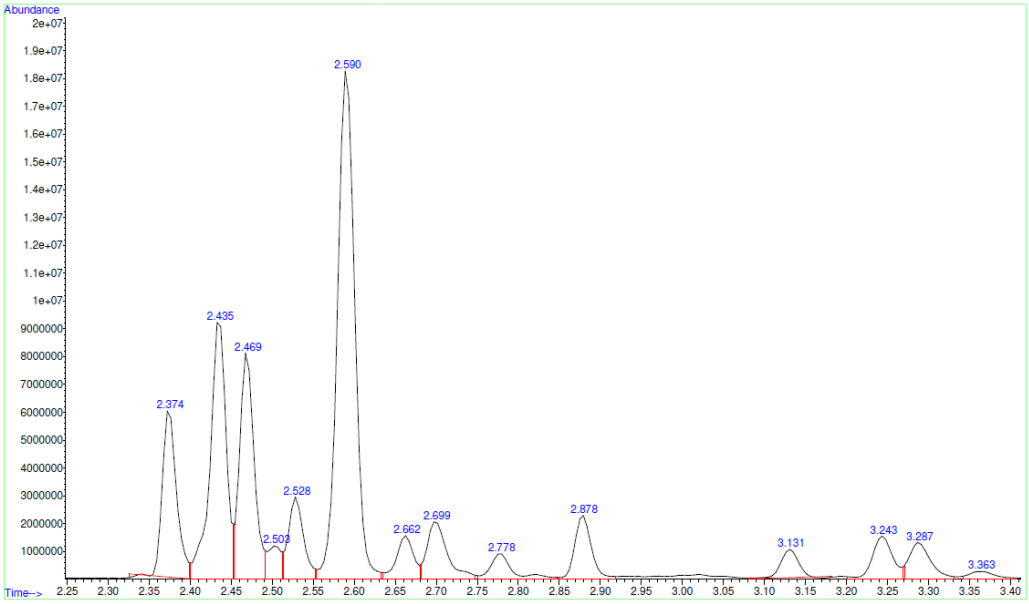


Figure H 17: Sample chromatogram for PYGAS GC-MS reaction experiment constituents between 2.3 RTmin and 3.4 RTmin at 320°C in heptane

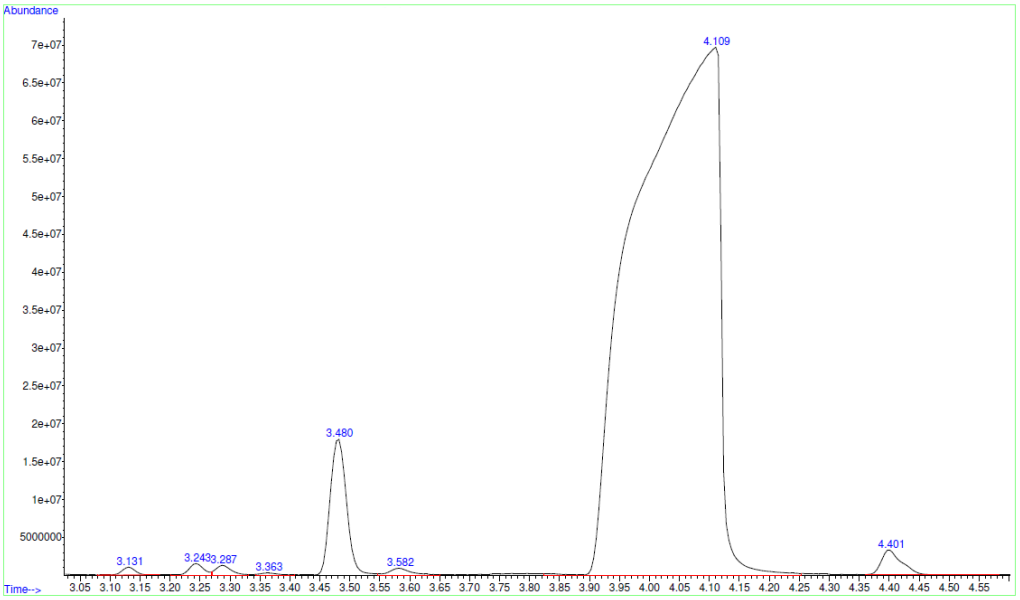


Figure H 18: Sample chromatogram for PYGAS GC-MS reaction experiment constituents between 3.05 RTmin and 4.55 RTmin at 320°C in heptane

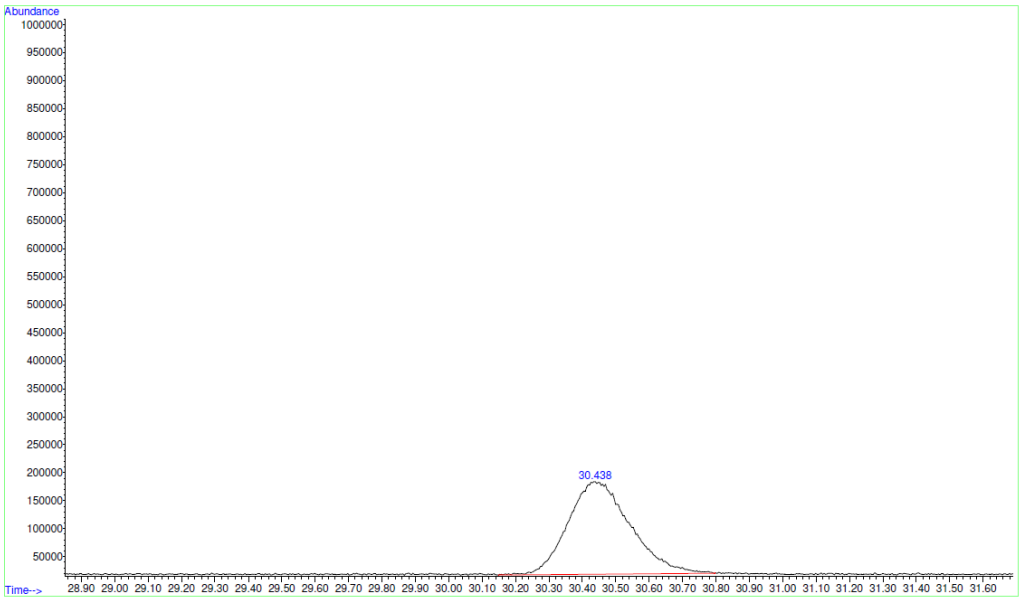


Figure H 19: Sample chromatogram for PYGAS GC-MS reaction experiment constituents between 28.9 RTmin and 31.6RTmin at 320°C in heptane



Figure H 20: Sample chromatogram for PYGAS GC-MS reaction experiment constituents between 2 RTmin and 58 RTmin at 350°C in heptane

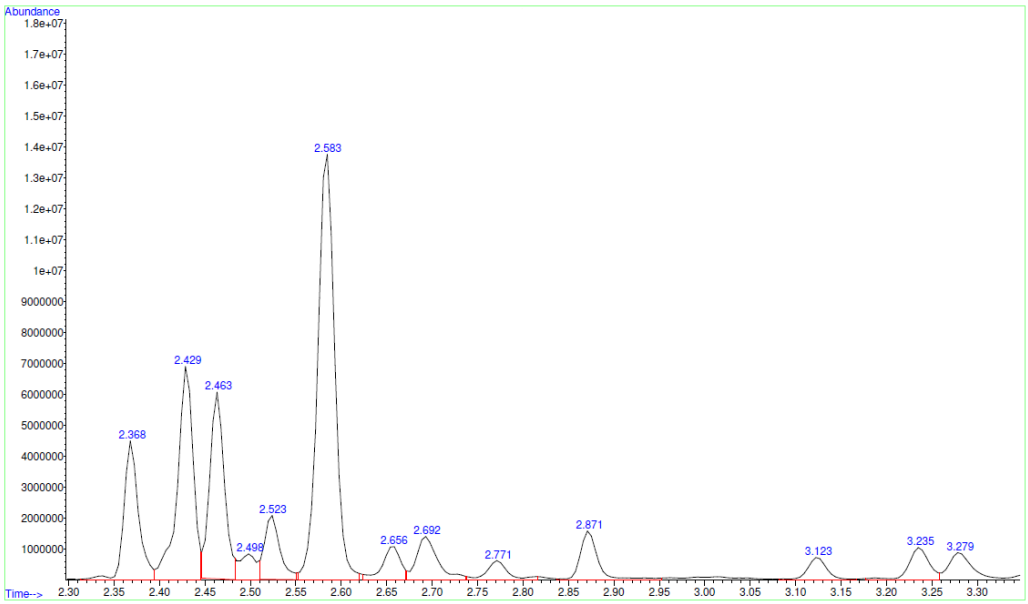


Figure H 21: Sample chromatogram for PYGAS GC-MS reaction experiment constituents between 2.3 RTmin and 3.3 RTmin at 350°C in heptane

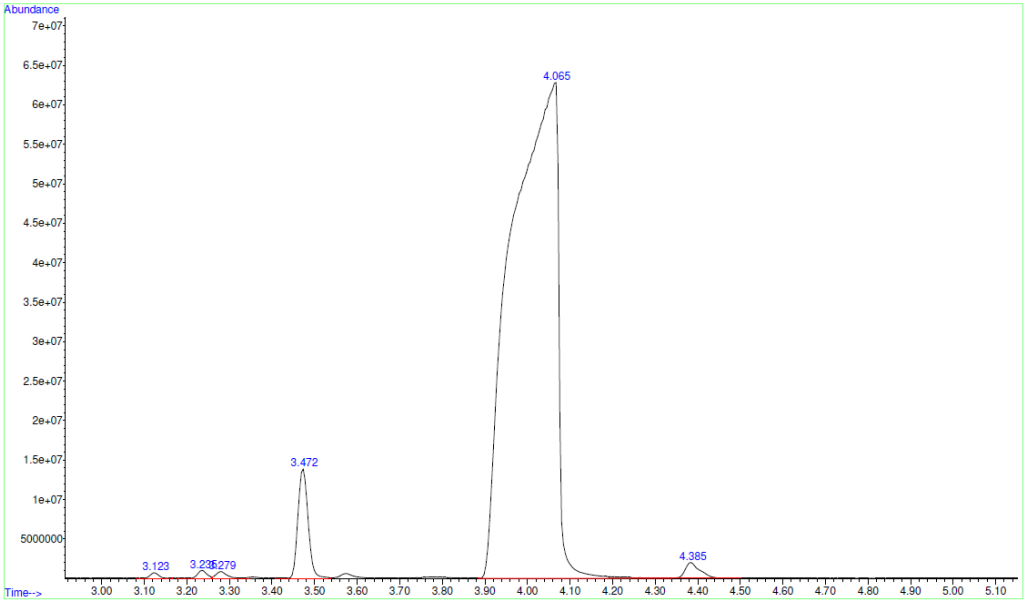


Figure H 22: Sample chromatogram for PYGAS GC-MS reaction experiment constituents between 3 RTmin and 5 RTmin at 350°C in heptane

I. Sample Chromatogram for Reactive Distillation Experiment 27 Liquid Compositions

Reactive Distillation Experiment 27 chromatograms are given in Figure I1 through I12. Mass spectras are given in Figure I13 through Figure I17. Method information are given in Table I1.

Table I 1: Method information for Reactive Distillation Experiment 27 samples

GC-MS Parameters	*Value*
Column	HP-5 ms
Inlet Type	Split (50:1)
Inlet Temperature	180°C
Injection Volume	0.2 µL
Inlet Gas Flow	He, 24 mL/min
Column Gas Flow	1.2 mL/min
Column Pressure	1.1 bar
Oven Program	80°C for 40 min
MS Gain Factor	2
Acquisition Type	Scan
Frequency	3.9 scans/sec
MS Step Size	0.1 m/z
MS Scan Range	30-500



Figure I 1: Sample chromatogram of liquid phase at 15 minute for Reactive Distillation Experiment 27



Figure I 2: Sample chromatogram of liquid phase at 30 minute for Reactive Distillation Experiment 27



Figure I 3: Sample chromatogram of liquid phase at 45 minute for Reactive Distillation Experiment 27

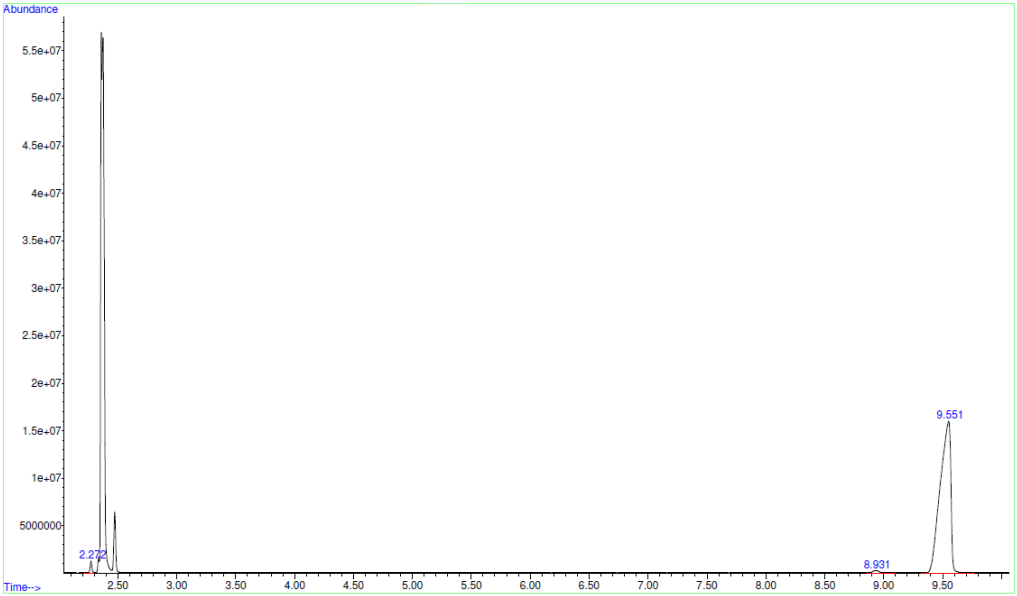


Figure I 4: Sample chromatogram of liquid phase at 60 minute for Reactive Distillation Experiment 27

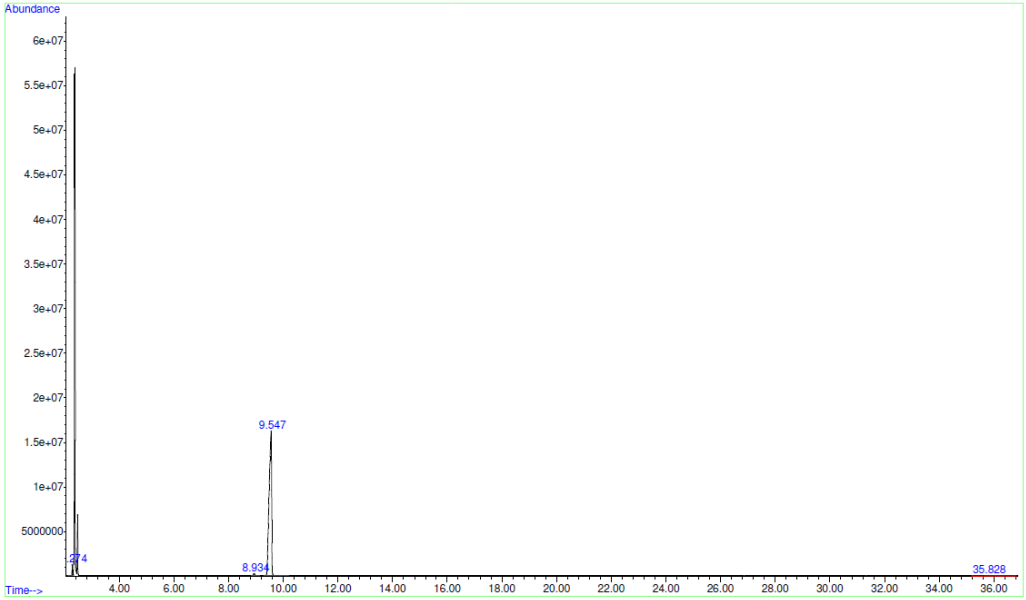


Figure I 5: sample chromatogram of liquid phase at 75 minute for Reactive Distillation Experiment 27

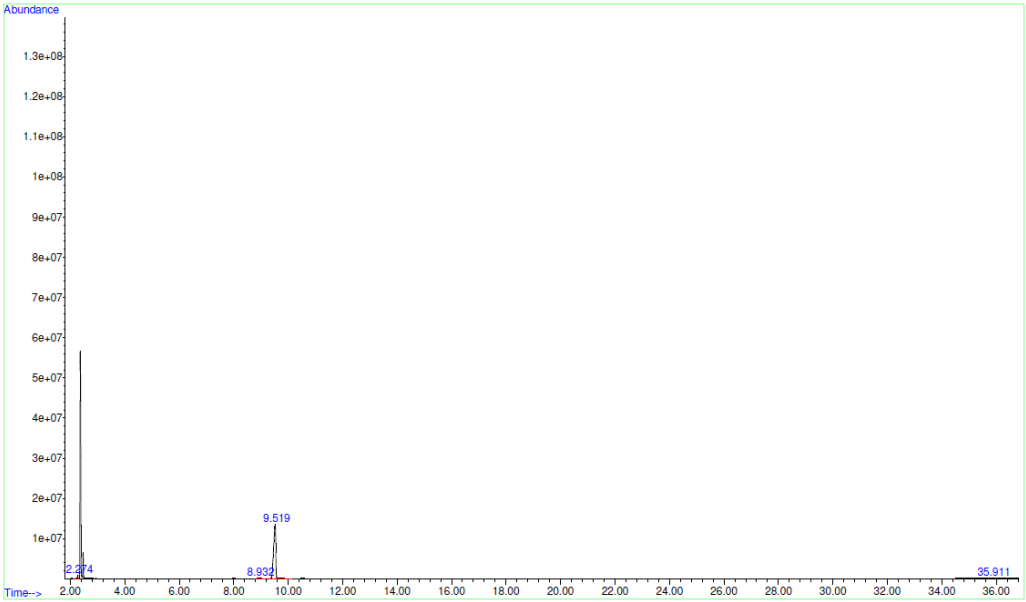


Figure I 6: Sample chromatogram of liquid phase at 90 minute for Reactive Distillation Experiment 27

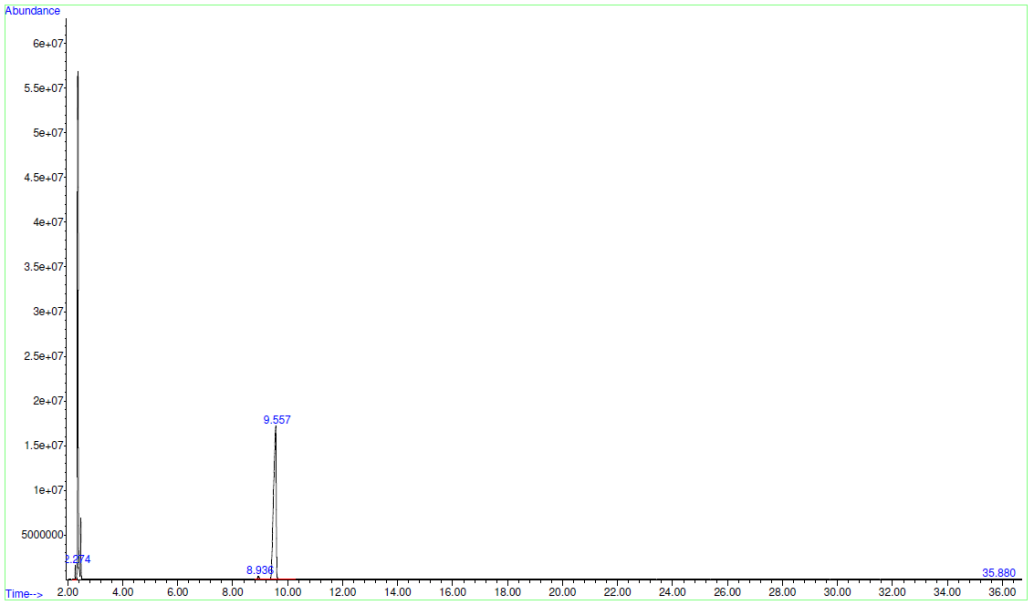


Figure I 7: Sample chromatogram of liquid phase at 105 minute for Reactive Distillation Experiment 27

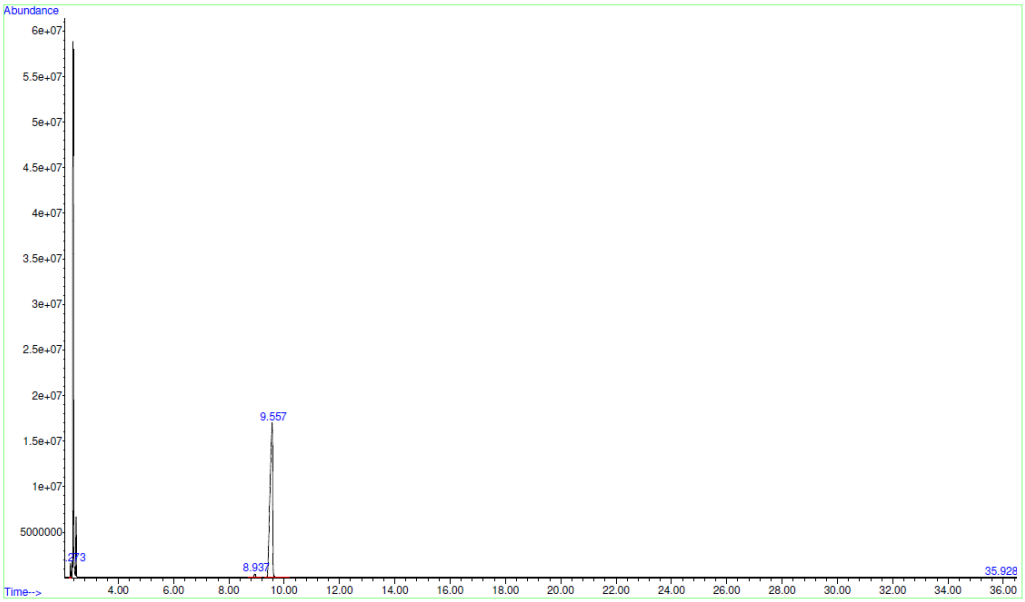


Figure I 8: Sample chromatogram of liquid phase at 120 minute for Reactive Distillation Experiment 27

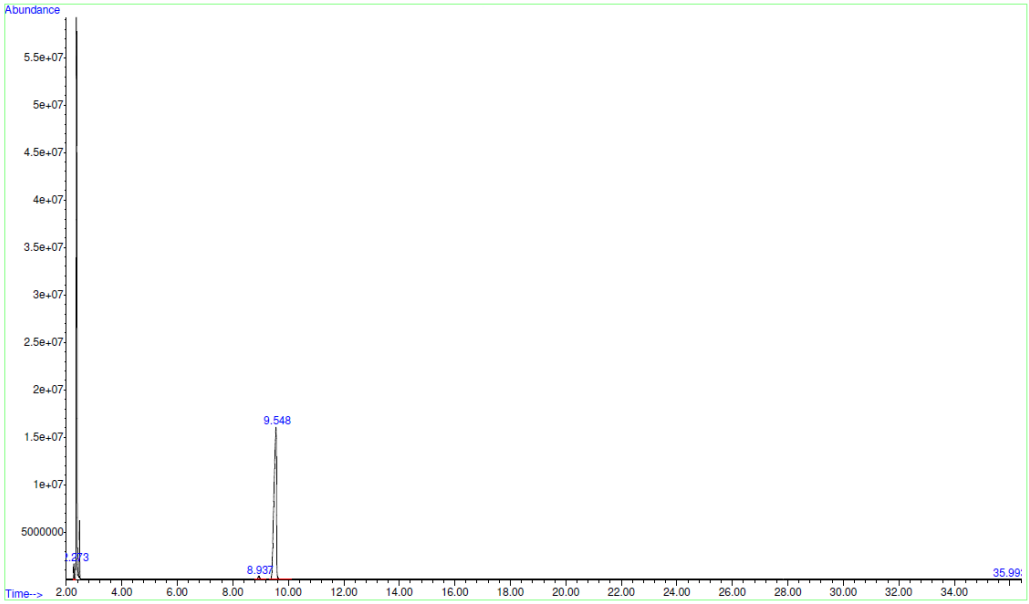


Figure I 9: Sample chromatogram of liquid phase at 135 minute for Reactive Distillation Experiment 27

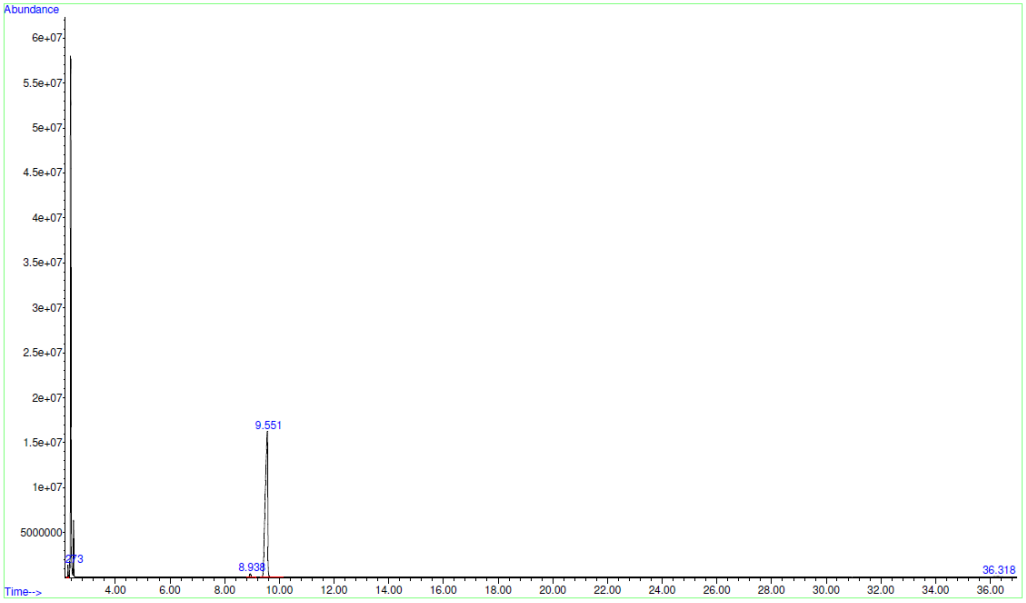


Figure I 10: Sample chromatogram of liquid phase at 150 minute for Reactive Distillation Experiment 27

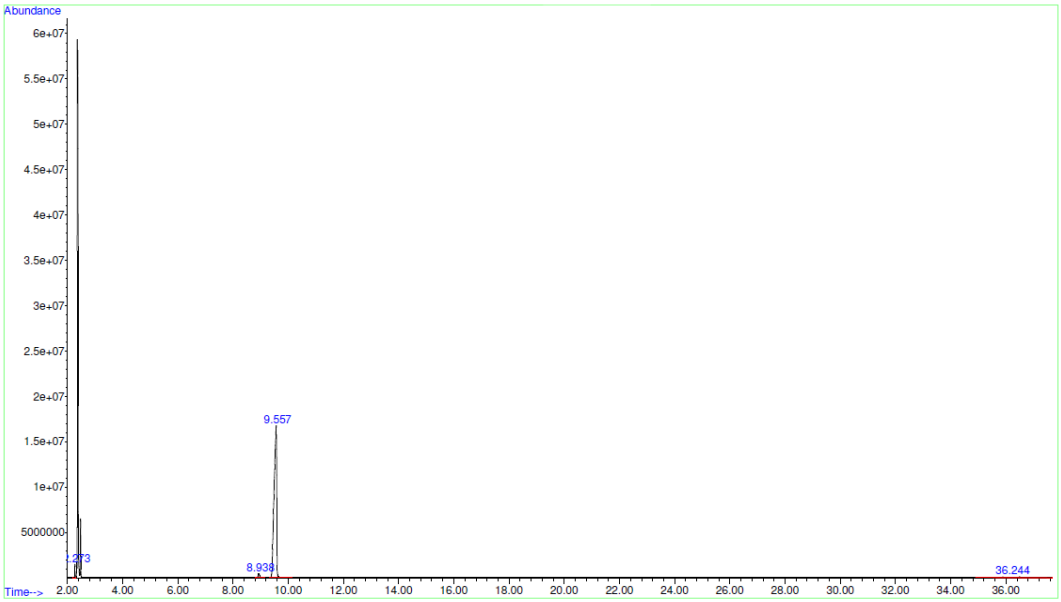


Figure I 11: Sample chromatogram of liquid phase at 165 minute for Reactive Distillation Experiment 27

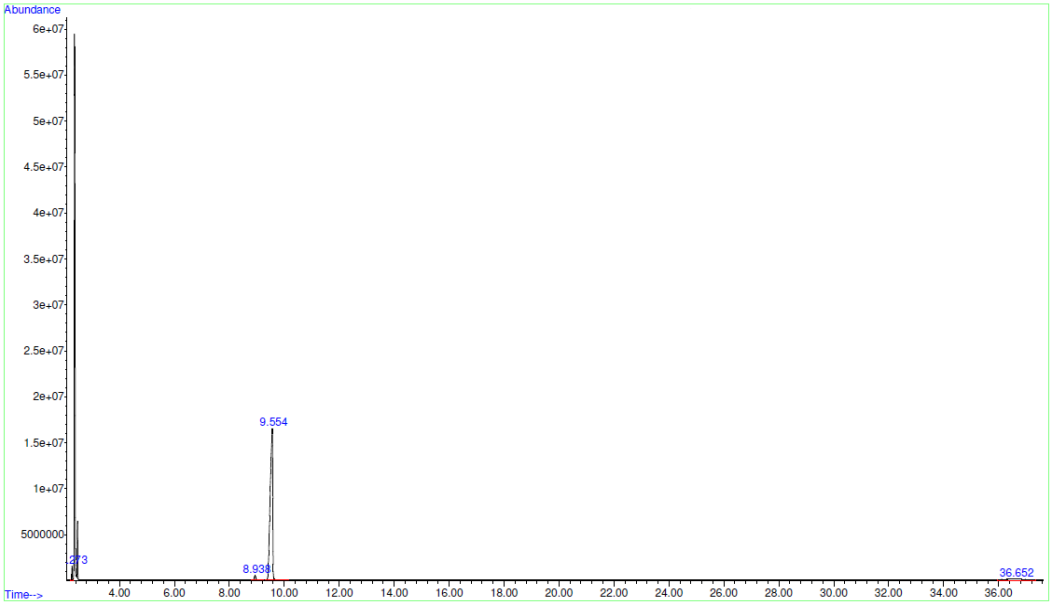


Figure I 12: Sample Chromatogram of Liquid Phase at 180 Minute for Reactive Distillation Experiment 27

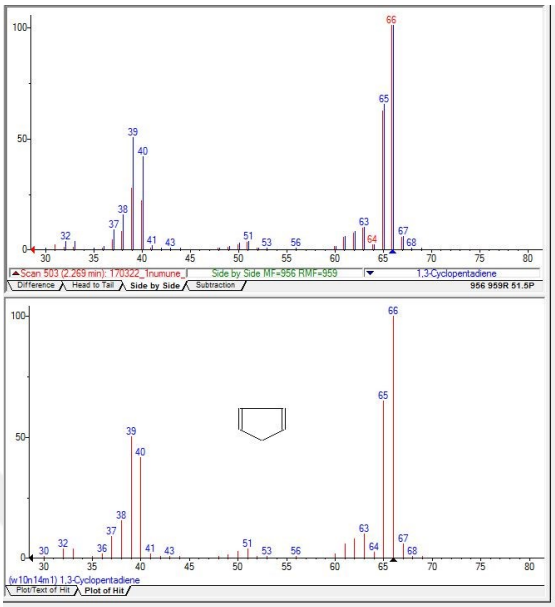


Figure I 13: Mass Spectra and Library Match for Peak at 2.27 RTmin

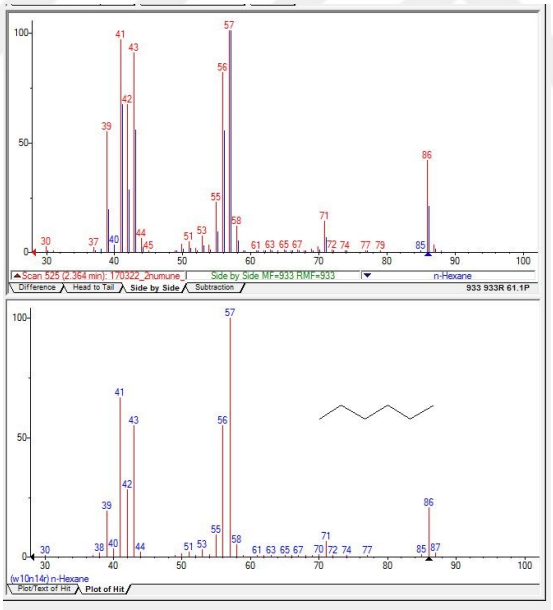


Figure I 14: Mass Spectra and Library Match for Peak at 2.36 RTmin

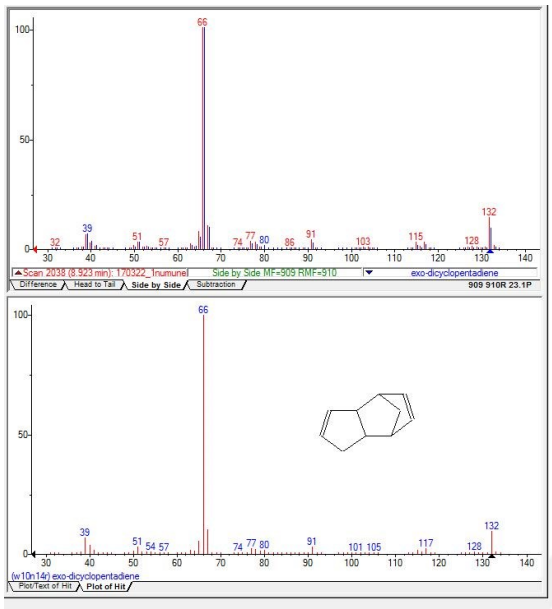


Figure I 15: Mass Spectra and Library Match for Peak at 8.92 RTmin

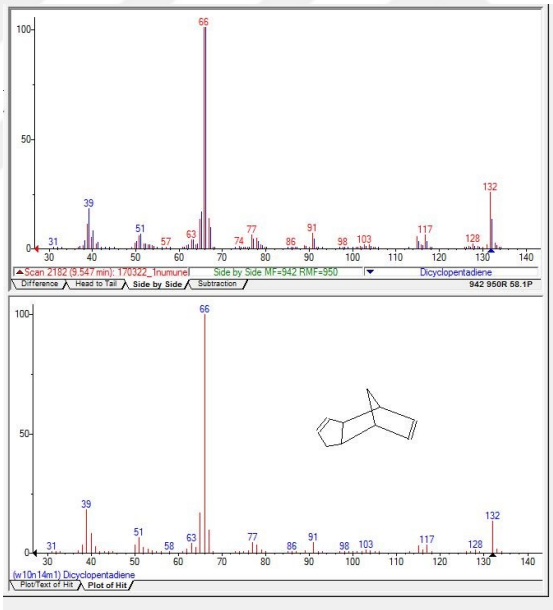


Figure I 16: Mass Spectra and Library Match for Peak at 9.55RTmin

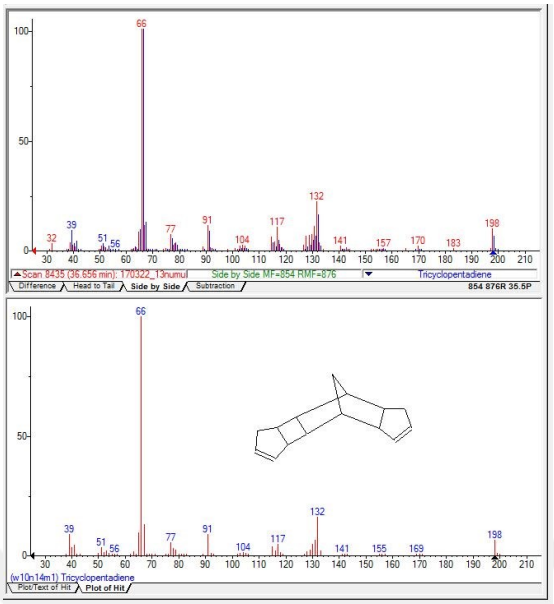


Figure I 17: Mass Spectra and Library Match for Peak at 36.66 RTmin

J. Sample Chromatogram for Reactive Distillation Experiment 39 Vapor and Liquid Compositions

DCPD constituents taken from vapor and liquid phases from Reactive Distillation Experiment 39, were analyzed by GC-MS. Chromatographic grade hexane was used as a dilution solvent. Abundance at corresponding retention times (RTmin) are given in Figure J1 where peaks at 2.7 through 3 RTmin are solvent peaks for hexane while the method parameters are given in Table J1.

Table J 1: Method information for Reactive Distillation Experiment 39 samples

GC-MS Parameters	*Value*
Column	HP-5 ms
Inlet Type	Split (50:1)
Inlet Temperature	180°C
Injection Volume	0.2 µL
Inlet Gas Flow	He, 24 mL/min
Column Gas Flow	1.2 mL/min
Column Pressure	1.1 bar
Oven Program	80°C for 40 min
MS Gain Factor	2
Acquisition Type	Scan
Frequency	3.9 scans/sec
MS Step Size	0.1 m/z
MS Scan Range	30-500

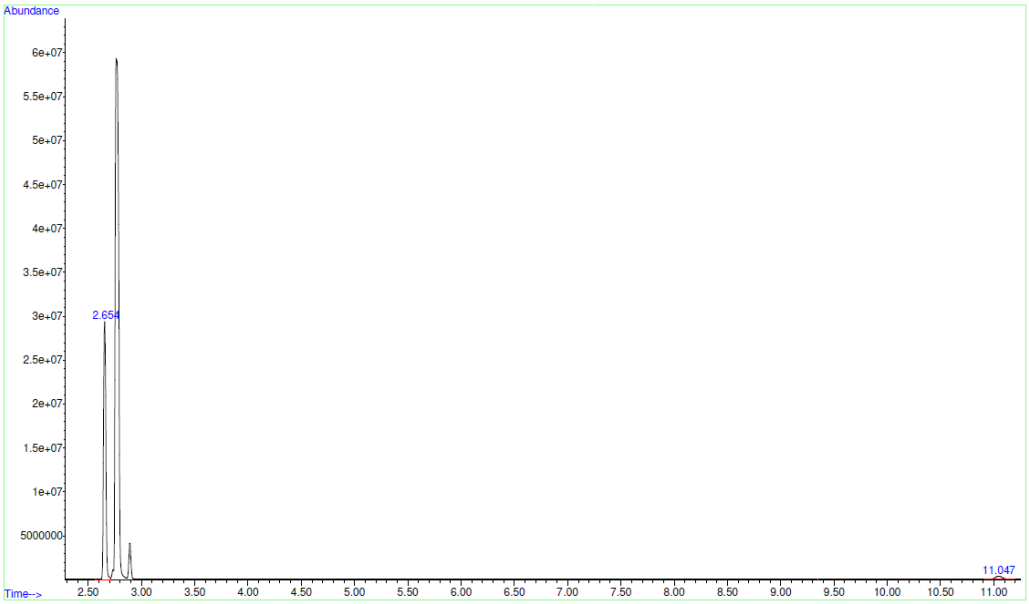


Figure J 1: Sample chromatogram of vapor phase at 10 minute for Reactive Distillation Experiment 39

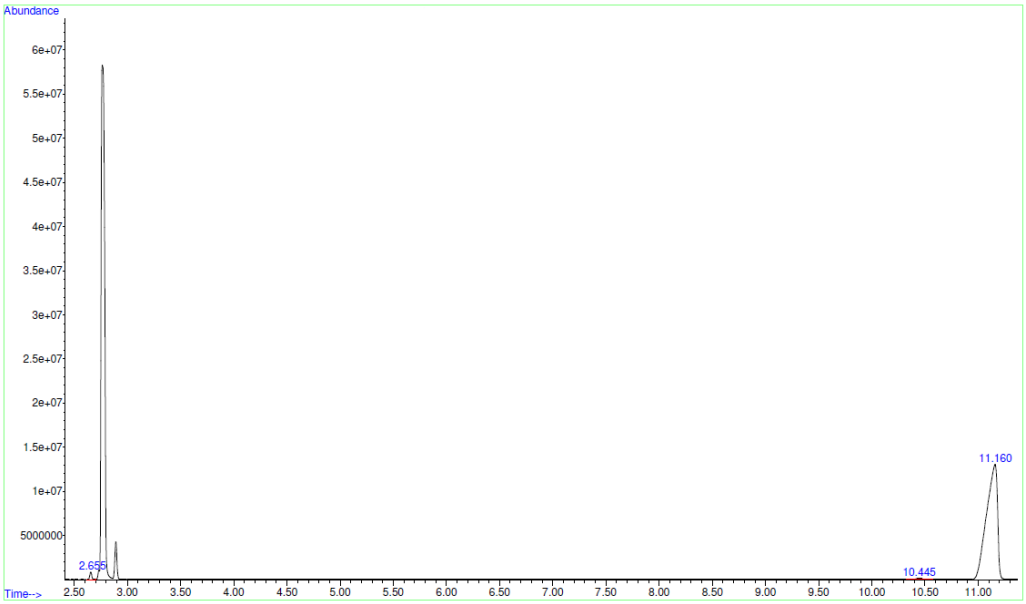


Figure J 2: Sample chromatogram of liquid phase at 10 minute for Reactive Distillation Experiment 39

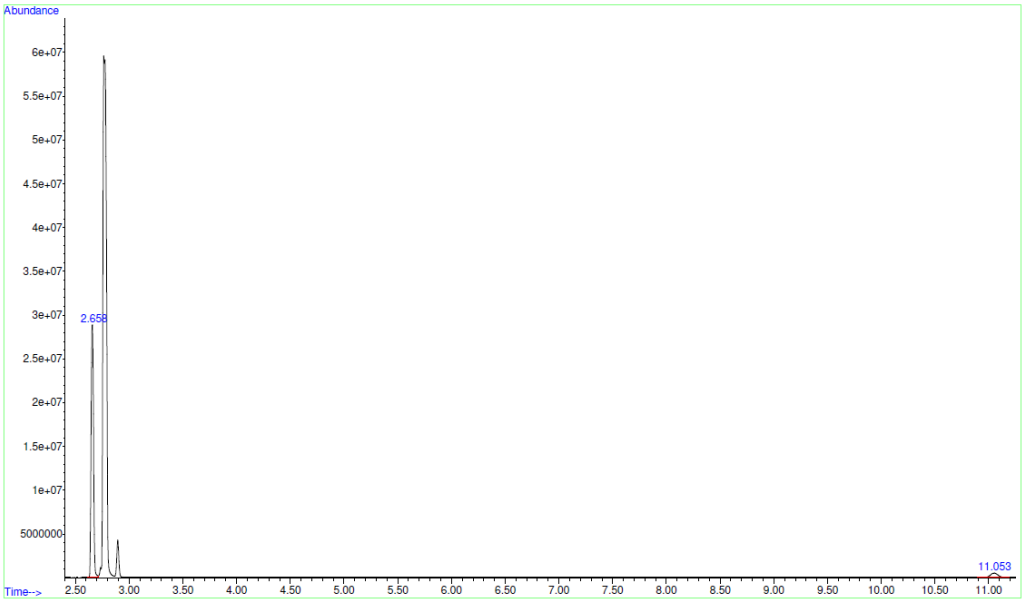


Figure J 3: Sample chromatogram of vapor phase at 20 minute for Reactive Distillation Experiment 39

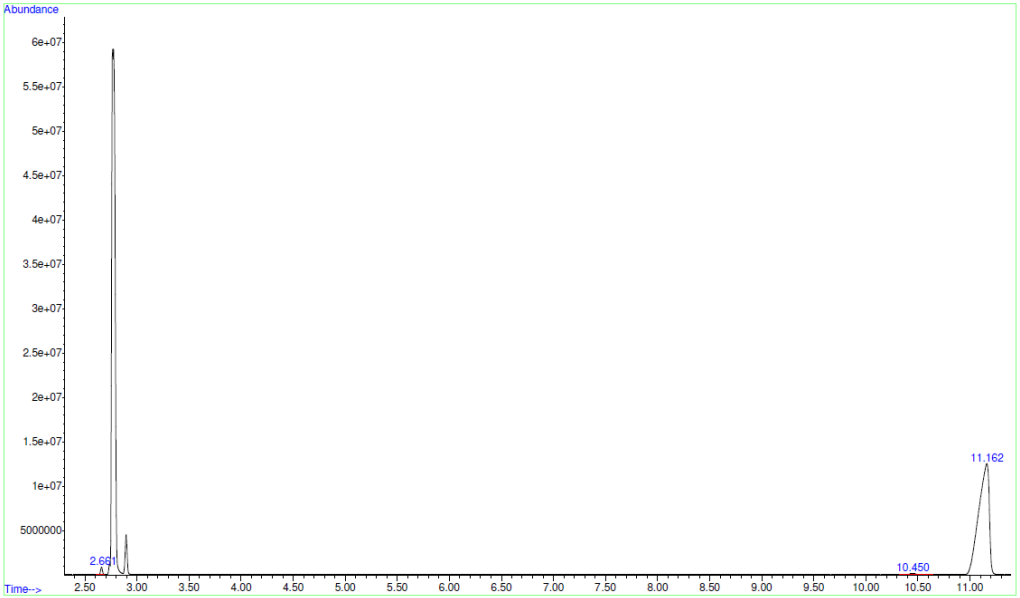


Figure J 4: Sample chromatogram of liquid phase at 20 minute for Reactive Distillation Experiment 39

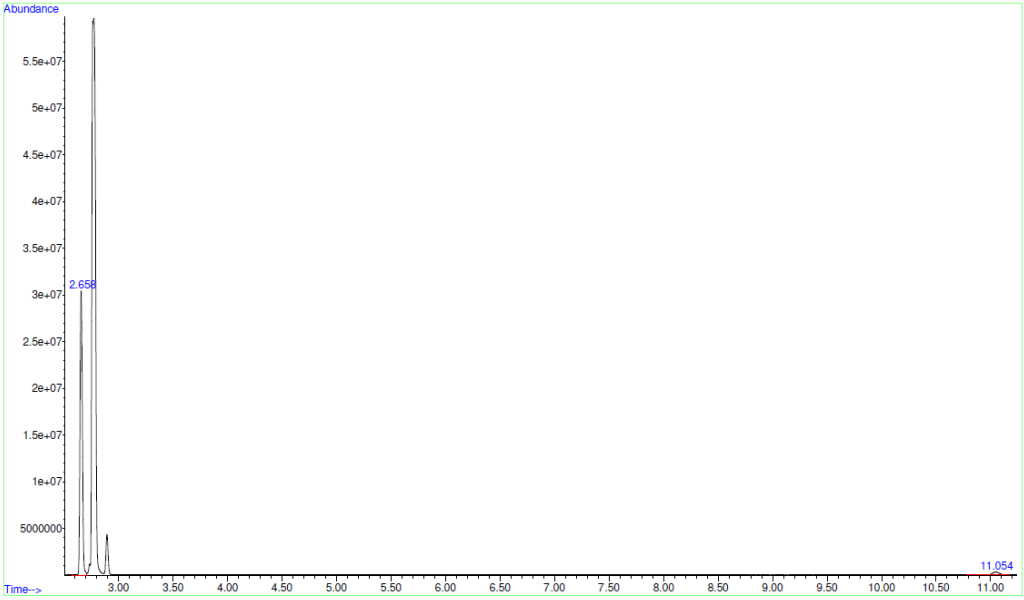


Figure J 5: Sample chromatogram of vapor phase at 30 minute for Reactive Distillation Experiment 39

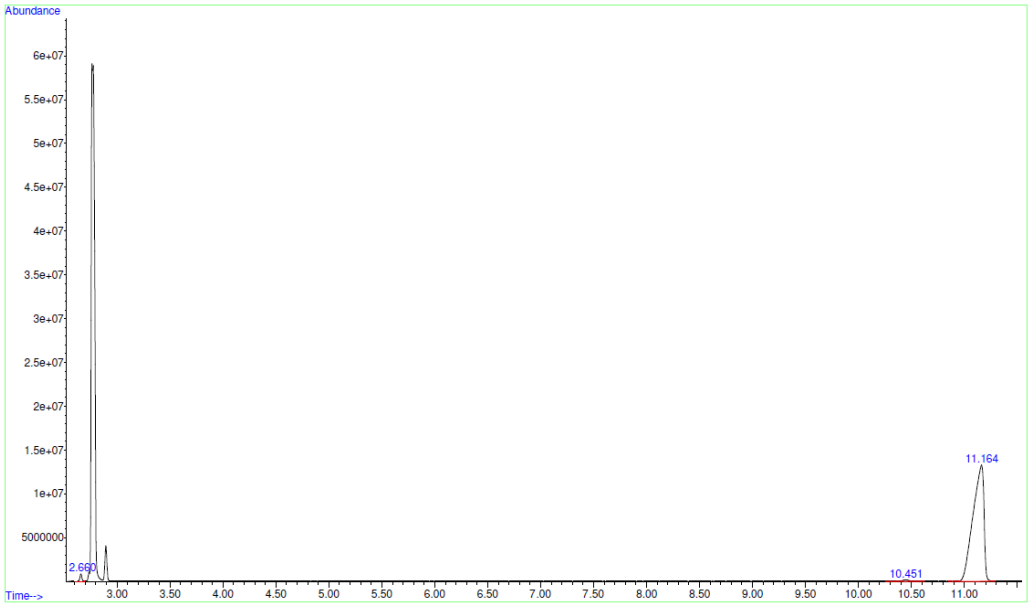


Figure J 6: Sample chromatogram of liquid phase at 30 minute for Reactive Distillation Experiment 39

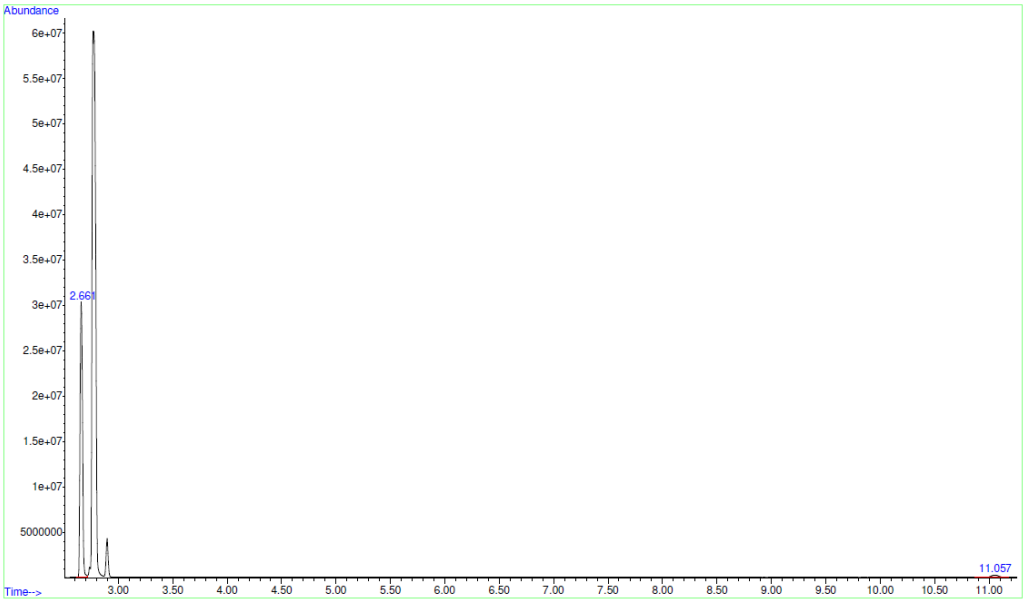


Figure J 7: Sample chromatogram of vapor phase at 40 minute for Reactive Distillation Experiment 39

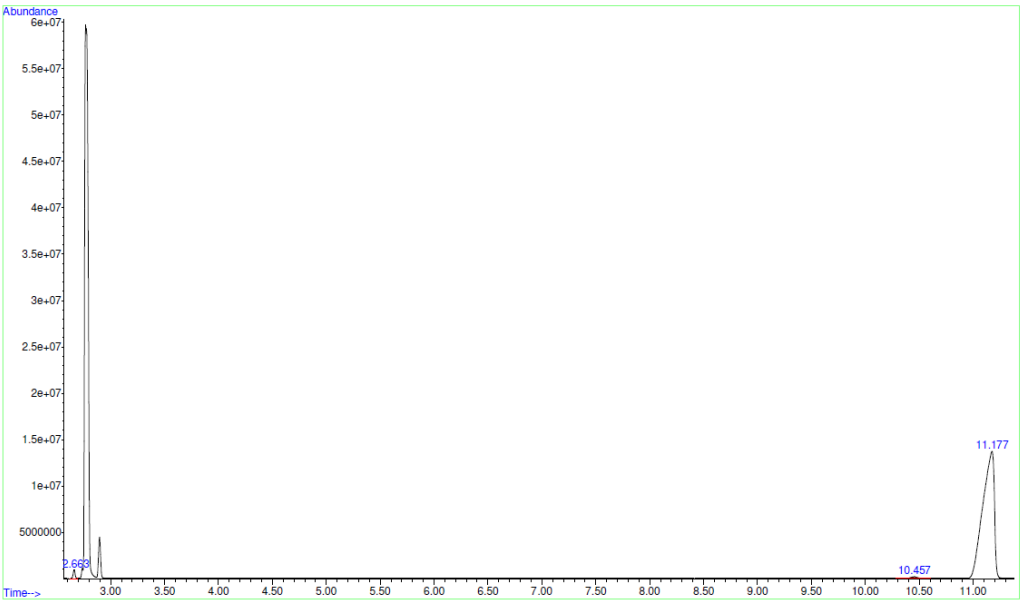


Figure J 8: Sample chromatogram of liquid phase at 40 minute for Reactive Distillation Experiment 39

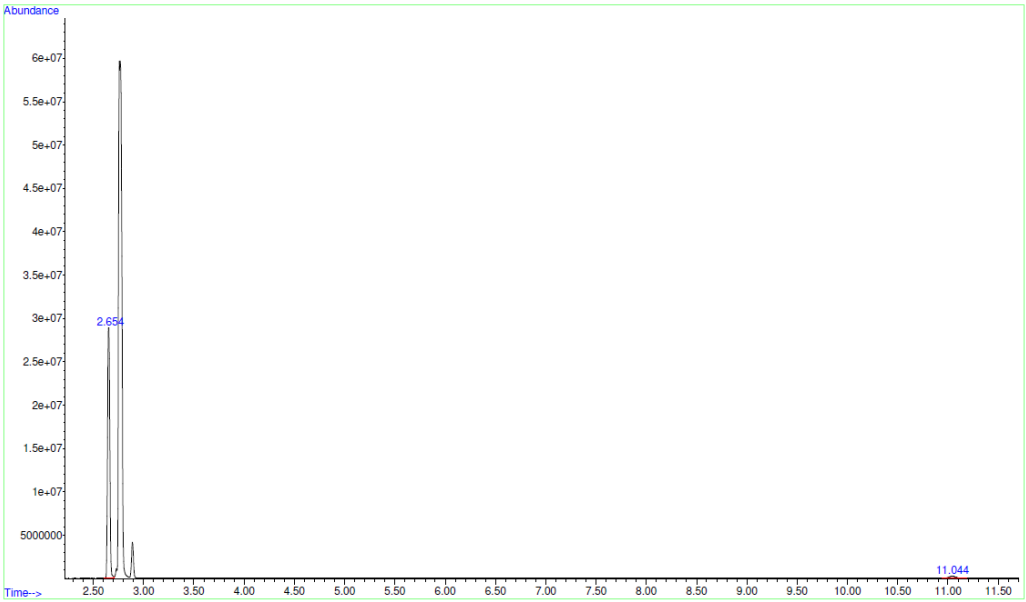


Figure J 9: Sample chromatogram of vapor phase at 50 minute for Reactive Distillation Experiment 39

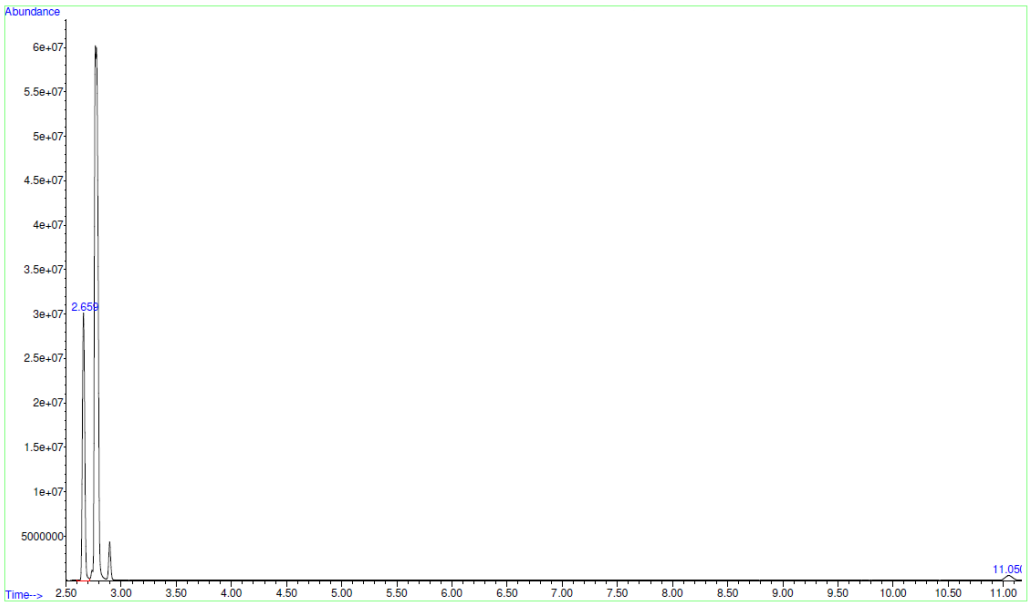


Figure J 10: Sample chromatogram of liquid phase at 50 minute for Reactive Distillation Experiment 39

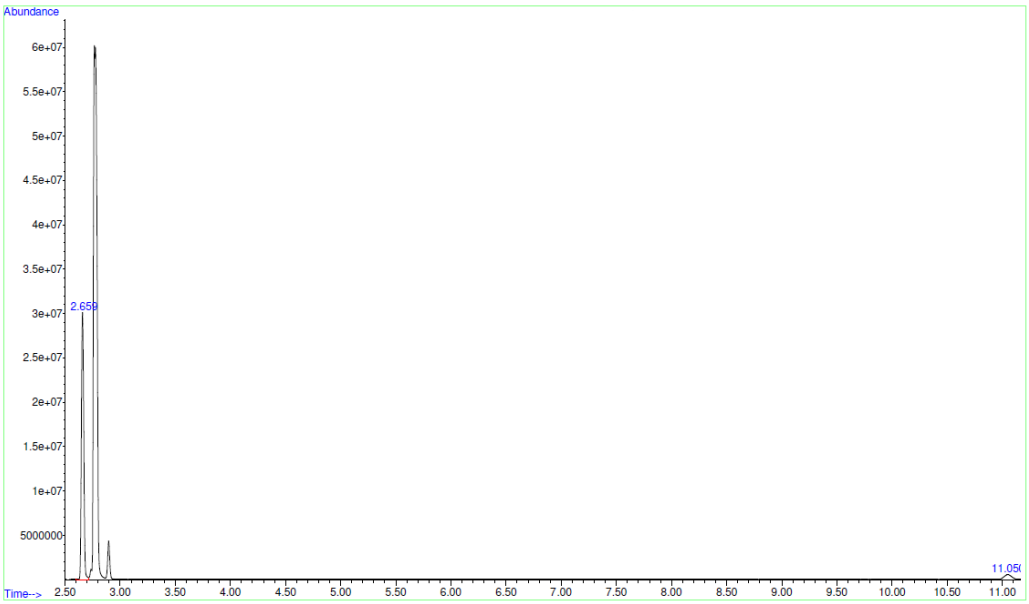


Figure J 11: Sample chromatogram of vapor phase at 60 minute for Reactive Distillation Experiment 39

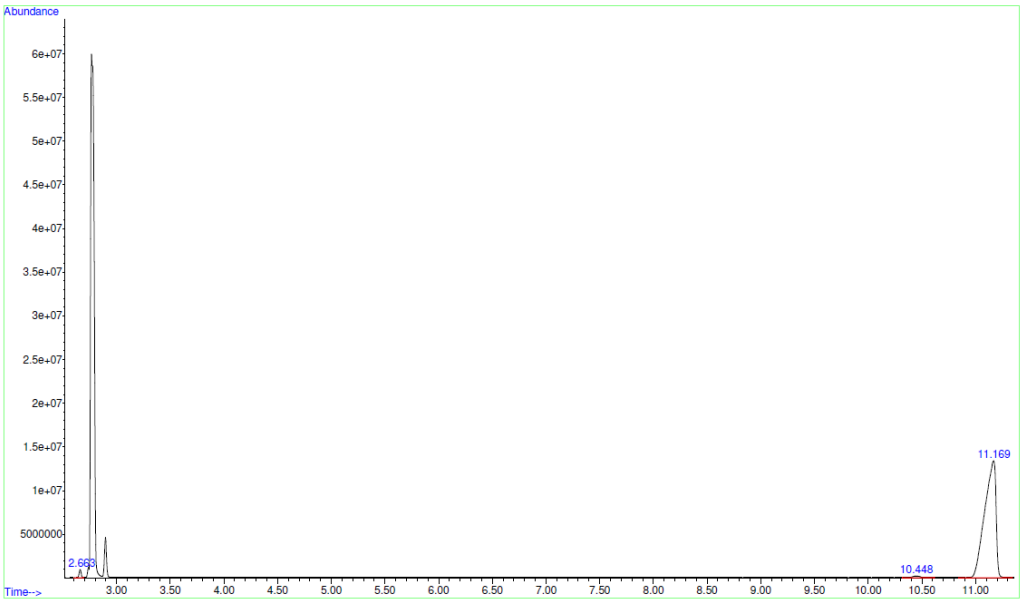


Figure J 12: Sample chromatogram of liquid phase at 60 minute for Reactive Distillation Experiment 39

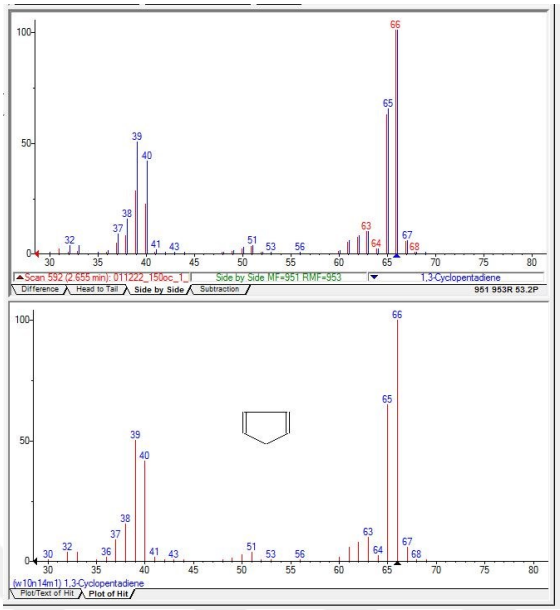


Figure J 13: Mass spectra and library match for peak at 2.665 RTmin

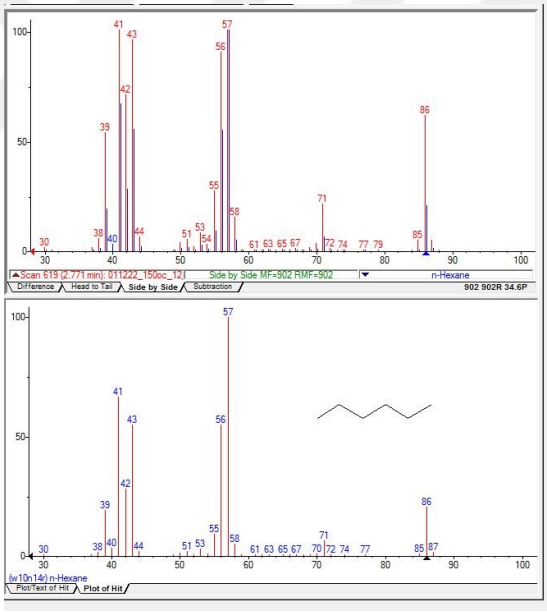


Figure J 14: Mass spectra and library match for peak at 2.771 RTmin

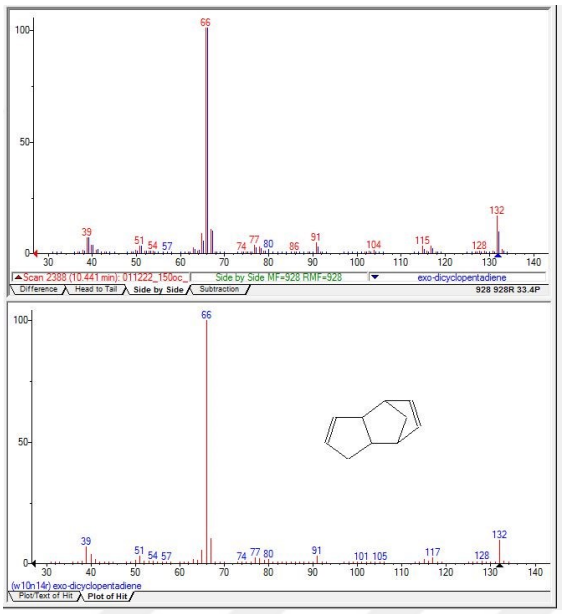


Figure J 15: Mass spectra and library match for peak at 10.441 RTmin

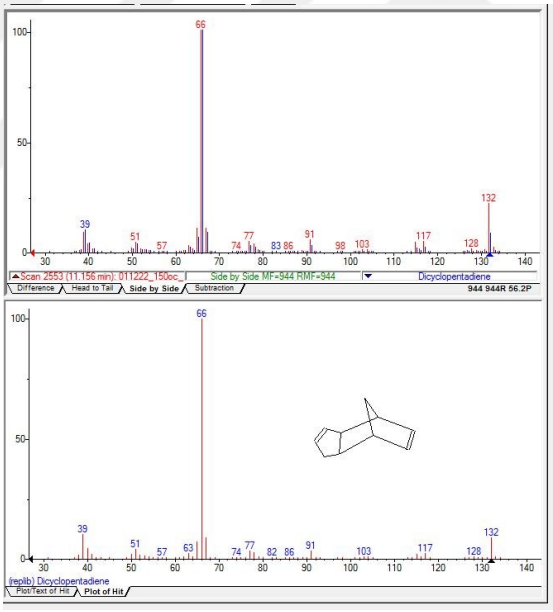


Figure J 16: Mass spectra and library match for peak at 11.156 RTmin